OF-WTWI-1984-8

NUMERICAL MODELING OF REGIONAL GROUND-WATER FLOW IN THE DEEP-BRINE AQUIFERS OF THE PALO DURO BASIN, TEXAS PANHANDLE

by

Prakob Wirojanagud

Charles W. Kreitler

D. Anderson Smith

CAUTION

This report describes research carried out by staff members of the Bureau of Economic Geology that addresses the feasibility of the Palo Duro Basin for isolation of high-level nuclear wastes. The report describes the progress and current status of research and tentative conclusions reached. Interpretations and conclusions are based on available data and state-of-the-art concepts, and hence, may be modified by more information and further application of the involved sciences.

Prepared for the
U. S. Department of Energy
Office of Nuclear Waste Isolation
under contract no. DE-AC-97-83WM46615

Bureau of Economic Geology
W. L. Fisher, Director
The University of Texas at Austin
University Station, P. O. Box X
Austin, Texas 78712

1984

CONTENTS

ABSTRACT

GENERAL GEOLOGIC AND HYDROGEOLOGIC SETTING

Major Hydrogeologic Units

Deep-Basin Brine Aquifer

Permian Evaporite Aquitard

Ogallala-Dockum Aquifer

A Conceptual Ground-Water Flow Model

HYDROGEOLOGIC PROPERTIES OF THE FLOW SYSTEM

Fluid Properties

Permeability and Hydraulic Conductivity

Porosity

HYDRAULIC AND BOUNDARY CONDITIONS

Head Map of the Ogallala-Dockum Aquifer

Map of the Deep-Basin Brine Aquifer

Head Map of the Wolfcamp Aquifer

Boundary Conditions

NUMERICAL SIMULATIONS

General Description of Numerical Modeling

The Wolfcamp Aquifer

Simulation A-1

Simulation A-2

Simulation A-3

Simulations B and C

Simulation D-1

Simulation D-2

Simulation E

Leakage Across Evaporite Aquitard

The Deep-Basin Brine Aquifer

Simulation A

Simulation B

Simulation C

HYDROGEOLOGIC IMPLICATIONS

CONCLUSIONS

REFERENCES

APPENDIX

ABSTRACT

A conceptual hydrogeologic model of the Palo Duro Basin, Texas Panhandle, subdivides the basin into three hydrogeologic units: the shallow Ogallala and Dockum aquifers, the Permian evaporite aquitard, and the deep confined, underpressured Permian and Pennsylvanian brine aquifer. The first permeable units beneath the thick Permian evaporite section are Wolfcamp strata composed of carbonates, shales, and arkosic sand and gravels (granite wash) with average effective permeability values of 8.9, 0.0001, and 8.6 md, respectively. Ground waters in the Wolfcamp aquifer flow to the northeast toward the semi-impermeable, granitic Amarillo Uplift. This anomalous hydrologic condition (flow toward a low-transmissivity barrier) may result from the presence of highly permeable granite-wash deposits that flank the uplift and function as "hydrologic sinks."

A two-dimensional, vertical-averaging finite-element model, incorporating the different lithologies and their different permeabilities as well as leakage through the overlying evaporite aquitard, has been used to simulate the observed potentiometric surface of the Wolfcamp aquifer. The conditions that best simulate the observed Wolfcamp potentiometric surface are a combination of specified head and no-flow conditions along the uplift, permeability values greater than 260 md for the granite-wash deposits that flank the uplift (in contrast to the average value of 8.6 md), and an increased permeability value of 50 md for the highly porous carbonate zone. The best estimate of the vertical permeability of the evaporite aquitard is 0.00008 md.

Treating the whole deep-brine aquifer as a single permeable unit beneath the evaporite aquitard, ground-water flow is to the northeast toward the uplift with a slightly larger west-to-east component than that found when considering only flow in Wolfcamp strata. The conditions that best simulate the averaged potentiometric surface are those from the best simulation of Wolfcamp strata, with increased permeability values of 260 md for the Pennsylvanian granite-wash close to the uplift and 250 md for the high-porosity Pennsylvanian carbonates.

This report describes research carried out by staff members of the Bureau of Economic Geology. The report describes the progress and current status of research, not definitive conclusions reached. Interpretations and conclusions are based on available data and state-of-the-art models, and hence, may be modified by more information and further application of the involved sciences.

GENERAL GEOLOGIC AND HYDROGEOLOGIC SETTINGS

The Palo Duro Basin is a Paleozoic depositional subbasin of the larger Permian Basin of southwest Texas and southeastern New Mexico. The basin is bounded on the north by the Amarillo Uplift and Bravo Dome, on the south by the Matador Arch, and on the west by the Tucumcari Basin and the Sierra Grande Uplift and on the east by the Hardeman Basin (fig. 1). The transition between the Palo Duro and the Tucumcari and the Hardeman is poorly defined. The detailed stratigraphy and depositional systems of the basin have been discussed in several research reports (Gustavson and others, 1981; Handford, 1980; Dutton and others, 1982). A simplified stratigraphic column consisting of different hydrogeologic elements and hydrogeologic units is defined for the study of regional ground-water movement and mass transport in the present work.

Major Hydrogeologic Units

Table 1 summarizes the stratigraphic and hydrogeologic divisions of the Palo Duro Basin. The hydrogeologic elements were designated according to their relative water-conducting or water-retarding character. The hydrogeologic units are composed of one or more of the hydrogeologic elements, and represent assemblages of vertically contiguous strata that have different primary lithologies, but have the same general hydraulic properties (Bassett and Bentley, 1983). Some of the hydrogeologic elements are composed of a sequence of relatively high and low permeability lithologies, reflecting the heterogeneity and complexity of the system. Nevertheless, there are three major hydrogeologic units overlying the impermeable crystalline basement: the Deep-Basin Brine Aquifer; the Permian evaporite aquitard; and the shallow Ogallala-Dockum Aquifer.

Deep-Basin Brine Aquifer

The Deep-Basin Brine Aquifer is composed of the pre-Pennsylvanian, Pennsylvanian, and Wolfcampian (Lower Permian) strata extending from the top of the Precambrian crystalline

rock up to the top of the Wolfcampian dolomite. The aquifer is generally composed of shelf and shelf-margin carbonates and fluvial-deltaic arkosic/nonarkosic sandstones interbedded with basinal shale (mudstone).

The pre-Pennsylvanian strata contain three depositional units: a basal clastic unit; a Lower Ordovician, predominantly dolomitic unit; and a relatively thick sequence of Mississippian carbonates (predominantly limestones). These units are not continuous, but occur in various combinations throughout the basin (Dutton and others, 1982). The crystalline basement deepens toward the southern center of the basin with the deepest part occurring just north of the Matador Arch in Floyd and Motley Counties (fig. 2). The same trend is observed for the structure contours of the top of the Mississippian system (fig. 3), but with a smaller slope, indicating that the pre-Pennsylvanian strata thicken toward Floyd and Motley Counties. The thickest pre-Pennsylvanian sequence is, however, encountered in the faulted, northeastern part of the basin. The thickness of the pre-Pennsylvanian strata can be determined from the structure contour maps of figures 2 and 3.

The Pennsylvanian and Wolfcampian strata are the most laterally and vertically extensive elements of the Deep-Basin Brine Aquifer with four genetic stratigraphic units of (1) shelf and shelf-margin carbonates, (2) fan-delta, coarse arkosic deposits (granite wash), (3) deltaic-nonarkosic sandstones, and (4) basinal shale. The depositional patterns and total thickness of the Pennsylvanian strata were strongly influenced by regional subsidence which was actively shaping the basin geometry. The northwest-trending area of thickest Pennsylvanian strata occurs in the basin center and thins onto the bounding Precambrian basement highlands and western edge of the basin (fig. 4). Thick, coarse-grained clastics were deposited adjacent to the sources, the Amarillo Uplift to the north and east, and the Bravo Dome to the northwest, and prograded away from the source area forming the "granite-wash" deposits (fig. 5). Deltaic-nonarkosic sandstones in the southeastern Palo Duro Basin extend westward into the basin (fig. 6), probably originating in the Wichita Mountains in Oklahoma (Dutton and others, 1982). Basinward from these peripheral terrigenous clastics are interbedded shelf carbonates which

grade basinward into thicker, more vertically persistent, shelf-margin carbonate buildups. The interbedded shelf carbonates in the lower Pennsylvanian strata are relatively thin (fig. 7), whereas thick, well-defined shelf-margin carbonates are common in the upper Pennsylvanian strata (fig. 8). High-porosity trends in the Pennsylvanian carbonates follow the shelf margins (fig. 9) and excellent correlation exists between high-porosity zones and dolomite occurrence (Dutton and others, 1982).

There is no major lithic change from the Pennsylvanian rocks to the Wolfcampian rocks; therefore, it is difficult to place the system boundary. The operational marker for the boundary is a thin, widespread limestone unit which was deposited near the end of the Pennsylvanian. Where the limestone was not deposited, the boundary is conventionally placed at the top of a widespread shale (Dutton and others, 1982). A typical cross section in figure 10 illustrates thick, widespread sequences of fine-grained sediments of silty shales and dark micritic limestones which filled the deeper portions of the basin during late Pennsylvanian and early Wolfcampian time. Depositional environments during the Wolfcampian are the same as those existing in the Pennsylvanian, although the basin was transforming from a relatively deep basin to a restricted carbonate platform. Wolfcampian strata thin onto and over the Precambrian basement uplifts with the thickest parts trending north-northwest (fig. 11). Granite-wash deposition was confined primarily to the flanks of the uplifts due to reduction in the supply of clastic sediment during the Wolfcamp. Some deltaic-nonarkosic sandstones extend westward into the basin through the southeastern boundary in similar patterns as those of the Pennsylvanian system (fig. 12). The thickness of Wolfcamp carbonate varies from 120 to 580 m (400 to 1,900 ft), with the thickest part lying approximately along the shelf margins (figs. 11 and 13). High-porosity trends in the Wolfcamp carbonates also follow the shelf margins (fig. 14) and correlate with zones of dolomitization.

CAUTION

This report describes research carried out by staff members of the Bureau of Economic Geology that addresses the feasibility of the Palo Duro Basin for [illegible] wastes. This report describes the [illegible] of research and tentative conclusions reached. [illegible] state-of-the-[illegible] modified by more information and further application of the involved sciences.

Permian Evaporite Aquitard

The term, "Permian Evaporite Aquitard," in this study refers to the relatively low-permeability, Permian evaporite-bearing strata extending from the top of the Wolfcampian strata (fig. 15) to the top of the Alibates Formation (fig. 16). Ground-surface elevation (fig. 17) was used as an approximation of the strata's upper boundary east of the Caprock Escarpment where the Alibates does not exist. The Permian evaporite-bearing strata consist almost entirely of four major lithofacies: halite, anhydrite, dolomite, and fine-grained siliciclastic red beds (Handford, 1980). A core study of the Permian section in the DOE-Gruy Federal No. 1 Grabbe test well in Swisher County (fig. 18) indicates that the section consists of 58 percent salt and anhydrite, 32 percent red beds, and 10 percent dolomite. Another rough estimation from the sample log of Castro County No. 1 well shows a combination of 67 percent salt and anhydrite, 30 percent red beds, and 3 percent dolomite (A. Dutton, personal communication, 1983). Total thickness of the evaporite aquitard estimated from figures 15 and 16 varies from 650 to 1,550 m (2,100 to 5,100 ft), and the aquitard thickens toward the southwestern part of the basin.

Ogallala-Dockum Aquifer

Overlying the Permian evaporite aquitard in the central and western parts of the Palo Duro Basin are the fluvial, deltaic, and lacustrine deposits of the Triassic Dockum Group and the alluvial deposits of the Tertiary Ogallala Formation. The Dockum Group is composed dominantly of terrigenous clastic red beds, mudstones, siltstones, sandstones, conglomerates, and minor facies of dolomite and chert (McGowen and others, 1979). The Ogallala Formation is made up of large alluvial fans of sand, gravel, and clay resulting from the eastward fluvial transport of eroded clastics from the Rocky Mountains (Seni, 1980). In contrast to the Dockum sandstones, which have low specific capacities and produce waters that range widely in salinity, the Ogallala aquifer has supplied most of the water used in the High Plains for agricultural, industrial, and domestic purposes. In the Palo Duro Basin, the aquifer is about 120 m (400 ft)

thick along a northwest-southeast trend and thins in the southwest direction to about 30 m (100 ft) and in the east and northeast directions to zero (Seni, 1980, fig. 5). The percentage of sand and gravel decreases from 70 percent to 20 percent in the same patterns as those of the aquifer's thickness (Seni, 1980, fig. 10).

A Conceptual Ground-Water Flow Model

Figure 19 depicts the conceptualized regional ground-water flow patterns in the Texas Panhandle (after Bassett and Bentley, 1983). The flow system is characterized by the geometry of the region, its hydraulic conditions, the relative average permeabilities of major hydrogeologic units, and the permeability distribution within each major hydrogeologic unit. The preliminary values of the relative average permeabilities given in figure 19 are intended only for illustrating their effects on the conceptual flow patterns. The distribution of the actual permeability values is far more complicated in the real system. The flow regime is bounded vertically by the land surface with a water table that essentially follows the topography, and by the basement aquiclude. The flow system is assumed to be currently under steady-state conditions.

The low-permeability evaporite aquitard separates the flow regime into two distinctly different flow systems: the upper unconfined aquifer (Ogallala-Dockum) and the Deep-Basin Brine Aquifer. Considering the ratio of average thickness to average areal extent of the aquifer in the Palo Duro Basin, which is about 1 to 400 for the upper unconfined and 1 to 190 for the deep brine, both aquifers can be treated as extensive ones in which losses of head due to the vertical velocity components may be neglected. Thus, flow in both systems is essentially horizontal. The results of pressure-depth analysis of the deep-basin fluids indicates vertical uniformity of heads (Bentley, 1981; E. Orr, personal communication, 1982), suggesting that: (1) the whole deep-brine aquifer is interconnected, probably by depositional thinning of the shale aquitards that are interbedded with the carbonates and sandstones and/or by faults and fractures and (2) the assumption of predominantly horizontal flow in the aquifer is valid. The

same pressure-depth results also indicate that the deep-brine aquifer is underpressured in most parts of the basin, especially beneath the High Plains, and that it is artesian. In other words, the piezometric heads in the deep basin are below the land surface, but are well above the top of the deep-basin aquifer and are within the salt section.

Recharge to the deep aquifer probably takes place in the updip areas to the west in New Mexico where the aquifer crops out (fig. 19) and along the upper boundary where vertical leakage from the upper aquifer moves through the evaporite aquitard. The amount of local recharge from leakage depends on the potentiometric-head difference between the upper and the deep-brine aquifers and the thickness and vertical permeability of the evaporite aquitard. Although average vertical-permeability of the evaporite section may be very small, vertical leakage across the aquitard may be significant due to the large contact area between formations. Locating areas where leakage is relatively high is also difficult because of the low density and unreliability of data.

Flow in the Ogallala-Dockum Aquifer is essentially horizontal and the flow system is effectively separated from the deep-brine system. Although flow patterns in the aquifer are not the subject of this study, long-term, equilibrium, potentiometric head contours of the aquifer are necessary for the evaluation of flow patterns in the deep aquifer because the upper aquifer is a factor controlling the vertical leakage across the evaporite aquitard. The Ogallala and Dockum Formations may not constitute a unified and interconnected aquifer, but may represent two separate aquifers. Available data are not sufficient to separate the two formations into two separate aquifers. A conservative approach is maintained by assuming the potentiometric surface of the Ogallala is representative for both formations.

The Wolfcamp is the first permeable strata beneath the proposed repository site and is a possible pathway for contaminant transport from the repository to the biosphere. The whole Deep-Basin Brine Aquifer can also be treated as a major pathway for contaminant transport, owing to the hydraulic interconnection of the aquifer by cross-formational flow. Additional

CAUTION

This report describes research carried out by staff members of the Bureau of Economic Geology and addresses the suitability of the Palo Duro Basin for isolation of high-level nuclear waste. The report describes the progress and current status of research and tentative conclusions reached. Interpretations and conclusions are based on available data and state-of-the-art concepts, and hence, may be modified by more information and further application of the involved sciences.

pathways may exist in continuously permeable dolomites (e.g., San Andres dolomites, Dutton, in press) in the evaporite section.

HYDROGEOLOGIC PROPERTIES OF THE FLOW SYSTEM

Fluid Properties

Procedures for computing salinity values of the deep-basin fluids from geophysical logs and from chemical analyses of fluid samples were described in Bassett and Bentley (1983). The average salinity in terms of total dissolved solids (TDS) of brines in the Wolfcamp-carbonate section of the Palo Duro Basin is 130,000 mg/L, determined from 110 data points (Bassett and Bentley, 1983, fig. 10). Similarly, the average salinity of brines in the deep-basin granite wash of the Palo Duro Basin was estimated, from 87 data points, to be 123,000 mg/L (Bassett and Bentley, 1983, fig. 11). In this study, an average salinity value of 127,000 mg/L was used for the deep-basin brines. Using the average geothermal gradient of 0.6°C/100 ft for the region, the average temperatures of brines in the Wolfcamp carbonates and in the granite wash were computed to be 41°C (105°F) and 52°C (125°F), respectively. It is expected that a small temperature gradient will have a negligible effect on regional ground-water flow patterns and, therefore, an average temperature of 46°C (115°F) was used to represent the fluid temperature. Using these average fluid properties (salinity and temperature) to convert units of permeability to hydraulic conductivity for the flow system. 1 md equals 0.00115 m/day.

Permeability and Hydraulic Conductivity

In order to do numerical simulations of ground-water flow patterns and calculate travel times in the deep brine aquifer of the Palo Duro Basin, knowledge of the permeability of the various hydrogeologic units is necessary. It is also necessary to recognize that when two-dimensional flow takes place in a stationary and isotropic medium under a uniform gradient, the

effective permeability of the medium is given by the geometric mean of permeability values at data points (Neuman, 1982). For problems of two-dimensional areal flow, each horizontally distributed point quantity must represent the vertically averaged permeability of the aquifer at that point which can be determined, for example, from pumping test data. The geometric mean of these point quantities is then used as an effective permeability value for the aquifer. The following is a discussion about the availability of permeability data for the deep-basin aquifer system and the use of the data in the numerical simulations.

Permeability data are available for Wolfcamp carbonates, Pennsylvanian carbonates, granite wash, and pre-Pennsylvanian rocks (Table 2). Much of the permeability data is from petroleum exploration testing in basins adjacent to the Palo Duro Basin and is included in the data base. Permeability data for Wolfcamp carbonates are available from 25 DSTs (drill-stem tests), described by Bassett and Bentley (1983), from six pumping tests and 70 core sample tests. The six pumping tests are multiple tests of a single Wolfcamp interval in the DOE-Stone and Webster No. 1 Sawyer test well in Donley County, Texas. The 70 core sample permeability values are from oil fields in the Anadarko, Midland, and Dalhart Basins (Texas Water Development Board, 1972). Pennsylvanian permeability data are available from 25 DSTs and 118 analyses of core samples. Upper and lower Pennsylvanian samples are not differentiated in the core data. Granite-wash permeability data are available from 10 DSTs, 10 pumping tests in a single granite-wash interval in the No. 1 Sawyer test well, and 426 laboratory core analyses. Of the core sample analyses, 415 are from six wells in the Mobeetie Field in the Anadarko Basin. Pre-Pennsylvanian permeability data are very limited and consist of values from 4 DSTs of the Ellenburger Group, 6 DSTs of Mississippian carbonates, 1 pumping test of the Ellenburger Group, and 14 pumping tests in a single Mississippian carbonate interval in the No. 1 Sawyer test well. From this data base, Smith (1983) summarized the permeability values of each hydrogeologic unit and computed the geometric mean, arithmetic mean, and variance of the permeability for each type of data. Additional permeability data from five pumping tests in the Pennsylvanian granite-wash at DOE's SWEC-J. Friemel No. 1 well indicate a permeability range

of 10 to 400 md with the average of 140 md. Laboratory tests on a granite-wash core sample from the same well indicate a permeability range of 97 to 267 md.

It should be noted that none of the above permeability data represent a vertically averaged permeability of the hydrogeologic unit at a given location which is the desirable nodal point value in two-dimensional areal flow simulations. Although each permeability value from pumping tests represents the average fluid-conducting property of a relatively large volume of the medium compared with that of a core sample, the tested zone of the medium is still a small portion of the whole section of the hydrogeologic unit. No attempt was made to compute the vertically averaged permeability at data points where there are more than one permeability value because of the insufficiency of information and the variety of testing techniques used to obtain the permeability data. Instead, all the permeability data for each hydrogeologic unit (including those of the neighboring basins) were used in the computation of the unit's geometric mean and variance.

Table 2 summarizes the effective permeability values and the variances for each hydrogeologic unit of the Palo Duro Basin. The variances given in the table are those of DST permeability data which, for all strata, are the highest. The range of variance from 5.08 to 5.70 for the carbonates seems high compared with the typical range of 1.12 to 1.49 from 24,222 core samples of limestone (Bennion and Griffiths, 1966). The variance of 7.13 for the granite wash is also high compared with the range of .21 to 5.30 from more than 60,000 core samples of conglomerate and sandstone (Bennion and Griffiths, 1966; Law, 1944). The large values of variance indicate that there is a large natural variation in the permeability of each hydrogeologic unit and also suggest a lack of sufficient data. The effective-average permeability value is slightly increased with the inclusion of permeability data from neighboring basins for the Wolfcamp and Pennsylvanian carbonates, but slightly decreased for the granite wash. A conservative approach is maintained by using the larger value in each case.

The vertical permeability of 0.00028 md for the evaporite aquitard was derived from the harmonic means of permeabilities of two typical cross sections of the evaporite strata using

typical or measured values of permeability for each substrata. A typical cross section of the evaporite strata is illustrated in figure 19. The typical or measured values of permeability of the evaporite's substrata are: 0.0001 md for red-bed shale (Davis and DeWiest, 1966), 0.0073 to 0.012 md for salt and anhydrite (Davis and DeWiest, 1966; Peterson and others, 1981), and 0.1 md for dolomite (DST results, A. Dutton, personal communication, 1983). Table 2 includes the typical values of permeability of carbonates, shale, and granite wash taken from the literature.

Porosity

There are no direct measurements of porosity available for the deep-brine aquifer of the Palo Duro Basin. An indirect method using neutron-density logs was employed to make quantitative determinations of porosity of the Wolfcamp and Pennsylvanian strata (R. Conti, personal communication, 1983). From two neutron-density logs which penetrate the Pennsylvanian strata at the DOE-No. 1 Sawyer test well in Donley County and the DOE-No. 1 Mansfield test well in Oldham County, porosity values of the Wolfcamp and Pennsylvanian carbonates and the granite wash were estimated at 50 ft intervals according to the procedure described in Schlumberger (1979). Results of the analyses are given along with some typical values in Table 3. Conti (1983, personal communication) has determined the porosity distributions of the Wolfcampian carbonates using 20 neutron-density logs in the Palo Duro Basin (fig. 20).

HYDRAULIC AND BOUNDARY CONDITIONS

Head Map of the Ogallala-Dockum Aquifer

Potentiometric heads in the Dockum Group indicate hydraulic conditions on the upper boundary of the underlying evaporite aquitard. Available head data are insufficient for constructing a reliable potentiometric head map of the Dockum unit. Published information on the characteristics of the Ogallala Formation is readily available. Using these data, combined

with Dockum head data, Bassett, Bentley, and Simpkins (1981) constructed a head map of the unconfined Upper Aquifer that overlies the evaporite aquitard in the Palo Duro Basin (fig. 21).

Head Map of the Deep-Basin Brine Aquifer

The whole deep-brine aquifer can be treated as a single permeable unit beneath the salt section provided that there is adequate vertical communication of flowing fluid between units comprising the aquifer. Based on the available geologic information and the results of pressure-depth analysis (which indicate general vertical uniformity of heads in the deep basin), this simplification seems to be justified for the evaluation of ground-water flow patterns on a regional scale. Therefore, it can be assumed that heads in the Wolfcamp and the Pennsylvanian strata are similar and that regional flow patterns in the deep basin may be characterized by an average potentiometric head surface.

Almost all of the head data from the Deep-Basin Brine Aquifer used in this study were derived from the results of drill-stem tests (DST) conducted in petroleum wildcat wells and from bottomhole pressures measured in oil fields (data available from the Petroleum Information Corporation (PI) commercial file). There are about 1,460 sets of data for the Palo Duro Basin and the northern part of the Midland Basin, just south of the Matador Arch. Sixty-six more sets of data with pressure/time charts were obtained directly from operators in the Palo Duro Basin in the form of DST technical reports. This type of data, classified as "class H" data, is considered to be the best since the pressure/time charts are available for analysis (Matthews and Russell, 1967; Bassett and Bentley, 1983). The Petroleum Information Corporation data are ranked according to number and quality of shut-in period data. With decreasing reliability, data are classified as: "class A" data if there are two shut-in pressures and both agree within 10 percent, "class B" if both shut-in pressures do not agree within 10 percent, and "class C" if there is only one shut-in pressure. Note that, in fact, class C group may include some good data such as those of class A, although good data could not be differentiated from bad with a single

shut-in pressure. The higher pressure of the two shut-in pressures was chosen and then converted to equivalent fresh-water head.

An average head surface for the deep-brine aquifer was constructed by averaging head values at data points where there are multiple values. By doing this and by choosing not to use class B and class C data, because of their lesser reliability, the data base of measured heads was reduced to 42 class H heads and 305 class A heads.

For a better understanding of the characteristics of each class of head data, class H and class A data were first separately investigated and then merged. Class H head data are sparsely distributed and are very rare in the middle-north and northeast of the basin (fig. 22). The head contours indicate a decline of head from west to east and from southwest to northeast. Class A head data are sparsely distributed within the Palo Duro Basin but densely packed in the northern parts of the Midland Basin, south of the Matador Arch (fig. 23). An average head map constructed from class A data (fig. 24) indicates that: (1) there is a general trend of head decline from west to east and from southwest to northeast across the Palo Duro Basin but with variability of localized zones of low and high head, and (2) there is no well-defined direction of regional head decline south of the Matador Arch due to the high density and variability of localized zones of low and high head. The zones of low head are probably created by depressurization of the aquifer from oil and gas production, especially south of the Matador Arch; or they may be due to measurement errors. The zones of high head could be due to local, high intensity recharge from the overlying evaporite aquitard. Since we are interested in studying the ground-water flow patterns on a regional scale and the available information is neither sufficient nor accurate enough for a detailed investigation of the effects of locally high recharge or depressurization due to oil and gas production, the irregularities of the head contours are treated as noise in the head data due to small-scale variations of head and measurement errors.

To obtain a smoother head map, a statistically moving-average technique called "kriging" was employed to filter out the noises. The programs for the kriging technique employed in this

study (GAMM and UKRIG) were developed by Knudson and Kim (1978) based on Matheron's (1963) intrinsic hypothesis that the first order difference (or increment) of observed values of the phenomenon (the head values in this case) forms a stationary process (has the same probability distribution at different locations). In other words, the programs assume a constant drift of head values over the area from which data are selected to make an estimate. In general, the kriging technique provides unbiased estimates of values of a variable at the nodal points of a regular or irregular grid given measured values of the variable at arbitrary points in space. The method differs from other spatial interpolation and averaging techniques in that it also provides estimates of the variance of the corresponding errors of estimation.

The first step in applying the kriging technique is to compute a representative variogram from a given set of observed data (using program GAMM). The variogram provides information about the form of relationship between two observations as a function of the intervening distance. Different functions can then be used to fit the computed variogram in order to describe it mathematically. The kriging program employed in this study (UKRIG) uses a spherical function for describing a variogram which can be defined by parameters: c, a, and co, respectively called the sill, the range, and the nugget effect. The reader is referred to Clark (1979), David (1977), and Royle and others (1980) for comprehensive discussions of geostatistical theory and mathematical methods. The next step after obtaining a representative variogram is to specify a block system of either regular or irregular sizes. Kriged estimates of the variable are then computed for each block by weighted averaging of the values of the surrounding data points (using program UKRIG). The weight of each surrounding data point in weighted averaging depends on the variogram structure and the location and orientation of the data relative to the kriged point.

An extensive variogram study of class A head data resulted in an anomalous representative variogram. The variogram indicates, from its periodic-sine-function shape, that class A head data belong to a purely random process with highly irregular patterns of data points. This phenomenon is mainly due to the highly inaccurate and fluctuating head values in the densely-

packed groups of data in the northern parts of the Midland Basin which may be due to depressurization from oil and gas production. Since the highly inaccurate head values are in the area outside the Palo Duro Basin, they are rejected and only those of class A data located above the 33°49' latitude used in this study.

By combining the best classes of head data, the new data base consists of 118 selected class A and 42 class H head values (fig. 25). The representative variogram of these 160 head values (fig. 26) gives the following information: (1) The range, the distance at which the variogram levels off, is 45,000 m, meaning that all the head data points within a distance of 45,000 m from a given point are related to the head value at that point and thus are used in the estimate of kriged head at the point. (2) The nugget effect is 2,700 m^2, indicating that the average standard error of the head data is about - 52 m which is relatively high compared to the head difference of about 500 m across the basin. (3) The average square difference of the head values (Gamma) increases from the nugget effect with distance until it levels off at a distance equal to the range and gamma equal to the sill, that is, head data nearby have similar values, and data far away are likely to have less similar values. (4) The average square difference of the head values begins to increase approximately linearly at some distance after it levels off. This indicates that the mean trend (or drift) of head begins to exert its influence and that a regional trend of head distribution is expressed in these head values. Note that drift, a large-scale phenomenon, does not exert its influence on data points separated by a distance less than the range.

The study area (fig. 25) was divided into a system of regular blocks, 20,000 m on a side. Based on the 160 selected class A and class H head data and their variogram structure (fig. 25), head values at the center of each block were computed using program UKRIG (Table A-1 in Appendix). A head map constructed from these computed head values (fig. 27) clearly shows a decline of head from southwest to northeast across the basin with a slightly larger decline from east to west along the basin's southern boundary. The kriging program not only provided the estimate of head value at a kriged point but also the estimation variance (and hence the

standard error of estimate) at each point. The estimation variance refers to the variance of the error between the true head value and the estimated head value of a block. The standard error of estimate is the square root of the estimation variance and represents the magnitude of error associated with an estimated value. A contour map of the standard errors of estimate for the kriged heads in figure 28 shows that the error is very high in the middle-north and northeast areas of the basin where there are almost no data.

Head Map of the Wolfcamp Aquifer

Due to the limited amount of Wolfcamp head data in the Palo Duro Basin, Smith (1983) used all classes of head data in both the Palo Duro and Anadarko Basins to construct a Wolfcamp head map. His data base consists of 23 class H heads, 71 class A heads, 19 class B heads, and 167 class C heads. His variogram analysis resulted in a representative variogram having a range of 20,000 m, a nugget effect of 5,340 m^2 (57,500 ft^2), and a sill of 9,530 m^2 (102,500 ft^2). The Wolfcamp nugget effect is larger than the nugget from the averaged heads variogram of the Deep-Basin Brine Aquifer, indicating that the Wolfcamp head data have a higher standard random error which, in this case, is mainly due to measurement errors. The Wolfcamp head map (fig. 29) is based on kriged estimates of head at the center of blocks 20,000 m on a side. The standard error of estimate associated with the kriged head is given in figure 30.

Boundary Conditions

There are generally two types of boundary conditions in any ground-water flow system: specified head and specified flow conditions. The eastern and western boundaries of the Palo Duro Basin are treated as head boundaries along which values are specified according to the relevant head map, that is, from figure 27 for the Deep-Basin Brine Aquifer simulations and from figure 29 for the Wolfcampian aquifer simulations. The same head maps also indicate that

the southern boundary along the Matador Arch is a no-flow boundary since the equipotential lines of both aquifer systems are essentially perpendicular to the boundary.

The conditions on the northern boundary along the Amarillo Uplift are more complicated due to the presence of the basement uplift that was exposed throughout the entire Pennsylvanian and a major part of the Wolfcampian and due to the presence of oil and gas fields. Geologic information indicates that the eastern section of the northern boundary is a no-flow boundary. This is supported by hydrologic information (the head maps). The massive block of the Amarillo Uplift apparently acts as an impervious barrier, directing most of the approaching fluid from the Palo Duro Basin eastward along the downthrown block of the uplift. There is a thin layer of Wolfcampian brown dolomite overlying the uplift (fig. 31; Handford, 1980, fig. 5; Dutton and others, 1982, figs. 12, 22, plate II) that may provide channels for fluid flowing over the uplift. However, this fluid conducting unit has a relatively small transmissivity compared with those of the adjacent Wolfcamp aquifer and the whole deep-brine aquifer in the Palo Duro Basin. Based on the average thickness of 60 m (200 ft) and the permeability of Wolfcamp carbonates, the permeable unit on the uplift has a transmissivity of 0.6 m^2/day compared with 5 to 50 m^2/day for the adjacent Wolfcampian aquifer and 10 to 80 m^2/day for the whole deep-brine aquifer. Therefore, flow in this small transmissivity unit is not expected to have any significant effect on the regional flow field of the Palo Duro Basin. Moreover, the presence of oil and gas in the Wolfcampian brown-dolomite unit on the Amarillo Uplift (Pippin, 1968) may reduce the effective permeability of water flow and act as another impervious barrier preventing ground water from flowing over the uplift. The head map of the whole deep-brine aquifer (fig. 27) clearly indicates that the northern boundary along the Amarillo Uplift can be treated as a no-flow boundary, although the Wolfcamp head map (fig. 29) and the Brown Dolomite isopach map (fig. 31) does not obviously reveal a no-flow condition along the uplift. Further discussion on the boundary conditions is given in the following section.

NUMERICAL SIMULATIONS

General Description of Numerical Modeling

For detailed characterization and evaluation of regional ground-water flow in the deep-brine aquifer, the conceptualized physical flow-system is represented by a steady-state, two-dimensional, vertical-averaging mathematical model of a confined aquifer with vertical leakage. The mathematical model is then numerically solved using the computer program "TRAVEL." Program TRAVEL is a general purpose program for two-dimensional steady-state ground-water flow analysis. It can be used to investigate two-dimensional, profile or areal, flow and mass transport problems. Program TRAVEL was written based on the Galerkin Finite-Element technique and the use of quadratic-quadrilateral elements in discretizing a flow region. Background materials, as well as some examples of application, are available in a report by Charbeneau and Street (1978). Full descriptions of the program's use and capabilities, as well as an example of application, are available in the user's guide for the program (Wirojanagud, 1983).

The studied flow region of the Palo Duro Basin was discretized into a finite element mesh of 120 elements with 405 nodes (fig. 32). The X and Y coordinates of the finite element mesh have their origin at 103.7500° longitude and 33.3870° latitude, respectively, the same as that of the well-control points mentioned earlier. The coordinate of each node point is given in meters from the origin. A data file called "PALOFL" was created to numerically represent the geometry of the flow region, thicknesses of the hydrogeologic units, and some hydraulic conditions of regional flow within the Palo Duro Basin. As Table A-2 in the Appendix illustrates, the PALOFL file consists of the following data at each node point (all length units are in meters):

(1) nodal point number;

(2) X-coordinate of node point;

(3) Y-coordinate of node point;

(4) elevation of top of the crystalline basement in meters from sea level (from fig. 2);

(5) thickness of pre-Pennsylvanian rock (from figs. 2 and 3);

(6) thickness of the Pennsylvanian carbonates (from figs. 7 and 8);

(7) thickness of the Pennsylvanian granite wash (from figs. 5 and 12);

(8) thickness of the Pennsylvanian shale in meters (from fig. 4, (6), and (7));

(9) thickness of the total Pennsylvanian rock (from fig. 4);

(10) thickness of the Wolfcamp carbonate (from figs. 11 and 13);

(11) thickness of the Wolfcamp granite wash (from fig. 12);

(12) thickness of the Wolfcamp shale (from fig. 11, (10), and (11));

(13) thickness of the total Wolfcampian rock (from fig. 11);

(14) thickness of the total granite wash (from fig. 5);

(15) thickness of the evaporite aquitard (from figs. 15, 16, and 17);

(16) potentiometric head in the upper unconfined aquifer (from fig. 21);

(17) thickness of the high-porosity Wolfcamp carbonates (from fig. 14);

(18) thickness of the high-porosity Pennsylvanian carbonates (from fig. 9); and

(19) NCODE, an integer identifying zones of granite-wash coarsening in the Pennsylvanian strata; it has the value of 2 for nodes in the coarsening zone, 1 for nodes at the boundary of the coarsening zone, and 0 for ordinary nodes.

In Table A-2, the deep-brine aquifer was divided into three subunits: the Wolfcamp, the Pennsylvanian, and the pre-Pennsylvanian strata. The Wolfcamp and the Pennsylvanian strata were further subdivided into carbonates, granite wash, and shales. The nonarkosic sandstones in the southeastern parts of the basin that are interbedded with carbonates were combined with the carbonates because of the relatively small thickness of these sandstones. The numerical values of elevation, thickness, head, and NCODE for each node point were obtained by superimposing a work map of the finite element mesh onto the relevant work map (or maps) as indicated above and either reading the values directly or computing them. Combined with information about the hydrogeologic properties (hydraulic conductivity and porosity) of the flow

system, the data in Table A-2 were used in preparing part of the input data file for the two-dimensional areal flow simulations.

Input data files for numerical simulations were prepared following the user's guide for TRAVEL (Wirojanagud, 1983). Although the whole procedure for preparing an input data file will not be described in this report, the computation of four parameters representing the hydrogeologic properties of the flow system will be briefly discussed. In an input data file, the aquifer's transmissivities in the X and Y directions (TRANSX and TRANSY) must be specified at each node, whereas the vertically integrated porosity (PORTH) and the leakage coefficient (COEF) must be specified element by element. In the Wolfcamp aquifer simulation, for example, the nodal point transmissivity is simply the summation of the products of the hydraulic conductivity and thickness of each Wolfcamp subunit (the carbonate, granite wash, and shale). The contribution of the shale subunit to the overall transmissivity value is practically negligible due to its very low permeability, but it is included in the computation for completeness. Nodal point values of the vertically integrated porosity were computed in the same manner and then averaged for each element. The leakage coefficient (defined as the aquitard's hydraulic conductivity divided by its thickness) was computed node by node and then averaged for element-wise values. The computational procedure for the properties of the whole deep-brine aquifer is similar.

The physically complex system has been represented by a numerical model whose behavior is governed by the boundary conditions and the values of four model-parameters: TRANSX, TRANSY, PORTH, and COEF. The reliability of a numerical result is, therefore, directly related to the availability and accuracy of the basic information required in computing the input parameters. Owing to the lack of accurate data on the potentiometric head and permeability of all of the major hydrogeologic units in the Palo Duro Basin, no single numerical simulation result presented in this report is intended to represent the actual regional flow patterns. Instead, each simulation result should be viewed as a possible representation of the actual flow system, and results from the so-called "best model" represent the most probable

CAUTION
This report [illegible] Bureau of Economic Geology that addresses the feasibility of the Palo Duro [illegible] the [illegible] conclusions reached. Interpretations and conclusions are based on available data and state-of-the-art concepts, and hence, may be modified by more information and further application of the involved sciences.

flow patterns. Numerical simulation is undertaken in an effort to better characterize the deep-basin ground-water flow system based on the available information and to evaluate changes in the flow patterns in response to any expected variations in the flow parameters and boundary conditions.

The Wolfcamp Aquifer

Regional ground-water flow patterns in the Wolfcamp aquifer are of concern because the Wolfcamp is the first permeable unit beneath the proposed repository level in the salt section. Major contributors to the transmissivity of the Wolfcamp aquifer are the carbonates and the granite wash. They would be the major pathways for any contaminant transport in the upper part of the deep-brine aquifer. The low permeability shale functions as an aquitard, underlying and interbedding with the carbonate aquifer.

Table 4 summarizes numerical simulations of the Wolfcamp aquifer. The specified head values along the eastern and western boundaries were set according to the Wolfcamp head map (fig. 29). The head value declines from 860 m (2,820 ft) in the south to 550 m (1,800 ft) in the north along the western boundary, and from 480 m (1,575 ft) to 380 m (1,250 ft) along the eastern boundary. The southern boundary along the Matador Arch is a no-flow boundary. The head map also indicates that the northern boundary along the uplift in Oldham and Potter Counties is a no-flow boundary, but this cannot be clearly seen along the eastern part of the boundary in Carson, Gray, Donley, and Collingsworth Counties, probably due to the lack of head data in these areas. Owing to the physical complexity imposed by the uplift and lack of head data along the northern boundary, two configurations of boundary conditions have been modeled (see figs. 34 and 35).

Simulation A-1

In Simulation A-1, the known values of permeability and porosity from Table 2 were used as input parameters for the numerical model (fig. 33) with the boundary conditions as shown in

figure 34. The resulting Wolfcamp transmissivity is fairly uniform throughout the basin (fig. 33). However, contours of computed head from the simulation results (fig. 34) are completely different in patterns from the contours of measured Wolfcamp head (fig. 29 and figure 4.18 in Stone & Webster, 1983) indicating that the specified model parameters do not satisfactorily represent the actual physical flow system. Therefore, the transmissivity values, the permeability of the evaporite aquitard, and the boundary conditions are modified in the subsequent simulations, based on geologic and hydrologic information, so that the simulated head surface is as much in agreement as possible with the measured head surface.

Simulation A-2

The model parameters for Simulation A-2 were the same as those of Simulation A-1 except that the boundary conditions along the uplift were modified (fig. 35). The contours of computed head (fig. 35) are still not in good agreement with those of measured head. It should be noted that a more restricted model was tried with specified values of head throughout the northern boundary along the uplift, but that model was also unable to satisfactorily simulate the measured Wolfcamp head surface.

Simulation A-3

Simulation A-3 investigated the effects of varying the transmissivity distribution of the aquifer. It is reasonable to expect that there are zones of high transmissivity in the northeastern part of the basin because the Wolfcamp head map indicates that there is regional ground-water flow toward that direction. High transmissivity zones may be related to the Wolfcamp granite wash that was primarily deposited in the northeastern part of the basin (fig. 12). The relatively thin granite-wash deposit with an expected high permeability may function as a high transmissivity zone (or sink) at the northeastern corner of the basin (fig. 36), pulling the ground water toward that direction. The granite-wash permeability was gradually increased to 260 md in Simulation A-3. Contours of computed head from Simulation A-3 (fig. 37) are similar to the contours of measured head except in the northwestern parts of the

basin where they indicate some flow toward the north and northwest directions. These unexpected flow directions may be caused by the specified no-flow condition along the northern boundary or by the high vertical leakage specified for the evaporite aquitard, which allows a large amount of leakage into the Wolfcamp aquifer, resulting in ground-water flow out of the basin through its western boundary.

Based on the results of Simulations A-1, A-2, and A-3, it can be concluded that zones of high transmissivity must exist in the northeastern parts of the basin for the model to reasonably simulate the measured Wolfcamp head map.

Simulations B and C

The effects of leakage on the simulation results were investigated in Simulation B by assuming a no-leakage condition (permeability of the evaporite aquitard equals zero). An improvement in the simulated head contours (fig. 38) indicates that the specified value of 0.00028 md for the vertical permeability of the evaporite aquitard in previous simulations was too high. The contours of computed head in figure 38 are generally in good agreement with the Wolfcamp head maps (fig. 29 and fig. 4.18, Stone & Webster, 1983), although they are smoother and more north-south. Increasing the permeability of the evaporite aquitard to 0.00008 md in Simulation C slightly improves the head distribution (fig. 39) such that it shows a more southwest to northeast flow direction than the results of Simulation B. The change of flow patterns from their original southwest-northeast direction to west-east direction along the northern boundary shows the effect of the no-flow condition imposed on that boundary. While a no-flow condition may be justified in the eastern part of the northern boundary where the uplift was almost completely exposed throughout Wolfcampian time, it may be an unrealistic restriction in the western part of the boundary where the brown dolomite over the uplift is up to 100 m (350 ft) thick (fig. 31). This unrealistic no-flow assumption may also be the reason for the east-to-west flow direction in the northwest part of the basin (fig. 40), an unacceptable condition according to the measured Wolfcamp head maps. The streamlines and travel times in

figure 40 were computed assuming a number of starting points along the western boundary. The spaces between streamlines do not constitute flow tubes as in a flow net and, therefore, there is not equal flow between streamlines. The travel-time interval between marks along streamlines is 400,000 years.

Simulation D-1

The numerical model was further refined in Simulation D-1 by imposing a specified head condition along the western part of the northern boundary, keeping all the other boundary conditions the same (fig. 41). This, in effect, allows a possibility of flow over the uplift. The resulting head distribution and streamlines (figs. 41 and 42) illustrate a significant improvement of the flow patterns in the northwestern part of the basin with the head contours being more similar to the measured head maps than the previous simulation results. The streamlines are essentially parallel to the uplift along the western part of the northern boundary in Oldham County but show some components of flow across the boundary (over the uplift) in Potter and Carson Counties where the overlying brown dolomite thickens to about 240 m (fig. 31). It should be noted that the northern boundary of the numerical model is on the downthrown (southern) side of the uplift. Therefore, the model does not recognize any physical configurations on the uplift, such as the existence of brown dolomite, although the existence of the uplift itself is recognized by the model in Carson, Gray, and Wheeler Counties through the assumption of the no-flow condition. The occurrence of larger flow components across the northern boundary through the zone of thick brown dolomite is considered to reflect a reasonable representation of the physical system by the model parameters and boundary conditions.

Simulation D-2

The model was refined in Simulation D-2 by using the averaged porosity distribution of the Wolfcamp (fig. 20), keeping all the other parameters the same as those of Simulation D-1. As such, only the travel times differ from the results of Simulation D-1 (fig. 43). Owing to the smaller average Wolfcamp porosity from figure 20 (0.064) compared to the porosity values used

in Simulation D-1, the travel times in figure 43 are less than those in figure 42. The time it takes for ground water to flush through the modeled section of the basin within the Wolfcamp aquifer is computed to be about 1.4 to 1.8 million years (fig. 43). Travel times across the entire Palo Duro Basin (biosphere to bio (115°F) was used to represent the fluid temperature unit beneath the salsphere) are larger.

Simulation E

Simulation E is another alternative for refining the numerical model using a qualitative isopach map of highly porous carbonate in the Wolfcamp aquifer (fig. 14). Porosity and permeability values of the highly porous carbonates were increased to 0.10 and 50 md from the average values of 0.08 and 8.9 md, respectively. The resulting transmissivity distribution (fig. 44) shows a significant increase in transmissivity along the shelf margins and a low transmissivity zone trending from south to northwest across the basin center. The boundary conditions in Simulation E are the same as those imposed in Simulations D-1 and D-2. As expected, the contours of computed head (fig. 45) indicate a high hydraulic gradient along the low-transmissivity zone, a phenomenon that can also be observed from the measured head map (fig. 29). The total travel time for ground-water to flow across the modeled section of the basin varies from 1.2 to 2.0 million years (fig. 46), which is the same range as the previous estimate from Simulation D-2. Total discharges through the western part of the northern boundary and the eastern boundary are about 280,000 and 400,000 m^3/year, respectively.

Leakage Across the Evaporite Aquitard

Using the results of Simulation E as the best representation of the flow system, the potential for leakage across the evaporite aquitard was computed at each point by taking the difference between the head in the unconfined Upper Aquifer (fig. 21) and the computed Wolfcamp head (fig. 45). The potential for leakage was then contoured (fig. 47). Contours of the leakage gradient (fig. 49), obtained by dividing each head difference by the corresponding thickness of the evaporite aquitard (fig. 48), indicate that the gradient for downward leakage is

high along the northern boundary of the basin and becomes smaller toward the south and southeast directions. The negative gradient in the southeastern part of Cottle County indicates the potential for upward flow from the Wolfcamp aquifer to the ground surface. Note that the results in figures 47 and 49 are based on the computed Wolfcamp head from Simulation E which assumed a permeability value of 0.00008 md for the evaporite aquitard. Local variations in the amount of leakage depend directly on the heterogeneity of the aquitard's permeability which needs to be further investigated on a local scale. The amount of leakage through the evaporite aquitard was estimated for each element (Table 5) based on the numerical results (fig. 49 and an average value of 0.00008 md for the aquitard's permeability) using a numerical-integration scheme. The total amount of leakage is estimated to be 359,000 m^3/year, about 52 percent of the total discharge from the Wolfcamp aquifer of the Palo Duro Basin.

The Deep-Basin Brine Aquifer

Because of the differences in the potentiometric surfaces and geologic conditions between the Wolfcamp and the deeper strata (Stone and Webster, 1983; Dutton and others, 1982), flow patterns in the deeper strata may be different from those of the Wolfcamp aquifer. The limited information available, however, does not allow a three-dimensional study of flow in the deep-brine aquifers with reasonable accuracy. A more appropriate approach is to treat the deep-brine aquifers as a single permeable unit with perfect cross-formational communication. All model parameters representing the aquifer properties, as well as the head value at a given point, are the vertically-averaged values throughout the deep basin. This approach is adequate for the study of averaged flow-patterns and averaged flow-velocities of the deep brines as well as the total amounts and rates of basin discharge, especially when there are only limited amounts of information available for the flow system.

The numerical model of the whole deep-brine aquifer is similar to the model of the Wolfcamp aquifer. In fact, some studied results of the Wolfcamp model can be directly useful for

deep-brine aquifer simulations, such as the most probable values of the leakage coefficient and the permeability of Wolfcamp granite-wash, and the proper types of boundary conditions.

Simulation A

Table 6 summarizes the deep-brine aquifer simulations. In Simulation A, the known values of permeability and porosity from Tables 2 and 3 were used, except that the permeability values of 260 md and 0.00008 md were specified for the Wolfcamp granite wash and evaporite aquitard, respectively, based on the best Wolfcamp model. The boundary conditions and head values were specified according to figures 51 and 27, respectively. The head value declines from 900 m (2,950 ft) in the south to 620 m (2,030 ft) in the north along the western boundary and from 480 m (1,575 ft) to 370 m (1,210 ft) along the eastern boundary. The model transmissivities for this simulation are as given in figure 50. The contours of computed head (fig. 51) and streamlines (fig. 52) indicate the expected southwest to northeast flow direction but with a slightly larger west-to-east flow component than the Wolfcampian flow, mainly due to the more west-to-east trend of heads specified along the western boundary (see figs. 27 and 29). Flow in the northwestern part of the study area is parallel to the uplift in Oldham and Potter Counties and discharges through the northern boundary in eastern Potter and Carson Counties (fig. 52). The coincidence of the discharge boundary with the zone of thick brown dolomite over the uplift indicates proper functioning of the model parameters.

Simulation B

Although the simulated head contours in figure 51 generally have similar patterns to those of the measured heads (fig. 27), the 450 m contour extends further to the east than expected. Increasing transmissivity values in the northeastern part of the study area will adjust the 450 m contour line further to the west. The permeability of the Pennsylvanian granite wash in certain areas close to the uplift (fig. 53) was, therefore, increased in Simulation B to 260 md to account for a possible granite-wash coarsening toward the source and/or high permeability in the fault zone that flanks the uplift. (In Simulation A, only the permeability of the Wolfcamp granite

wash was increased to 260 md.) This, in effect, creates a high transmissivity zone extending along the uplift (fig. 54) and the simulation results are slightly improved compared to the previous ones (figs. 55 and 56).

Simulation C

Finally, permeabilities of the more porous Wolfcamp and Pennsylvanian carbonates (figs. 14 and 9) were increased to 50 md in Simulation C. The resulting transmissivity contours are as given in figure 57 and the simulation results in figures 58 and 59 give an estimate of discharges of 60,000 and 1,020,000 m^3/year across the northern and the eastern boundaries, respectively. The approximate travel time across the basin is in the range of 1.2 to 2.2 million years, which is in the same range as that of the Wolfcamp aquifer.

HYDROGEOLOGIC IMPLICATIONS

Ground water in the Wolfcamp aquifer flows mainly from southwest to northeast across the basin and discharges through the eastern boundary and part of the northern boundary (in Potter and Carson Counties) where the Wolfcamp brown dolomite overlying the Amarillo Uplift is thick and acts as a conduit for fluid flow over the uplift. For the given boundary conditions, this flow direction can be maintained only when there is a high transmissivity zone in the northeastern part of the basin that functions as a sink and "pulls" the ground water toward the uplift. The expected high transmissivity zone can be related to the existence of the Wolfcamp granite wash that was deposited primarily along the flanks of the uplift. The results of numerical simulations indicate that a permeability value of 250 md or higher for the granite wash is needed to cause the observed flow direction (fig. 45). Although there are no data to justify the expected permeability value of the Wolfcamp granite wash, five pumping tests in Pennsylvanian granite wash at DOE's SWEC-J. Friemel No. 1 well indicate a permeability range of 10 to 400 md with an average of 140 md. Because of the similarity in depositional environments between the tested Pennsylvanian granite wash and the Wolfcampian granite wash

(both are close to their sources, Bravo Dome and Amarillo Uplift, respectively), a similar range of permeability values is expected. Bentley (1981) and Bassett and Bentley (1983) noted that the fluid pressures in the deep-basin aquifer were below hydrostatic. Because the thick granite-wash deposits cause a shift in direction of lateral ground-water flow, it is also expected that this hydrologic sink could cause the observed subhydrostatic pressures. This numerical model, however, cannot confirm this relationship, because the prescribed heads used for part of the boundary condition force the simulation to be subnydrostatic.

An alternate explanation as to why ground-water flow is toward the Amarillo Uplift may be the extensive hydrocarbon production from the Panhandle oil and gas field. Hydrocarbon production along the Matador Arch (southern boundary of the model) has caused an artificial depressuring in that area. The possibility of this occurring in the Amarillo Uplift region needs to be considered. Simulation E does show, however, that the high permeability zone of granite-wash sediment can cause the northeastern flow.

Toth (1978) suggested that elevated potentiometric surfaces beneath topographic highs can be translated through low permeability formations and affect potential distributions in deep-basin aquifers. In the Palo Duro Basin, the low-permeability evaporite aquitard separates the flow regime into two different flow systems: the topographically high, upper, unconfined aquifer and the Deep-Basin Brine Aquifer. The translation of topographic effects from the elevated potentiometric surface of the Ogallala through the evaporite aquitard to the Deep-Basin Brine Aquifer, however, appears to be small compared to the effects of permeability distributions of the aquifer system. Comparing the results of numerical Wolfcamp Simulations B, C, and E demonstrates the relative importance of topographic effects and permeability distributions. In Simulation B where there was no leakage, the head distribution (fig. 38) was governed by the transmissivity distribution of the Wolfcamp aquifer and the boundary conditions. In Simulation C where topographic control was allowed by assuming an average permeability value of 0.00008 md for the aquitard, the head distribution (fig. 39) remains essentially the same without showing any topographic effects. On the other hand, when the

permeability of the highly-porous Wolfcamp carbonates along the shelf margins was increased to 50 md in Simulation E, a bunching of contours (fig. 45) was observed, a phenomenon that can be also observed on the kriged head map (fig. 29). The flow direction follows more along the shelf carbonates in Simulation E (fig. 46), and the average travel time across the basin decreases from 2.2 (fig. 42) to 1.4 million years.

Based on the results of Simulation E as the best representation of the Wolfcampian flow system, the travel time across the model area of the basin ranges from 1.2 to 2.2 million years (fig. 46). The flow velocities in Wolfcamp carbonates computed in the present work are roughly one order of magnitude higher than those of INTERA's model (INTERA, 1982), mainly due to the differences in the permeability values used in each model. INTERA (1982) used an earlier compiled data set of permeability values which had lower statistical means. Using this study's computed travel times and assuming that the present flow system started in the late Cretaceous, about 30 to 55 pore volumes of the Wolfcamp aquifer have been flushed through the basin. The saline waters in the Wolfcamp and Deep-Basin Brine Aquifer are considered hydrodynamic and of meteoric origin. Because of this multiple flushing, these aquifers do not represent a stagnant system containing original conate waters.

In spite of the small average permeability value of the evaporite aquitard, leakage through the aquitard may be large because of the large contact areas between formations. The amount of leakage was estimated to be 359,000 m^3/year, about 50 percent of the total flow through the Wolfcamp aquifer. An approximate average linear velocity ($\bar{v} = 9/\theta$) for vertical flow through the salt section is 3.8×10^{-5} m/day. A particle of water would travel 139 m in 10,000 years or 1,390 m in one million years. These calculations are based on a vertical permeability of 0.00008 md, a hydraulic gradient as defined in figure 48, and an effective porosity of .001 (from Peterson and others, 1981).

The most sensitive parameter in the calculated values for the amount of leakage and the average linear velocity is the permeability. A change in permeability from 0.00008 md to 0.000008 md decreases leakage volume and travel times correspondingly by an order of

magnitude. The permeability value of 0.00008 md is considered conservative. In-situ permeability testing of salt at the WIPP Site (Carlsbad, New Mexico) indicates permeabilities of 0.018 to 0.021 md (Peterson and others, 1981). Laboratory permeability tests of salts from the DOE WIPP tests indicate permeabilities of approximately 0.001 md (C. Christiansen, personal communication). These results are one to two orders of magnitude higher than the value used in this study. The chosen permeability value of 0.00008 md also produces the best simulated potentiometric surface for the Wolfcamp aquifer.

Two additional factors affect calculated transit times through the evaporite aquitard. Calculations of hydraulic conductivity within the basin were based on brines with a TDS of 127,000 mg/L. Brines moving through the evaporite section would have TDS values over 300,000 mg/L. This increase in TDS would also change the viscosity and density of the fluid. To obtain the required leakage for Simulation E, the permeability of the evaporite section would have to increase. The flow velocity would probably remain about the same because the increased resistance to flow of the fluid would be balanced by the increased permeability of the evaporites needed to maintain the calculated leakage.

The second factor in calculating transit times in the evaporite section is whether Darcian assumptions for flow are valid at these low permeabilities and low flow velocities. Future research on water flow through the aquitard is critical. It is a significant parameter controlling flow patterns and chemical compositions of water in the deep-brine aquifer, as well as indicating that there may be fluid movement through the evaporite section.

Average ground-water flow in the Deep-Basin Brine Aquifer is similar to flow in the Wolfcamp aquifer but, with more west-to-east flow components. Results of numerical deep-basin Simulations B and C (figs. 55 and 58) indicate that the model is not as sensitive as the Wolfcamp model to the increases in permeability values of the Wolfcamp and Pennsylvanian high-porosity carbonates. This is probably due to the presence of thick, widespread, Pennsylvanian granite wash that helps smooth out the transmissivity contrast due to the shelf

This report describes research carried out by staff members of the Bureau of Economic Geology. The report describes the progress and current status of research and tentative conclusions reached. Interpretations and conclusions are based on available data and state-of-the-art concepts, and hence, may be modified by more information and further application of the involved sciences.

carbonates. The thick and widely-spread Pennsylvanian granite wash to the east (fig. 5) is also responsible for the higher west-to-east flow component of the whole deep-brine aquifer.

This modeling study has implications for the problem of radionuclide transport to the biosphere from a potential repository in the evaporite aquitard. There may be a natural component of ground-water flow through the evaporite aquitard. Release scenarios need to consider this natural flow component as well as potential flow through drilled and abandoned wells. The potential for flow through the evaporite aquitard appears to be downward rather than upward which is a favorable characteristic of this basin.

If radionuclides reach deep-basin aquifers such as the Wolfcamp, transport time to the biosphere will be long. Transit times across the modeled area of the basin range from 1.2 to 2.2 million years. Discharge zones to land surface or shallow ground waters cannot be determined from this study. The granite wash along the Amarillo Uplift should be considered as the discharge zone for calculating conservative transit times for two reasons. First, flow velocities in granite-wash facies along the Amarillo Uplift are significantly higher than in other facies within the basin and presumably, once water reached the granite wash, it could flow rapidly to a discharge point. Second, the hydrologic importance of the Amarillo Uplift is not known. Some ground water may flow across the uplift or it may all flow along its flanks in the granite wash. Until the detailed hydrology and geology of the uplift are understood, a conservative approach in determining transit time would assume the uplift as the point of discharge.

The simulated flow lines and flow velocities have been constructed and computed from a very limited data base. More detailed hydrologic and geologic information is needed to accurately characterize flow directions and flow velocities within the basin. The inclusion of permeable Wolfcamp shelf margins (Simulation E) significantly alters flow directions and velocities from previous simulations. The incorporation of this permeable zone into the model is based on geologic interpretation and not on actual hydrologic testing of the zone. Other

aquifer heterogeneities, such as faulting and fracturing of the evaporite aquitard and the deep-basin aquifers, may have similar but unidentified effects on deep-basin flow.

CONCLUSIONS

The hydrologic information in the Palo Duro Basin in terms of hydraulic properties of the aquifer-aquitard system and deep-brine pressures is limited, but when used in conjunction with a larger data base of geologic information, approximations of the aquifer-aquitard properties can be made.

A potentiometric head map of the Wolfcamp aquifer derived from the measured head data indicates a regional flow direction from southwest to northeast across the basin and from west to east along the Matador Arch. This flow pattern is best simulated by the numerical model using modified permeability values of 0.00008 md for the evaporite aquitard, 260 md for the granite wash, and 50 md for the high-porosity carbonate and a combination of specified head condition (in the western part) and no-flow condition (in the eastern part) along the Amarillo Uplift. It takes about 1.2 to 2.0 million years for ground water to flow across the modeled area of the basin. The amount of discharge through the western part of the northern boundary is probably 280,000 m^3/year, while discharge through the eastern boundary is probably 400,000 m^3/year.

The average head map for the Deep-Basin Brine Aquifer also indicates flow from southwest to northeast across the basin with a slightly larger west-to-east flow component. Numerical simulations of the deep-brine aquifer show that the simulated flow patterns are not critically sensitive to variations in the permeability distribution of Pennsylvanian carbonate and granite wash as long as the Wolfcamp aquifer's properties and the leakage coefficient are according to the best Wolfcamp model. The best deep-brine aquifer model was obtained with increased permeability values of 260 md for the Pennsylvanian granite-wash coarsening zone and 50 md for the Pennsylvanian high-porosity carbonate. The total travel time across the modeled part of the basin is about 1.2 to 2.2 million years, the same range as travel times

through the Wolfcamp aquifer. The amount of discharge through the northern boundary is 60,000 m^3/year, and discharge through the eastern boundary is 1,020,000 m^3/year.

Additional hydrogeologic information, especially from future exploratory drilling, is essential for improving and evaluating the numerical simulation results of this study. Information such as local variations of the aquifer and aquitard properties as well as more accurate head data are necessary for local characterization of the ground-water flow system in the Palo Duro Basin.

CAUTION

This report describes research carried out by staff members of the Bureau of Economic Geology that addresses the feasibility of the Palo Duro Basin for isolation of high-level nuclear wastes. The report describes the progress and current status of research and tentative conclusions reached. Interpretations and conclusions are based on available data and state-of-the-art concepts, and hence, may be modified by more information and further application of the involved sciences.

REFERENCES

Bassett, R. L., and Bentley, M. E., 1983, Deep brine aquifers in the Palo Duro Basin: regional flow and geochemical constraints: The University of Texas at Austin, Bureau of Economic Geology Report of Investigations No. 130, 59 p.

Bassett, R. L., Bentley, M. E., and Simpkins, W. W., 1981, Regional ground-water flow in the Panhandle of Texas: a conceptual model, in Gustavson, T. C., and others, Geology and geohydrology of the Palo Duro Basin, Texas Panhandle, a report on the progress of nuclear waste isolation feasibility studies (1980): The University of Texas at Austin, Bureau of Economic Geology Geological Circular 81-3, p. 102-107.

Bassett, R. L., and Duncan, E. A., 1982, Regional salinity and chemical composition of waters in deep aquifers in the Palo Duro Basin, in Gustavson, T. C., and others, Geology and geohydrology of the Palo Duro Basin, Texas Panhandle, a report on the progress of nuclear waste isolation feasibility studies (1981): The University of Texas at Austin, Bureau of Economic Geology Geological Circular 82-7, p. 138-145.

Bennion, D. W., and Griffiths, J. C., 1966, A stochastic model for predicting variations in reservoir rock properties: Transactions AIME, v. 237, part 2, p. 9-16.

Bentley, M. E., 1981, Regional hydraulics of brine aquifers, Palo Duro and Dalhart Basins, Texas, in Gustavson, T. C., and others, Geology and geohydrology of the Palo Duro Basin, Texas Panhandle, a report on the progress of nuclear waste isolation feasibility studies (1980): The University of Texas at Austin, Bureau of Economic Geology Geological Circular 81-3, p. 102-107.

Charbeneau, R. J., and Street, R. L., 1978, Finite element modeling of groundwater injection-extraction systems: Technical Report No. 231, Department of Civil Engineering, Stanford University, 118 p.

Clark, I., 1979, Practical Geostatistics: London, Applied Science Publishers, Ltd., 129 p.

David, M., 1977, Geostatistical Ore Reserve Estimation: New York, Elsevier, 340 p.

Davis, S. N., 1980, Hydrogeologic effects of natural disruptive events on nuclear waste repositories: Research Report No. PNL-2858, Pacific Northwest Laboratory, 33 p.

Davis, S. N., and DeWiest, R. J., 1966, Hydrogeology: New York, John Wiley & Sons, 463 p.

Dutton, A. R., in press, Regional ground-water flow systems of San Andres Formation, in Gustavson, T. C., and others, Geology and geohydrology of the Palo Duro Basin, Texas Panhandle, A report on the progress of nuclear waste isolation feasibility studies (1982): The University of Texas at Austin, Bureau of Economic Geology Geological Circular.

Dutton, S. P., Goldstein, A. G., and Ruppel, S. C., 1982, Petroleum potential of the Palo Duro Basin, Texas Panhandle: The University of Texas at Austin, Bureau of Economic Geology Report of Investigations No. 123, 87 p.

Freeze, R. A., and Cherry, J. A., 1979, Groundwater: Englewood Cliffs, Prentice-Hall, Inc., 604 p.

Gustavson, T. C., Bassett, R. L., Finley, R. J., and others, 1981, Geology and geohydrology of the Palo Duro Basin, Texas Panhandle, a report on the progress of nuclear waste isolation

feasibility studies (1980): The University of Texas at Austin, Bureau of Economic Geology Geological Circular 81-3, 173 p.

Handford, C. R., 1980, Lithofacies and depositional environments of evaporite-bearing strata based on Randall and Swisher County cores, in Gustavson, T. C., and others, Geology and geohydrology of the Palo Duro Basin, Texas Panhandle, a report on the progress of nuclear waste isolation feasibility studies (1979): The University of Texas at Austin, Bureau of Economic Geology Geological Circular 80-7, p. 5-7.

Handford, C. R., 1980, Lower Permian facies of the Palo Duro Basin, Texas: depositional systems, shelf-margin evolution, paleogeography, and petroleum potential: The University of Texas at Austin, Bureau of Economic Geology Report of Investigations No. 102, 31 p.

Handford, C. R., and Dutton, S. P., 1980, Pennsylvanian-Lower Permian depositional systems and shelf-margin evolution, Palo Duro Basin, Texas: American Association of Petroleum Geologists Bulletin, v. 64, no. 1, p. 88-106.

INTERA, 1982, Status report on regional ground-water flow modeling for the Palo Duro Basin, Texas: ONWI/E512-02900/TR-13, Intera Environmental Consultants, Inc., Houston, Texas, 170 p., Draft.

Knudsen, H. P., and Kim, Y. C., 1978, A short course on geostatistical ore reserve estimate: Department of Mining and Geological Engineering, University of Arizona, 224 p.

Law, J., 1944, A statistical approach to the interstitial heterogeneity of sand reservoirs: Transactions AIME, v. 155, p. 202-222.

Matherton, G., 1963, Principles of geostatistics: Economic Geology, v. 58, p. 1246-1266.

Matthews, C. S., and Russell, D. G., 1967, Pressure buildup and flow test in wells: Society of Petroleum Engineers, Henry L. Doherty Series, v. 1, 167 p.

McGowen, J. H., 1981, Depositional sequences and associated sedimentary diagenetic facies: an ongoing investigation of salt-bearing core, Swisher County, Texas, in Gustavson, T. C., and others, Geology and geohydrology of the Palo Duro Basin, Texas Panhandle, a report on the progress of nuclear waste isolation feasibility studies (1980): The University of Texas at Austin, Bureau of Economic Geology Geological Circular 81-3, p. 90-92.

McGowen, J. H., Granata, G. E., and Seni, S. J., 1979, Depositional framework of the lower Dockum Group (Triassic), Texas Panhandle: The University of Texas at Austin, Bureau of Economic Geology Report of Investigations No. 97, 60 p.

Neuman, S. P., 1982, Statistical characterization of aquifer heterogeneities: Geological Society of America Special Paper 189, p. 81-102.

Peterson, E. W., Lagus, P. L., and Broce, R. D., 1981, In situ permeability of rock salt: Report No. SAND81-7073, prepared for Sandia National Laboratories, Albuquerque, New Mexico, 65 p.

Pippin, L., 1968, Panhandle-Hugoton Field, Texas-Oklahoma-Kansas--the first fifty years: Geology of Giant Petroleum Fields: American Association of Petroleum Geologists, Memoir No. 14, p. 204-222.

Royle, A. G., Brooker, P. I., Clark, I., Grant, D. C., Journel, A. G., Mousset-Jones, P., Parker, H., Rendu, J. M., and Sandefur, R. I., 1980, Geostatistics: New York, McGraw-Hill, Inc., 168 p.

Schlumberger, 1979, Log interpretation charts: Schlumberger Well Surveying Corporation, 97 p.

Seni, S. J., 1980, Sand-body geometry and depositional systems, Ogallala Formation, Texas: The University of Texas at Austin, Bureau of Economic Geology Report of Investigations No. 105, 36 p.

Smith, D. A., 1983, Permeability of the deep-basin aquifer system, Palo Duro Basin, in Gustavson, T. C., and others, Geology and geohydrology of the Palo Duro Basin, Texas Panhandle, a report on the progress of nuclear waste isolation feasibility studies (1982): The University of Texas at Austin, Bureau of Economic Geology Geological Circular (in press).

Stone and Webster Engineering Corporation, 1983, Hydrogeologic investigations based on drill-stem test data, Palo Duro Basin area, Texas and New Mexico: Topical Report, August, 1983.

Texas Department of Water Resources, 1982, Evaluating the ground-water resources of the high plains of Texas: Report No. LP-173, v. 1.

Texas Water Development Board, 1972, A survey of the subsurface saline water of Texas: Report 157, v. 1, 113 p.

Toth, J., 1978, Gravity induced cross-formational flow of formation fluids, Red Earth Region, Alberta, Canada: analysis, patterns and evolution: Water Resources Research, v. 14, p. 805-843.

Wirojanagud, P., 1983, User's guide for TRAVEL: The University of Texas at Austin, Bureau of Economic Geology, QA Document, 50 p.

FIGURE CAPTIONS

Figure 1. Structural features of the Texas Panhandle and adjacent areas (modified from Handford, 1980).

Figure 2. Structure contour map on top of the crystalline basement, Texas Panhandle (from Dutton and others, 1982).

Figure 3. Structure contour map of the top of Mississippian System, Palo Duro Basin (from Dutton and others, 1982).

Figure 4. Isopach map of Pennsylvanian System, Texas Panhandle. Sediment thins onto uplifts that were exposed during Pennsylvanian Period (Dutton and others, 1982).

Figure 5. Isolith map of Pennsylvanian and Wolfcampian granite wash in the Texas Panhandle (Dutton and others, 1982).

Figure 6. Net-sandstone map of upper part of the Pennsylvanian System, including both granite wash and nonarkosic sandstone (Dutton and others, 1982).

Figure 7. Net-carbonate map of lower part of Pennsylvanian System (Dutton and others, 1982).

Figure 8. Net-carbonate map of upper part of Pennsylvanian System. Position of older shelf margin is shown by dark hachured lines, and younger (retreated) position is shown by lighter hachures (Dutton and others, 1982).

Figure 9. Isopach map of porous carbonate strata in upper part of the Pennsylvanian System. Map is made on the basis of qualitative sample log descriptions, so actual porosity values are unknown (Dutton and others, 1982).

Figure 10. East-west cross section A-A'. Datum is the top of Wolfcampian Series; depths are in feet. See figure 1 for location (Dutton and others, 1982).

Figure 11. Isopach map of Wolfcampian Series, Palo Duro Basin (Handford, unpublished data).

Figure 12. Sandstone isolith map of Lower Permian strata, Palo Duro Basin (Handford, 1980).

Figure 13. Percent-carbonate map of Lower Permian strata in the Palo Duro Basin (Handford, 1980).

Figure 14. Isopach map of porous carbonate strata in Wolfcampian Series. Map is made on the basis of qualitative sample by descriptions, so actual porosity values are unknown (Handford and Dutton, 1980).

Figure 15. Structure contour map of top of Wolfcampian Series, Texas Panhandle. See figure 14 for county locations.

Figure 16. Structure contour map on top of Alibates, Texas Panhandle. (D. Johns, personal communication, 1983.) See figure 14 for county locations.

Figure 17. Simplified topographic map of the Palo Duro Basin region.

Figure 18. Swisher County core test well DOE-Gruy Federal, Grabbe No. 1: percent lithologic type per stratigraphic unit (McGowen, 1981).

Figure 19. Regional east-west section illustrating conceptual flow patterns based on hydraulic conditions and relative average permeabilities of major hydrogeologic units (Bassett and Bentley, 1983).

Figure 20. Weighted-average porosity of the Wolfcamp strata estimated from neutron-density log data (R. Conti, personal communication, 1983).

Figure 21. Head map (1979-1980) of the unconfined upper aquifer that overlies the Evaporite Aquitard in the Palo Duro Basin (Bassett and others, 1981).

Figure 22. Average head map of the whole deep-brine aquifer constructed from class H data.

Figure 23. Location of wells for class A head data of the whole deep-brine aquifer. See figure 22 for county locations.

Figure 24. Average head map of the whole deep-brine aquifer constructed from class A data. See figure 22 for county locations.

Figure 25. Locations of selected class A and class H head data. See figure 22 for county locations.

Figure 26. Representative variogram of the 118 selected class A and 42 class H average head data for the whole deep-brine aquifer.

Figure 27. Potentiometric head map of the whole deep-brine aquifer of the Palo Duro Basin, constructed from kriged estimates of head for regular blocks of 20,000 m^2. See figure 22 for county locations.

Figure 28. Standard error of estimate of the kriged deep-brine head in figure 27. See figure 22 for county locations.

Figure 29. Potentiometric head map of the Wolfcamp aquifer of the Palo Duro Basin, constructed from kriged estimates of head for regular blocks of 20,000 m^2 (Smith, 1983). See figure 22 for county locations.

Figure 30. Standard error of estimate of the kriged Wolfcamp-head shown in figure 29. See figure 22 for county locations.

Figure 31. Isopach map of the Wolfcamp brown dolomite, based on sample log information (M. Herron, personal communication, 1983). Location of Amarillo Uplift from figure 5.

Figure 32. Discretized flow region of the Palo Duro Basin. See figure 22 for county locations.

Figure 33. Contours of transmissivity for Wolfcamp aquifer Simulations A-1 and A-2. See figure 22 for county locations.

Figure 34. Contours of computed head, Wolfcamp aquifer Simulation A-1. See figure 22 for county locations.

Figure 35. Contours of computed head, Wolfcamp aquifer Simulation A-2. See figure 22 for county locations.

Figure 36. Contours of transmissivity for Wolfcamp aquifer Simulations A-3, B, C, D-1, D-2. See figure 22 for county locations.

Figure 37. Contours of computed head, Wolfcamp aquifer Simulation A-3. See figure 22 for county locations.

Figure 38. Contours of computed head, Wolfcamp aquifer Simulation B. See figure 22 for county locations.

Figure 39. Contours of computed head, Wolfcamp aquifer Simulation C. See figure 22 for county locations.

Figure 40. Streamlines and travel times, Wolfcamp aquifer Simulation C. See figure 22 for county locations.

Figure 41. Contours of computed head, Wolfcamp aquifer Simulation D-1. See figure 22 for county locations.

Figure 42. Streamlines and travel times, Wolfcamp aquifer Simulation D-1. See figure 22 for county locations.

Figure 43. Streamlines and travel times, Wolfcamp aquifer Simulation D-2. See figure 22 for county locations.

Figure 44. Contours of transmissivity for Wolfcamp aquifer Simulation E. See figure 22 for county locations.

Figure 45. Contours of computed head, Wolfcamp aquifer Simulation E. See figure 22 for county locations.

Figure 46. Streamlines and travel times, Wolfcamp aquifer Simulation E. See figure 22 for county locations.

Figure 47. Contours of head difference between the Upper Ogallala-Dockum Aquifer and the Wolfcampian aquifer, computed from figure 21 and the computed head of Simulation E. See figure 22 for county locations.

Figure 48. Contours of the evaporite strata's thickness. See figure 22 for county locations.

Figure 49. Contours of leakage gradient through the evaporite strata. The leakage gradient is obtained from dividing the head difference (fig. 47) by the evaporite's thickness (fig. 48). See figure 22 for county locations.

Figure 50. Contours of transmissivity for the Deep-Basin Brine Aquifer Simulation A. See figure 22 for county locations.

Figure 51. Contours of computed head, Deep-Basin Brine Aquifer Simulation A. See figure 22 for county locations.

Figure 52. Streamlines and travel times, Deep-Basin Brine Aquifer Simulation A. See figure 22 for county locations.

Figure 53. Deep-Basin Brine Aquifer Simulations B and C; zone of granite-wash coarsening in Pennsylvanian strata is assumed as indicated by the shaded area. See figure 22 for county locations.

Figure 54. Contours of transmissivity for the Deep-Basin Brine Aquifer Simulation B. See figure 22 for county locations.

Figure 55. Contours of computed head, Deep-Basin Brine Aquifer Simulation B. See figure 22 for county locations.

Figure 56. Streamlines and travel times, Deep-Basin Brine Aquifer Simulation B. See figure 22 for county locations.

Figure 57. Contours of transmissivity for the Deep-Basin Brine Aquifer Simulation C. See figure 22 for county locations.

Figure 58. Contours of computed head, Deep-Basin Brine Aquifer Simulation C. See figure 22 for county locations.

Figure 59. Streamlines and travel times, Deep-Basin Brine Aquifer Simulation C. See figure 22 for county locations.

LIST OF TABLES

Table 1. Generalized stratigraphic column of the Palo Duro Basin (modified from Bassett and Bentley, 1982).

Table 2. Permeability of hydrogeologic units of the Palo Duro Basin.

Table 3. Porosity of hydrogeologic units of the Palo Duro Basin.

Table 4. Summary of numerical simulations of the Wolfcamp aquifer.

Table 5. Amount of leakage through the evaporite aquitard computed from the results of Simulation E.

Table 6. Summary of numerical simulations of the Deep-Basin Brine Aquifer.

Table 1. Generalized stratigraphic column of the Palo Duro Basin (modified from Table 1 of Bassett and Bentley, 1982).

System	Series	Group	General lithology and depositional setting	Hydrogeologic element	Hydrogeologic unit
Quaternary			Fluvial and lacustrine clastics	Ogallala aquifer	Shallow aquifer
Tertiary					
Cretaceous			Nearshore marine clastics		
Triassic		Dockum	Fluvial deltaic and lacustrine clastics and limestones	Dockum aquifer	
Permian	Ochoa		Salt, anhydrite, red beds and peritidal dolomite	Evaporite aquitard	Evaporite aquitard
	Guadalupe	Artesia			
		Pease River			
	Leonard	Clear Fork			
		Wichita			
	Wolfcamp		Shelf and platform carbonates, basin shale and deltaic sandstones	Wolfcamp carbonate aquifer	Deep-basin brine aquifer
Pennsylvanian				Pennsylvanian carbonate aquifer	
			Basin shale aquitard	Upper Paleozoic granite wash aquifer	
Mississippian			Shelf limestone and chert	Lower Paleozoic carbonate aquifer	Basin shale aquitard
Ordovician		Ellenburger	Shelf dolomite		
Cambrian			Shallow marine (?) sandstone	Lower Paleozoic sandstone aquifer	
Precambrian			Igneous and metamorphic	Basement aquiclude	Basement aquiclude

Table 2. Permeability of hydrogeologic units of the Palo Duro Basin.

Hydrogeologic unit		y = ln(k)		Geometric mean of k ($e^{\bar{y}}$), md	Number and source of data	Typical value md
		Average value, $\bar{y}$	Variance, s^2			
Evaporite strata		—	—	—	—	.00028 (vertical permeability)
Deep brine aquifer	Wolfcampian carbonate	2.19	5.08	8.90	25 - DST data 70 - TWDB core data 6 - Sawyer #1 pumping test data	.07—$\frac{16}{300}$ *
	Pennsylvanian carbonate	2.88	5.61	17.90	25 - DST data 118 - TWDB core data	
	shale	—	—	—	—	.00001—.0001 *
	granite wash	1.27 (2.15 without Mobeetie data)	7.13	3.55 (8.60 without Mobeetie data)	10-DST data 10-Sawyer #1 pumping test 415-Mobeetie field core data 11- TWDB core data	.01—380 *
	Pre-Pennsylvanian rock	1.56	5.70	4.76	11- DST data 14- Sawyer #1 pumping test data	—

199
415

* from Davis and DeWiest (1966), Davis (1980), Freeze (1979)

Note (1). 1 md = 0.00115 m/day for saline water having salt concentration of 127,000 mg/ℓ at 115°F

(2) DST = drill-stem test, TWDB = Texas Water Development Board

15

Hydrogeologic unit		Porosity from neutron-density log analysis			Typical value**
		Mean	Standard deviation	Number of data	
Evaporite strata		—	—	—	less than .01
Deep brine aquifer	Wolfcampian carbonate	.08 (.064)*	.055	53 data points of 50 ft interval at Sawyer #1 and Mansfield #1 wells	.063 — .12
	Pennsylvanian carbonate	.08	.055		
	Shale	—	—	—	.05 — .15 — .25
	Granite wash	.23	.12	18 data points of 50 ft interval	.11 — .14 — .27
	Pre-Pennsylvanian rock	—	—	—	—

* Average value for Wolfcampian strata from R. Conti (personal communication, 1983).

** From Davis and Dewiest (1966), Davis (1980).

Table 4 Summary of numerical simulations of Wolfcamp aquifer.

Simulation	Permeability and porosity values	Boundary conditions
A-1	Best estimated values (from Table 2): $k_{carb.}$ = 8.9 md, $\phi_{carb.}$ = .08, k_{GW} = 8.6 md, ϕ_{GW} = .14, $k_{sh.}$ = .0001 md, $\phi_{sh.}$ = .05, k_{salt} = .00028 md.	Figures 30 and 35
A-2	The same as A-1	Figures 30 and 36
A-3	Best estimated values except, k_{GW} = 260 md (typical value for friable sandstones)	Figures 30 and 38
B	Best estimated values except, k_{GW} = 260 md k_{salt} = 0 (no leakage).	Figures 30 and 39
C	Best estimated values except, k_{GW} = 260 md k_{salt} = .00008 md.	Figures 30 and 40
D-1	The same as C	Figures 30 and 42
D-2	The same as D-1 with average porosity distribution of the Wolfcampian strata from Figure 31.	Figures 30 and 44
E	The same as D-1 with permeability and porosity of 50 md and 0.10, respectively for the highly porous carbonate zone (fig. 8).	Figures 30 and 46

Table 5. Amount of leakage through the evaporite aquitard computed from the results of Simulation E.

ELEMENT NO.	AMOUNT OF LEAKAGE, CU.M/YEAR	ELEMENT NO.	AMOUNT OF LEAKAGE, CU.M/YEAR
1	6169.9	61	3780.6
2	6584.4	62	3726.9
3	6197.8	63	3590.7
4	6186.6	64	2462.7
5	6192.9	65	1807.2
6	5467.2	66	1758.0
7	4792.2	67	2455.3
8	3916.9	68	2428.0
9	3110.9	69	2755.1
10	2231.0	70	2568.8
11	6230.3	71	3352.4
12	6336.7	72	3286.1
13	5859.2	73	2943.3
14	5707.4	74	2189.1
15	5021.5	75	1295.4
16	4715.6	76	966.0
17	4384.1	77	1515.0
18	3743.9	78	1605.4
19	2950.1	79	1802.7
20	2109.1	80	1945.2
21	6890.9	81	3147.4
22	6638.3	82	2705.0
23	5727.0	83	2872.8
24	5391.4	84	2333.0
25	4343.1	85	1255.3
26	4245.0	86	808.4
27	4148.9	87	993.5
28	3374.1	88	898.6
29	2592.5	89	1120.4
30	2010.6	90	1448.3
31	6687.8	91	2978.7
32	6127.1	92	2590.9
33	5411.9	93	2385.8
34	5580.9	94	2084.6
35	3904.6	95	1216.7
36	3740.1	96	692.6
37	3790.8	97	764.8
38	3069.4	98	553.6
39	2676.3	99	685.9
40	2381.8	100	1019.9
41	5144.3	101	2262.5
42	4661.5	102	2101.4
43	4693.4	103	2026.8
44	4873.5	104	1575.7
45	3777.4	105	1010.6
46	3123.8	106	526.3
47	3289.8	107	582.1
48	2905.4	108	298.8
49	2689.9	109	382.4
50	2635.4	110	504.3
51	4707.7	111	1902.7
52	4437.3	112	1619.6
53	4107.1	113	1517.7
54	3267.7	114	1062.5
55	3441.0	115	598.3
56	2876.7	116	343.4
57	3237.1	117	434.4
58	2961.5	118	156.4
59	2931.5	119	175.9
60	2624.6	120	21.4

Total amount of leakage = 359,000 cu.m/year

Table 6. Summary of numerical simulations of the whole deep-brine aquifer

Simulation	Permeability and porosity values	Boundary conditions
A	Wolfcampian aquifer: $k_{carb.}$ = 8.9 md, $\phi_{carb.}$ = .08, k_{GW} = 260 md, ϕ_{GW} = .14, k_{sh} = .0001 md, ϕ_{sh} = .05. Pennsylvanian aquifer: $k_{carb.}$ = 17.9 md, $\phi_{carb.}$ = .08, k_{sh} = .0001 md, ϕ_{sh} = .05, k_{GW} = 8.6 md (no fault zone), ϕ_{GW} = .11. Pre-Pennsylvanian rock: k = 4.8 md, ϕ = .08 Salt section: k_{salt} = .00008 md.	Figures 28 and 52
B	The same as A with permeability in the coarsening zone of Pennsylvanian granite-wash of 260 md.	Figures 28 and 56
C	The same as B with permeability and porosity of 50 md and .10, respectively, for the highly porous carbonate zones (figs. 10 and 15).	Figures 28 and 59

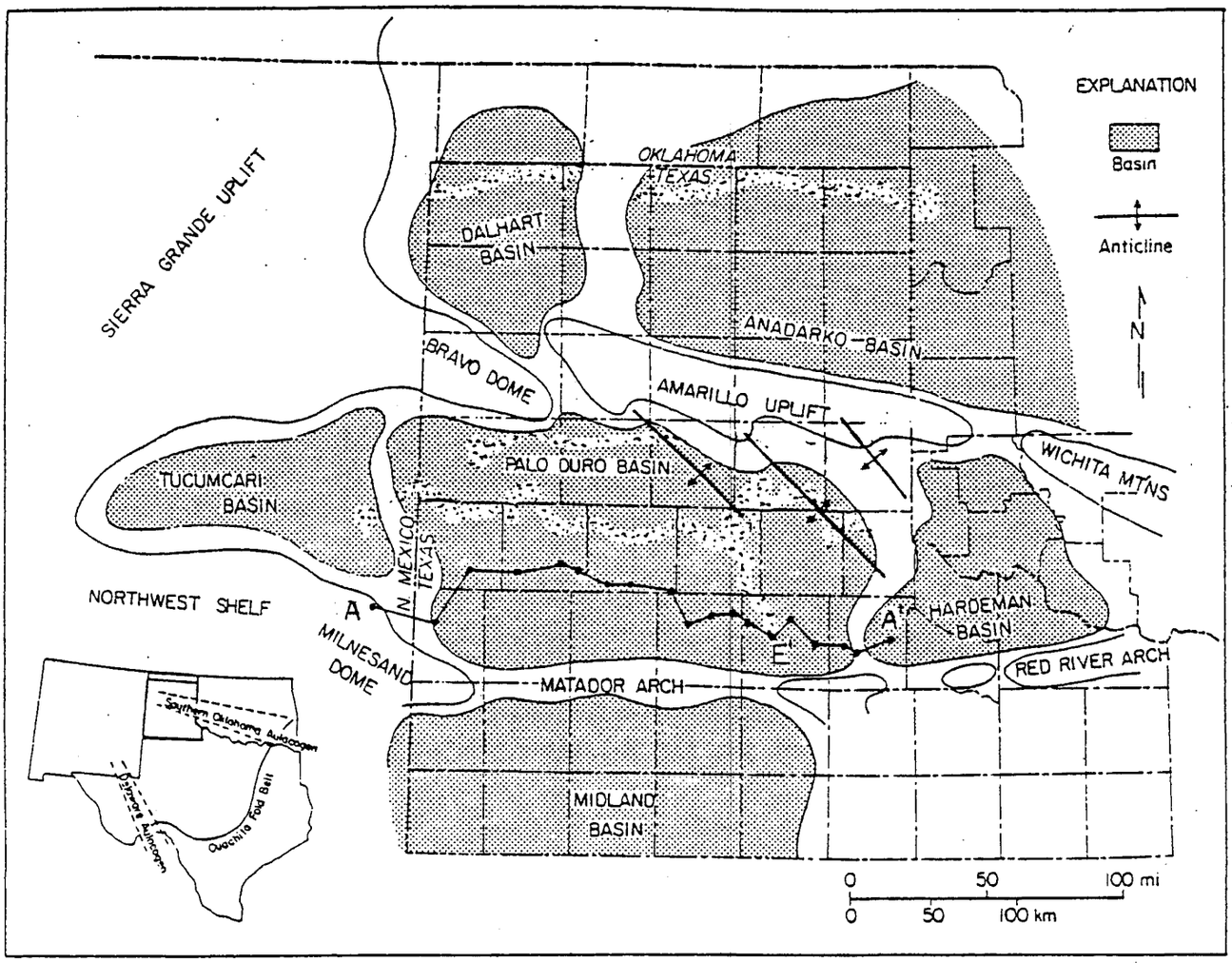

Figure 1. Structural features of Texas Panhandle and adjacent areas (modified from Handford, 1980).

THE UNIVERSITY OF TEXAS AT AUSTIN
BUREAU OF ECONOMIC GEOLOGY
W.L. FISHER, DIRECTOR

REPORT OF INVESTIGATIONS NO. 123
PLATE V

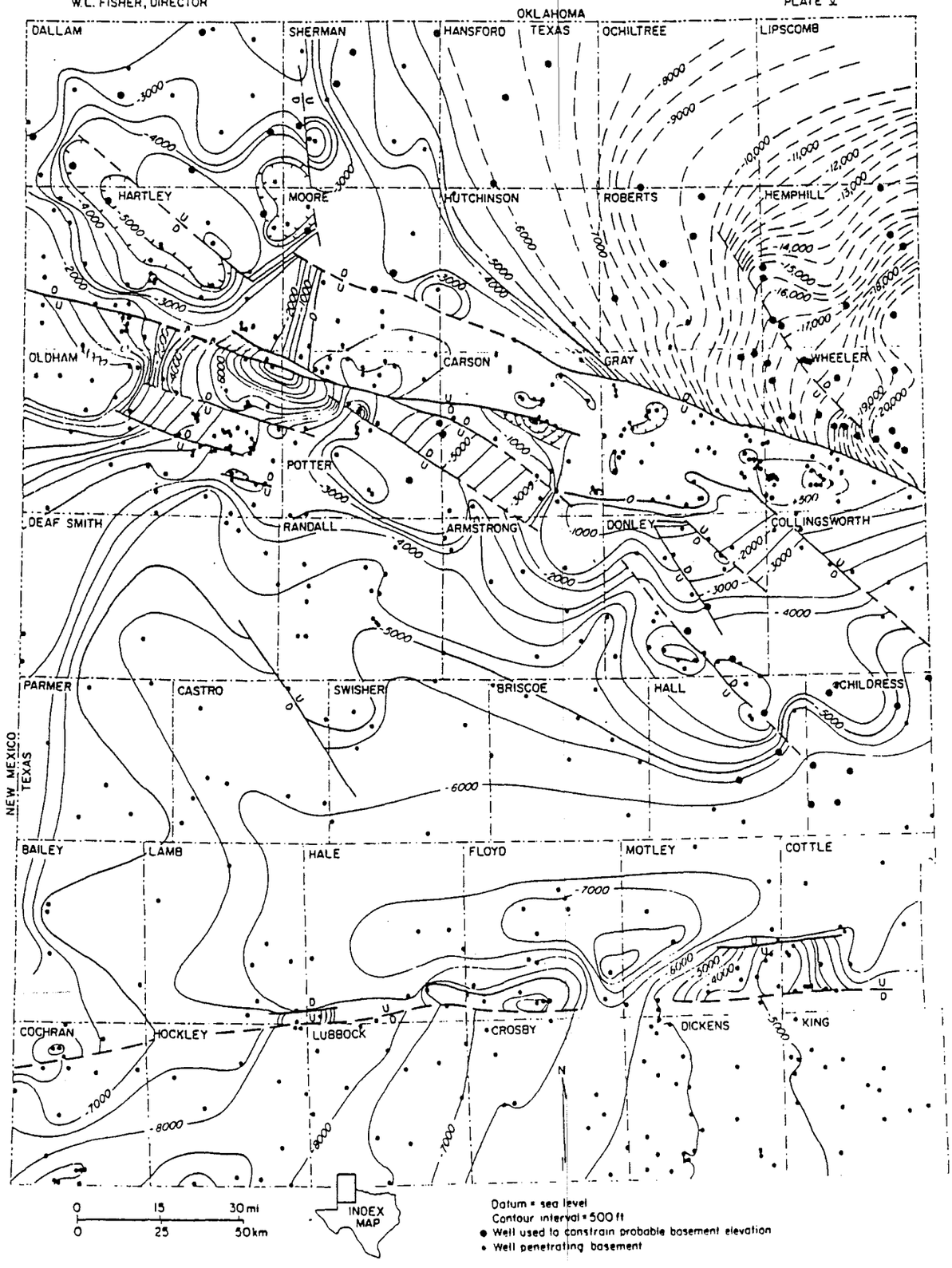

Figure 2. Structure contour map on top of crystalline basement in Texas (from Dutton and others, 1982).

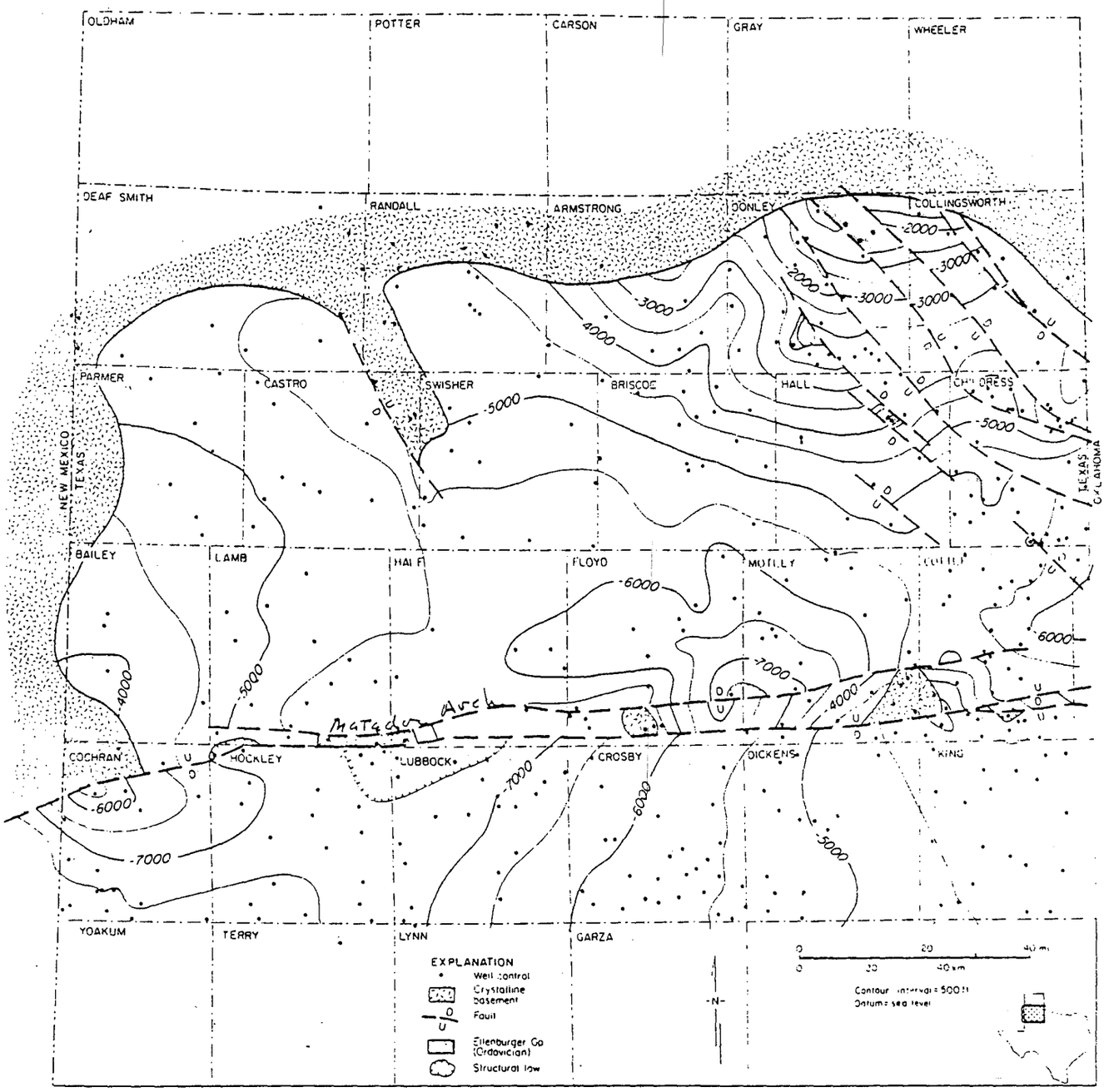

Figure 5. Structure contour map of top of Mississippian System, Palo Duro Basin (from Dutton and others, 1982).

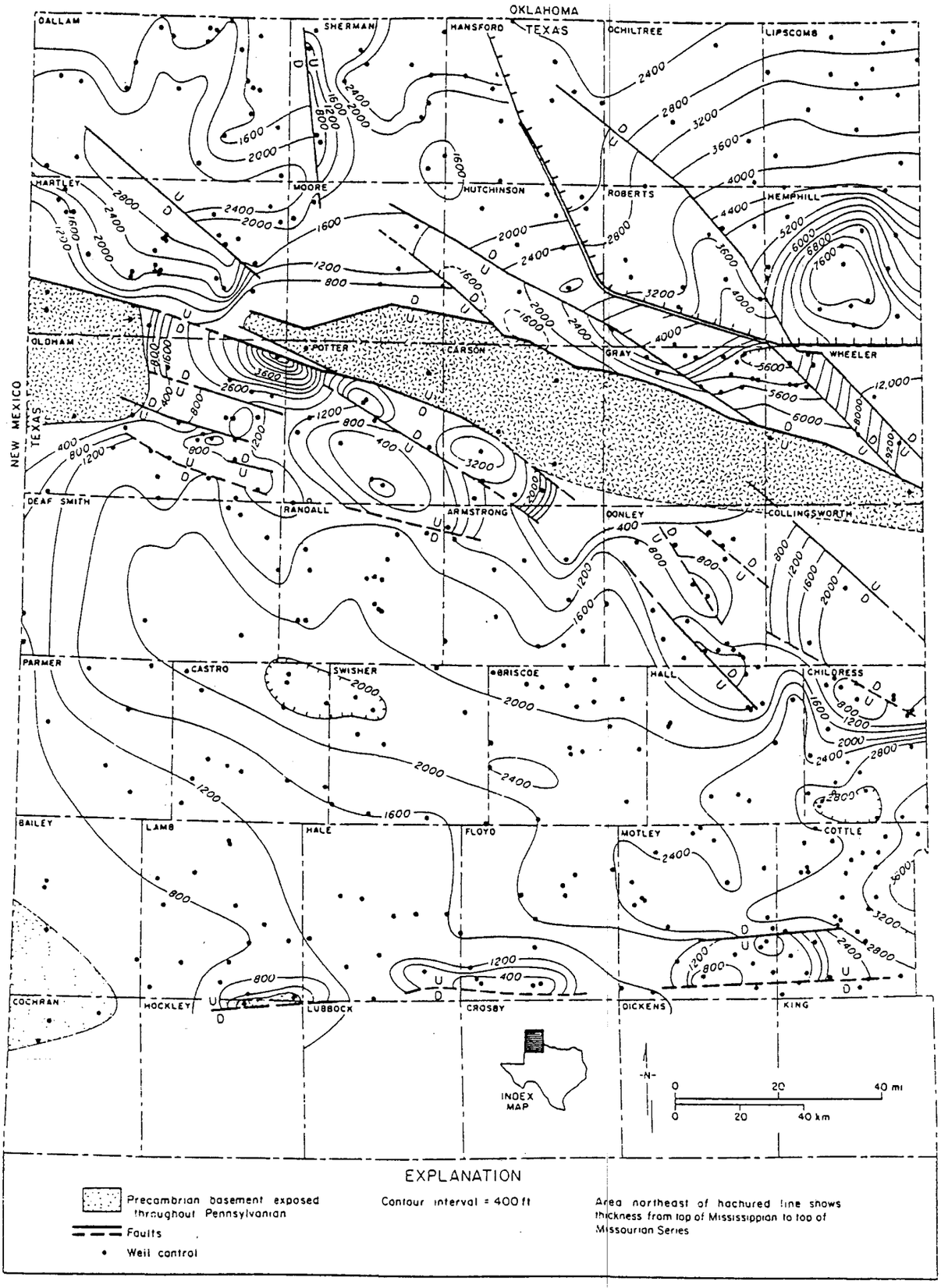

Figure 4. Isopach map of Pennsylvanian System, Texas Panhandle. Sediments thin onto uplifts that were exposed during Pennsylvanian Period(from Dutton and [illegible]

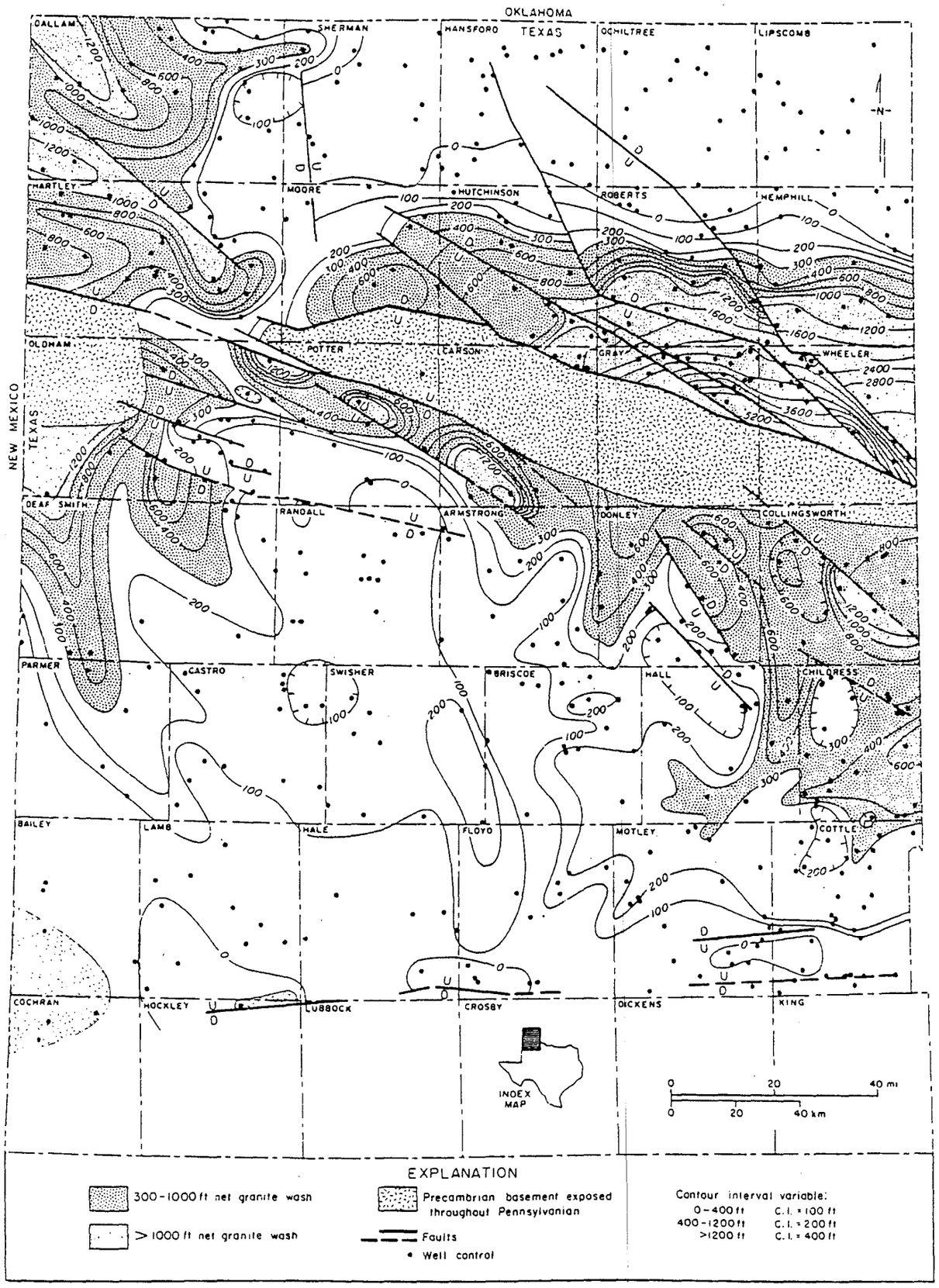

Figure 5 **Isolith map of Pennsylvanian and Wolfcampian granite wash in the Texas Panhandle** (from Dutton and others, 1982).

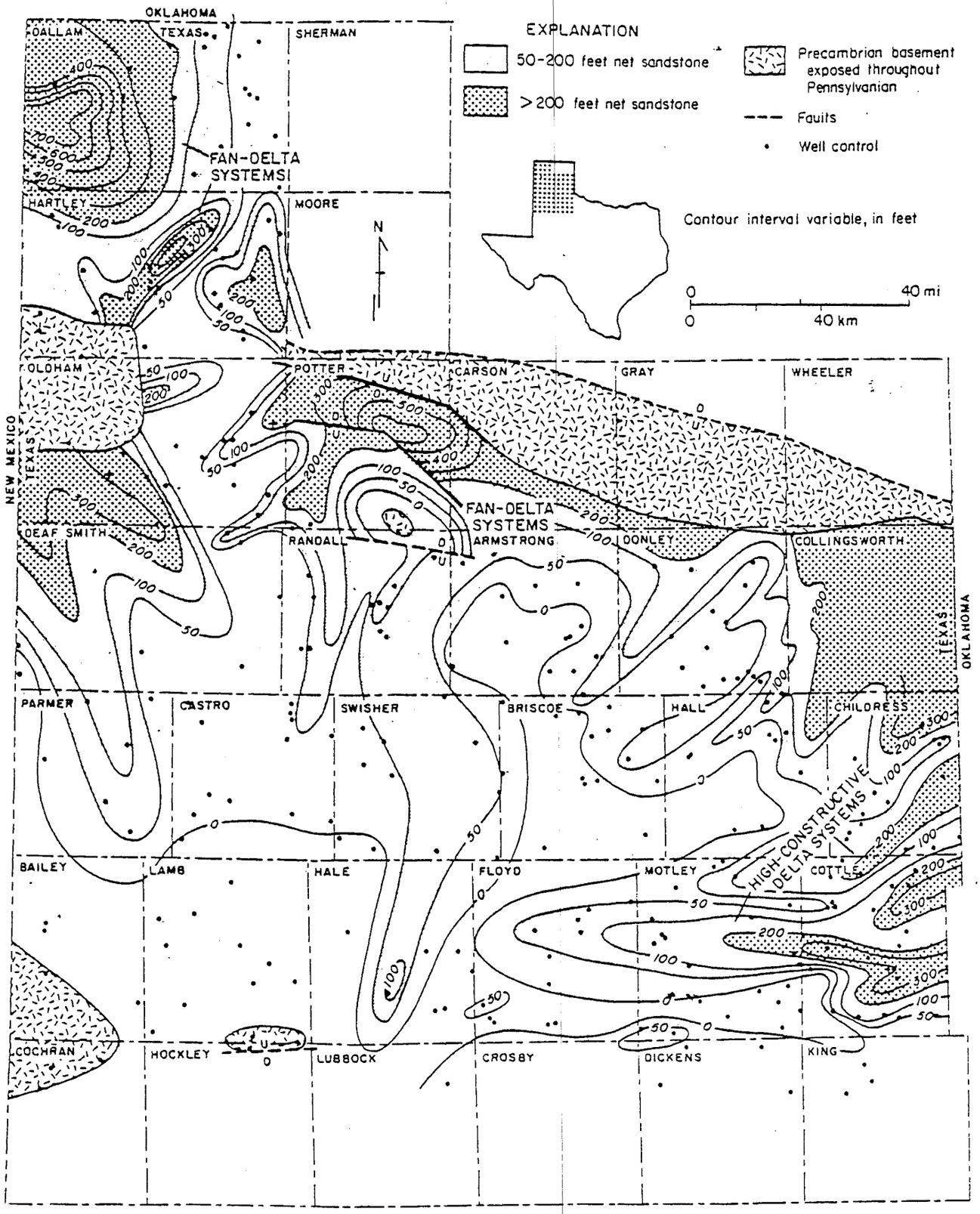

Figure 6 . **Net-sandstone map of upper part of the Pennsylvanian System, including both granite wash and nonarkosic sandstone** (from Dutton and others, 1982).

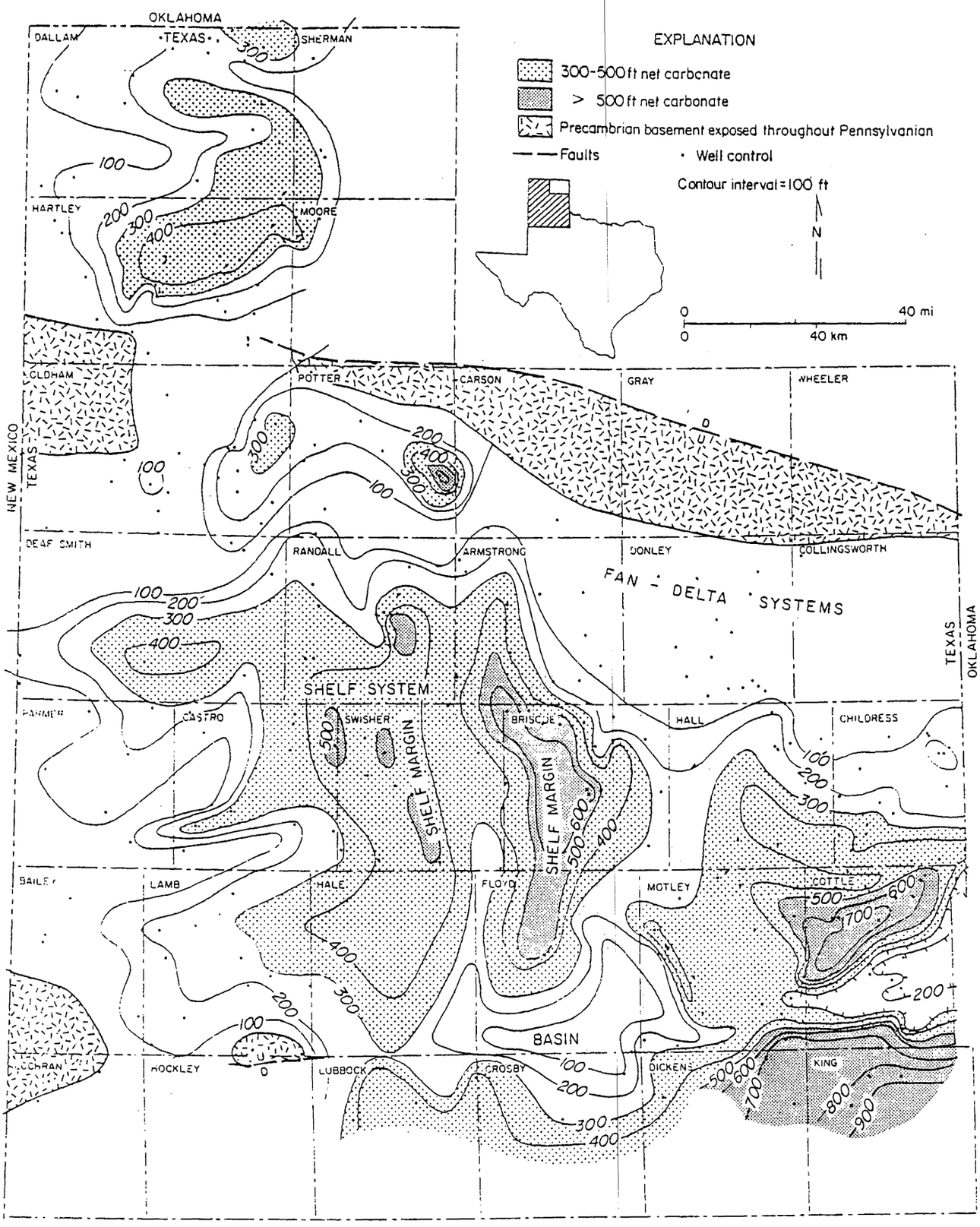

Figure 7 . Net-carbonate map of lower part of Pennsylvanian System (from Dutton, 1982).

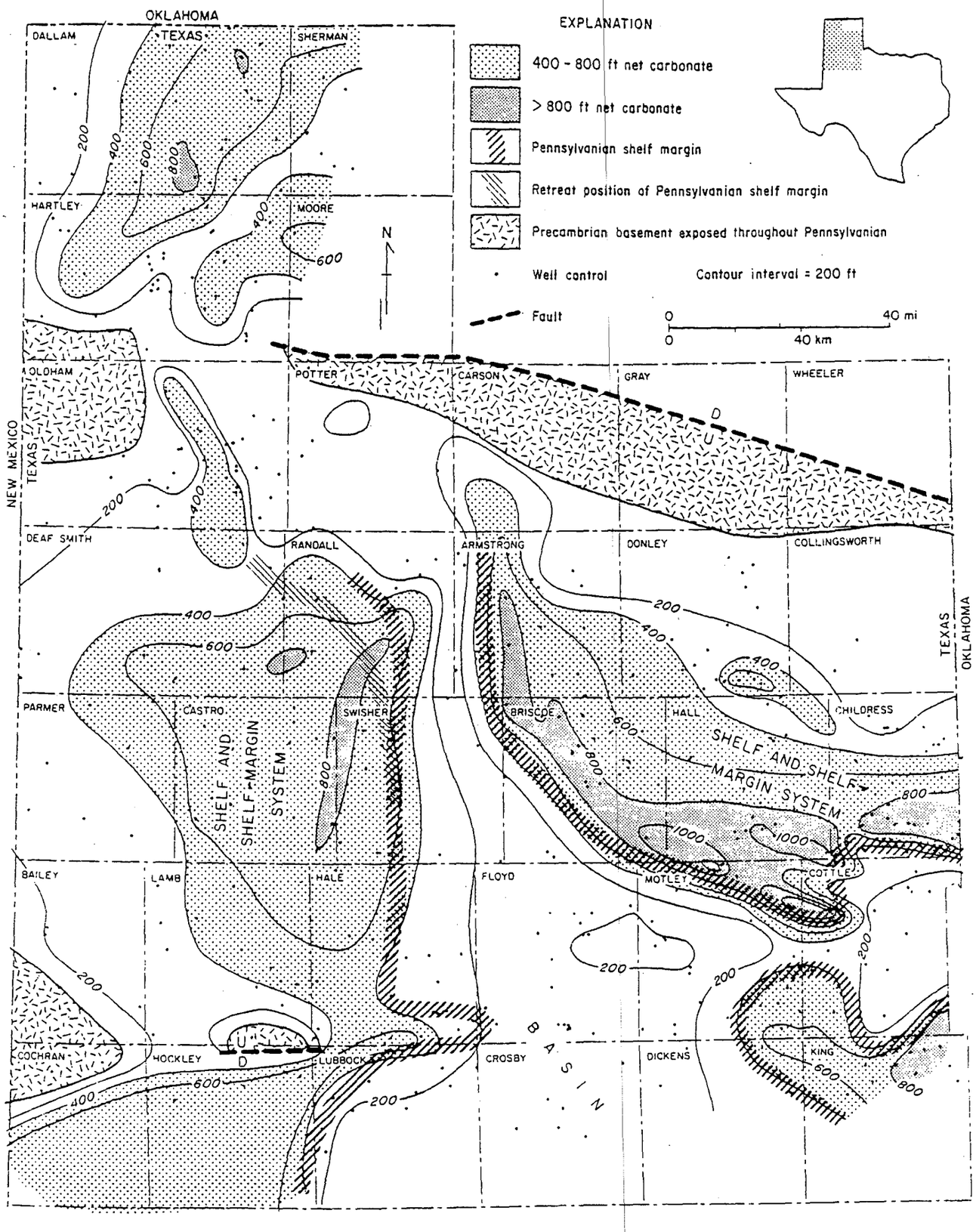

Figure 8 . Net-carbonate map of upper part of Pennsylvanian System. Position of older shelf margin is shown by dark hachured lines, and younger (retreated) position is shown by lighter hachures(from Dutton and other [illegible] .

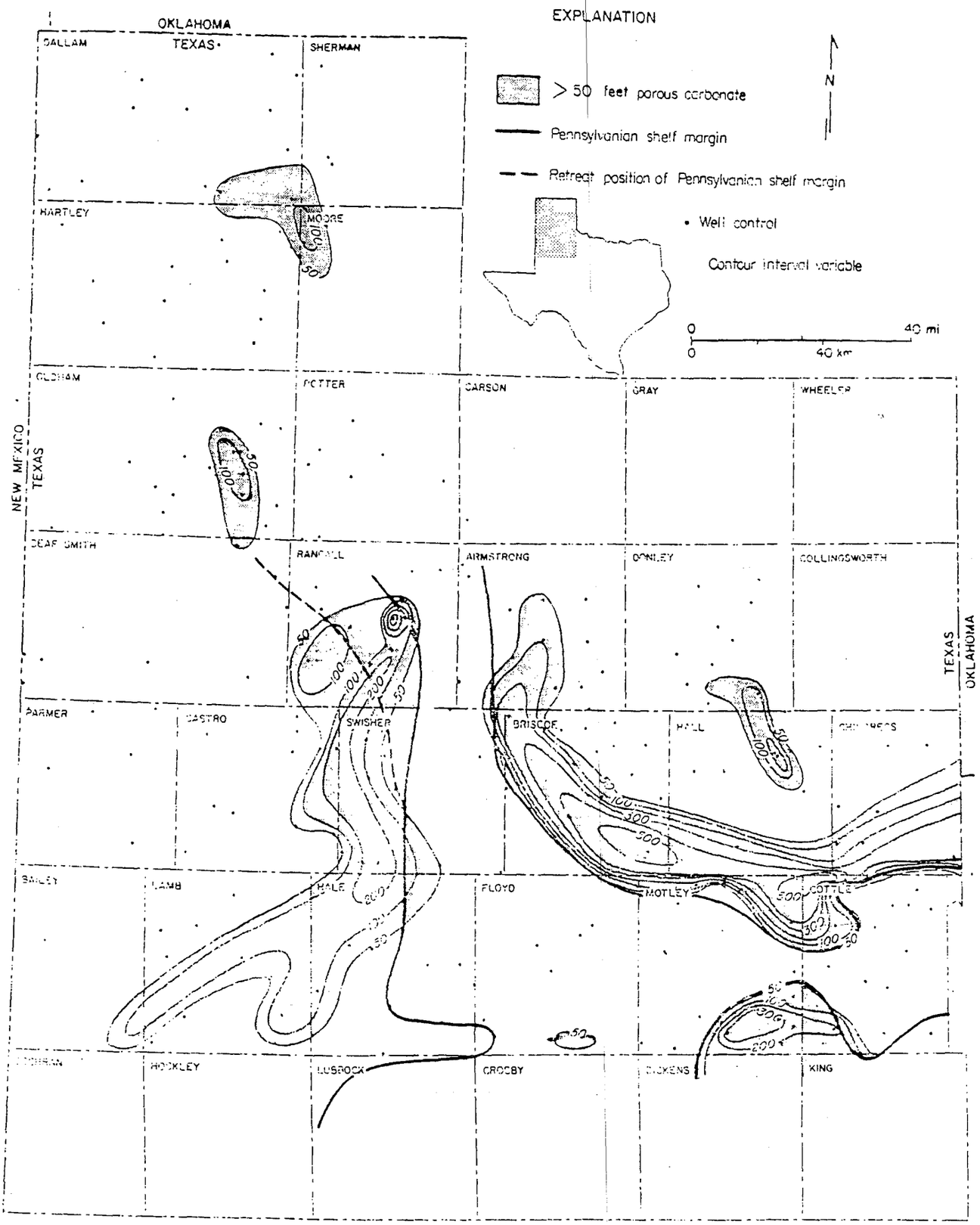

Figure 3. Isopach map of porous carbonate strata in upper part of the Pennsylvanian System. Map is made on the basis of qualitative sample log descriptions, so actual porosity values are unknown (from Dutton and others, 1979).

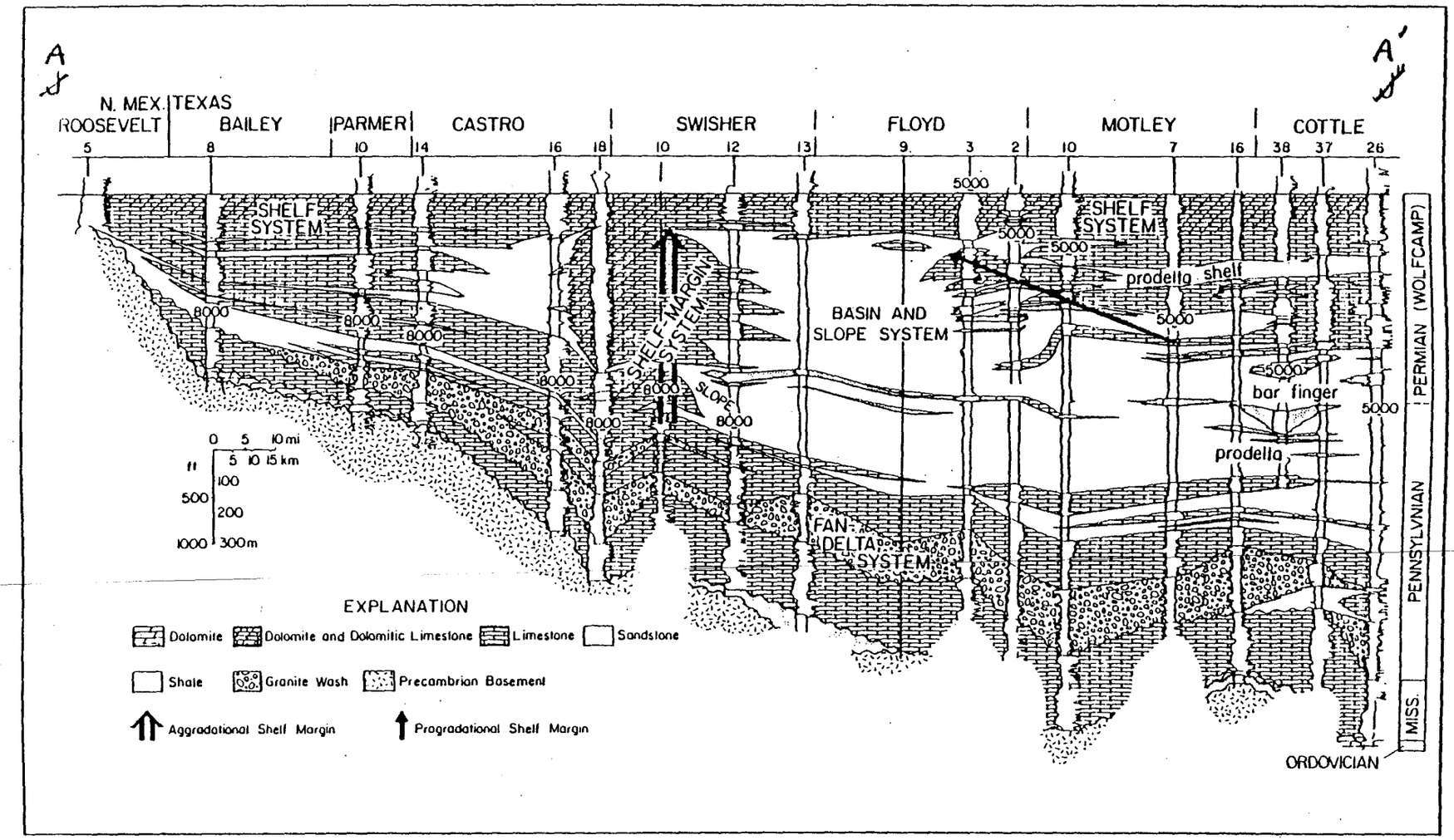

Figure 10 ft. **East-west cross section A-A'. Datum is top of Wolfcampian Series; depths are in feet.** See figure 1 for location. (from Dutton and others, 1982).

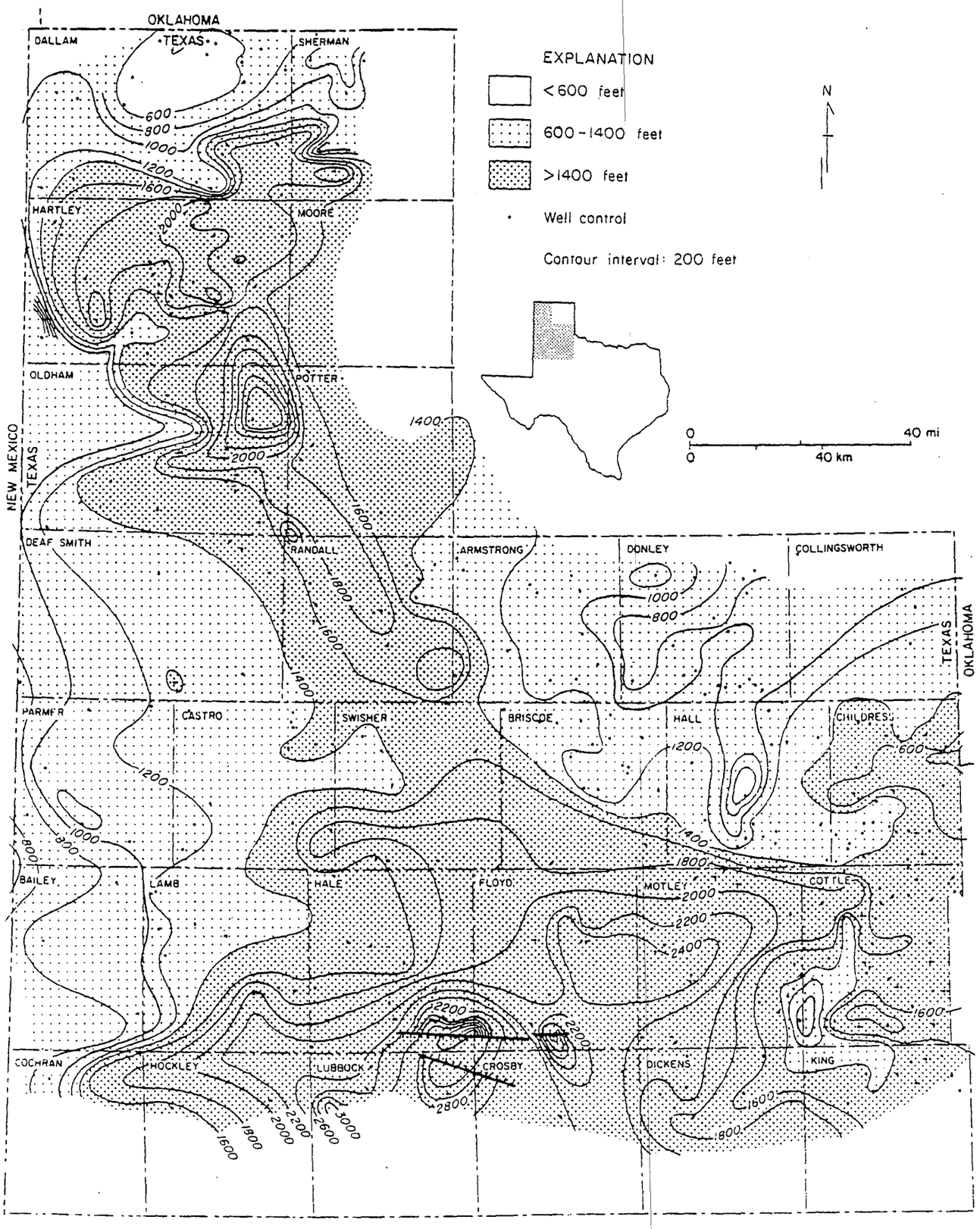

Figure 12. Isopach map of Wolfcampian Series, Palo Duro Basin (Handford, unpublished data).

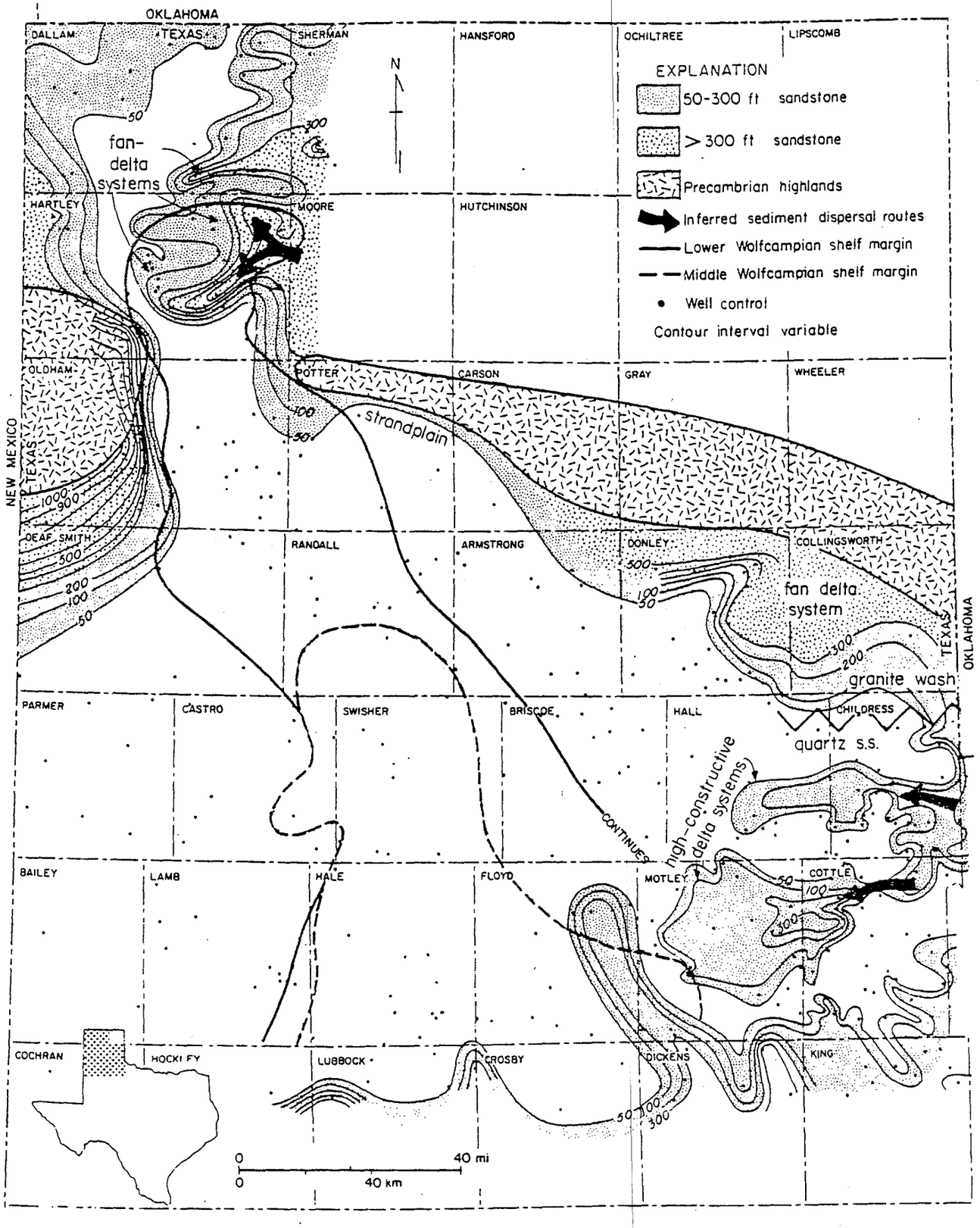

Figure 12. **Sandstone isolith map of Lower Permian strata, Palo Duro Basin. Inferred sand dispersal routes highlight delta systems** (from Handford, 1980).

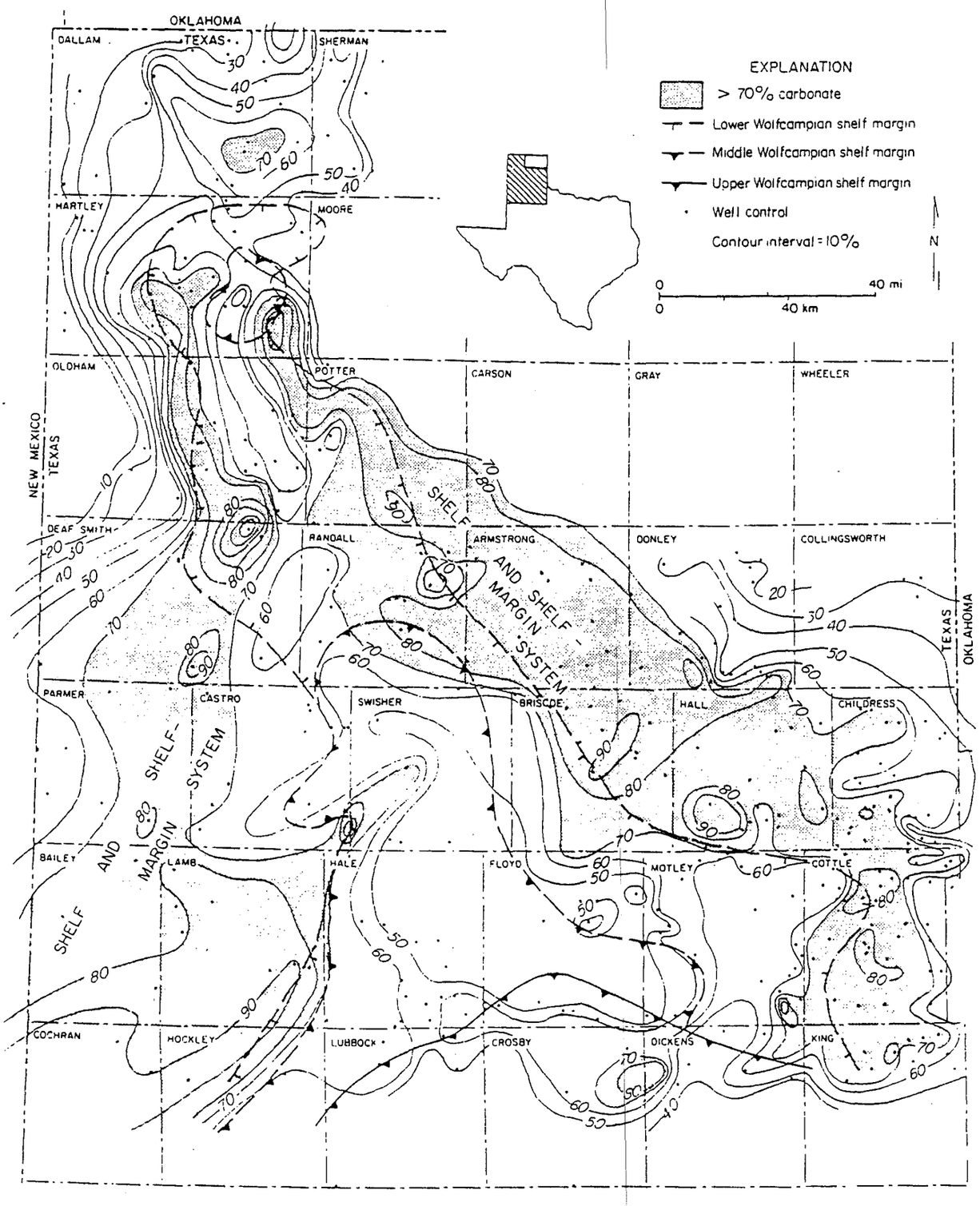

Figure 3. Percent-carbonate map of lower Permian strata in the Palo Duro Basin. Lines defining lower, middle, and upper Wolfcampian shelf-margin positions illustrate shelf-margin progradation through time (from Handford, 1980).

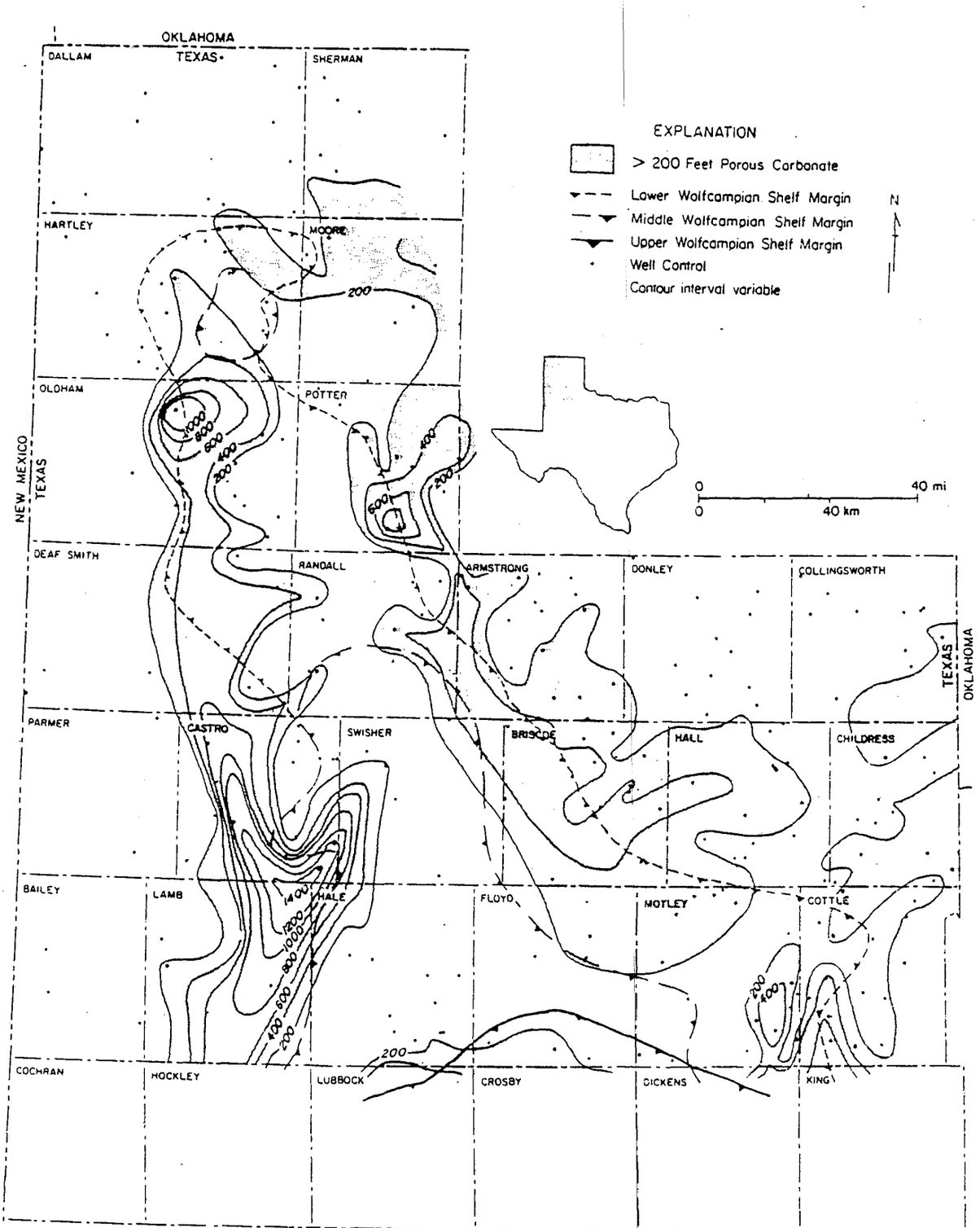

ure 14. Isopach map of porous carbonate strata in Wolfcampian Series. Map is made on the basis of qualitative sample log descriptions, so actual porosity values are unknown (from Handford and Dutton, 1980).

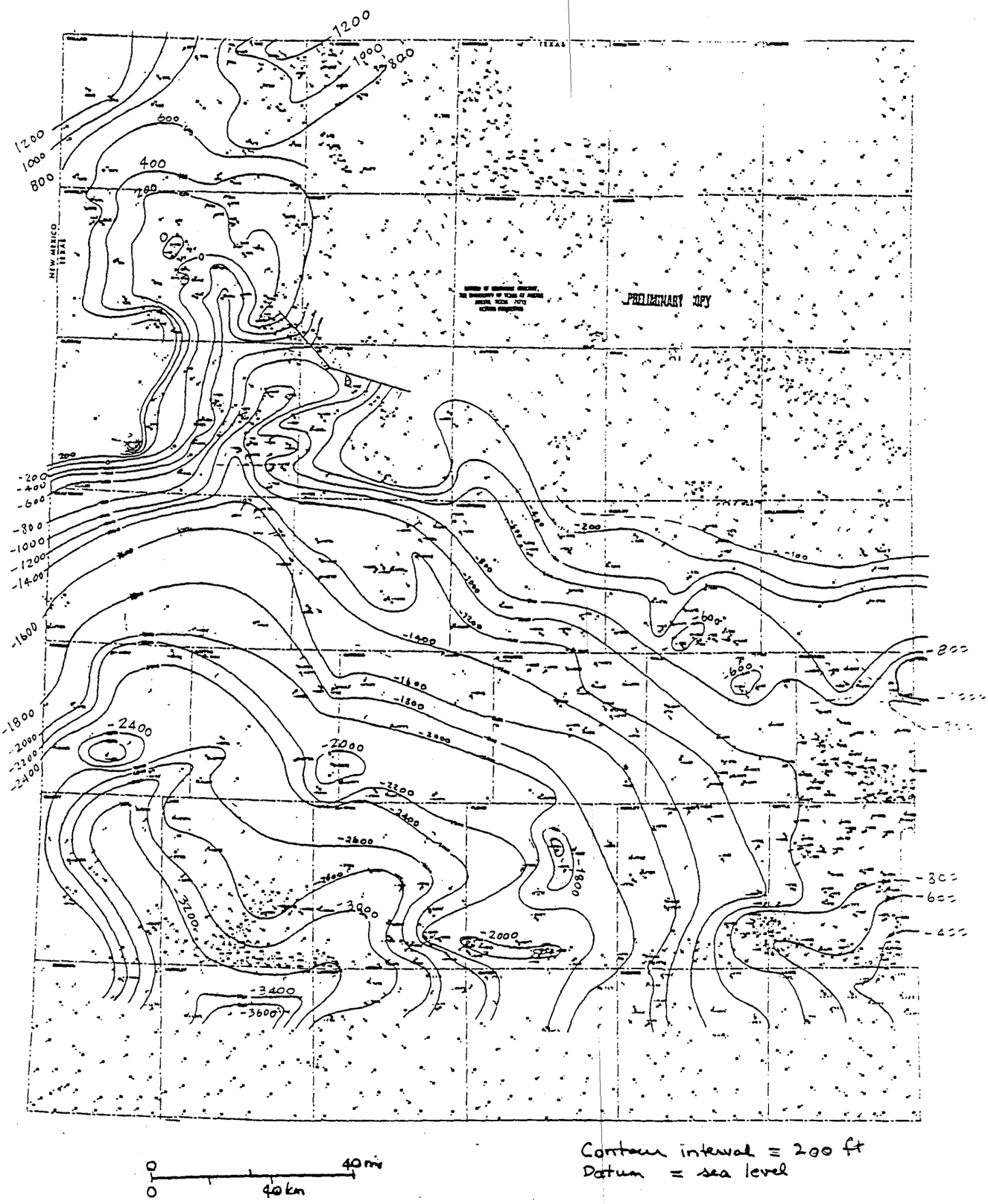

Contour interval = 200 ft
Datum = sea level

Figure 15 Structure contour map of top of Norfolk [illegible] Tom, Texas [illegible] (unpublished [illegible] of Economic Geology).

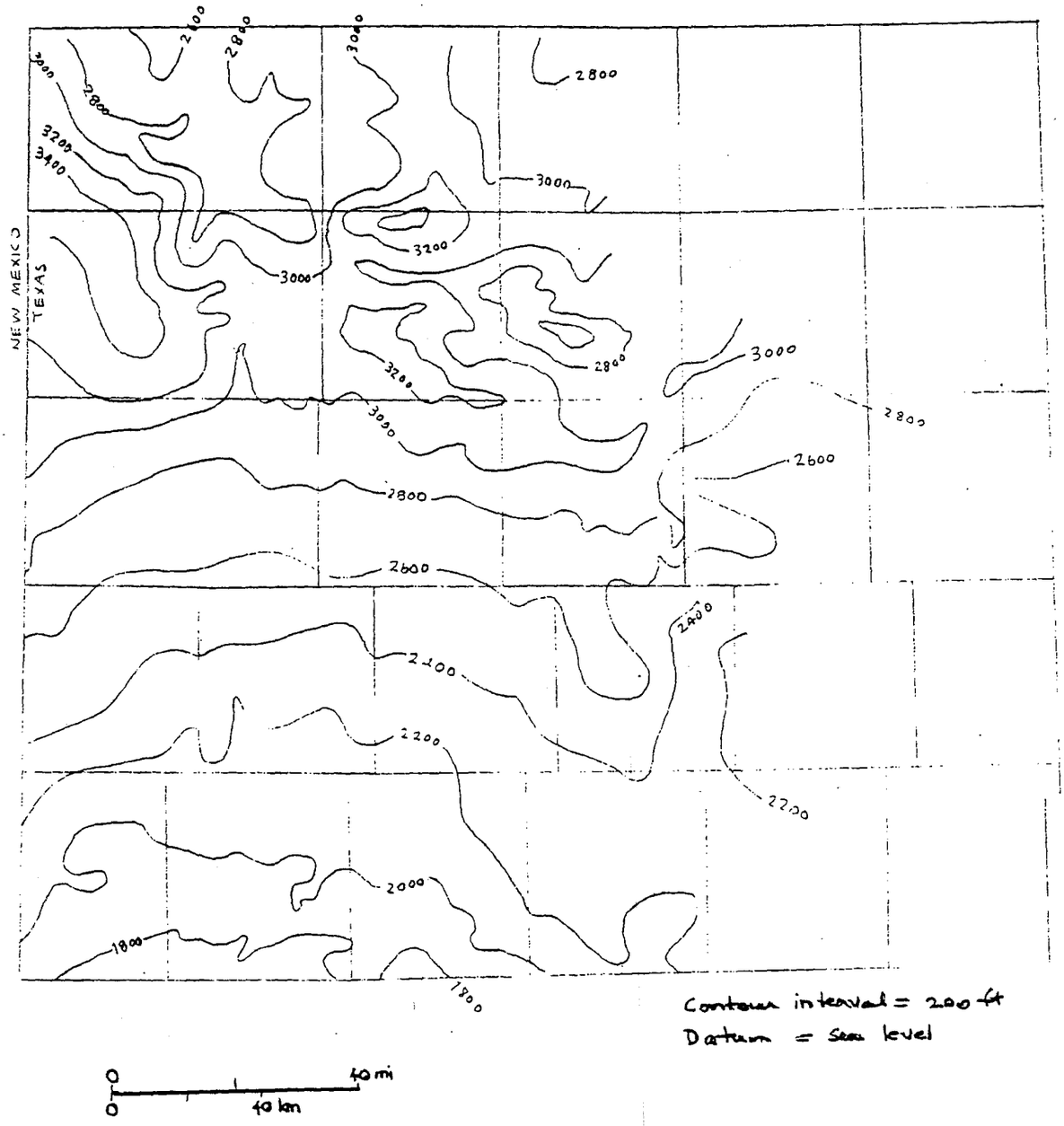

Figure 11 Structure contour map on top of Alibates, Texas Panhandle (D. Jones, personal communication, 1993).

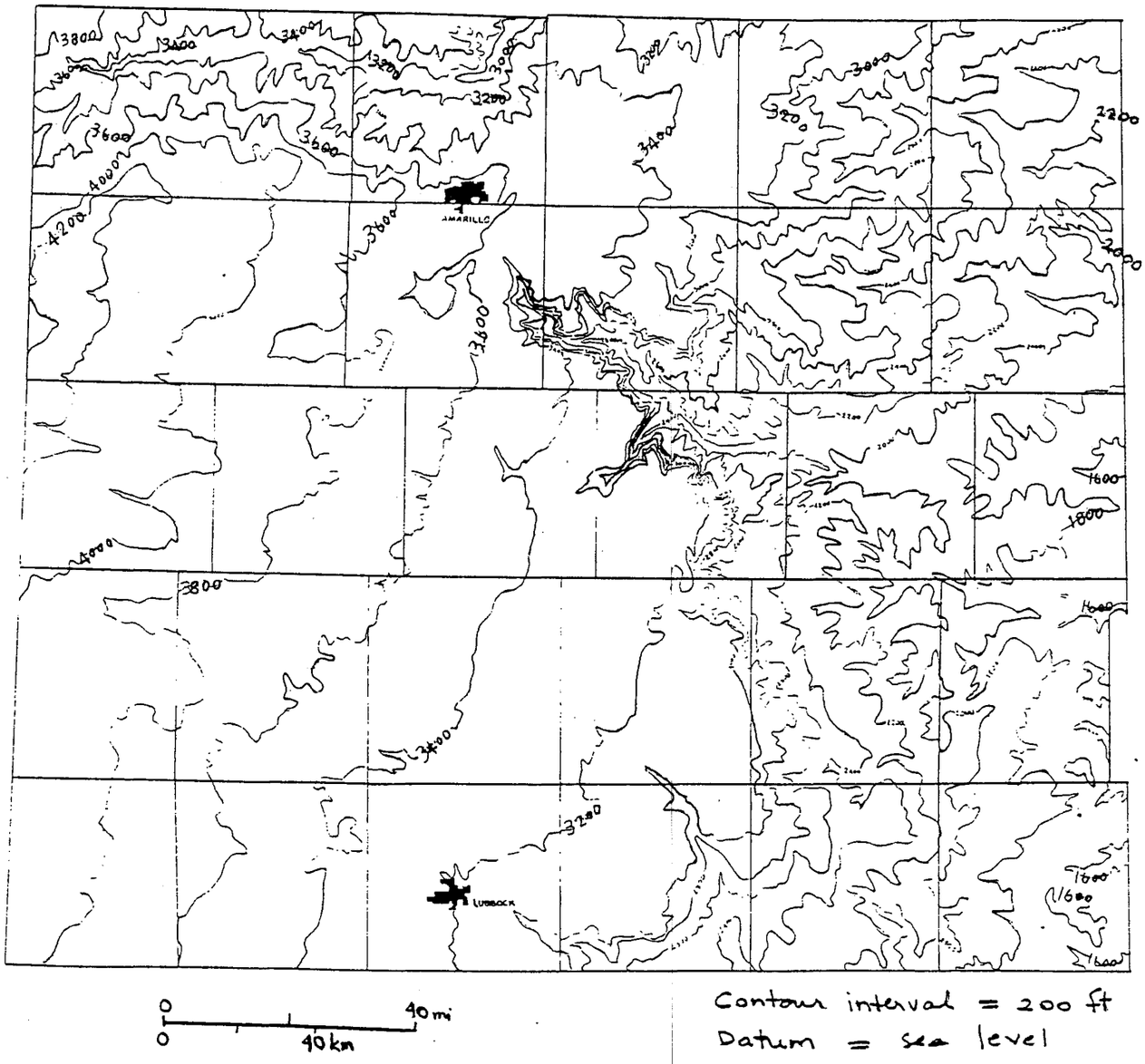

Figure 17. Simplified topographic map of the Palo Duro Basin.

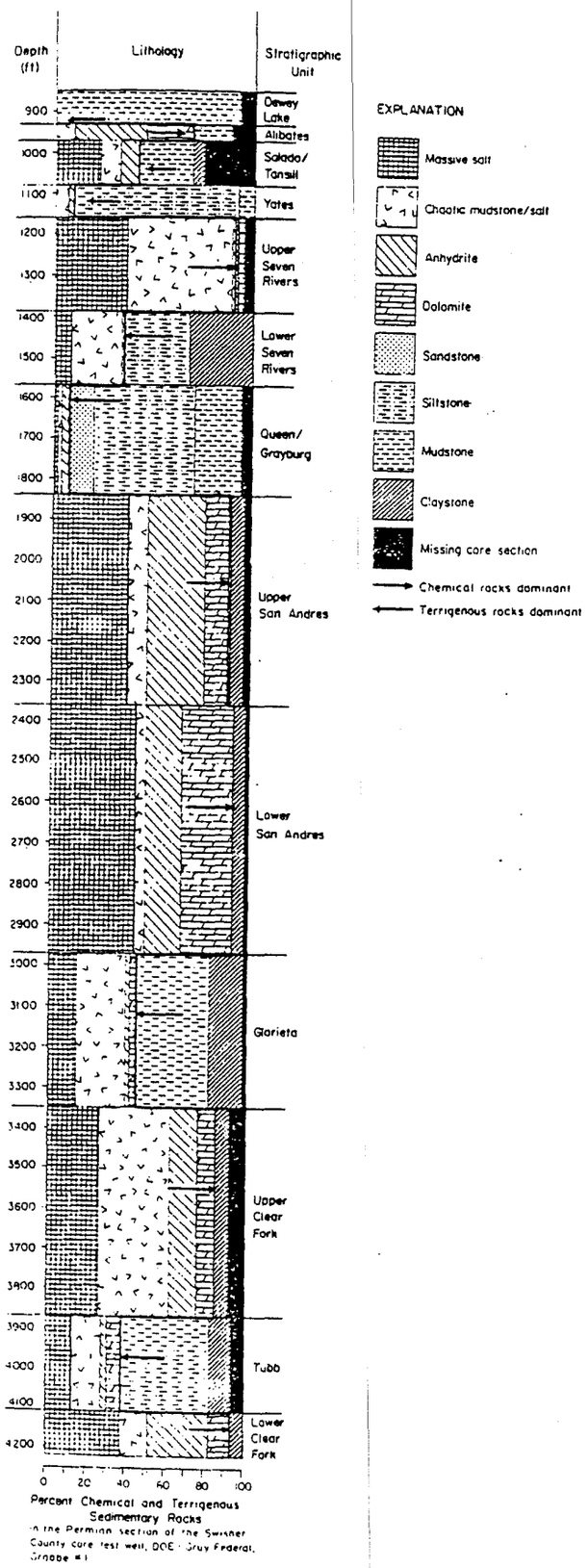

Figure 18. Swisher County core test well DOE-Gruy Federal, Grabbe no. 1: percent lithologic type per stratigraphic unit (McGowen,)

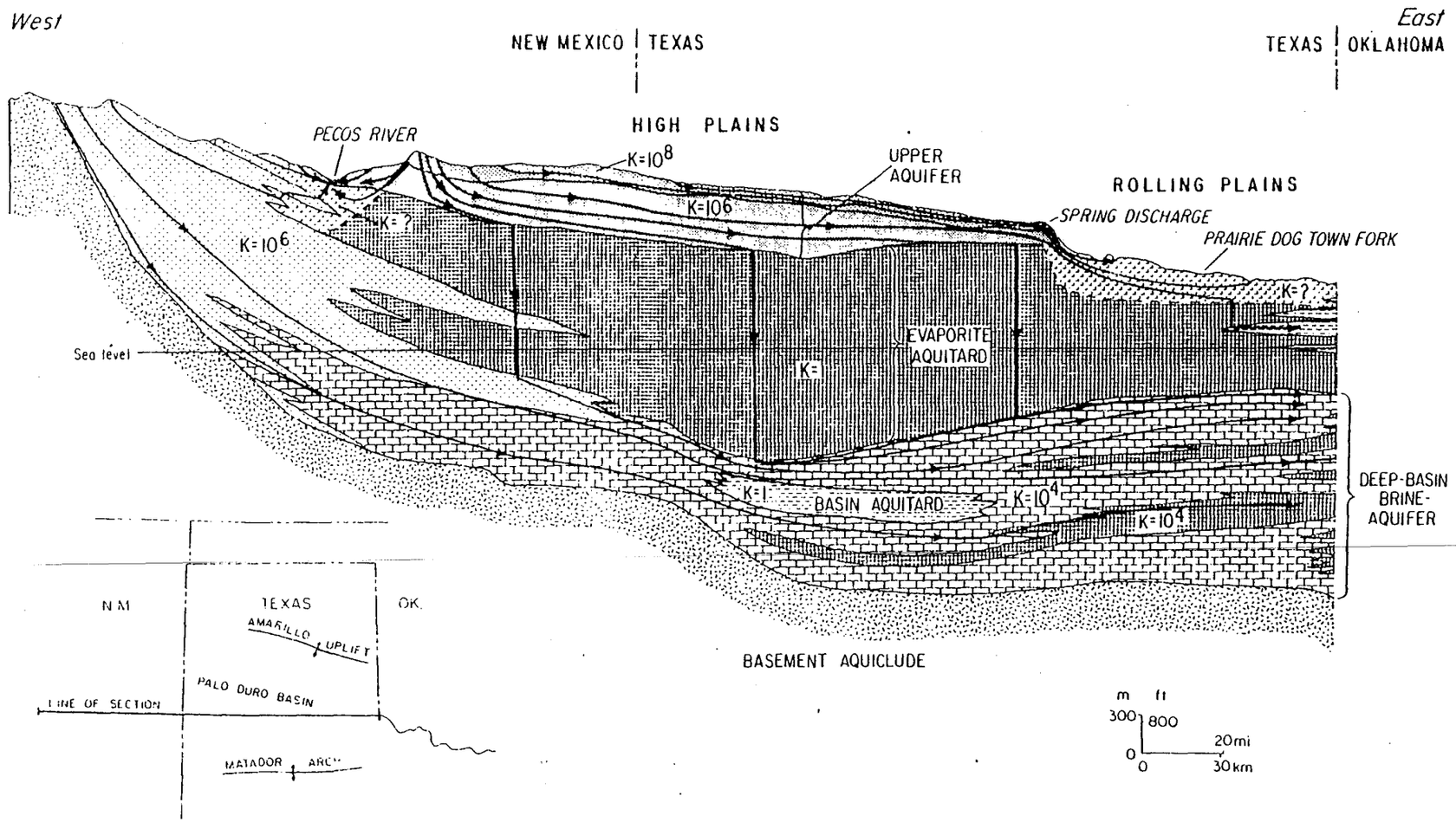

Figure 19. Regional east-west section illustrating conceptual flow patterns based on hydraulic conditions and relative average permeabilities of major hydrogeologic units (from Bassett and Bentley 1983).

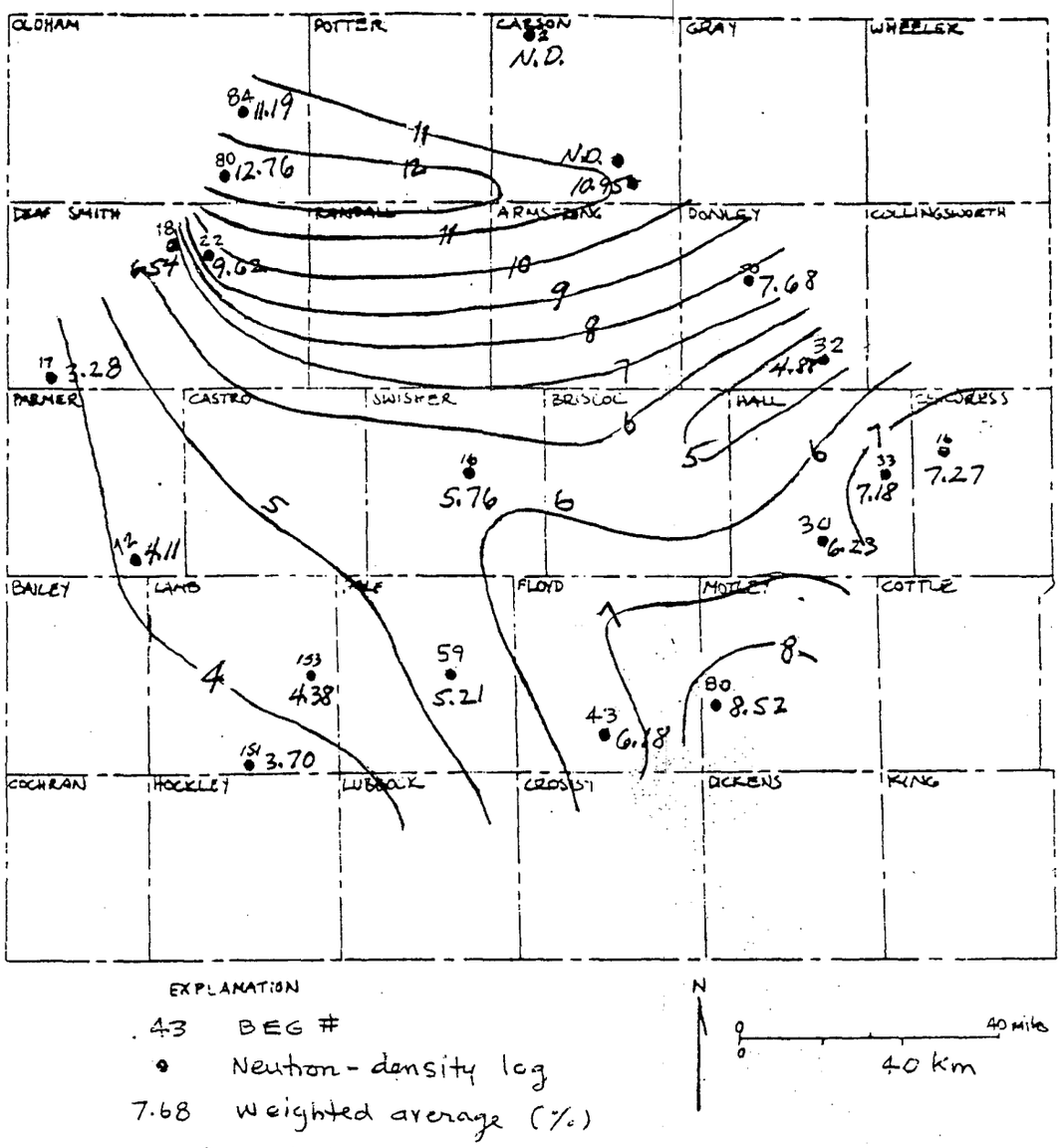

Figure 20. Weighted-average porosity of the Wolfcamp strata estimated from neutron-density log data (R. Corti, personal communication, 1983).

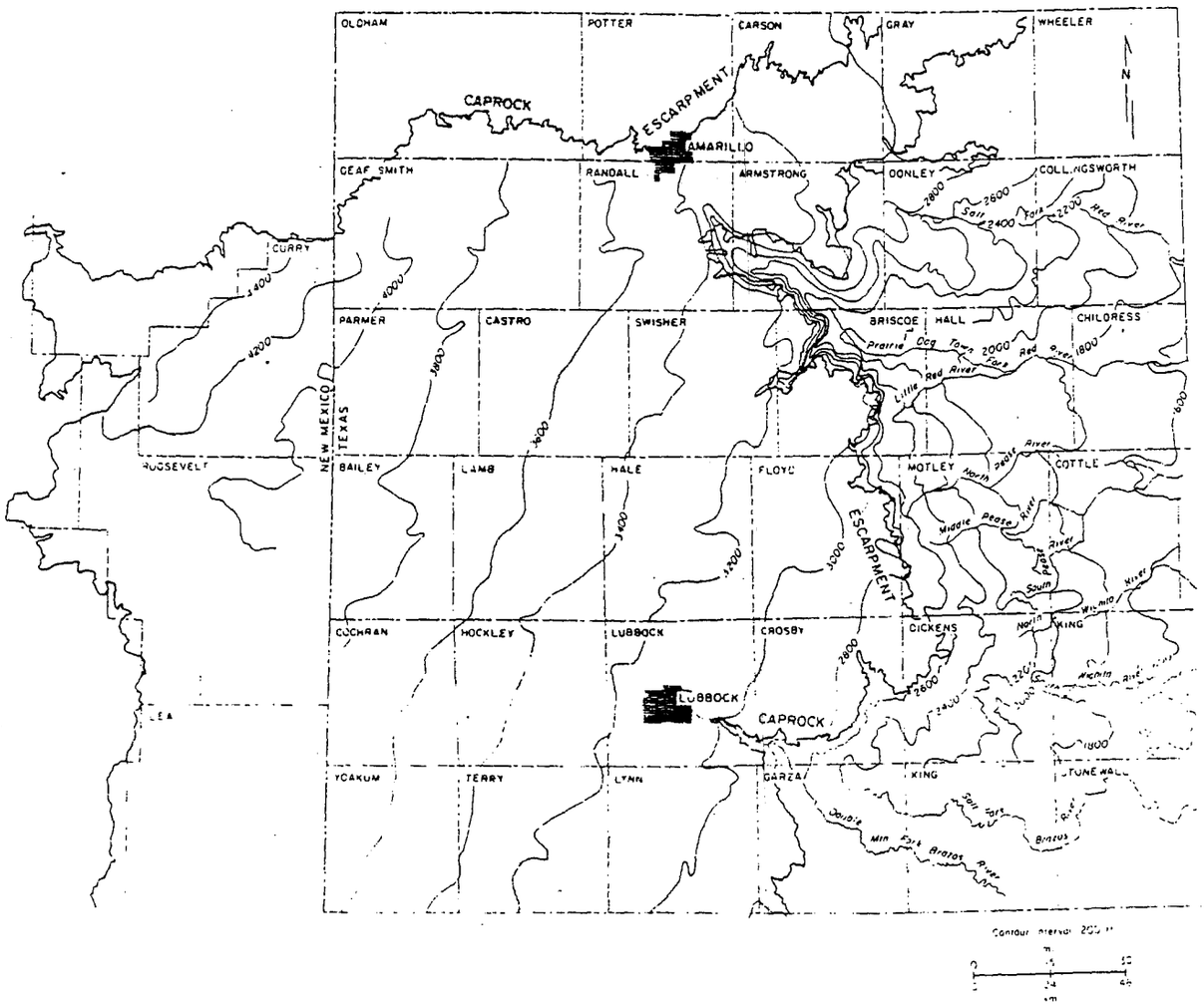

Figure 21. Head map (1979-1980) of the unconfined upper aquifer [illegible] escarpment [illegible]

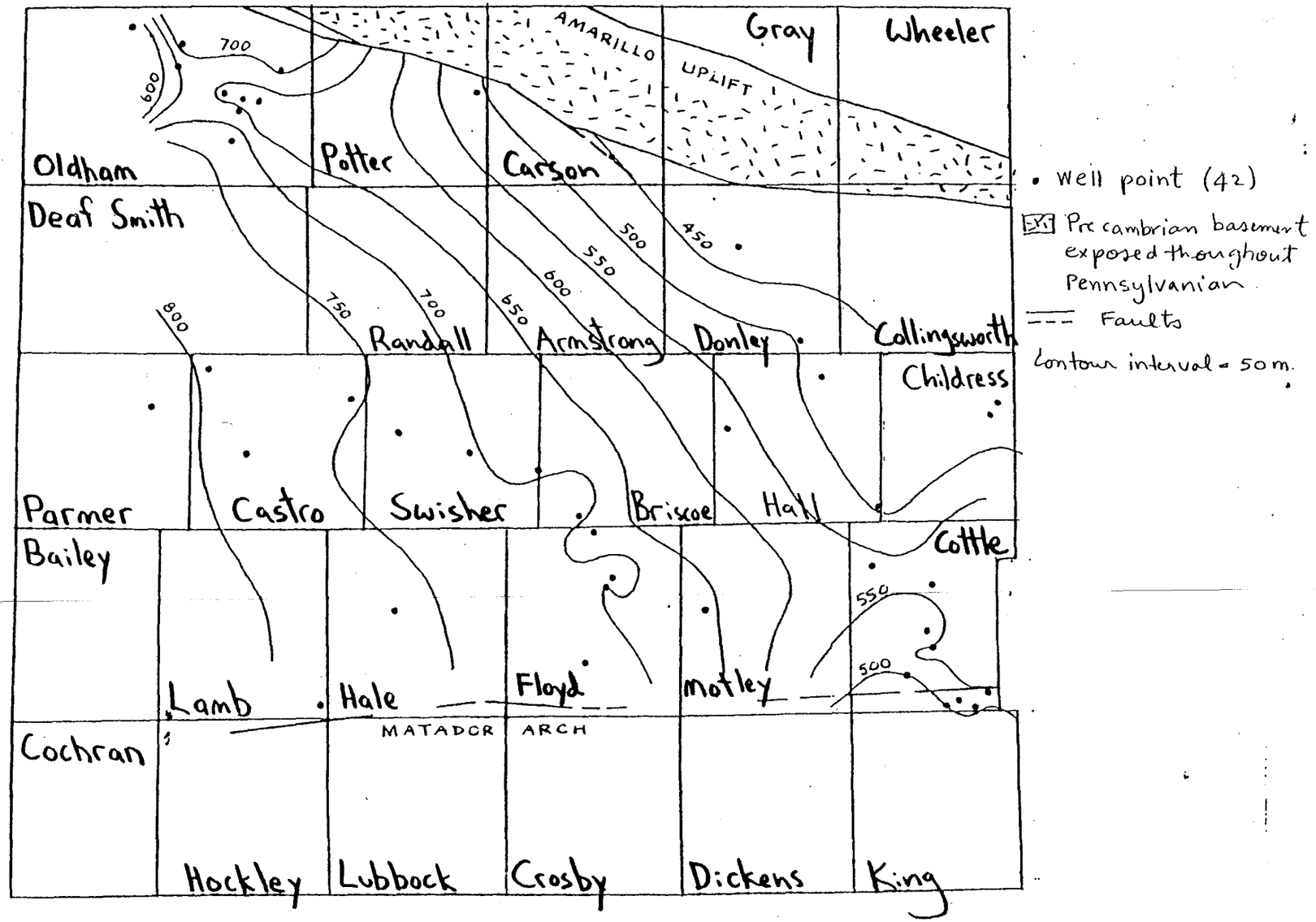

Figure 22. Average head map of the whole deep-brine aquifer constructed from claim H data.

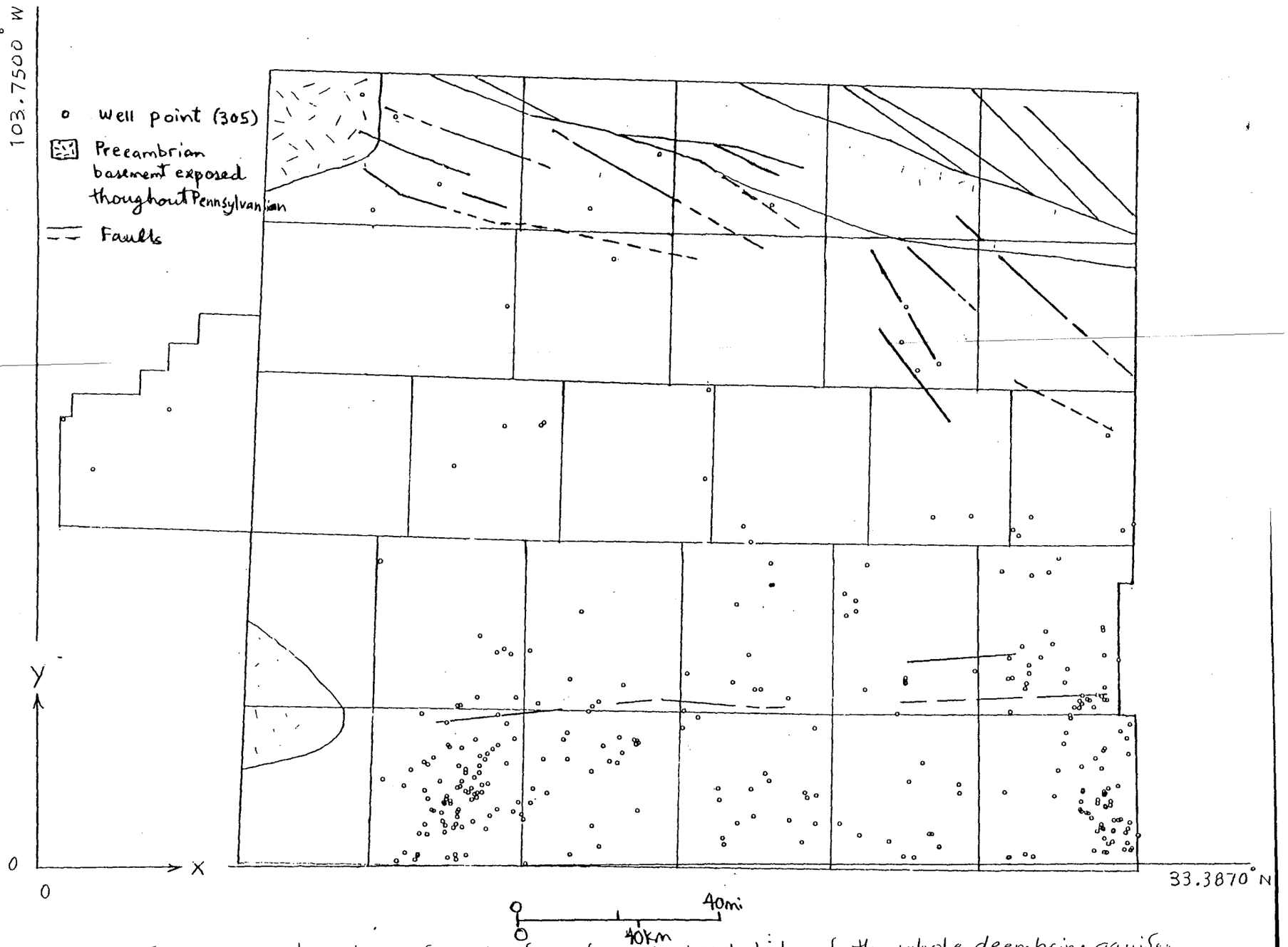

Figure 23. Location of well for class A head data of the whole deep-brine aquifer.

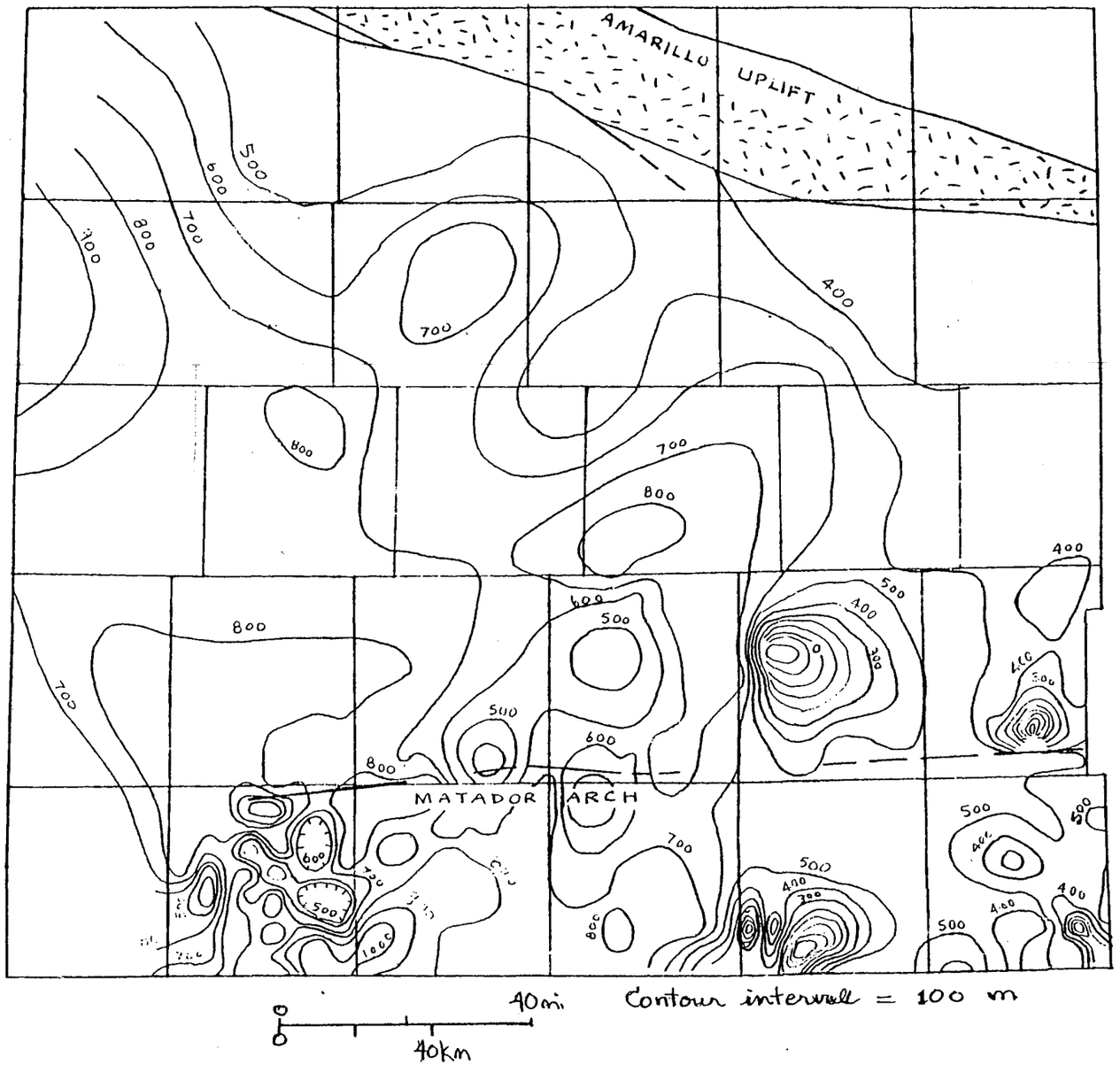

Figure 4. Average head map of the whole deep-brine aquifer constructed from class A data.

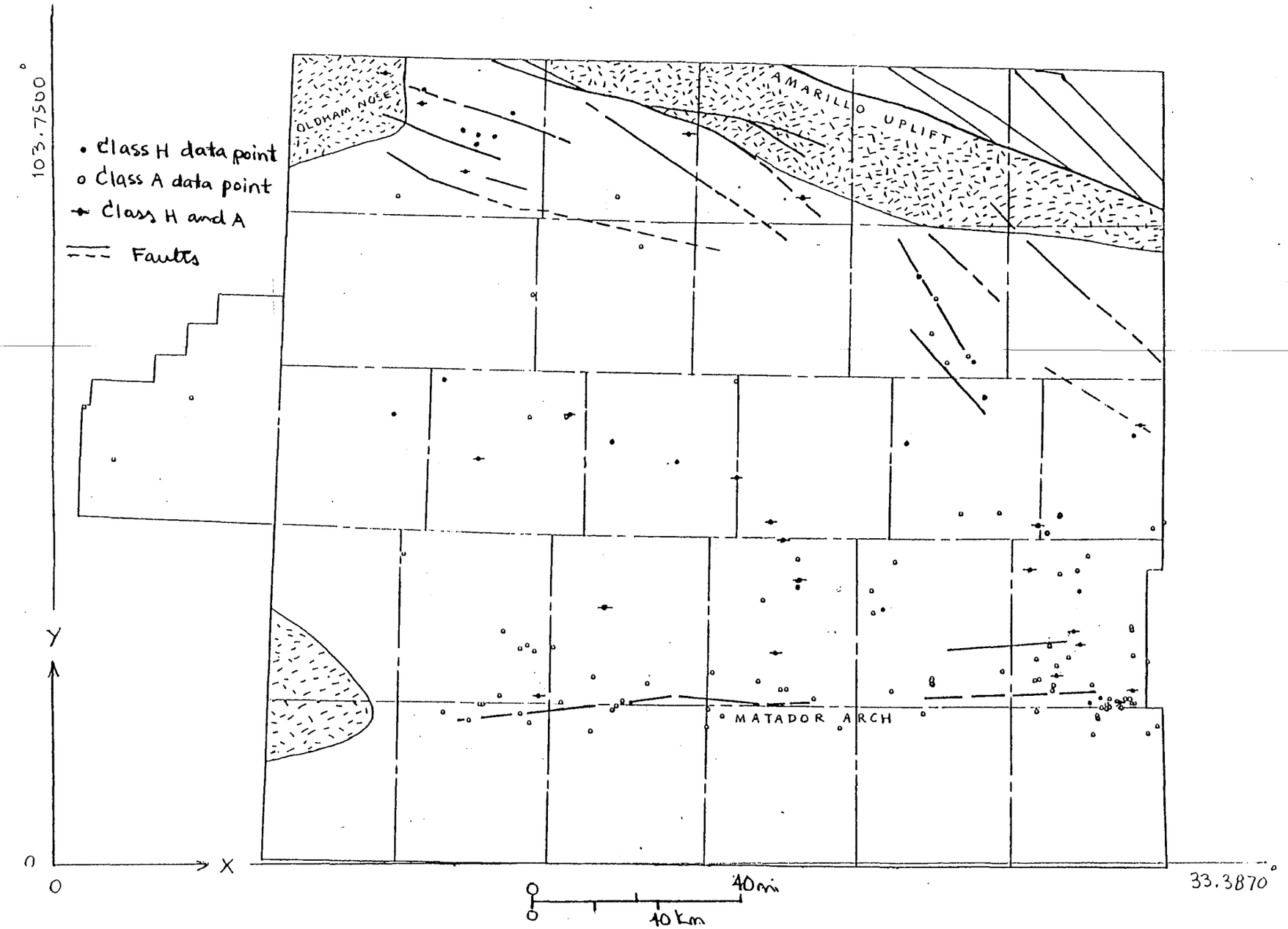

Figure 25. Location of selected class A and class H head data.

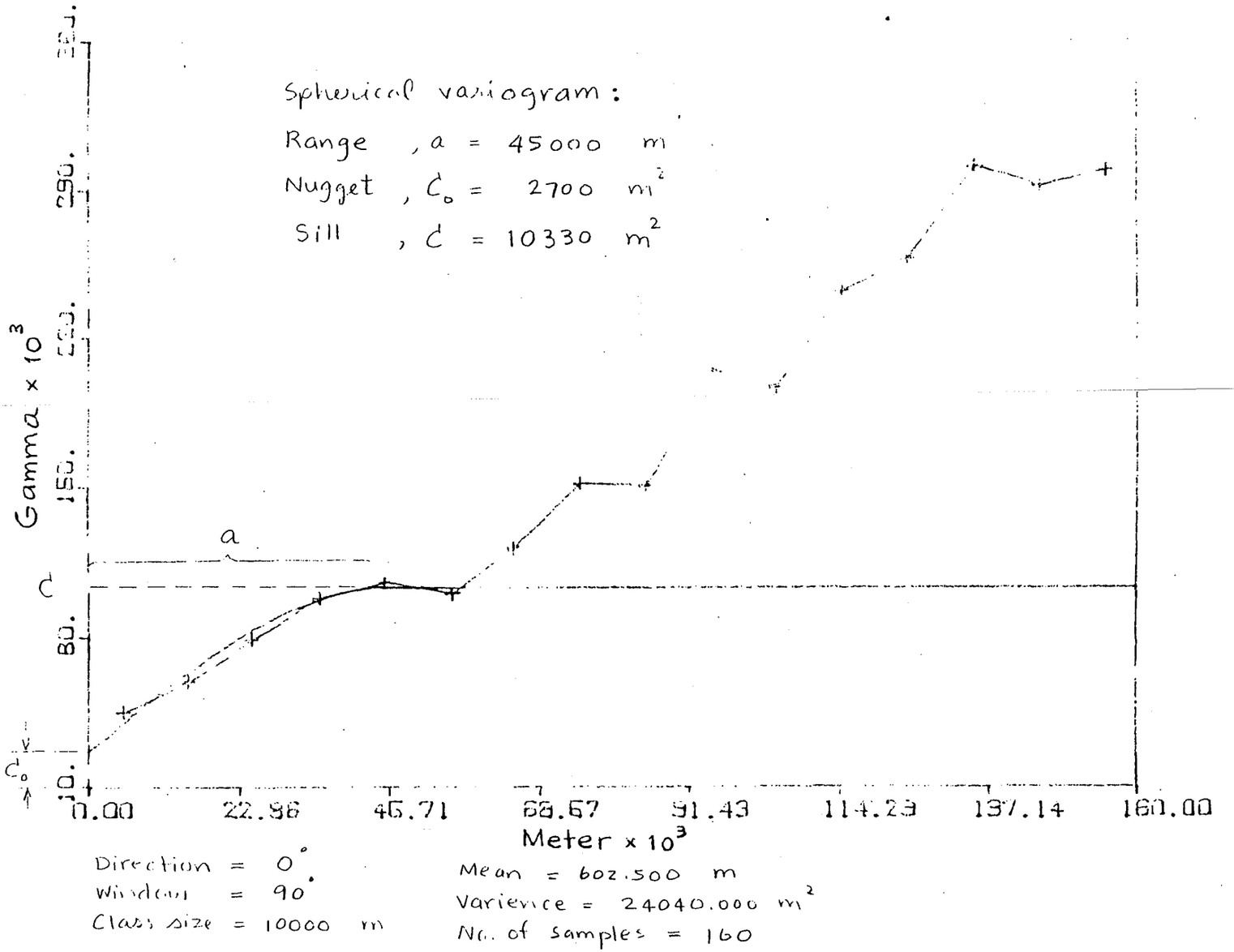

Figure 26. Representative variogram of the 118 selected class A and 42 class H average head data for the whole deep-brine aquifer.

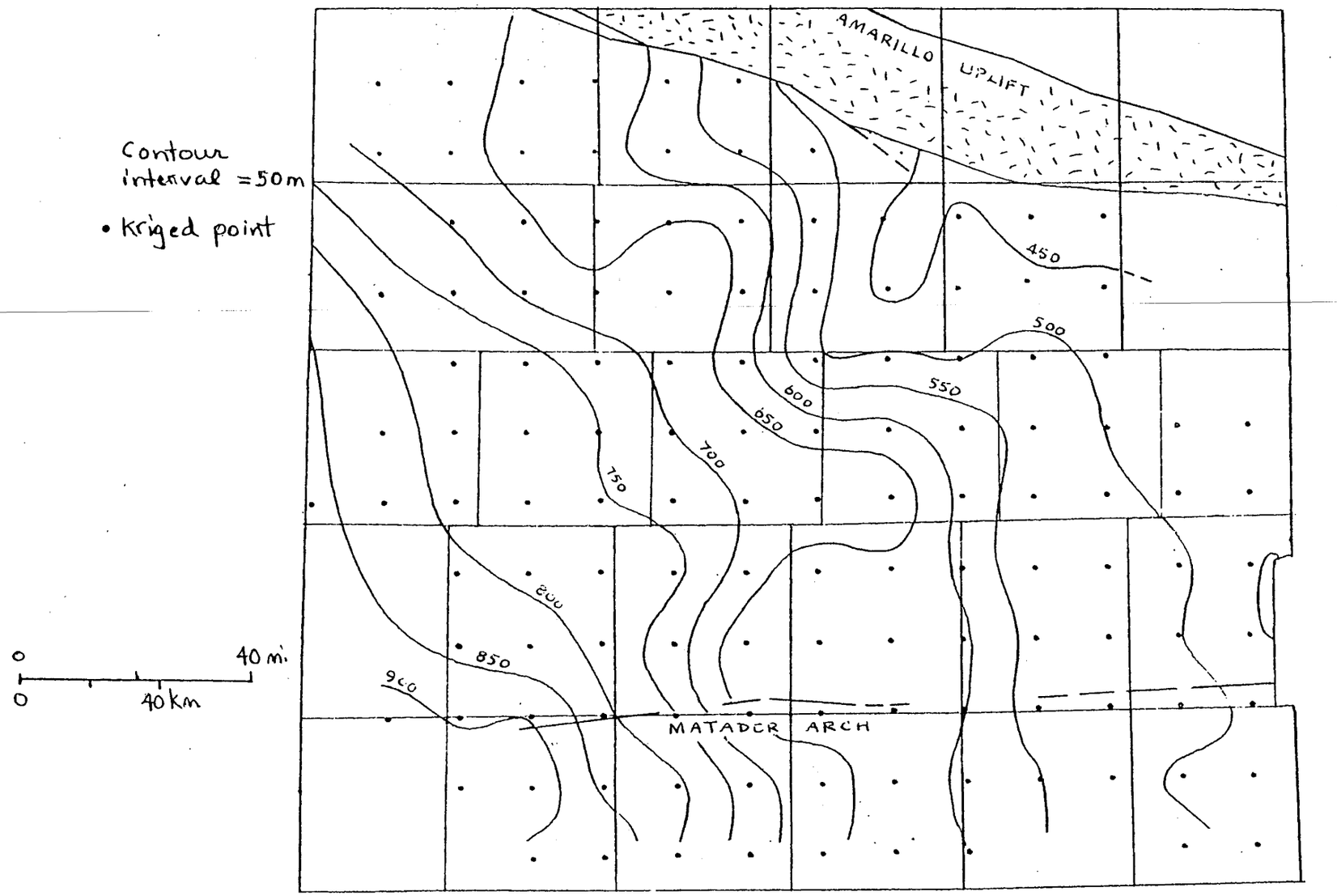

Figure 27. Potentiometric head map of the [illegible] deep-brine aquifer of Palo Duro [illegible] constructed from kriged estimates of head for regular blocks of

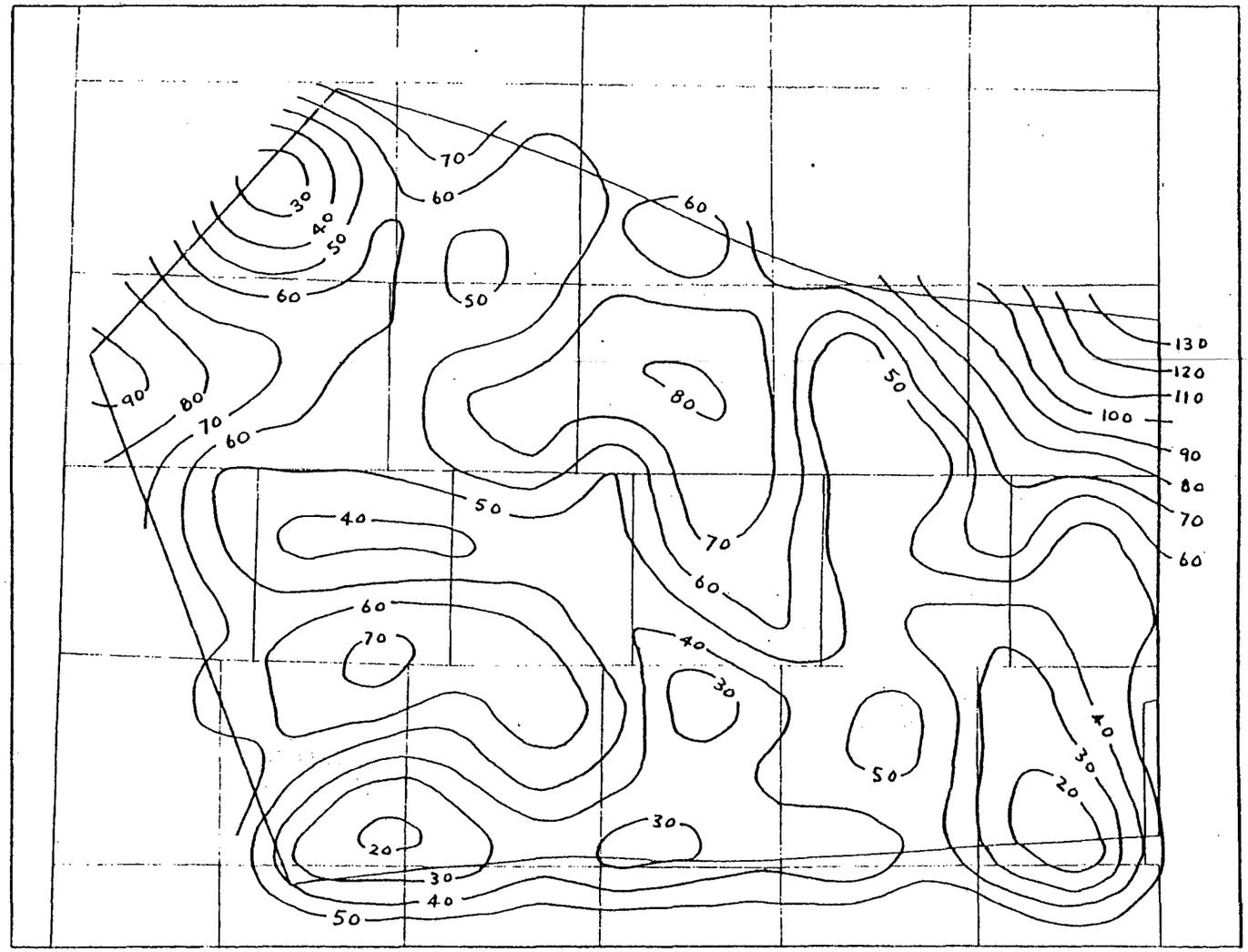

Figure 28. Standard error of estimate of the kriged deep-brine head in Figure 27.

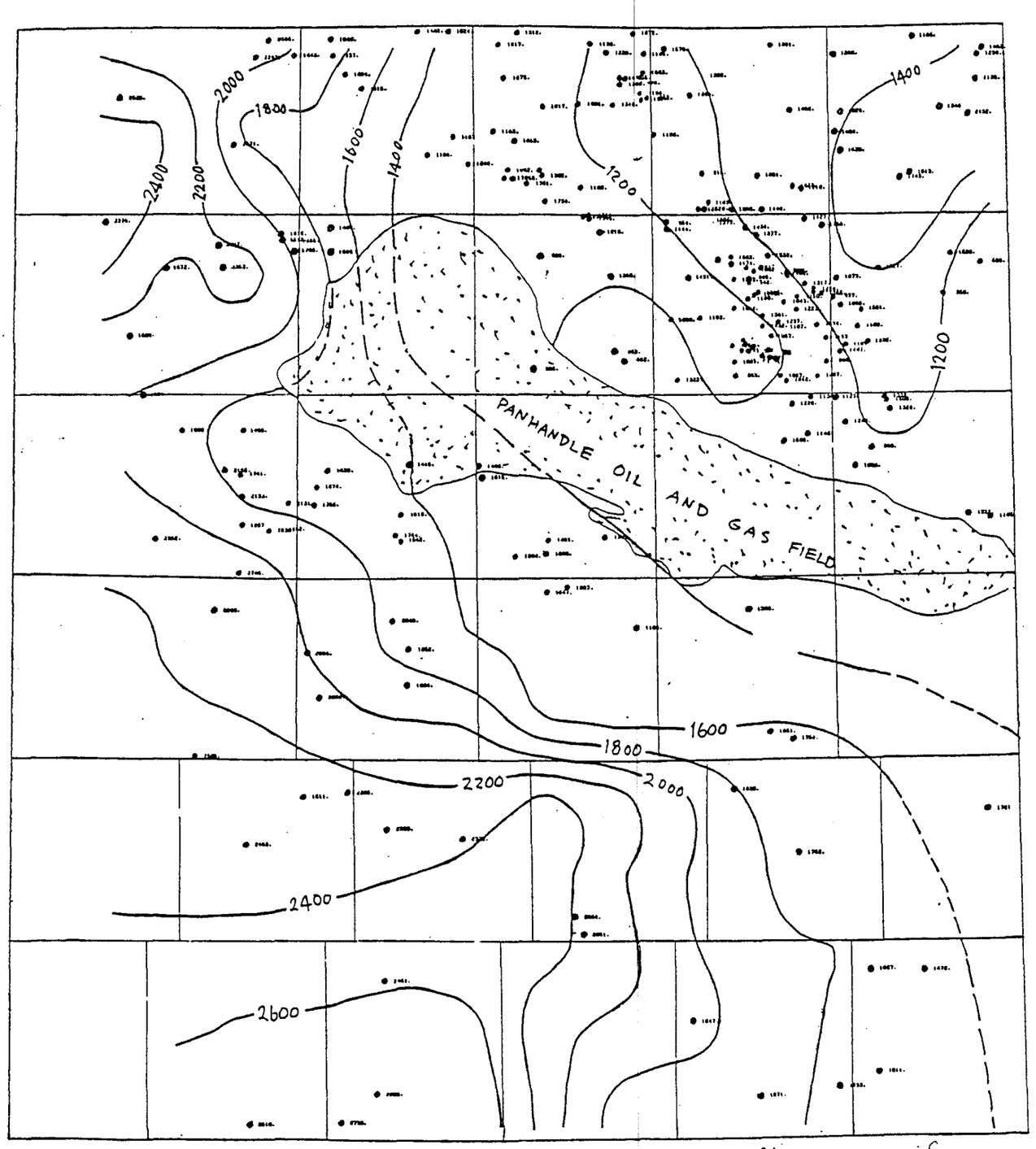

Figure 29. Potentiometric head map of the Wolfcamp aquifer of Palo Duro Basin constructed from kriged estimates of head for regular blocks of 20,000 meter square (from Smith, 1983).

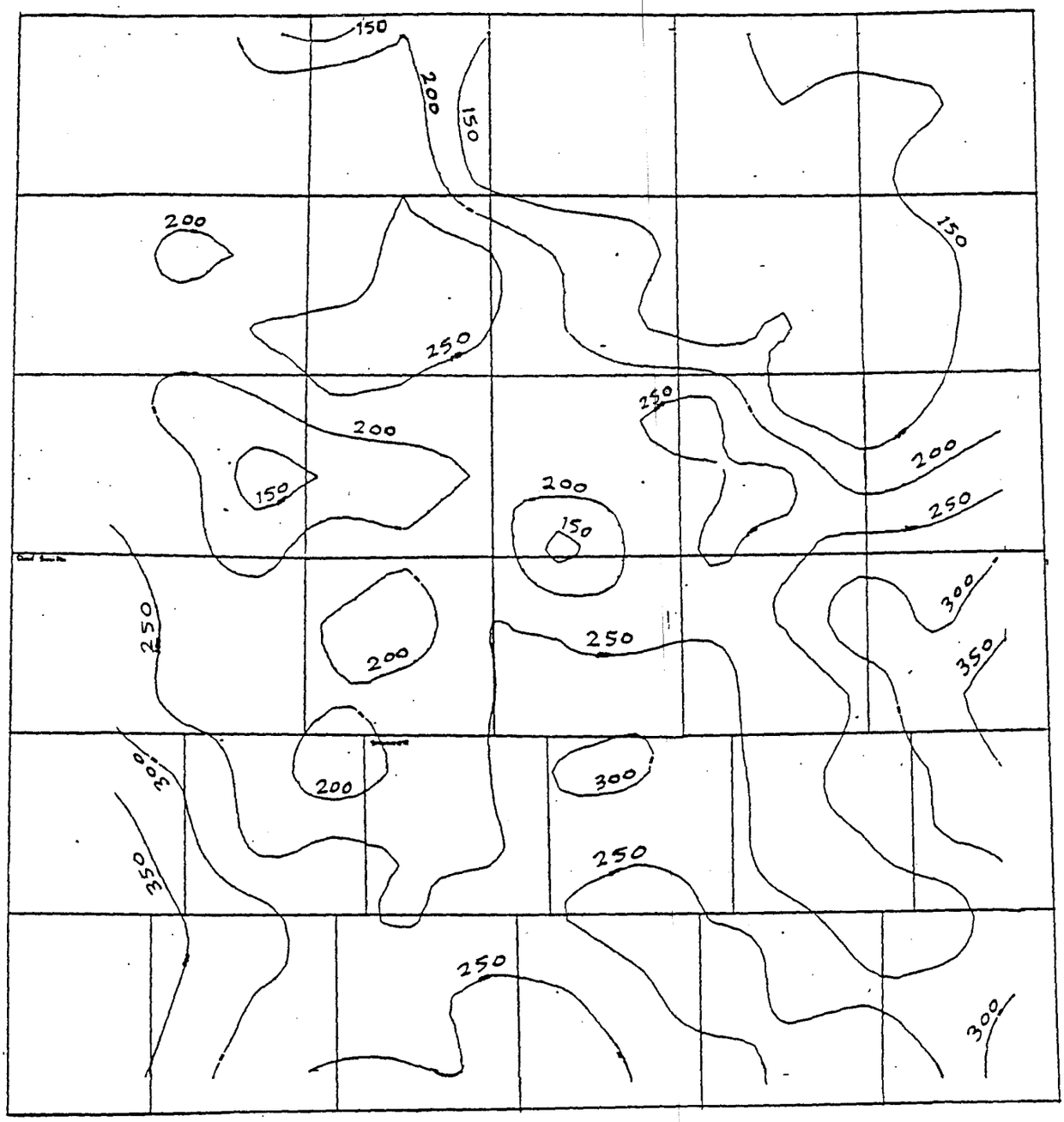

Figure 30. Standard error of estimate of the kriged Wolfcamp-head in Figure 29.

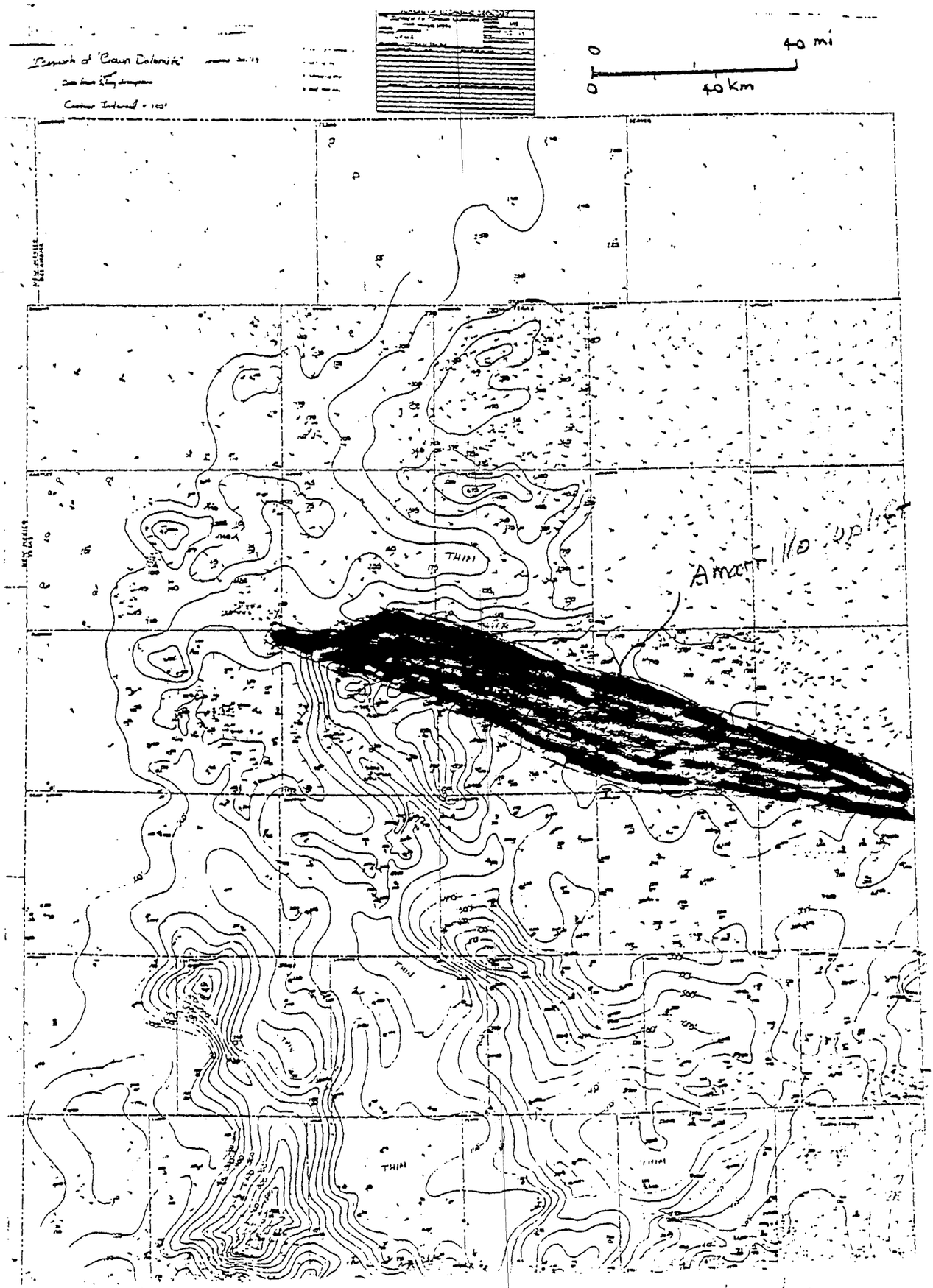

Figure 31. Isopach map of Wolfcamp Brown-Dolomite based on sample log information (M. Hamlin, personal communication, 1992). Location of Amarillo Uplift from Figure 5.

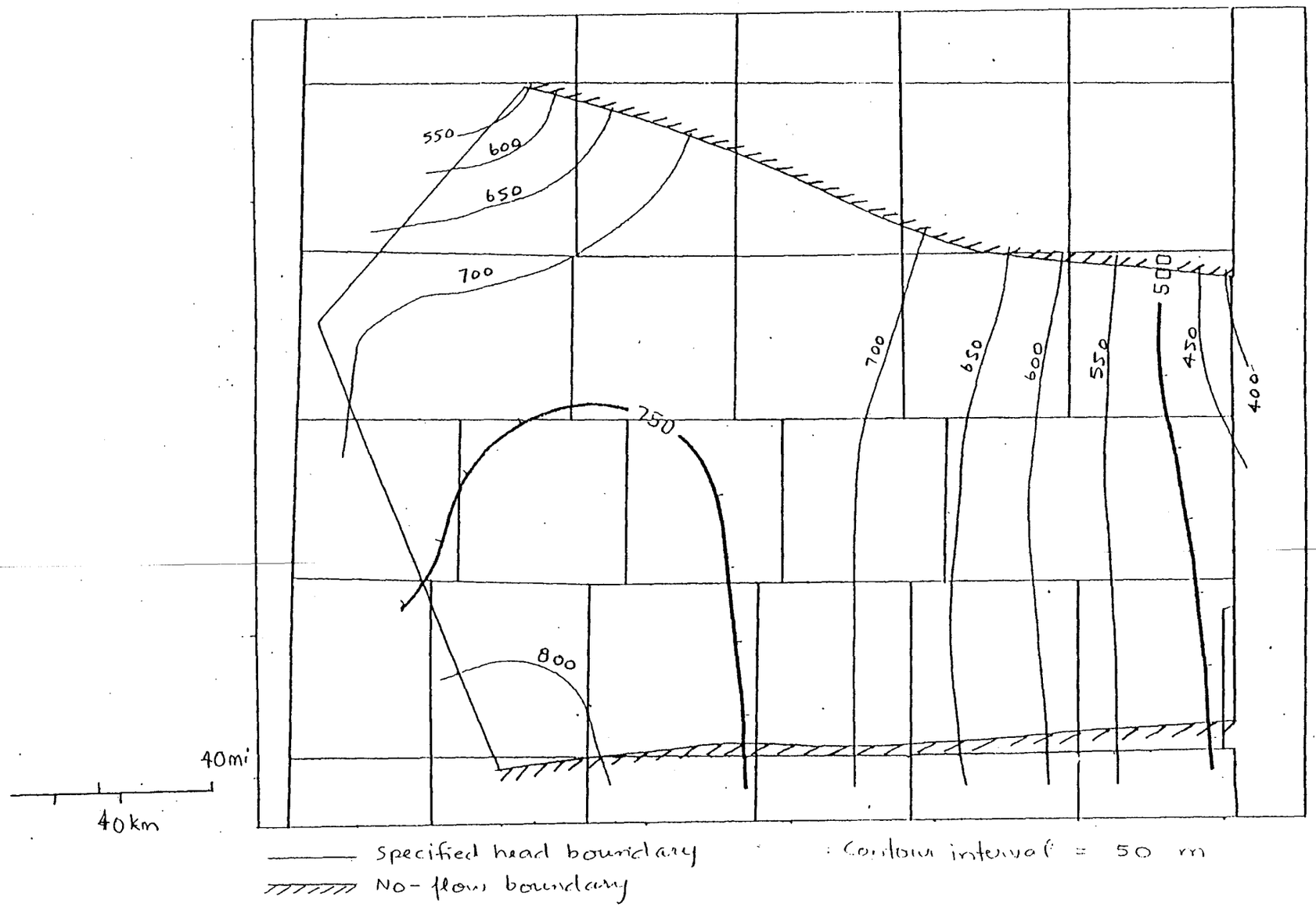

Figure 34. Contours of computed heads, Wolfcamp Aquifer Simulation A-1.

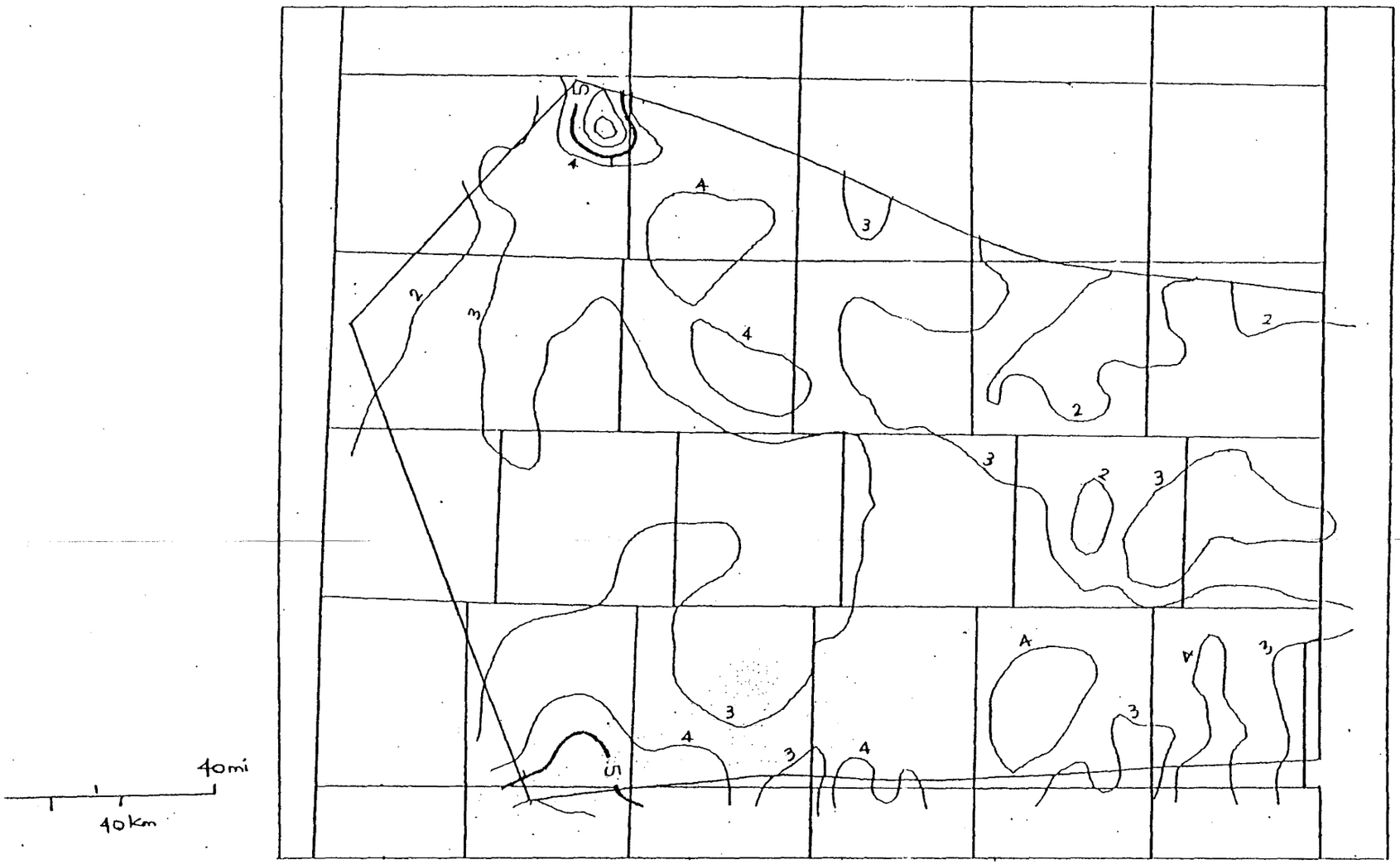

Transmissivity = summation of products of permeability and thickness, m/day
Contour interval = 1 m^2/day

Figure 33. Contours of transmissivity for Wolfcamp Aquifer Simulations A-1 and A-2

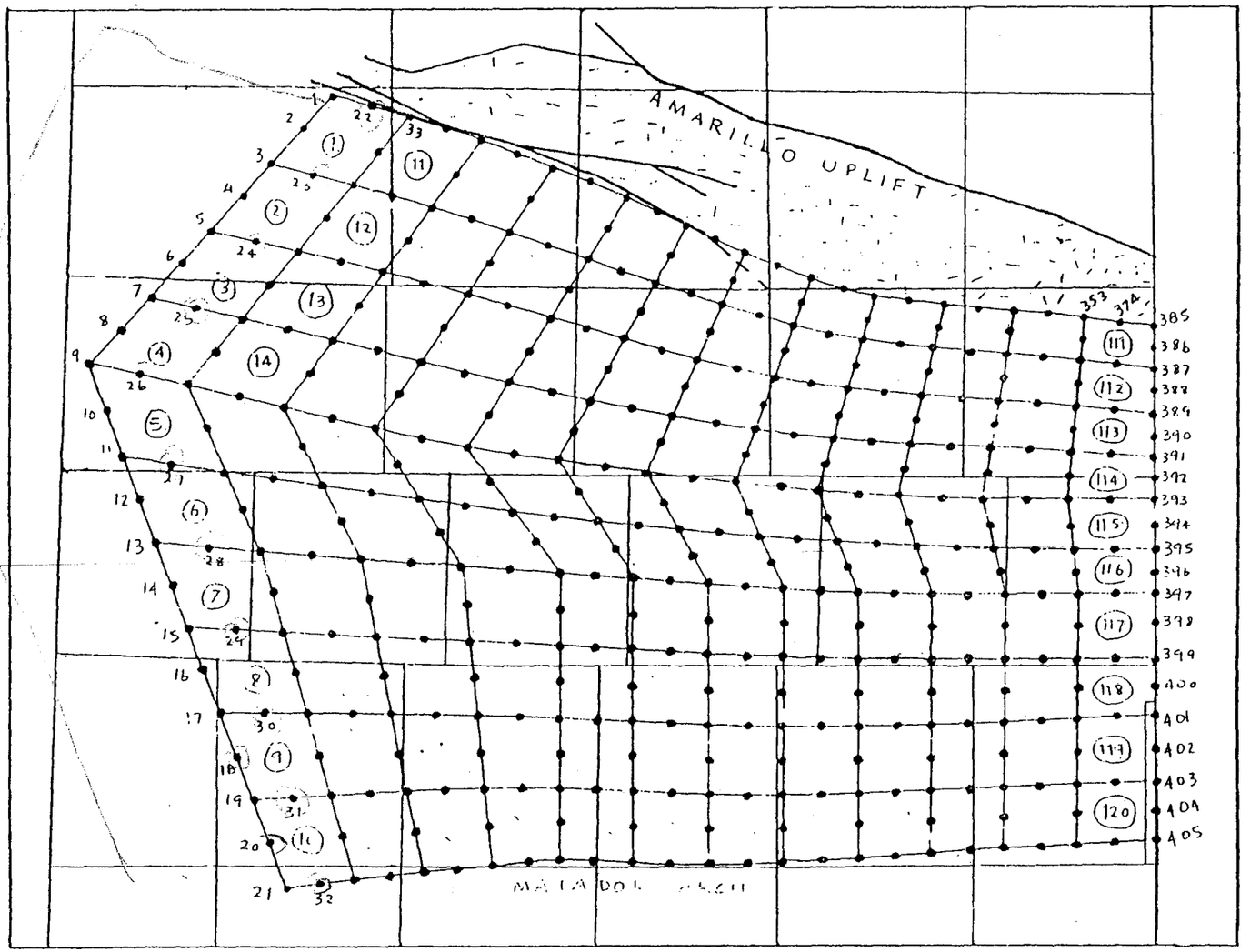

12 × 10
→ 120 el.

Figure 32. Discretized flow region of the Ogallala Aquifer

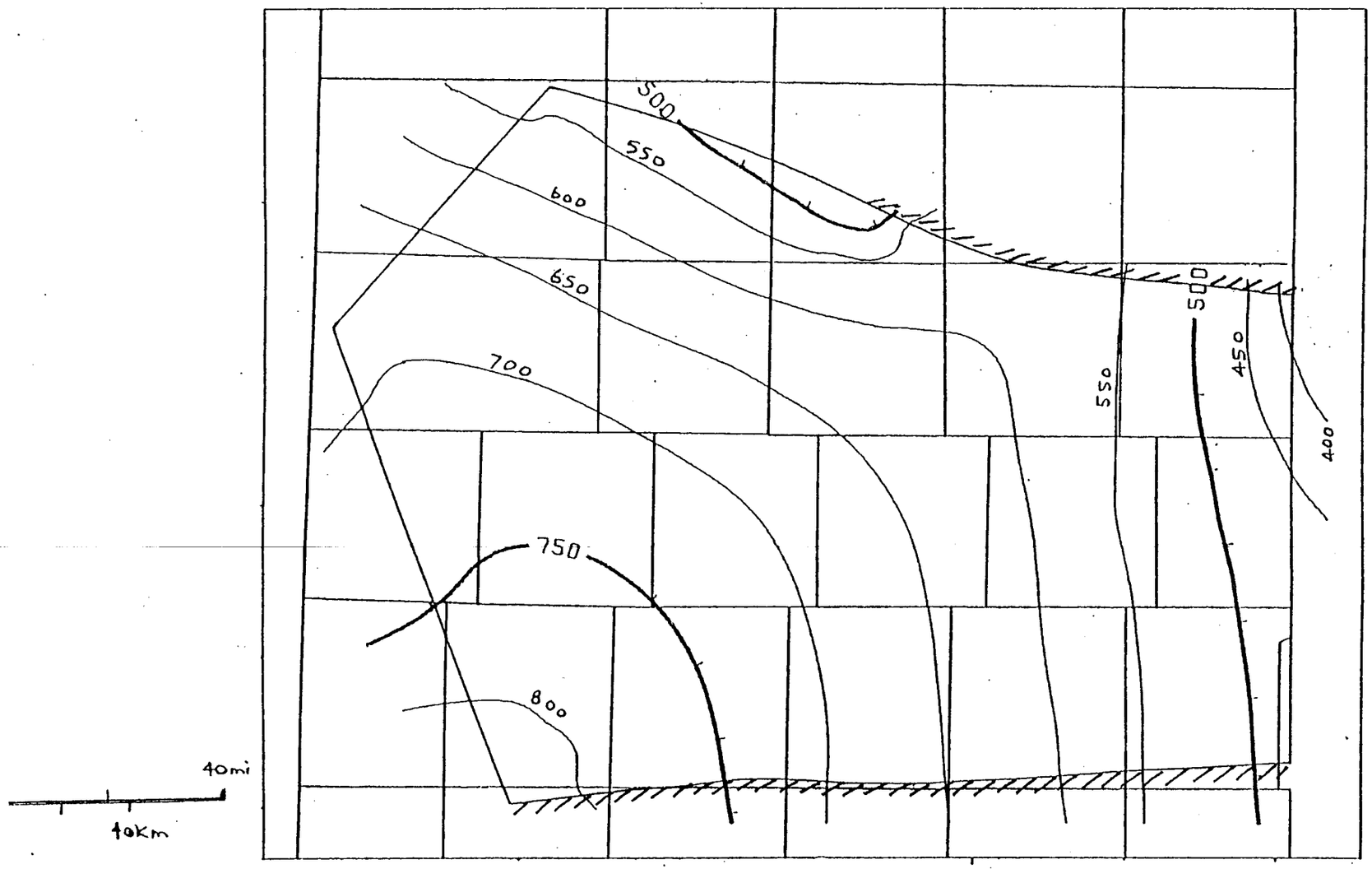

Figure 5. Contours of computed head, Wolfcamp Aquifer simulation A-2.

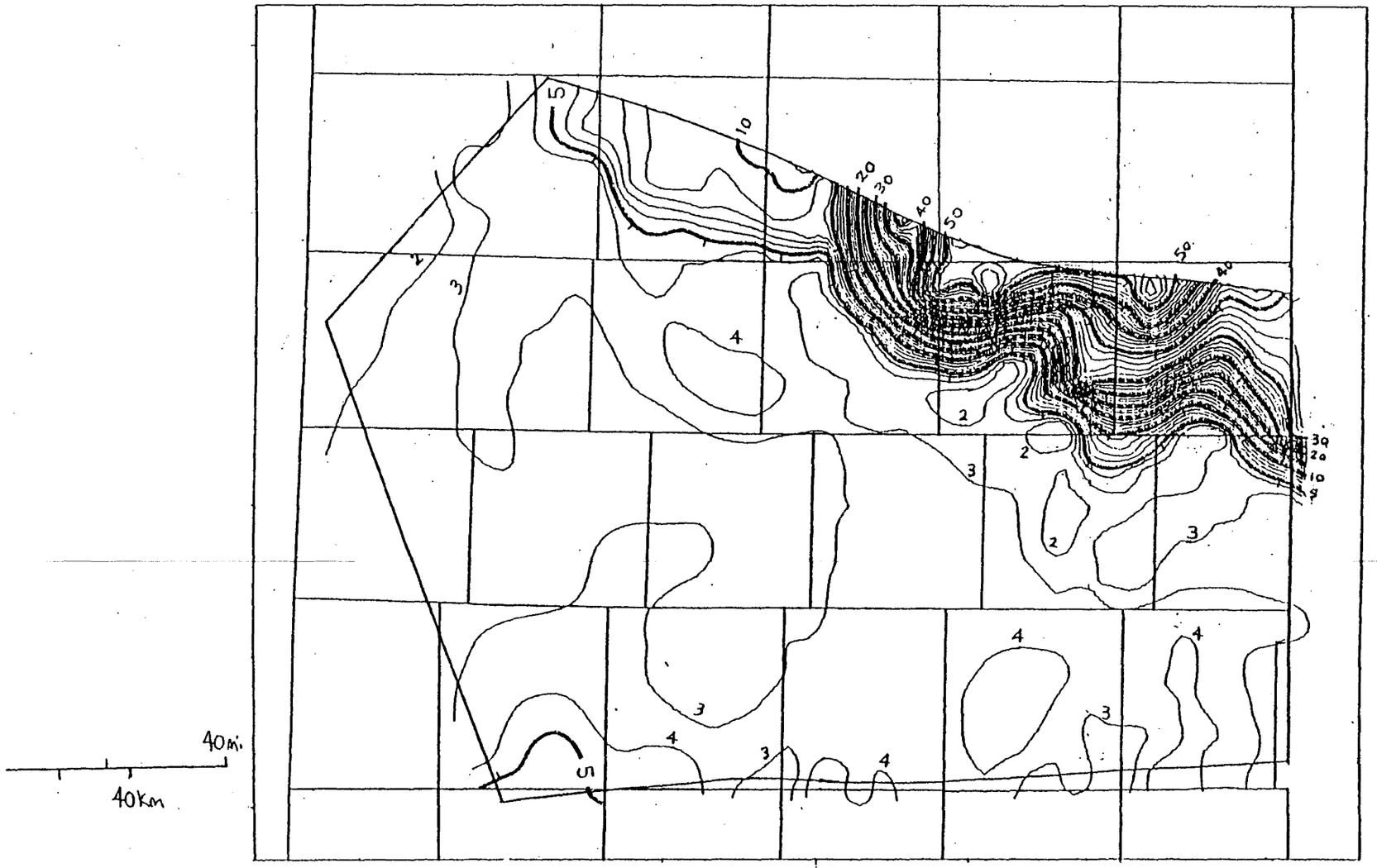

Transmissivity = summation of products of permeability and thickness, m^2/day
Contour interval = 1 m^2/day

Figure 36. Contours of transmissivity for Wolfcamp Aquifer Simulations A-3, B, C, D-1, and D-2.

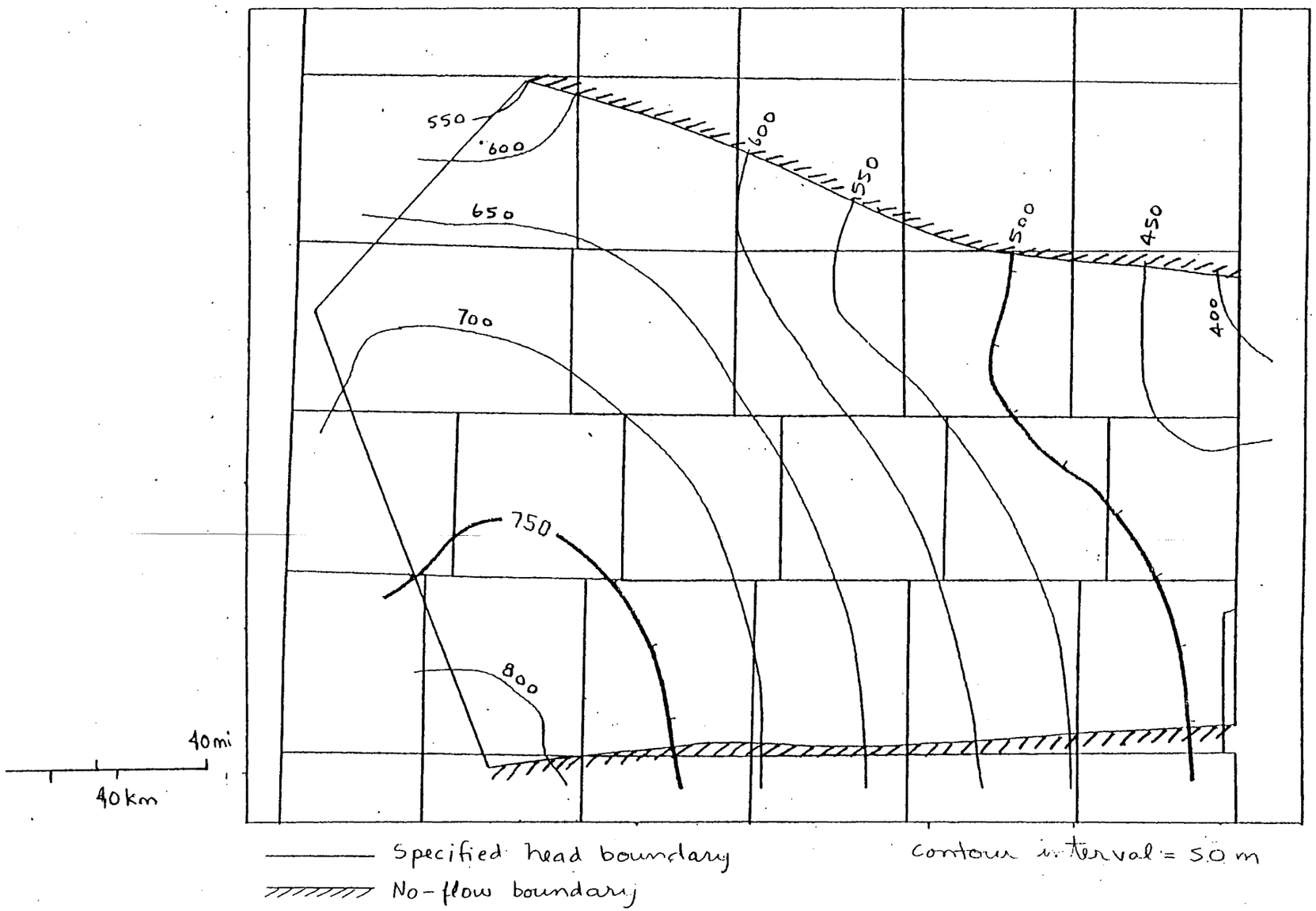

Figure 37. Contours of computed head, Wolfcamp Aquifer Simulation A-3.

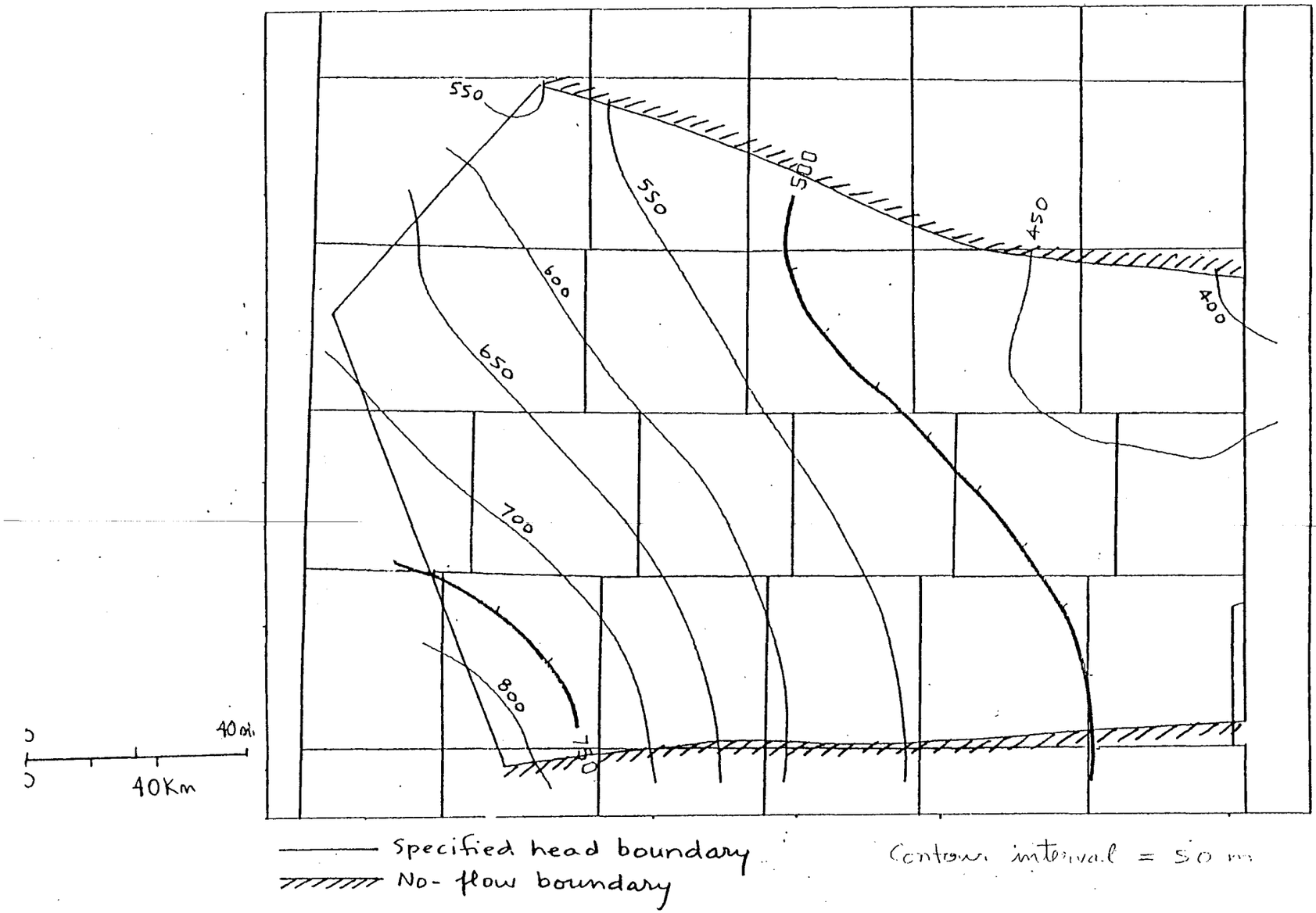

Figure 38. Contours of computed head, Wolfcamp Aquifer Simulation B.

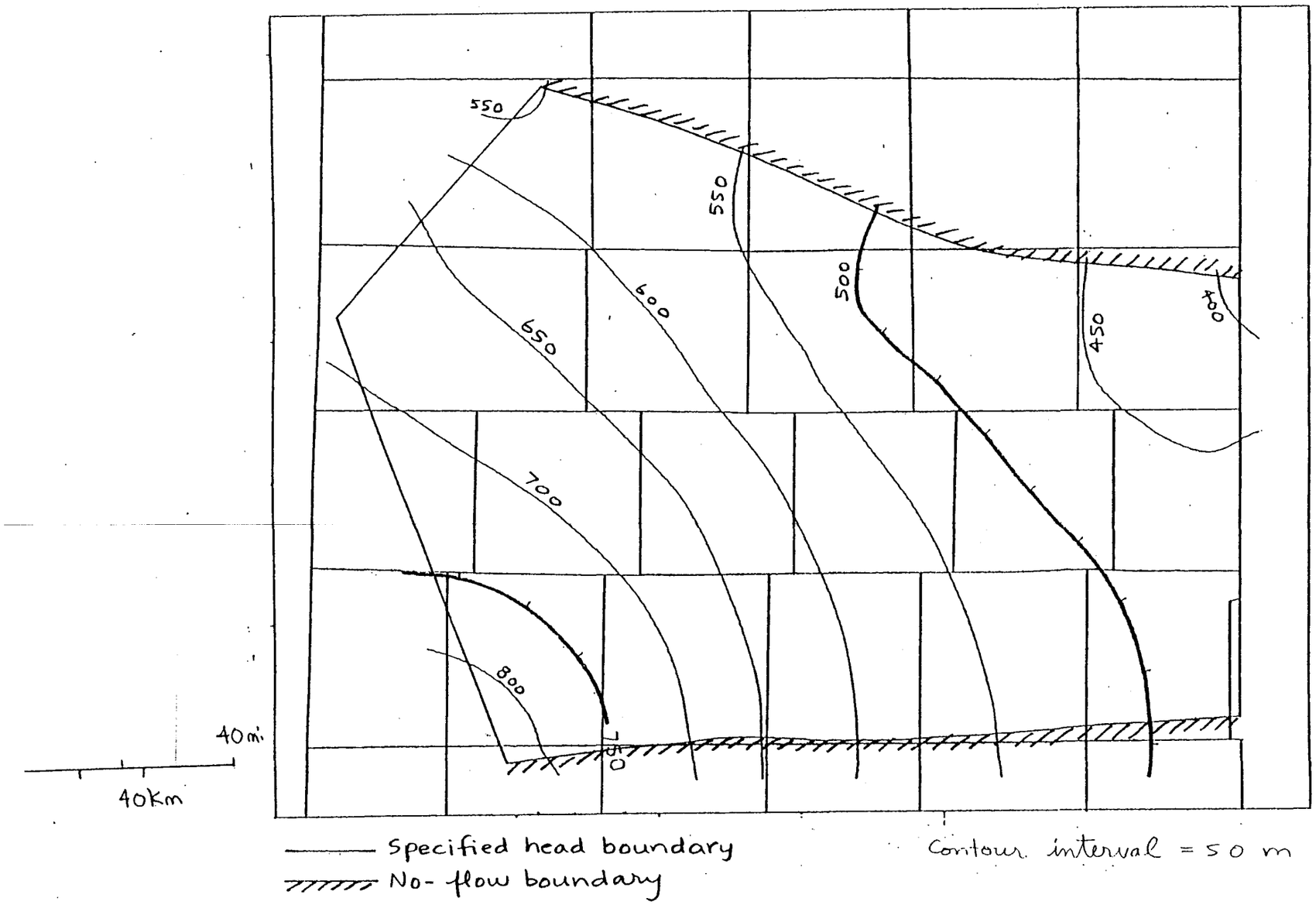

Figure 39. Contours of computed head, Wolfcamp Aquifer Simulation C

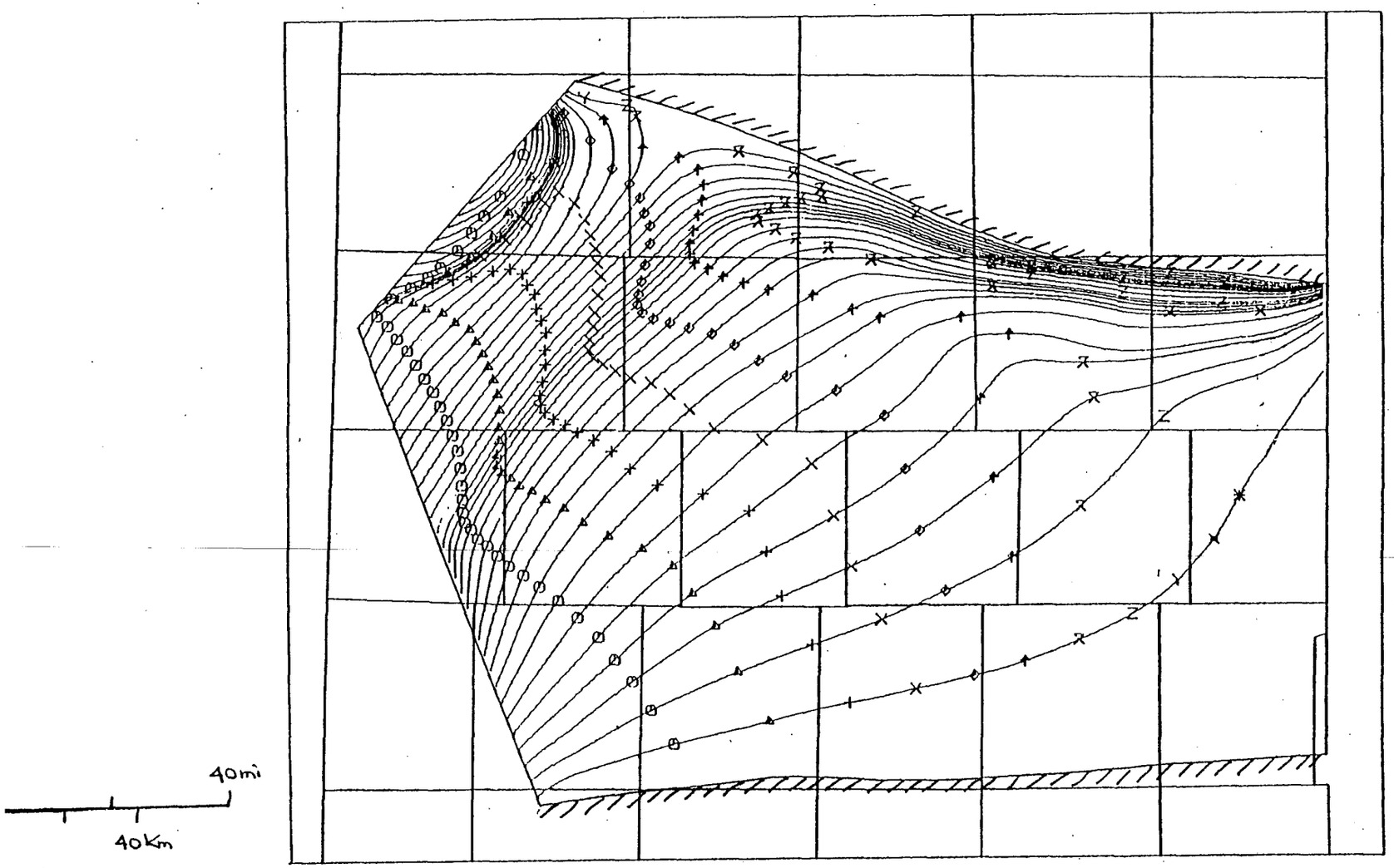

Travel-time interval between marks along streamlines = 400,000 years

——— Specified head boundary

/////// No-flow boundary

Figure 40 Streamlines and travel times, Wolfcamp Aquifer Simulation C.

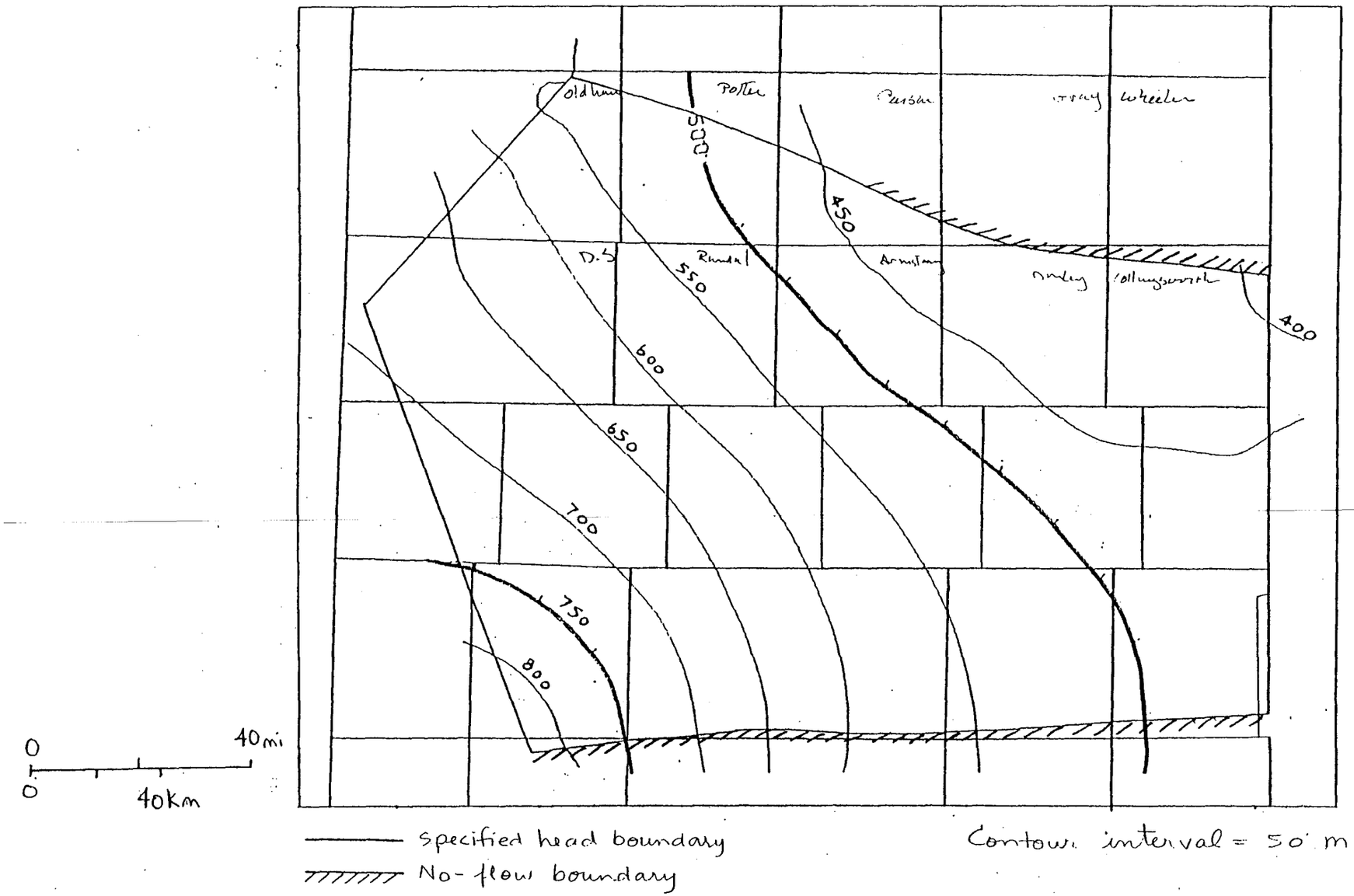

Figure 41. Contours of computed head, Wolfcamp Aquifer Simulation D-1.

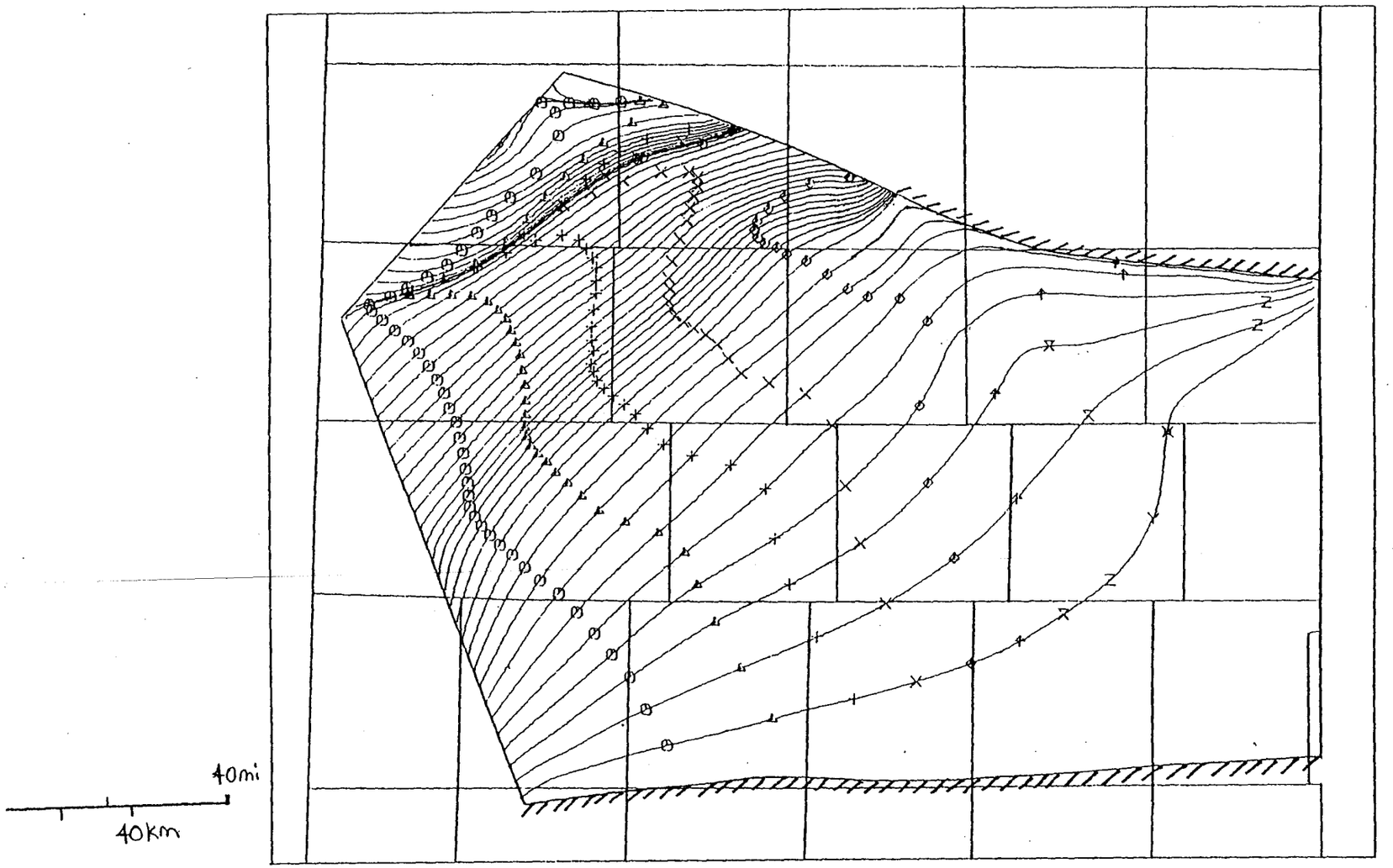

Travel-time interval between marks along streamlines = 400,000 years

——— Specified head boundary

////// No-flow boundary

Figure 42. Streamlines and travel times, Wolfcamp Aquifer Simulation D-1

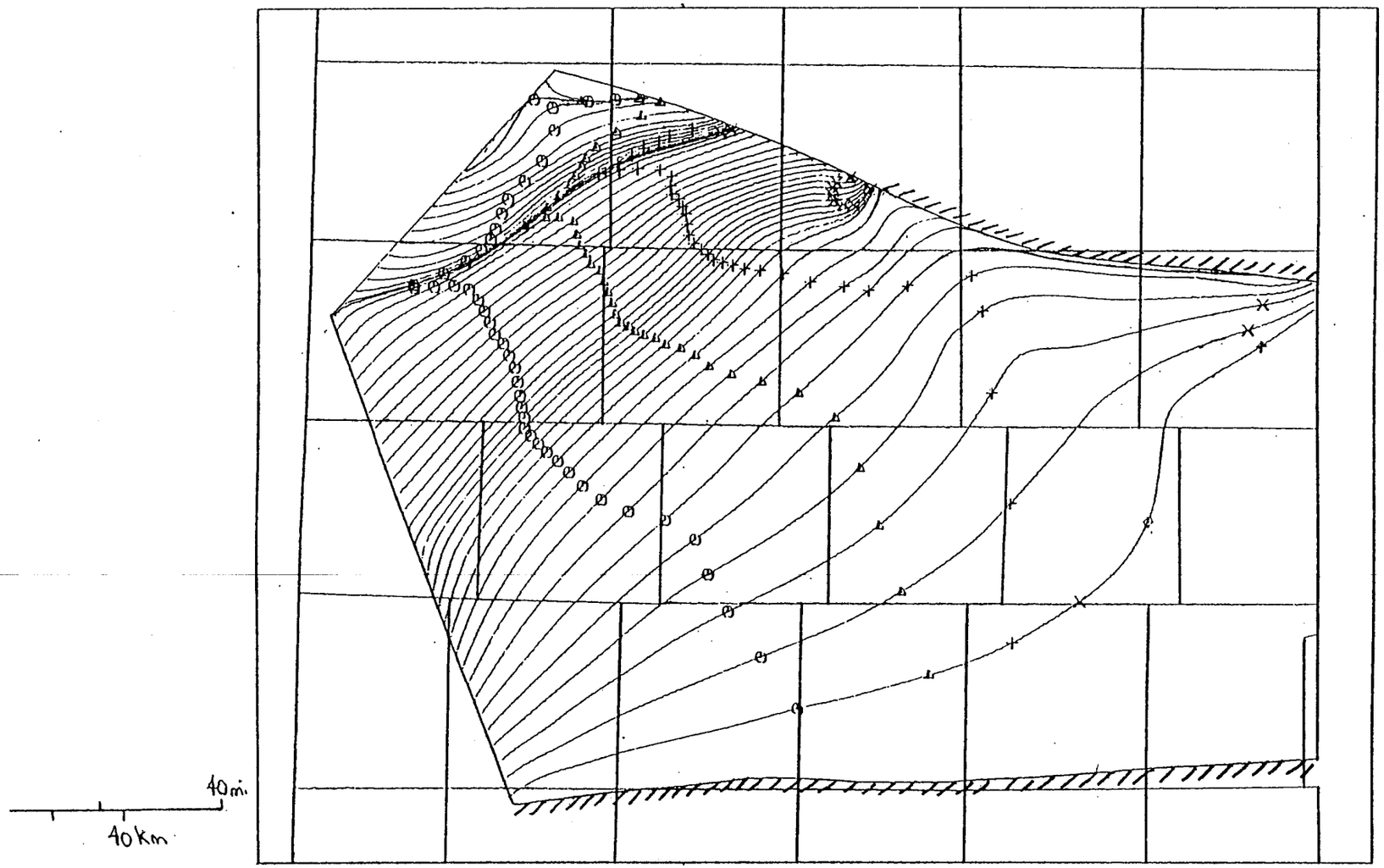

Travel-time interval between marked streamlines = 400,000 years

——— Specified head boundary

NO-flow boundary

Figure 43. Streamlines and travel times, Wolfcamp Aquifer Simulation D-2.

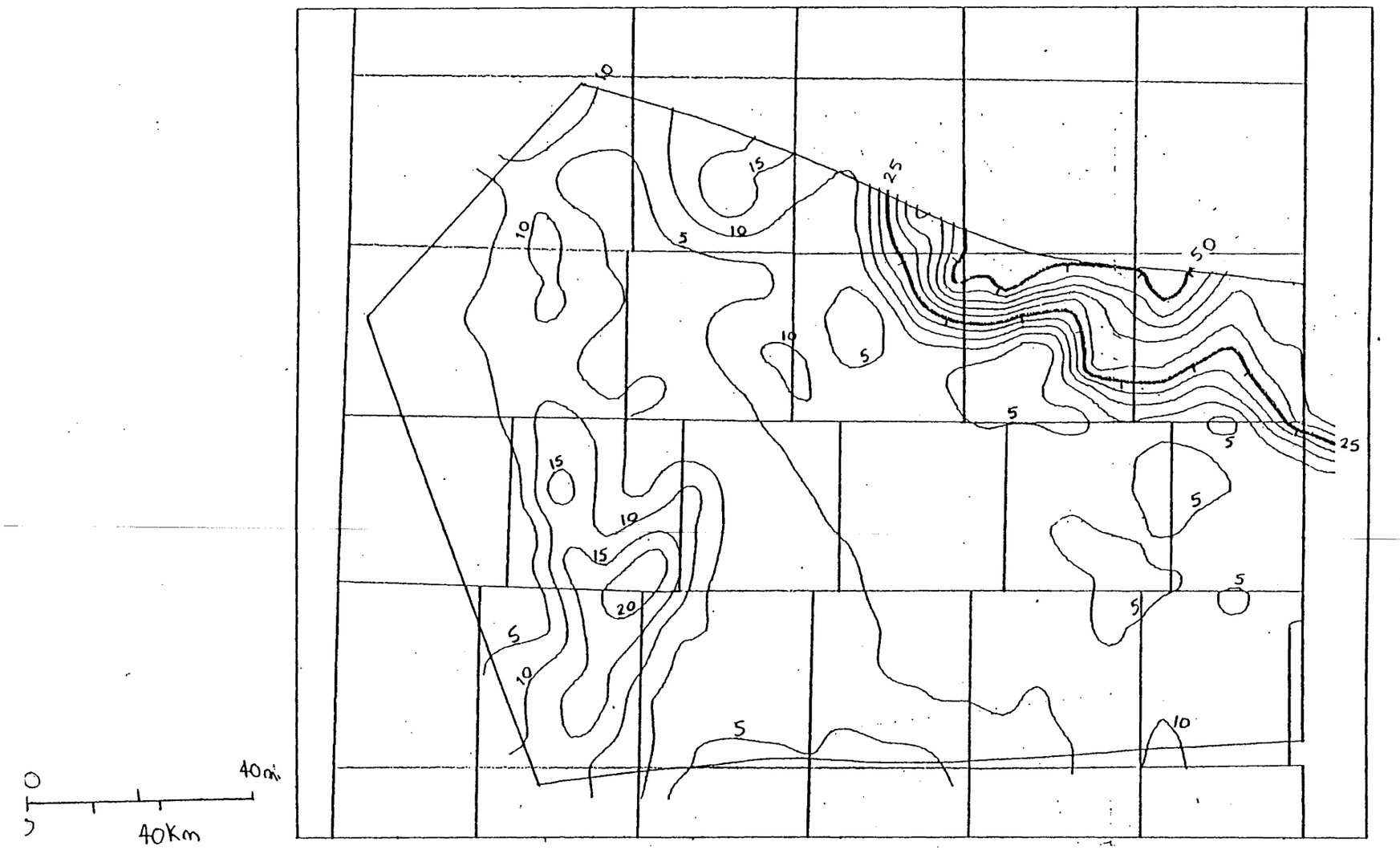

Transmissivity = summation of products of permeability and thickness, m^2/day
Contour interval = 5 m^2/day

Figure 14. Contours of transmissivity for Wolfcamp Aquifer Simulation E.

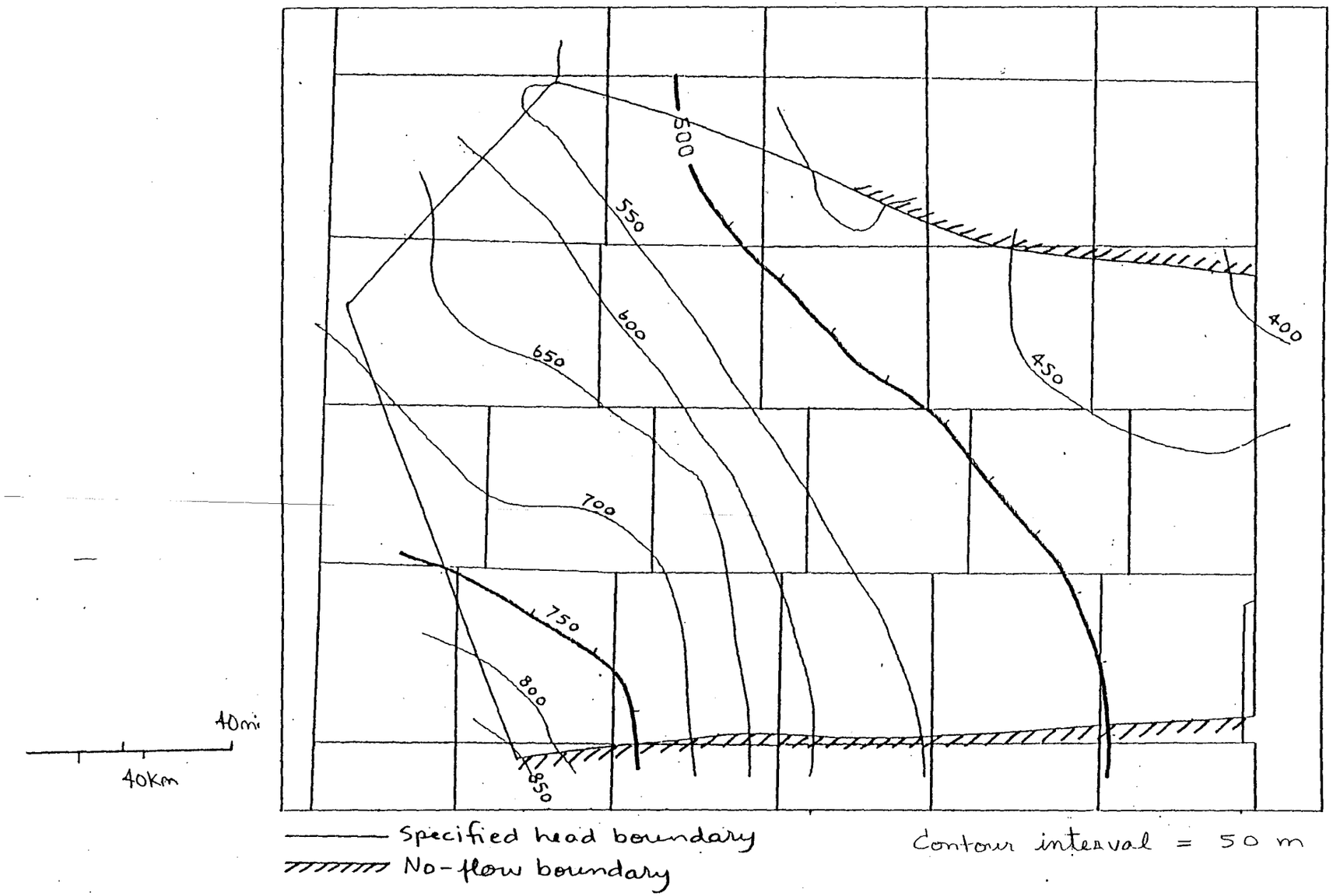

Figure 45. Contours of computed head, Wolfcamp Aquifer Simulation E.

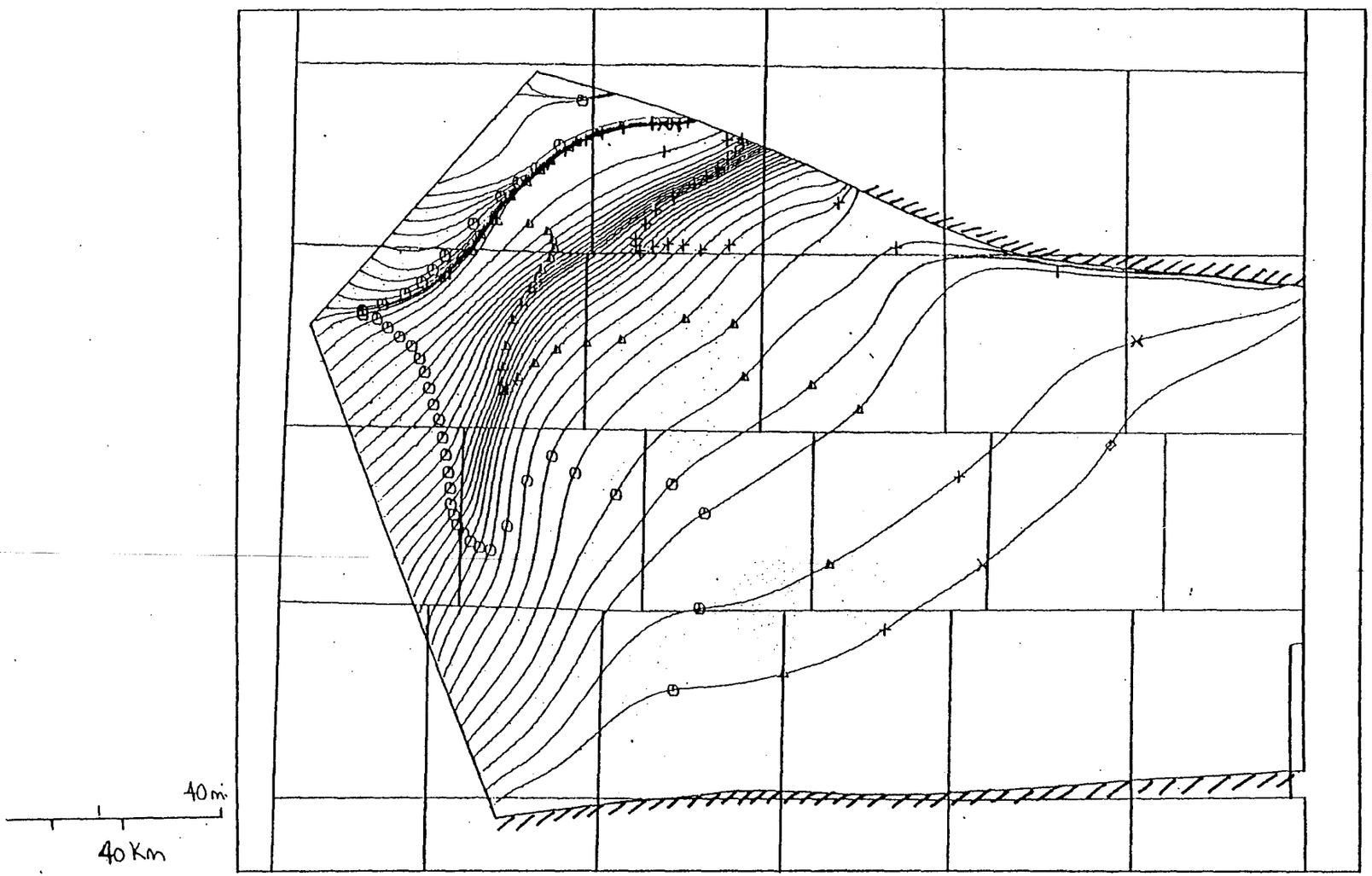

Travel-time interval between marks along streamlines = 400,000 years

——— Specified head boundary

//////// No-flow boundary

Figure 46. Streamlines and travel times, Wolfcamp Aquifer Simulation E.

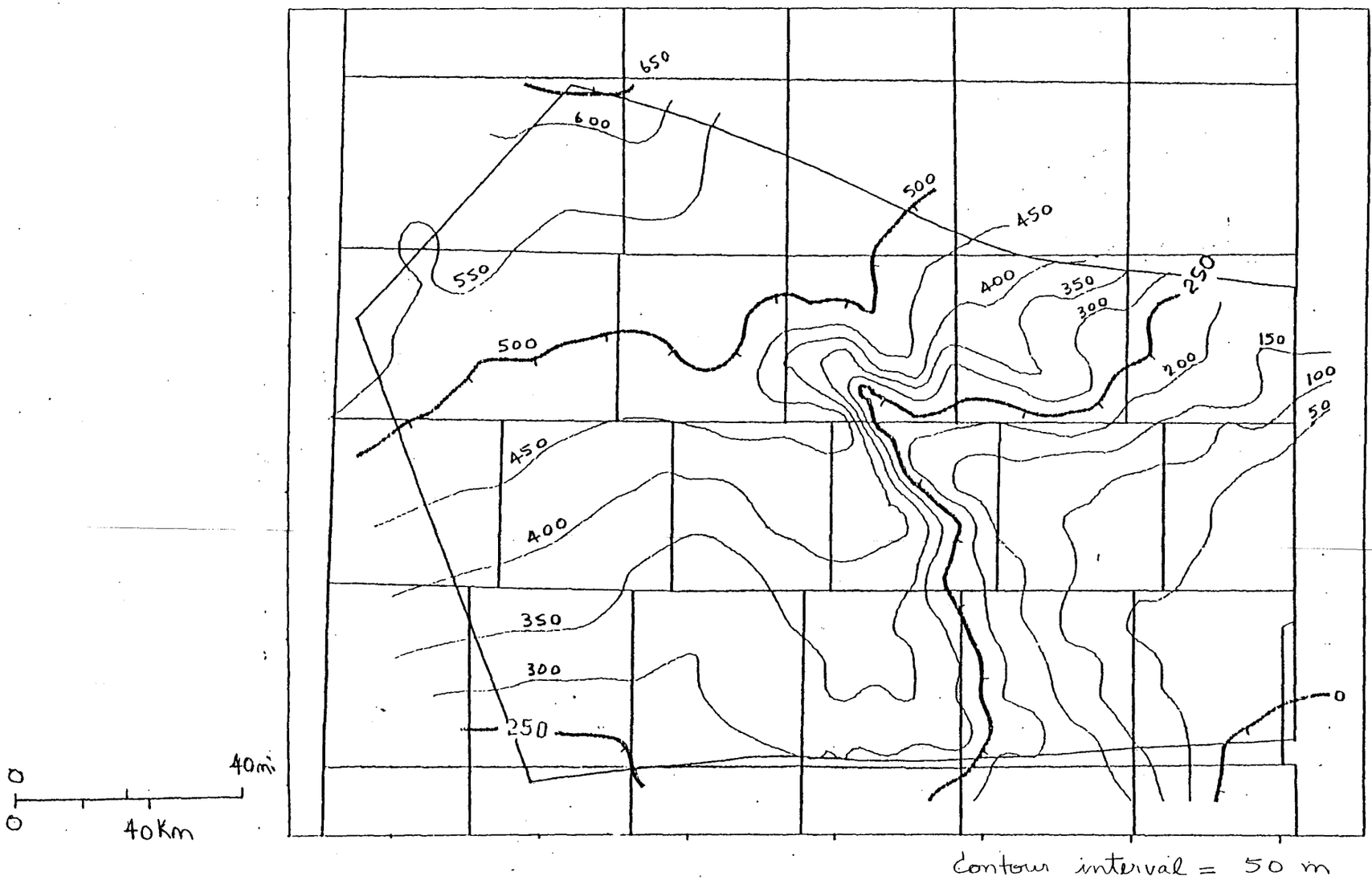

Figure 47. Contours of head difference between the Upper Ogallala - Dockum Aquifer and the Wolfcampian Aquifer (computed from Figure 22 and the computed head of Simulation E).

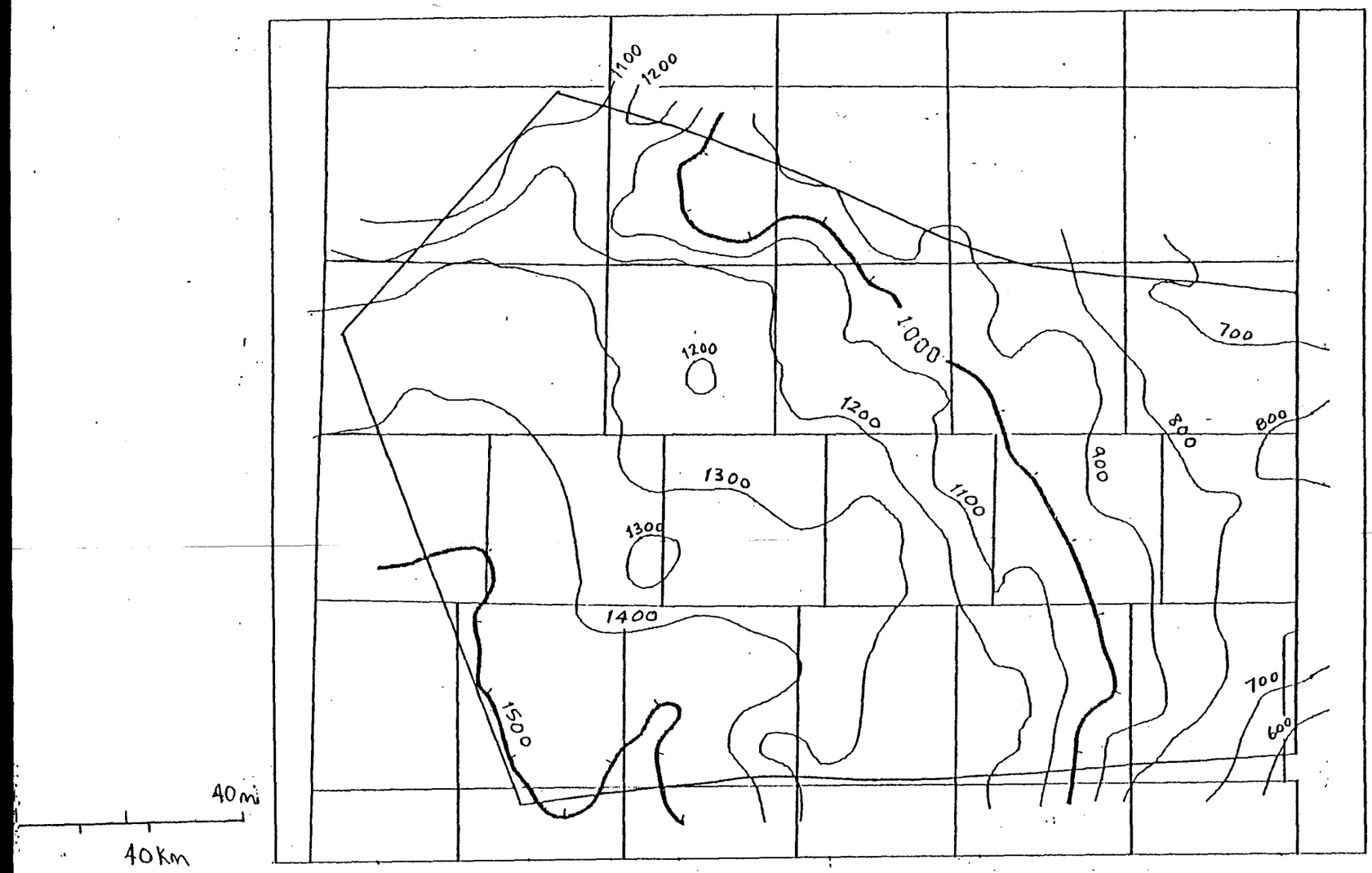

Figure 48. Contours of the Evaporite strata's thickness.

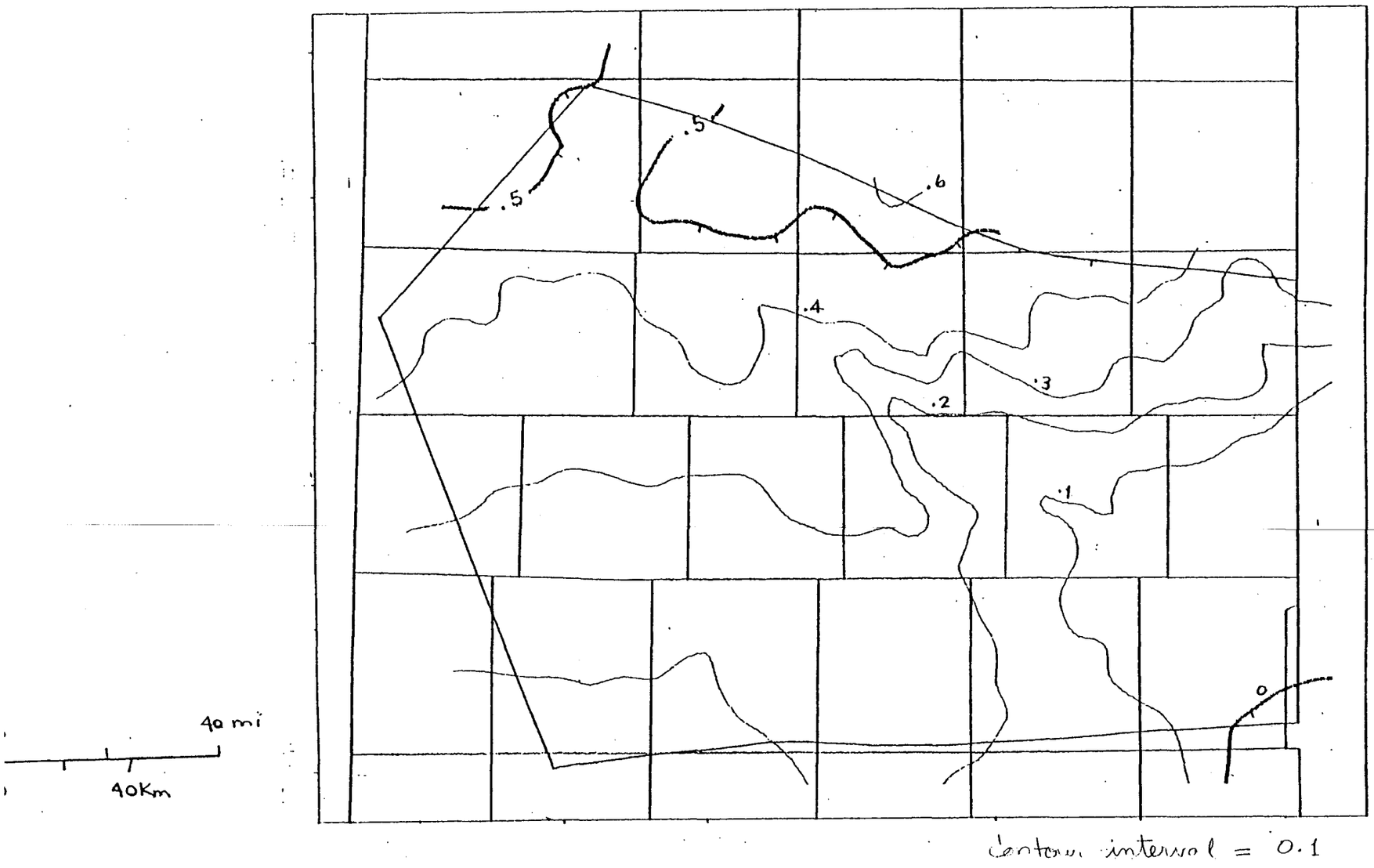

Figure 49. Contours of leakage gradient through the Evaporite strata. The leakage gradient is obtained from dividing the head difference (fig 50) by

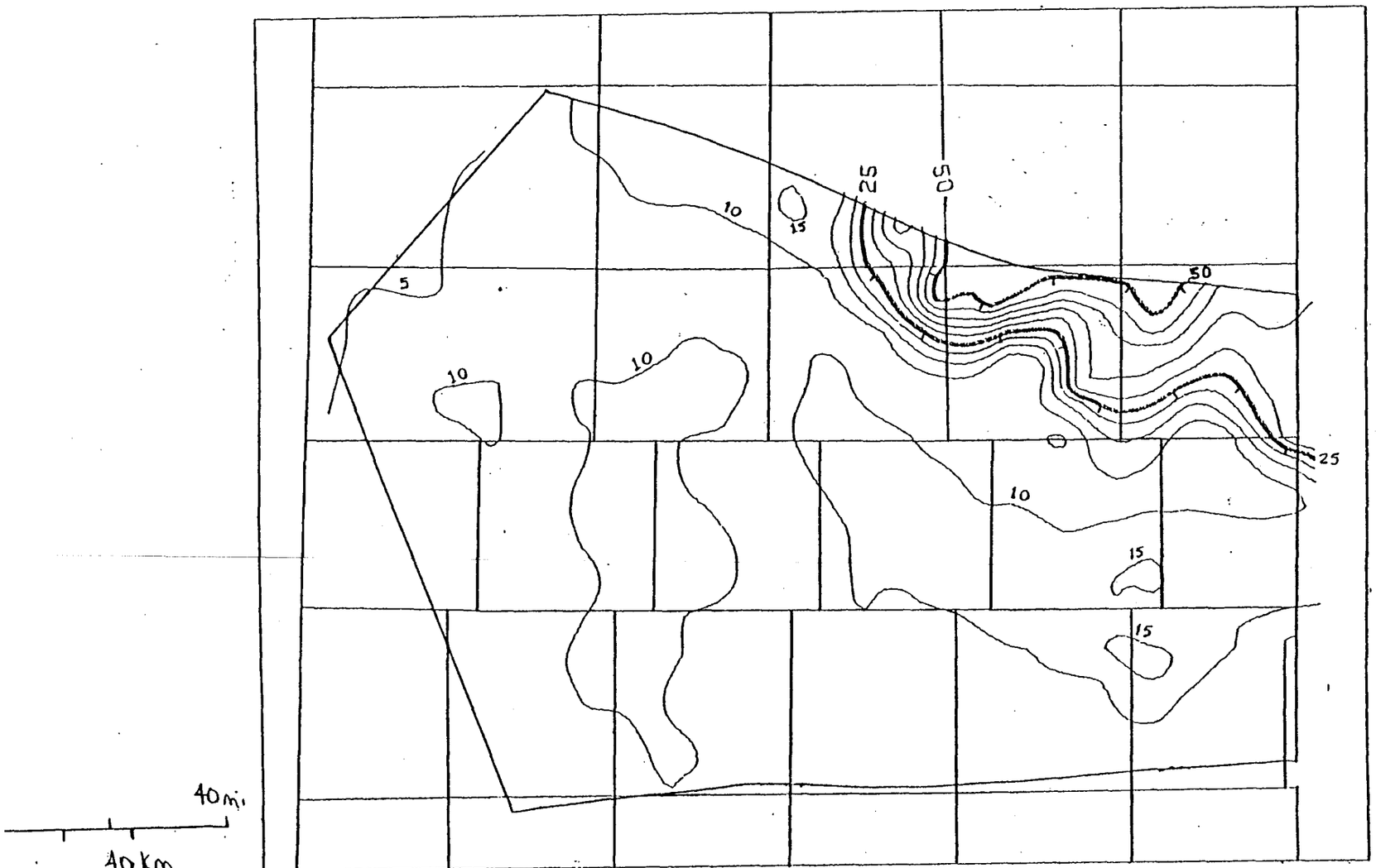

Transmissivity = summation of products of permeability and thickness, m^2/day
Contour interval = 5 m^2/day

Figure 50. Contours of transmissivity for Deep-Brine Aquifer Simulation A.

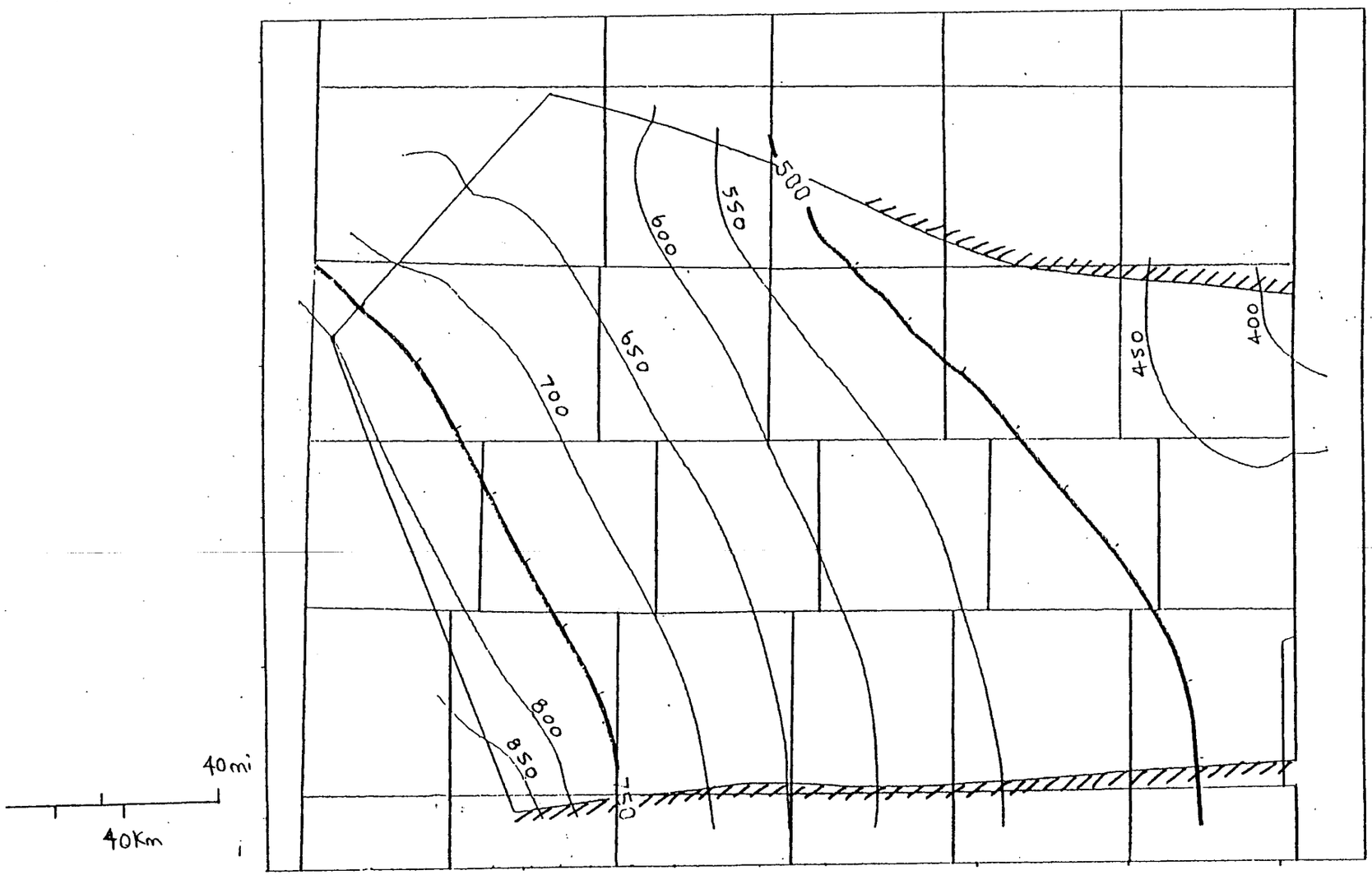

Figure 51. Contours of potential head, Deep-Brine Aquifer simulation A.

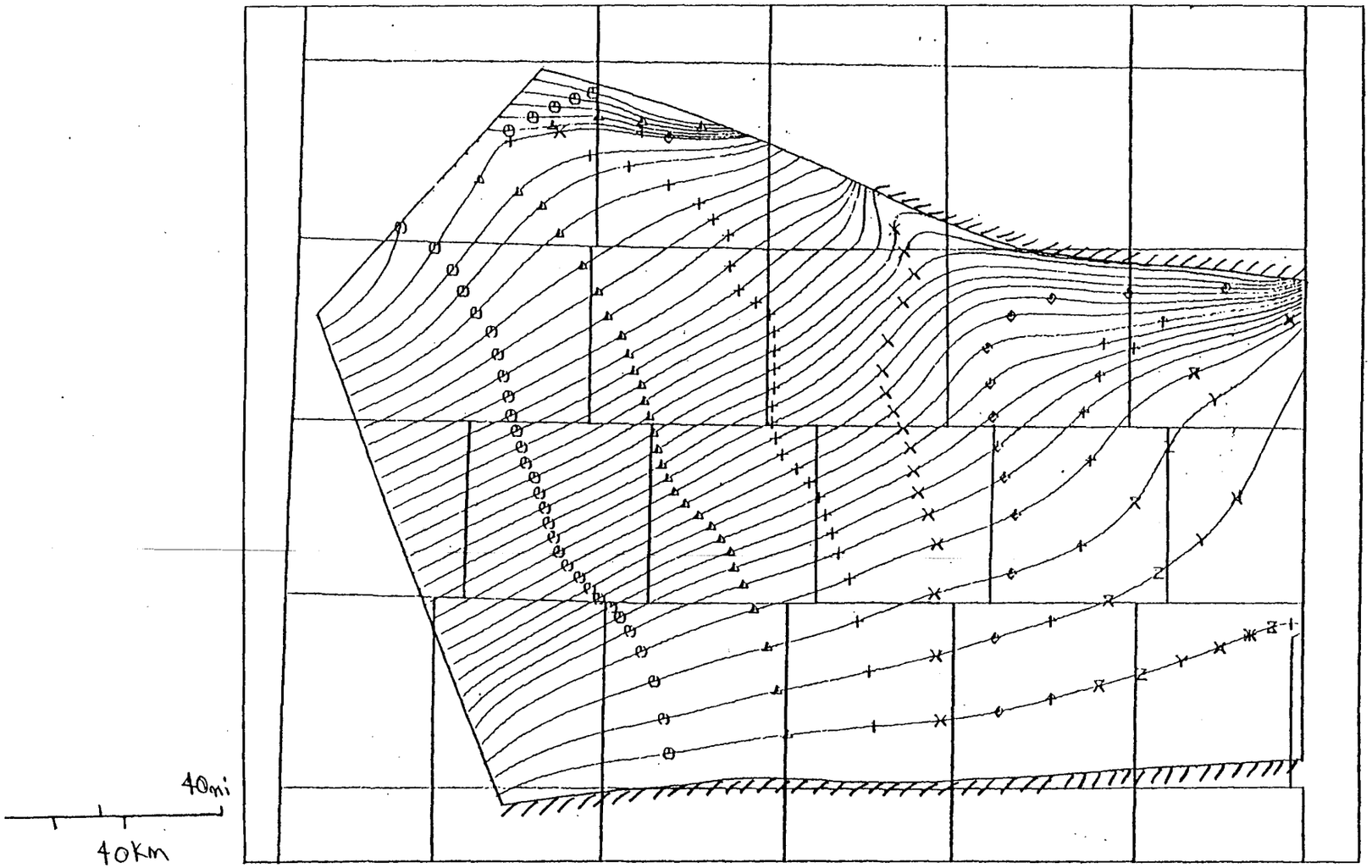

Travel-time interval between marks along streamlines = 400,000 years

——— Specified head boundary

////// No-flow boundary

Figure 52. Streamlines and travel times, Deep-Brine Aquifer Simulation A.

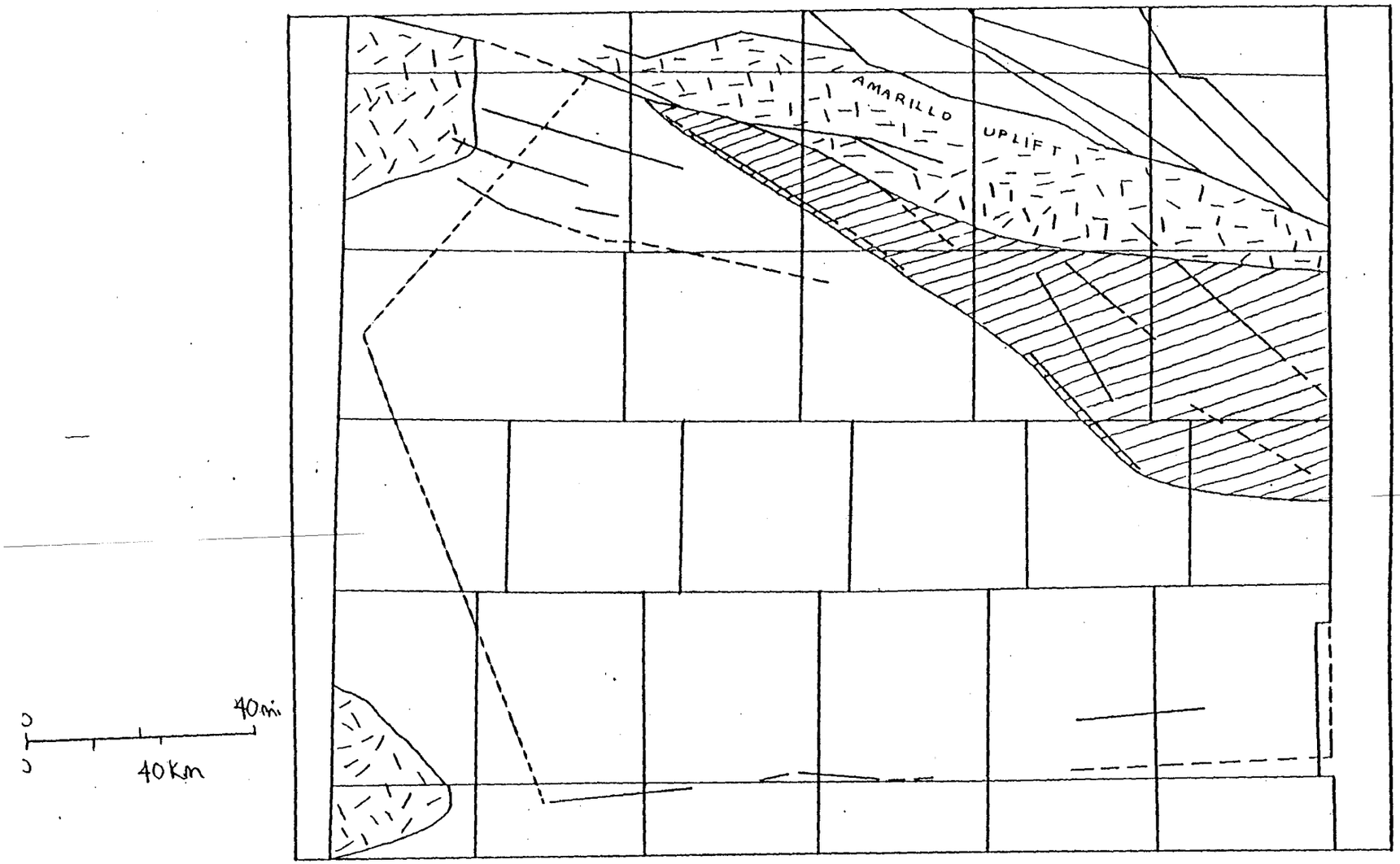

Figure 53. Deep-Brine Aquifer Simulations B and C; zone of granite-wash coarsening

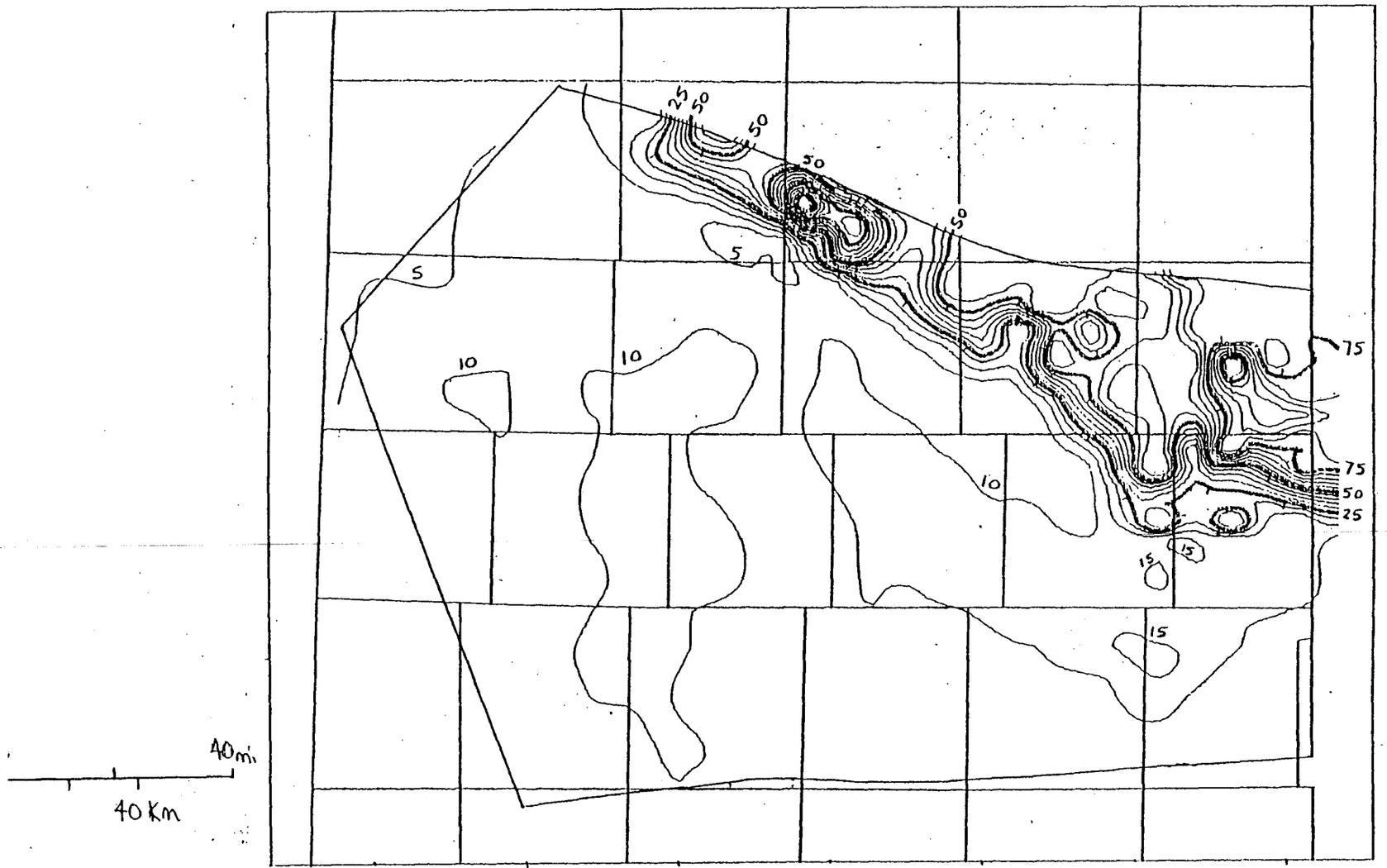

Transmissivity = summation of products of permeability and thickness, m^2/day
Contour interval = 5 m^2/day

Figure 54. Contours of transmissivity for Deep-Brine Aquifer Simulation B.

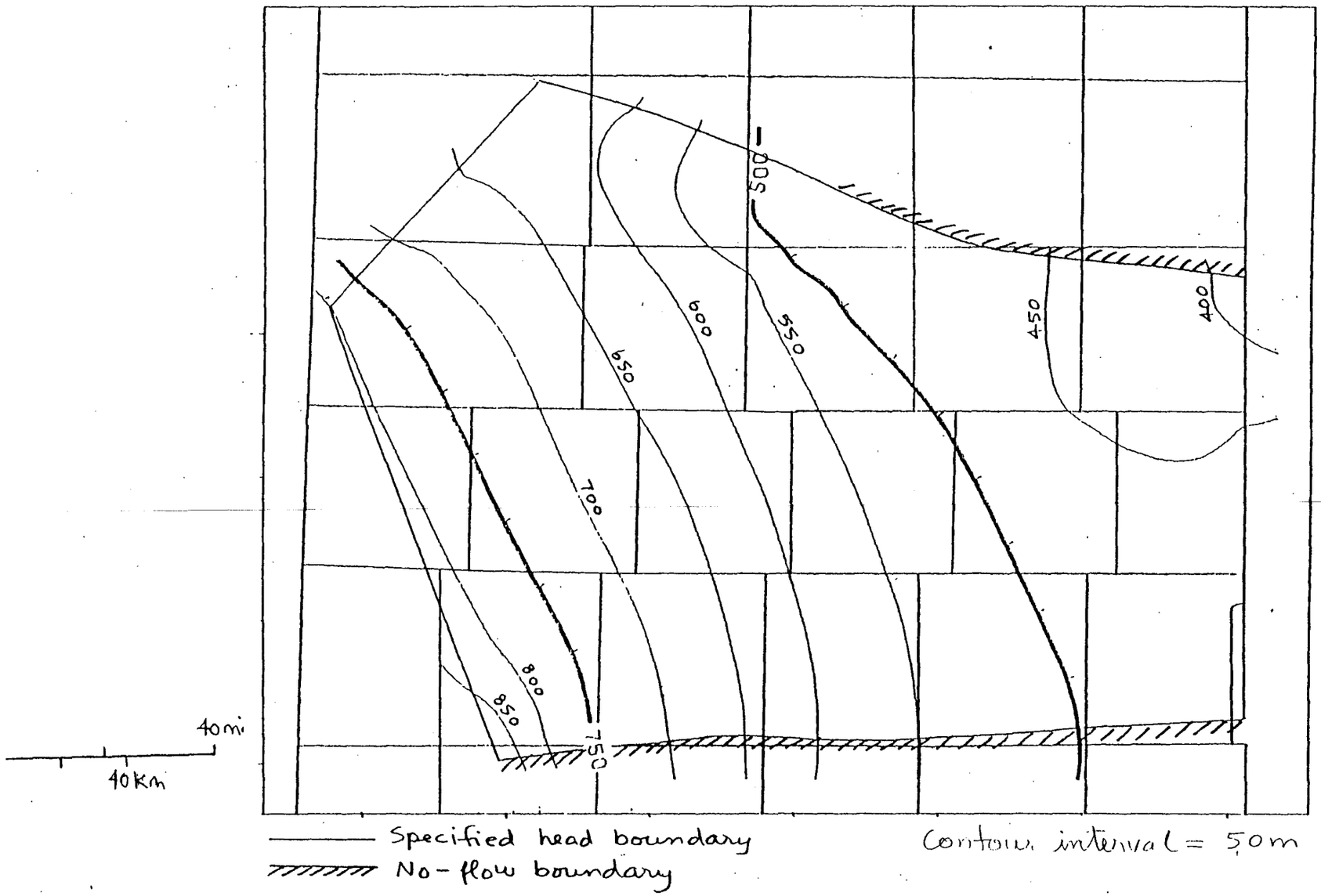

Figure 55. Contours of computed head, Deep-Brine Aquifer Simulation B.

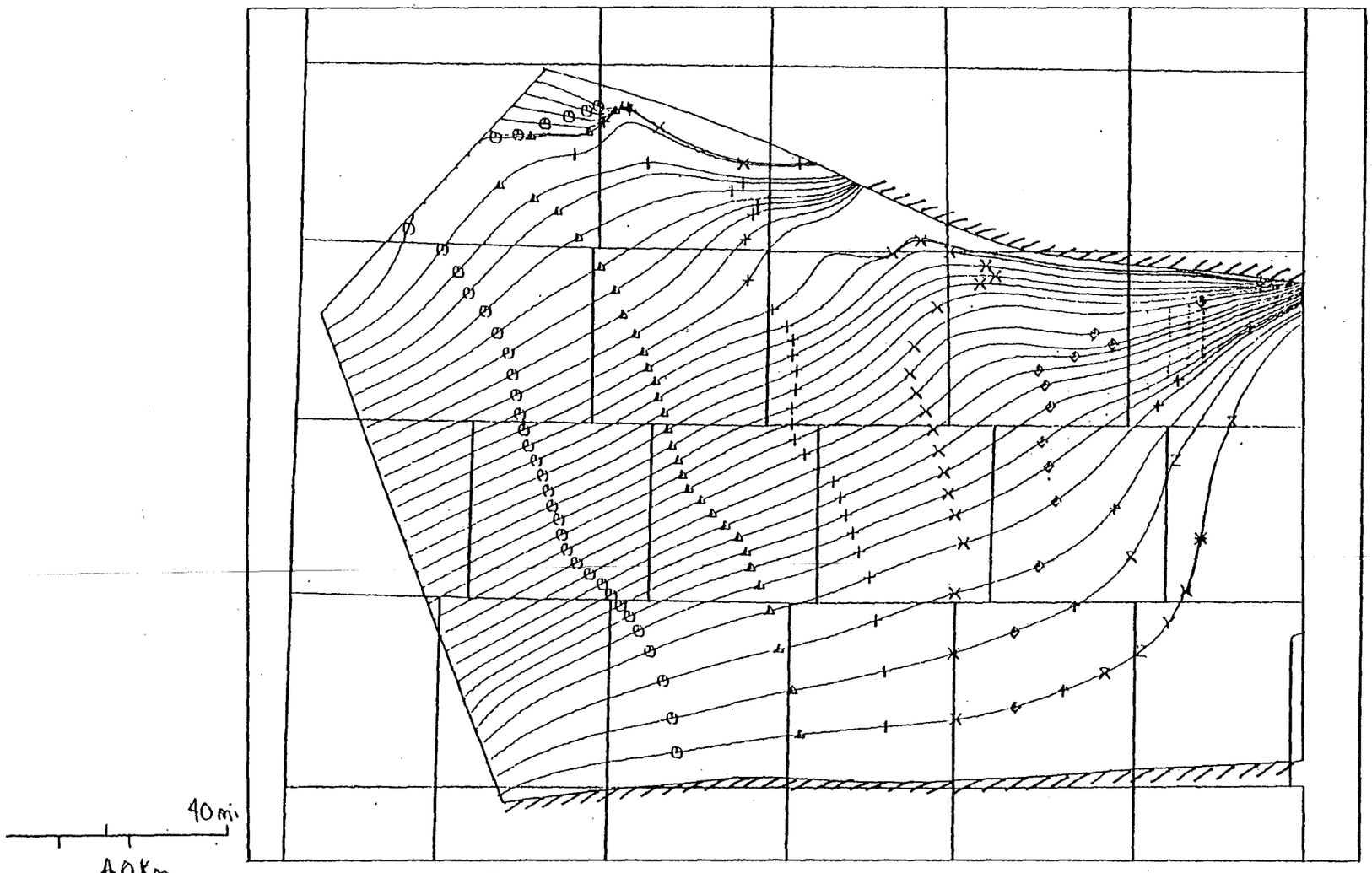

Travel-time interval between marks along streamlines = 400,000 years

——— Specified head boundary

///////// No-flow boundary

Figure 56. Streamlines and travel times, Deep-Brine Aquifer Simulation B.

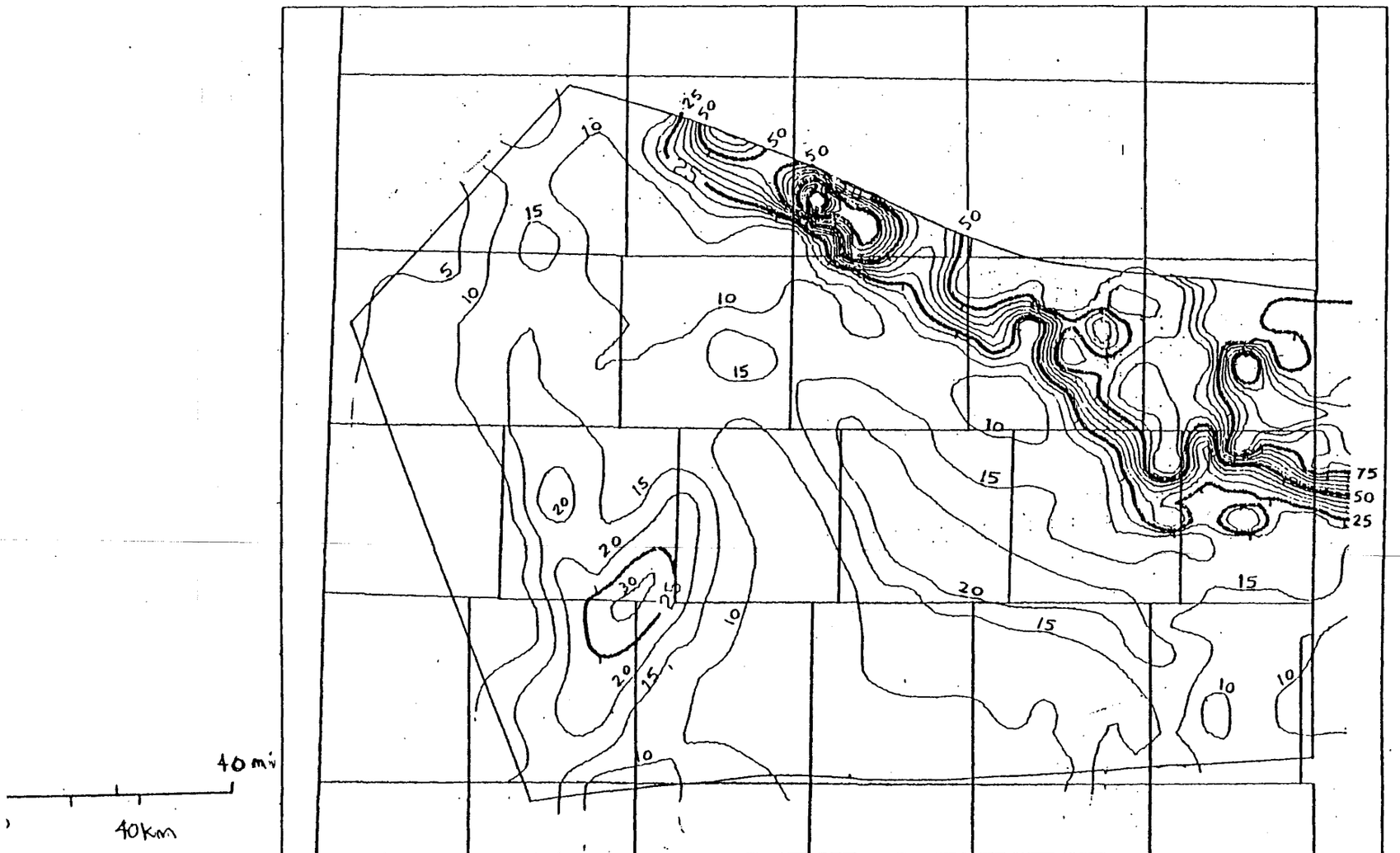

Figure 57. Contours of transmissivity for Deep-Brine Aquifer Simulation C.

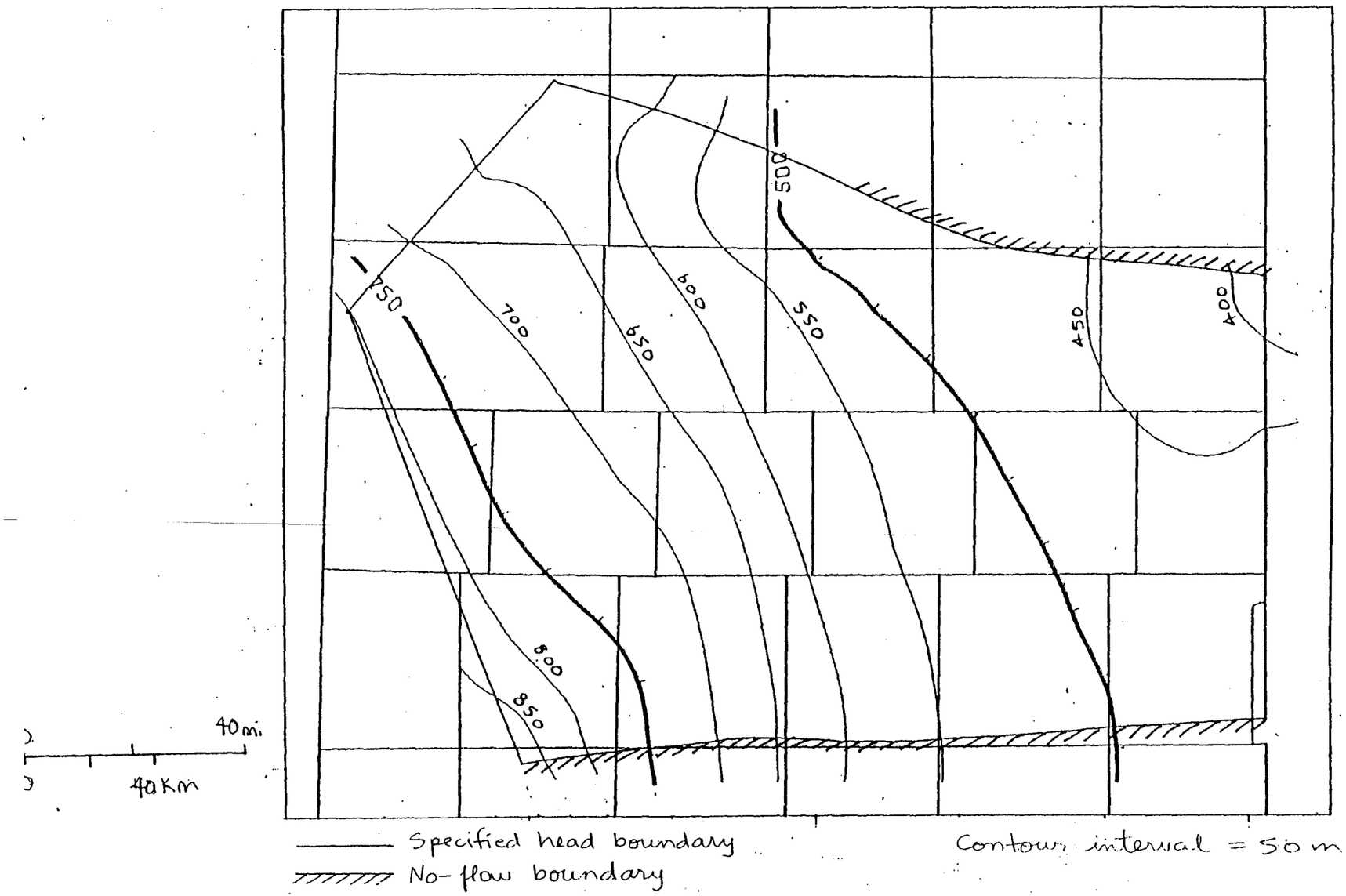

Figure 58. Contours of computed head, Deep-Living Aquifer Simulation C.

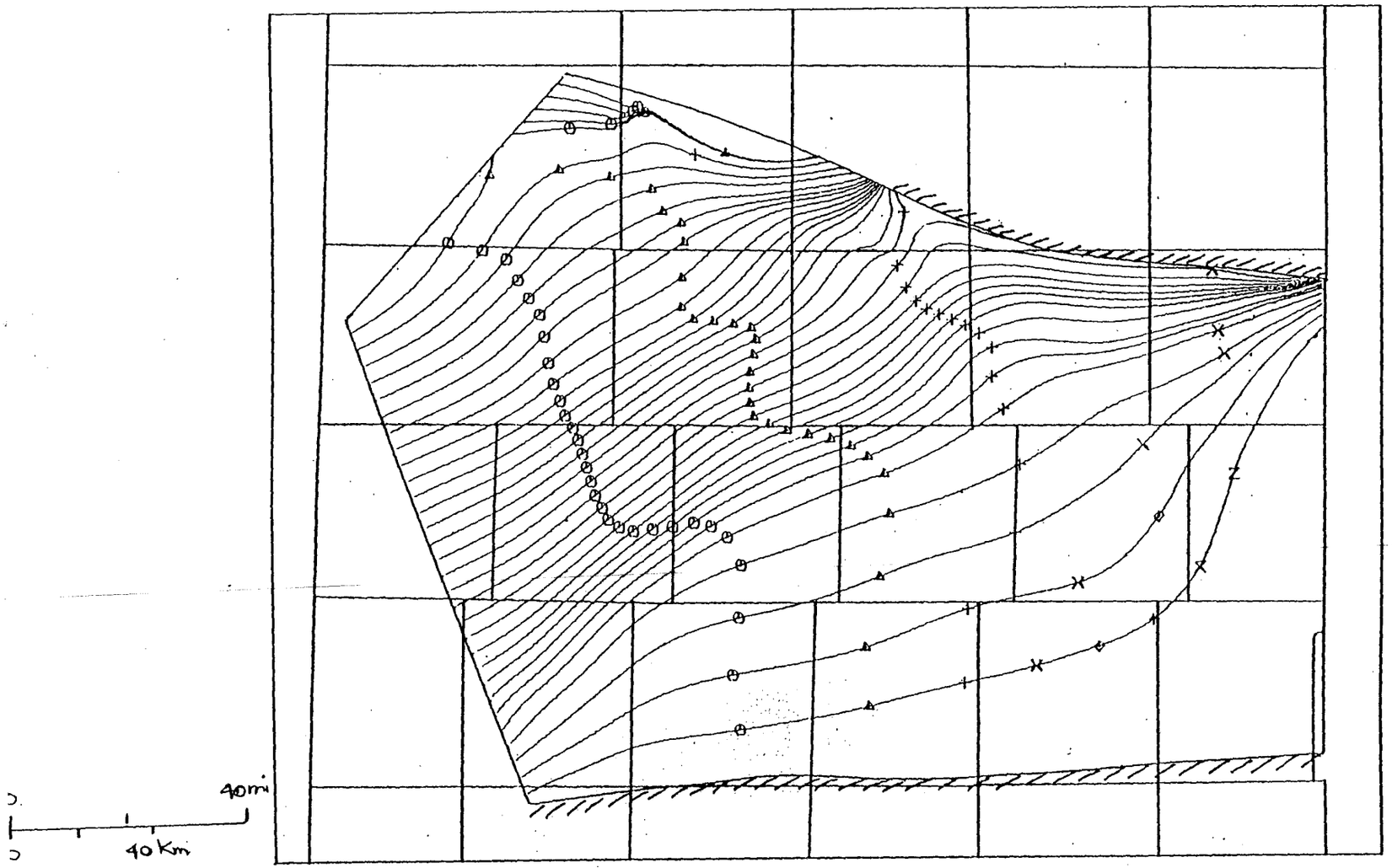

Travel-time interval between marks on streamlines = 400,000 years

——— Specified head boundary

≈≈≈≈≈ No-flow boundary

Figure 59. Streamlines and travel times, Deep-Bedrock Aquifer Simulation C.

APPENDIX

Table A-1. Vertically-averaged head data for the whole Deep-Brine Aquifer

Class H head data					
ID*	Latitude	Longtitude	X, m**	Y, m**	Head, m
			19.2"		
DOEM1	35.43778	102.38510	125468.	225176.	643.6
DOES1	35.02763	100.84681	266875.	180141.	426.9
DOEZ1	34.51282	101.66131	192002.	123615.	707.7
15	35.51130	102.52788	112343.	233248.	671.5
17	35.39428	102.39428	124624.	220399.	679.7
18	35.43734	102.45786	118780.	225127.	646.8
19	35.59620	102.65120	101007.	242570.	587.2
21	35.46904	102.23750	139036.	228608.	696.3
22	35.33622	102.20307	142201.	214024.	690.9
25	35.40704	102.34653	129014.	221800.	622.0
26	35.32053	102.37709	126204.	212302.	711.2
39	35.42839	101.62508	195333.	224145.	506.9
47	35.25780	101.24310	230446.	205414.	462.4
79	34.95307	102.32644	130860.	171954.	768.5
81	34.72496	102.48156	116601.	146908.	792.0
85	34.64046	102.02041	158992.	137630.	755.3
92	34.55616	101.90129	169942.	128374.	719.3
93	34.47893	101.47254	209355.	119894.	678.6
94	34.34615	101.33902	221629.	105315.	720.5
97	34.33302	100.41923	306180.	103873.	505.6
98	34.72449	100.57423	291932.	146856.	475.5
121	34.59698	100.09479	336004.	132856.	518.1
153	33.86040	102.11800	150021.	51979.	791.1
171	34.11000	101.89300	170704.	79385.	768.7
182	33.92680	101.53360	203742.	59270.	718.5
185	34.18340	101.24620	230161.	87445.	702.8
190	34.30365	101.31422	223909.	100648.	634.3
231	33.89070	100.09990	335535.	55306.	517.1
240	34.04620	100.30670	316525.	72380.	494.8
258	34.21860	100.45560	302837.	91310.	573.6
263	33.83680	100.18230	327960.	49388.	523.9
265	33.84610	100.15680	330304.	50409.	530.1
273	33.94220	100.33820	313629.	60961.	535.3
275	33.86080	100.13000	332768.	52023.	516.8
276	33.86096	100.22043	324455.	52041.	496.5
278	33.84708	100.10517	335050.	50517.	555.2
284	34.01007	100.28382	318628.	68413.	587.8
HALL2	34.56514	100.88108	263725.	129360.	566.9
DON31	34.78963	100.65931	284111.	154009.	531.5
PARM3	34.63941	102.61695	104155.	137515.	837.9
CHL10	33.38823	100.09077	336374.	134920.	591.5
FLOYD	34.19212	101.22584	232033.	88402.	729.0

Table A-1 (cont.)

Selected class A head data					
ID	Latitude	Longtitude	X, m	Y, m	Head, m
3	34.65315	103.66020	8255.	139023.	1095.5
5	34.68036	103.29772	41576.	142011.	943.1
7	34.51074	103.55887	17570.	123387.	776.6
15	35.51130	102.52787	112344.	233248.	566.3
19	35.59620	102.65120	101007.	242570.	575.2
26	35.32053	102.37708	126205.	212302.	485.9
33	35.24830	102.60463	105288.	204371.	726.0
37	35.24871	101.86406	173365.	204416.	521.5
39	35.42839	101.62508	195333.	224145.	462.7
47	35.25780	101.24309	230447.	205414.	450.5
61	35.10790	101.78184	180923.	188955.	766.0
63	34.97224	102.14690	147365.	174059.	610.8
67	34.78633	100.74777	275979.	153646.	567.8
68	34.80490	100.67699	282486.	155685.	449.6
73	34.96623	100.78648	272421.	173399.	398.1
75	34.86856	100.80087	271098.	162675.	502.0
79	34.51754	102.32643	130861.	124133.	706.5
83	34.63043	102.15478	146640.	136529.	873.9
85	34.64046	102.02040	158993.	137630.	662.3
86	34.63269	102.03013	158099.	136777.	625.1
93	34.47893	101.47253	209356.	119894.	711.7
94	34.34615	101.33901	221630.	105315.	838.8
96	34.73282	101.45845	210650.	147771.	402.3
97	34.33302	100.41921	306182.	103873.	467.9
105	34.36894	100.69507	280824.	107817.	552.9
107	34.37220	100.56361	292908.	108175.	466.6
108	34.31684	100.39984	307963.	102096.	539.5
109	34.33119	100.04085	340963.	103672.	412.4
121	34.59698	100.09477	336006.	132856.	495.0
122	34.36812	100.35810	311800.	107727.	491.6
123	34.34761	100.00261	344478.	105475.	484.6
137	34.00040	102.15720	146418.	67351.	753.2
147	33.99140	102.18149	144185.	66363.	785.8
148	33.83730	102.30580	132758.	49443.	984.8
150	33.98410	102.13369	148579.	65562.	799.5
152	34.03920	102.23860	138935.	71612.	824.8
153	33.86040	102.11799	150022.	51979.	786.1
154	34.25370	102.57789	107746.	95164.	780.0
155	33.86090	102.24960	137924.	52034.	792.5
156	33.83720	102.31580	131839.	49432.	761.4
158	33.84780	101.83539	176000.	50596.	703.8
160	33.83400	101.85619	174088.	49081.	734.0
161	33.99610	102.06850	154572.	66879.	781.5
165	33.89610	101.75089	183768.	55899.	399.0
170	33.84300	102.04130	157072.	50069.	832.1
171	34.11000	101.89299	170705.	79385.	784.6

Table A-1 (cont.)

ID	Latitude	Longtitude	X, m	Y, m	Head, m
172	33.91380	101.93359	166973.	57843.	694.6
178	34.18430	101.23980	230750.	87544.	579.4
179	33.88190	101.28239	226835.	54340.	696.2
180	33.88100	101.30239	224996.	54241.	602.3
181	33.85520	101.18939	235384.	51408.	721.8
182	33.92680	101.53359	203743.	59270.	684.6
183	34.12820	101.36299	219425.	81384.	432.2
184	33.98340	101.32199	223194.	65485.	595.6
185	34.18340	101.24619	230162.	87445.	660.5
186	34.24340	101.24718	230071.	94033.	679.1
187	33.90320	101.37740	218101.	56679.	609.6
190	34.30365	101.31420	223910.	100648.	650.1
192	33.93250	100.55040	294123.	59896.	492.6
196	34.09330	100.99029	253686.	77552.	586.7
198	34.15570	100.99600	253161.	84403.	586.1
202	33.87750	100.92708	259496.	53857.	532.8
215	33.90370	100.79200	271914.	56734.	557.8
216	33.89610	100.78909	272181.	55899.	514.2
219	34.23610	100.91819	260314.	93231.	451.7
224	33.89900	100.78829	272255.	56218.	449.6
226	33.91190	100.78888	272200.	57634.	570.3
229	33.88270	100.10378	335178.	54428.	521.8
237	33.88020	100.37839	309935.	54153.	561.4
240	34.04620	100.30669	316526.	72380.	464.8
245	33.85660	100.11519	334129.	51562.	532.8
246	33.89540	100.37419	310321.	55822.	563.6
248	33.89670	100.24248	322428.	55965.	516.0
249	33.96170	100.05389	339764.	63102.	344.4
250	33.91180	100.42239	305890.	57623.	530.0
254	33.83620	100.18358	327842.	49322.	531.6
255	34.05980	100.10938	334663.	73873.	447.1
256	33.97940	100.10358	335196.	65046.	388.0
258	34.21860	100.45559	302838.	91310.	550.8
260	33.94940	100.36498	311167.	61752.	319.4
262	34.05080	100.10739	334846.	72885.	519.4
263	33.83680	100.18228	327962.	49388.	514.5
264	33.84900	100.16469	329579.	50728.	491.9
265	33.84610	100.15678	330306.	50409.	501.4
266	33.90970	100.43709	304539.	57392.	520.9
268	33.96830	100.43248	304962.	63827.	552.0
269	34.00480	100.38778	309071.	67834.	490.1
270	34.25550	100.26129	320699.	95361.	390.4
271	33.97320	100.32318	315010.	64365.	420.9
274	34.20600	100.35439	312141.	89926.	507.8
275	33.86080	100.12999	332769.	52023.	504.1
277	33.84704	100.09645	335852.	50512.	495.0
278	33.84708	100.10516	335051.	50517.	484.9
279	33.85929	100.18209	327979.	51857.	486.8

Table A-1 (cont.)

ID	Latitude	Longtitude	X, m	Y, m	Head, m
280	33.92330	100.36407	311251.	58886.	517.2
281	33.84440	100.19146	327118.	50223.	329.8
282	34.21551	100.29466	317631.	90970.	448.7
284	34.01007	100.28381	318629.	68413.	426.7
369	33.81240	102.17919	144396.	46709.	783.6
370	33.78700	102.14880	147190.	43920.	824.2
389	33.81600	102.43960	120458.	47104.	887.6
452	33.79416	102.35213	128499.	44706.	1136.3
496	33.82320	101.86919	172893.	47895.	903.4
500	33.76500	101.94199	166201.	41504.	819.6
528	33.77720	101.55029	202208.	42844.	759.6
533	33.77530	101.09968	243630.	42635.	608.7
537	33.80700	101.49759	207052.	46116.	477.0
543	33.82550	101.54599	202603.	48147.	717.5
584	33.81490	100.81759	269561.	46983.	513.3
611	33.76400	100.05049	340077.	41395.	499.9
705	33.83100	100.19179	327088.	48751.	491.6
707	33.78380	100.01758	343102.	43569.	453.2
710	33.76060	100.23918	322731.	41021.	441.4
739	33.83420	100.14100	331757.	49103.	518.2
748	33.80400	100.22169	324339.	45787.	487.7
749	33.81200	100.22459	324073.	46665.	515.7
757	33.83434	100.20871	325532.	49118.	528.2
759	33.82274	100.43062	305133.	47844.	566.9

* DOEM1 - DOE's Mansfield #1 well.
79 - Well ID number in PI data file "ALLCOID".
HALL2 - Well #2 (BEG number) in Hall County.

** The origin is at latitude 33.3870° N and longtitude 103.7500° W.

Table A-2 Data file (PALOFL) for the deep-brine aquifer giving information at 405 finite-element nodal points.

Node No.	Coordinates, m		Elev. of cryst. basement, m	Thickness, m											Head in upper aquifer, m	Thickness, m		NCODE
	X	Y		Pre-Penn	Penn. carbonate	Penn. granite wash	Penn. shale	Penn., Total	Wolf. carbonate	Wolf. granite wash	Wolf. shale	Wolf., Total	Granite wash, total	Rock salt		Wolf. porous carbonate	Penn. porous carbonate	
1	137122.	245523.	-2073.	0	46.	122.	777.	945.	439.	0	293.	732.	122.	976.	1036.	158.	0	0
2	129479.	236866.	-1646.	0	76.	122.	411.	610.	319.	0	261.	579.	122.	1088.	1082.	229.	0	0
3	121835.	228267.	-792.	0	61.	122.	0	183.	293.	0	73.	366.	122.	1082.	1128.	198.	0	0
4	114192.	219725.	-671.	0	61.	91.	30.	183.	341.	0	146.	488.	91.	1037.	1180.	61.	0	0
5	106548.	211242.	-975.	0	91.	122.	213.	427.	137.	0	320.	457.	122.	1098.	1195.	0	0	0
6	98904.	202817.	-1006.	0	76.	91.	320.	488.	107.	0	320.	427.	91.	1204.	1207.	0	0	0
7	91261.	194449.	-1006.	0	76.	183.	168.	427.	119.	0	277.	396.	183.	1250.	1219.	0	0	0
8	83617.	186140.	-1006.	0	76.	244.	46.	366.	140.	0	210.	351.	244.	1305.	1244.	0	0	0
9	75973.	177888.	-1006.	0	91.	91.	122.	305.	116.	0	174.	290.	91.	1332.	1280.	0	0	0
10	80244.	166254.	-1067.	0	137.	91.	137.	366.	174.	0	116.	290.	91.	1348.	1265.	0	0	0
11	84511.	154751.	-1280.	30.	152.	91.	198.	442.	207.	0	89.	296.	91.	1384.	1219.	0	0	0
12	88775.	143380.	-1524.	55.	152.	98.	207.	457.	224.	0	96.	320.	98.	1466.	1204.	0	0	0
13	93036.	132140.	-1494.	46.	152.	79.	165.	396.	235.	0	101.	335.	79.	1488.	1189.	0	0	0
14	97167.	121467.	-1463.	61.	143.	61.	131.	335.	230.	0	99.	329.	61.	1418.	1167.	0	0	0
15	101263.	110712.	-1463.	58.	128.	30.	146.	305.	244.	0	61.	305.	30.	1546.	1152.	0	0	0
16	105322.	99876.	-1524.	58.	128.	21.	125.	274.	229.	0	76.	305.	21.	1524.	1140.	0	0	0
17	109345.	88958.	-1570.	79.	168.	9.	82.	259.	244.	0	61.	305.	9.	1518.	1128.	0	0	0
18	113332.	77959.	-1615.	98.	168.	0	76.	244.	293.	0	73.	366.	0	1503.	1119.	61.	0	0
19	117284.	66878.	-1676.	122.	171.	0	12.	183.	329.	0	82.	411.	0	1524.	1097.	91.	30.	0
20	121199.	55716.	-1707.	122.	134.	0	79.	213.	389.	0	69.	457.	0	1509.	1067.	122.	0	0
21	125078.	44472.	-2256.	122.	107.	0	137.	244.	576.	0	64.	640.	0	1524.	1061.	183.	0	0
22	146387.	243004.	-2591.	0	61.	366.	1036.	1463.	585.	0	146.	732.	366.	1037.	1036.	61.	0	0
23	131838.	225813.	-762.	0	152.	61.	91.	305.	352.	0	288.	640.	61.	1189.	1146.	91.	30.	0
24	117290.	208767.	-1067.	0	91.	244.	107.	442.	258.	0	211.	469.	244.	1235.	1177.	61.	0	0
25	102740.	191865.	-1280.	0	91.	79.	378.	549.	201.	0	201.	402.	79.	1341.	1198.	0	0	0
26	88191.	175109.	-1067.	0	146.	183.	98.	427.	168.	0	168.	335.	183.	1357.	1219.	0	0	0
27	97130.	152836.	-1768.	67.	213.	122.	204.	539.	245.	0	91.	335.	122.	1457.	1189.	0	0	0
28	106058.	131024.	-1753.	79.	177.	76.	158.	411.	256.	0	110.	366.	76.	1485.	1158.	0	0	0
29	113224.	110046.	-1524.	73.	149.	61.	125.	335.	245.	0	91.	335.	61.	1518.	1134.	0	0	0
30	120264.	88782.	-1615.	91.	189.	18.	73.	280.	305.	0	76.	381.	18.	1479.	1113.	0	0	0
31	127179.	67233.	-1768.	122.	183.	3.	27.	213.	389.	0	69.	457.	3.	1448.	1070.	183.	15.	0
32	133967.	45399.	-1829.	152.	1070	0	244.	244.	541.	0	135.	677.	0	1479.	1036.	183.	0	0
33	155652.	240312.	-2591.	0	91.	351.	1021.	1463.	293.	15.	180.	488.	366.	1189.	1036.	0	0	0
34	148732.	231763.	-1890.	0	122.	107.	381.	610.	683.	0	171.	853.	107.	1189.	1082.	0	0	0
35	141813.	223229.	-1189.	0	137.	30.	168.	335.	351.	0	351.	701.	30.	1189.	1128.	0	15.	0
36	134893.	214709.	-975.	0	198.	30.	15.	244.	311.	0	207.	518.	30.	1244.	1140.	0	30.	0
37	127973.	206204.	-1372.	0	152.	137.	198.	488.	343.	0	114.	457.	137.	1280.	1158.	137.	9.	0
38	121053.	197714.	-1433.	0	152.	183.	168.	503.	325.	0	108.	433.	183.	1296.	1167.	128.	0	0
39	114134.	189238.	-1494.	0	122.	116.	341.	579.	286.	0	123.	408.	116.	1372.	1180.	91.	0	0
40	107214.	180776.	-1524.	0	168.	61.	381.	610.	273.	0	117.	390.	61.	1341.	1189.	61.	0	0
41	100294.	172329.	-1524.	0	213.	82.	253.	549.	256.	0	110.	366.	82.	1372.	1189.	0	0	0
42	104970.	161584.	-1707.	61.	305.	61.	244.	610.	274.	0	91.	366.	61.	1387.	1170.	0	0	0
43	109645.	150938.	-1707.	61.	274.	67.	268.	610.	282.	0	84.	366.	67.	1448.	1158.	0	0	0
44	114316.	140391.	-1707.	61.	244.	70.	235.	549.	279.	0	93.	372.	70.	1491.	1152.	0	0	0
45	118986.	129942.	-1707.	94.	213.	61.	213.	488.	279.	0	93.	372.	61.	1479.	1137.	0	0	0
46	122057.	119704.	-1676.	131.	213.	30.	152.	396.	263.	0	102.	366.	30.	1479.	1128.	0	0	0
47	125101.	109405.	-1676.	125.	213.	30.	122.	366.	241.	0	124.	366.	30.	1463.	1113.	61.	0	0
48	128118.	99044.	-1646.	137.	189.	30.	116.	335.	277.	0	119.	396.	30.	1433.	1103.	61.	0	0

Table A-2 (cont.)

Node No.	Coordinates, m		Elev. of cryst. basement, m	Thickness, m											Head in upper aquifer, m	Thickness, m		NCODE
	X	Y		Pre-Penn	Penn. carbonate	Penn. granite wash	Penn. shale	Penn., Total	Wolf. carbonate	Wolf. granite wash	Wolf. shale	Wolf., Total	Granite wash, total	Rock salt		Wolf. porous carbonate	Penn. porous carbonate	
49	131108.	88623.	-1676.	143.	244.	18.	43.	305.	317.	0	79.	396.	18.	1445.	1097.	61.	9.	0
50	134070.	78140.	-1753.	143.	223.	12.	40.	274.	363.	0	64.	427.	12.	1439.	1079.	183.	30.	0
51	137006.	67596.	-1859.	152.	183.	9.	52.	244.	439.	0	49.	488.	9.	1433.	1058.	244.	9.	0
52	139915.	56991.	-1829.	122.	91.	0	152.	244.	544.	0	96.	640.	0	1433.	1036.	192.	18.	0
53	142797.	46325.	-1829.	122.	0	0	0	0	561.	0	140.	701.	0	1479.	1018.	61.	0	0
54	164917.	237445.	-1951.	0	107.	165.	338.	610.	341.	18.	67.	427.	183.	1204.	1067.	30.	0	0
55	151758.	220515.	-914.	0	168.	30.	168.	366.	347.	0	232.	579.	30.	1143.	1097.	0	0	0
56	138599.	203555.	-1219.	0	183.	76.	107.	366.	366.	0	91.	457.	76.	1229.	1134.	76.	15.	0
57	125440.	186567.	-1433.	0	152.	122.	335.	610.	334.	0	84.	418.	122.	1348.	1158.	187.	0	0
58	112280.	169550.	-1676.	18.	274.	55.	280.	610.	286.	0	95.	381.	55.	1381.	1158.	61.	0	0
59	122054.	149057.	-1737.	61.	287.	55.	268.	610.	310.	0	77.	387.	55.	1442.	1140.	122.	0	0
60	131819.	128893.	-1768.	122.	229.	55.	219.	503.	277.	0	119.	396.	55.	1448.	1116.	305.	0	0
61	136891.	108789.	-1829.	113.	213.	30.	152.	396.	247.	0	165.	411.	30.	1421.	1097.	305.	0	0
62	141874.	88480.	-1768.	128.	274.	21.	55.	351.	334.	0	84.	418.	21.	1418.	1082.	305.	24.	0
63	146767.	67968.	-1890.	183.	213.	9.	98.	320.	415.	0	73.	488.	9.	1457.	1042.	213.	30.	0
64	151570.	47252.	-1859.	152.	0	0	0	0	469.	0	201.	671.	0	1524.	1006.	30.	0	0
65	174182.	234405.	-1981.	0	122.	131.	479.	732.	341.	21.	64.	427.	152.	1082.	1052.	61.	0	2
66	167928.	226052.	-1067.	0	122.	104.	140.	366.	366.	18.	73.	457.	122.	1021.	1067.	61.	0	1
67	161674.	217670.	-914.	0	101.	15.	98.	213.	363.	15.	140.	518.	30.	1082.	1082.	0	0	0
68	155421.	209259.	-975.	0	91.	15.	259.	366.	368.	0	181.	549.	15.	1073.	1097.	0	0	0
69	149167.	200819.	-1006.	0	91.	55.	219.	366.	329.	0	219.	549.	55.	1198.	1109.	0	0	0
70	142913.	192350.	-1219.	0	122.	58.	247.	427.	320.	0	137.	457.	58.	1296.	1128.	61.	0	0
71	136659.	183852.	-1341.	0	183.	76.	259.	518.	320.	0	107.	427.	76.	1360.	1137.	128.	0	0
72	130405.	175326.	-1463.	0	198.	91.	320.	610.	296.	0	115.	411.	91.	1375.	1143.	137.	0	0
73	124151.	166770.	-1676.	30.	280.	61.	268.	610.	317.	0	79.	396.	61.	1381.	1149.	128.	0	0
74	129255.	156949.	-1707.	61.	280.	49.	280.	610.	277.	0	119.	396.	49.	1369.	1131.	137.	0	0
75	134358.	147193.	-1707.	91.	268.	46.	296.	610.	269.	0	127.	396.	46.	1384.	1128.	183.	0	0
76	139458.	137503.	-1737.	122.	274.	46.	290.	610.	276.	0	136.	411.	46.	1387.	1109.	183.	0	0
77	144557.	127878.	-1768.	122.	311.	46.	192.	549.	258.	0	139.	396.	46.	1372.	1097.	122.	0	0
78	146586.	118058.	-1798.	125.	311.	37.	140.	488.	256.	0	171.	427.	37.	1372.	1088.	122.	0	0
79	148597.	108198.	-1829.	128.	268.	30.	143.	442.	283.	0	189.	472.	30.	1363.	1067.	274.	0	0
80	150590.	98296.	-1859.	140.	305.	30.	76.	411.	320.	0	137.	457.	30.	1372.	1067.	427.	12.	0
81	152565.	88354.	-1859.	143.	314.	24.	58.	396.	320.	0	107.	427.	24.	1418.	1061.	305.	30.	0
82	154522.	78371.	-1890.	143.	290.	18.	64.	372.	331.	0	110.	442.	18.	1433.	1052.	183.	30.	0
83	156461.	68348.	-1920.	213.	244.	12.	110.	366.	341.	0	146.	488.	12.	1473.	1036.	61.	30.	0
84	158382.	58283.	-1920.	183.	198.	6.	131.	335.	393.	0	168.	561.	6.	1509.	1012.	30.	18.	0
85	160285.	48178.	-1920.	183.	152.	0	0	152.	449.	0	221.	671.	0	1540.	1024.	0	0	0
86	183447.	231191.	-2073.	0	122.	162.	448.	732.	299.	21.	107.	427.	183.	960.	1027.	91.	0	2
87	171562.	214695.	-610.	0	76.	15.	0	76.	378.	15.	79.	472.	30.	1006.	1061.	122.	0	0
88	159677.	197996.	-1067.	0	122.	52.	192.	366.	401.	0	148.	549.	52.	1204.	1088.	0	0	0
89	147791.	181095.	-1311.	0	213.	58.	186.	457.	274.	0	183.	457.	58.	1302.	1119.	61.	0	0
90	135906.	163991.	-1524.	0	244.	61.	305.	610.	247.	0	165.	411.	61.	1360.	1131.	61.	0	0
91	146556.	145345.	-1707.	91.	311.	37.	262.	610.	254.	0	143.	396.	37.	1341.	1106.	91.	0	0
92	157201.	126896.	-1753.	134.	360.	30.	219.	610.	256.	0	171.	427.	30.	1320.	1076.	61.	43.	0
93	160217.	107632.	-1829.	143.	320.	37.	131.	488.	384.	0	165.	549.	37.	1280.	1049.	396.	0	0
94	163179.	88245.	-1905.	152.	335.	24.	52.	411.	303.	0	130.	433.	24.	1433.	1036.	122.	46.	0
95	166088.	68736.	-1981.	213.	262.	12.	122.	396.	346.	0	203.	549.	12.	1509.	1006.	0	15.	0
96	168942.	49105.	-1920.	183.	213.	0	152.	366.	439.	0	247.	686.	0	1463.	975.	0	0	0

Table A-2 (cont.)

Node No.	Coordinates, m		Elev. of cryst. basement, m	Thickness, m											Head in upper aquifer, m	Thickness, m		NCODE
	X	Y		Pre-Penn	Penn. carbonate	Penn. granite wash	Penn. shale	Penn., Total	Wolf. carbonate	Wolf. granite wash	Wolf. shale	Wolf., Total	Granite wash, total	Rock salt		Wolf. porous carbonate	Penn. porous carbonate	
97	192712.	227804.	-1981.	0	122.	98.	573.	792.	299.	24.	104.	427.	122.	945.	997.	137.	0	2
98	187066.	219733.	-1890.	0	79.	165.	0	244.	343.	18.	96.	457.	79.	966.	1015.	137.	0	1
99	181420.	211590.	-610.	0	46.	15.	0	61.	378.	15.	79.	472.	30.	945.	1039.	244.	0	0
100	175775.	203374.	-610.	0	61.	0	0	61.	433.	0	48.	482.	0	1052.	1052.	122.	0	0
101	170129.	195086.	-1158.	0	91.	46.	320.	457.	422.	0	126.	549.	46.	1241.	1067.	0	0	0
102	164483.	186726.	-1311.	0	183.	46.	274.	503.	384.	0	165.	549.	46.	1232.	1085.	0	0	0
103	158837.	178293.	-1372.	0	244.	52.	207.	503.	327.	0	176.	503.	52.	1232.	1097.	0	15.	0
104	153191.	169788.	-1402.	0	290.	58.	201.	549.	274.	0	183.	457.	58.	1299.	1100.	0	15.	0
105	147545.	161211.	-1433.	0	351.	61.	198.	610.	256.	0	171.	427.	61.	1326.	1119.	0	15.	0
106	153098.	152346.	-1463.	0	351.	30.	229.	610.	256.	0	171.	427.	30.	1311.	1103.	61.	15.	0
107	158650.	143514.	-1494.	0	381.	30.	198.	610.	265.	0	177.	442.	30.	1280.	1079.	0	15.	0
108	164200.	134714.	-1524.	0	396.	30.	183.	610.	256.	0	171.	427.	30.	1287.	1067.	61.	61.	0
109	169750.	125948.	-1768.	61.	381.	37.	192.	610.	256.	0	171.	427.	37.	1329.	1055.	183.	61.	0
110	170755.	116530.	-1768.	137.	351.	43.	171.	564.	352.	0	151.	503.	43.	1299.	1036.	152.	61.	0
111	171752.	107091.	-1829.	162.	335.	37.	146.	518.	329.	0	219.	549.	37.	1326.	1030.	122.	61.	0
112	172739.	97632.	-1890.	183.	314.	30.	128.	472.	236.	0	236.	472.	30.	1387.	1021.	91.	61.	0
113	173718.	88153.	-1920.	192.	305.	24.	113.	442.	236.	0	236.	472.	24.	1448.	1006.	61.	30.	0
114	174687.	78653.	-1981.	180.	274.	18.	134.	427.	236.	0	236.	472.	18.	1479.	1006.	0	15.	0
115	175647.	69133.	-2012.	244.	244.	12.	171.	427.	293.	0	195.	488.	12.	1482.	1006.	0	0	0
116	176599.	59592.	-1981.	244.	235.	6.	125.	366.	375.	0	250.	625.	6.	1436.	975.	0	0	0
117	177541.	50031.	-1829.	91.	213.	0	152.	366.	439.	0	293.	732.	0	1454.	966.	61.	0	0
118	201977.	224242.	-1676.	0	122.	98.	604.	823.	299.	24.	104.	427.	122.	884.	972.	61.	0	2
119	191250.	208354.	-762.	0	110.	12.	0	122.	389.	12.	56.	457.	24.	915.	1012.	91.	0	1
120	180523.	192090.	-1219.	0	183.	40.	265.	488.	378.	0	94.	472.	40.	1265.	1036.	0	0	0
121	169796.	175449.	-1433.	0	229.	46.	290.	564.	384.	0	165.	549.	46.	1229.	1076.	0	21.	0
122	159068.	158432.	-1433.	0	366.	46.	198.	610.	274.	0	183.	457.	46.	1265.	1103.	61.	30.	0
123	170638.	141700.	-1494.	6.	381.	30.	198.	610.	213.	0	213.	427.	30.	1244.	1061.	0	30.	0
124	182205.	125033.	-1737.	152.	305.	52.	253.	610.	274.	0	183.	457.	52.	1338.	1024.	0	15.	0
125	183201.	106575.	-1890.	201.	305.	34.	180.	518.	274.	0	274.	549.	34.	1354.	1006.	0	37.	0
126	184179.	88077.	-1951.	213.	244.	21.	192.	457.	259.	0	259.	518.	21.	1439.	991.	0	15.	0
127	185140.	69538.	-2012.	183.	229.	9.	189.	427.	259.	0	259.	518.	9.	1418.	1024.	0	0	0
128	186082.	50958.	-1829.	152.	198.	0	168.	366.	335.	0	274.	610.	0	1433.	951.	61.	0	0
129	211242.	220507.	-1463.	0	91.	94.	668.	853.	277.	27.	91.	396.	122.	884.	960.	0	0	2
130	206146.	212805.	-1433.	0	152.	344.	479.	975.	313.	21.	83.	418.	366.	960.	969.	0	0	2
131	201051.	204988.	-762.	0	122.	46.	76.	244.	334.	15.	68.	418.	61.	1082.	988.	0	0	1
132	195955.	197055.	-762.	0	91.	0	30.	122.	334.	0	84.	418.	0	1159.	1012.	91.	0	0
133	190859.	189006.	-1067.	0	122.	34.	302.	457.	334.	0	84.	418.	34.	1220.	1021.	0	0	0
134	185763.	180841.	-1311.	0	168.	37.	314.	518.	303.	0	130.	433.	37.	1262.	1036.	61.	15.	0
135	180668.	172561.	-1372.	0	396.	40.	128.	564.	439.	0	110.	549.	40.	1210.	1067.	61.	61.	0
136	175572.	164164.	-1524.	21.	351.	43.	216.	610.	411.	0	123.	533.	43.	1189.	1073.	0	61.	0
137	170476.	155652.	-1524.	15.	344.	30.	235.	610.	293.	0	195.	488.	30.	1235.	1079.	0	61.	0
138	176499.	147777.	-1585.	27.	326.	30.	253.	610.	251.	0	206.	457.	30.	1235.	1055.	0	21.	0
139	182521.	139902.	-1676.	61.	265.	40.	305.	610.	229.	0	229.	457.	40.	1250.	1036.	0	0	0
140	188543.	132027.	-1737.	122.	213.	52.	375.	640.	229.	0	229.	457.	52.	1299.	1015.	0	0	0
141	194565.	124151.	-1768.	174.	213.	61.	396.	671.	244.	0	244.	488.	61.	1317.	1006.	0	0	0
142	194565.	115118.	-1829.	198.	229.	55.	326.	610.	267.	0	267.	533.	55.	1341.	1000.	0	0	0
143	194565.	106085.	-1859.	213.	229.	30.	259.	518.	280.	0	280.	561.	30.	1348.	981.	0	0	0
144	194565.	97051.	-1890.	219.	213.	24.	235.	472.	277.	0	277.	555.	24.	1363.	975.	0	0	0

Table A-2 (cont.)

Node No.	Coordinates, m		Elev. of cryst. basement, m	Thickness, m											Head in upper aquifer, m	Thickness, m		NCODE
	X	Y		Pre-Penn	Penn. carbonate	Penn. granite wash	Penn. shale	Penn., Total	Wolf. carbonate	Wolf. granite wash	Wolf. shale	Wolf., Total	Granite wash, total	Rock salt		Wolf. porous carbonate	Penn. porous carbonate	
145	194565.	88015.	-1951.	219.	213.	21.	207.	442.	274.	0	274.	549.	21.	1418.	975.	0	0	0
146	194565.	78985.	-2012.	216.	198.	15.	213.	427.	274.	0	274.	549.	15.	1433.	975.	0	0	0
147	194565.	69951.	-2042.	210.	183.	9.	204.	396.	290.	0	290.	579.	9.	1387.	975.	0	0	0
148	194565.	60918.	-1829.	168.	152.	0	213.	366.	366.	0	366.	732.	0	1296.	975.	0	0	0
149	194565.	51884.	-1768.	91.	168.	0	15.	183.	293.	0	195.	488.	0	1372.	945.	61.	0	0
150	218712.	216454.	-1280.	0	76.	91.	686.	853.	238.	30.	128.	396.	122.	884.	954.	0	0	2
151	209635.	201601.	-853.	0	183.	76.	107.	366.	317.	15.	64.	396.	91.	1113.	981.	0	0	1
152	200558.	186284.	-1036.	0	122.	34.	241.	396.	317.	0	79.	396.	34.	1189.	1006.	122.	0	0
153	191482.	170505.	-1311.	24.	274.	30.	229.	533.	390.	0	98.	488.	30.	1226.	1006.	122.	0	0
154	182405.	154262.	-1615.	49.	305.	30.	274.	610.	363.	0	155.	518.	30.	1223.	1042.	0	15.	0
155	193234.	138860.	-1737.	122.	152.	46.	411.	610.	244.	0	244.	488.	46.	1238.	1006.	30.	0	0
156	204062.	123456.	-1798.	189.	152.	61.	472.	686.	259.	0	259.	518.	61.	1290.	978.	30.	0	0
157	204062.	105361.	-1890.	219.	152.	61.	335.	549.	282.	0	282.	564.	61.	1357.	975.	0	0	0
158	204062.	87265.	-1951.	223.	152.	46.	305.	503.	290.	0	290.	579.	46.	1396.	960.	0	0	0
159	204062.	69169.	-2042.	213.	122.	37.	344.	503.	305.	0	305.	610.	37.	1348.	951.	0	0	0
160	204062.	51073.	-1524.	91.	91.	0	30.	122.	219.	0	146.	366.	0	1296.	924.	61.	0	0
161	226298.	212632.	-1067.	0	46.	46.	640.	732.	219.	76.	70.	366.	122.	838.	945.	0	0	2
162	222273.	205567.	-975.	0	113.	198.	482.	792.	238.	46.	82.	366.	244.	915.	963.	0	0	2
163	218249.	198387.	-914.	0	152.	347.	262.	762.	286.	18.	67.	372.	366.	1034.	975.	30.	0	1
164	214224.	191091.	-914.	0	244.	76.	107.	427.	297.	0	74.	372.	76.	1159.	988.	61.	0	0
165	210200.	183679.	-1067.	0	290.	34.	43.	366.	297.	0	74.	372.	34.	1159.	991.	61.	0	0
166	206175.	176151.	-1219.	0	244.	30.	183.	457.	317.	0	79.	396.	30.	1134.	975.	61.	0	0
167	202151.	168507.	-1280.	76.	152.	30.	335.	518.	366.	0	91.	457.	30.	1189.	914.	122.	0	0
168	198126.	160748.	-1372.	116.	152.	30.	366.	549.	439.	0	110.	549.	30.	1204.	945.	122.	0	0
169	194102.	152873.	-1585.	113.	152.	30.	411.	594.	384.	0	165.	549.	30.	1226.	1006.	91.	0	0
170	198966.	145345.	-1646.	137.	183.	37.	390.	610.	283.	0	189.	472.	37.	1235.	1003.	91.	0	0
171	203831.	137817.	-1676.	168.	183.	52.	405.	640.	260.	0	213.	472.	52.	1241.	985.	91.	0	0
172	208695.	130290.	-1737.	189.	183.	37.	451.	671.	268.	0	219.	488.	37.	1250.	981.	91.	0	0
173	213559.	122762.	-1768.	201.	183.	30.	503.	716.	277.	0	226.	503.	30.	1302.	975.	91.	0	0
174	213559.	113728.	-1829.	213.	183.	61.	427.	671.	267.	0	267.	533.	61.	1360.	969.	46.	0	0
175	213559.	104695.	-1890.	219.	183.	61.	305.	549.	282.	0	282.	564.	61.	1366.	957.	0	0	0
176	213559.	95662.	-1920.	232.	183.	61.	305.	549.	290.	0	290.	579.	61.	1366.	945.	0	0	0
177	213559.	86628.	-1981.	232.	198.	61.	305.	564.	297.	0	297.	594.	61.	1378.	945.	0	0	0
178	213559.	77595.	-2134.	232.	198.	49.	317.	564.	305.	0	305.	610.	49.	1369.	945.	0	0	0
179	213559.	68561.	-2073.	213.	168.	37.	299.	503.	320.	0	320.	640.	37.	1326.	951.	0	0	0
180	213559.	59528.	-1829.	174.	122.	0	244.	366.	343.	0	343.	686.	0	1311.	908.	30.	0	0
181	213559.	50494.	-1372.	46.	91.	0	30.	122.	439.	0	293.	732.	0	1287.	902.	61.	0	0
182	234000.	209042.	-457.	0	46.	0	76.	122.	216.	122.	22.	360.	122.	869.	945.	0	0	2
183	226892.	195347.	-610.	0	82.	122.	162.	366.	270.	61.	29.	360.	183.	945.	945.	0	0	1
184	219783.	181189.	-853.	0	198.	76.	61.	335.	280.	0	70.	351.	76.	1098.	975.	0	18.	0
185	212675.	166567.	-1219.	91.	366.	30.	91.	488.	293.	0	73.	366.	30.	1128.	853.	30.	15.	0
186	205567.	151483.	-1524.	143.	274.	30.	259.	564.	320.	0	107.	427.	30.	1204.	991.	137.	15.	0
187	214312.	136775.	-1676.	189.	351.	30.	229.	610.	247.	0	179.	427.	30.	1250.	975.	137.	70.	0
188	223055.	122067.	-1768.	213.	305.	30.	396.	732.	307.	0	165.	472.	30.	1320.	945.	137.	91.	0
189	223055.	104087.	-1890.	226.	244.	30.	335.	610.	347.	0	187.	533.	30.	1357.	936.	67.	0	0
190	223055.	86107.	-1981.	238.	213.	30.	366.	610.	320.	0	320.	640.	30.	1317.	924.	30.	0	0
191	223055.	68127.	-2134.	216.	152.	18.	347.	518.	320.	0	320.	640.	18.	1296.	920.	0	0	0
192	223055.	50147.	-1219.	0	91.	0	30.	122.	366.	0	244.	610.	0	1280.	884.	61.	0	0

Table A-2 (cont.)

Node No.	Coordinates, m		Elev. of cryst. basement, m	Thickness, m											Head in upper aquifer, m	Thickness, m		NCODE
	X	Y		Pre-Penn	Penn. carbonate	Penn. granite wash	Penn. shale	Penn., Total	Wolf. carbonate	Wolf. granite wash	Wolf. shale	Wolf., Total	Granite wash, total	Rock salt		Wolf. porous carbonate	Penn. porous carbonate	
193	241817.	205683.	0	0	15.	0	15.	30.	201.	122.	12.	335.	122.	899.	930.	0	0	2
194	238690.	199140.	-152.	0	30.	0	30.	61.	218.	110.	8.	335.	110.	899.	920.	0	0	2
195	235563.	192480.	-305.	0	52.	0	70.	122.	235.	94.	6.	335.	94.	936.	914.	0	0	1
196	232436.	185705.	-396.	0	70.	0	52.	122.	268.	61.	6.	335.	61.	1006.	930.	0	0	0
197	229309.	178815.	-610.	0	88.	15.	140.	244.	261.	15.	50.	326.	30.	1052.	945.	61.	0	0
198	226182.	171808.	-914.	15.	213.	30.	122.	366.	268.	0	67.	335.	30.	1113.	966.	61.	18.	0
199	223055.	164685.	-1067.	61.	274.	30.	137.	442.	268.	0	67.	335.	30.	1134.	914.	61.	30.	0
200	219928.	157447.	-1250.	101.	351.	30.	107.	488.	293.	0	73.	366.	30.	1174.	762.	76.	43.	0
201	216801.	150093.	-1463.	134.	411.	30.	107.	549.	293.	0	73.	366.	30.	1213.	945.	122.	61.	0
202	220739.	142913.	-1554.	171.	411.	30.	122.	564.	297.	0	99.	396.	30.	1250.	945.	131.	61.	0
203	224677.	135733.	-1615.	195.	427.	30.	152.	610.	317.	0	79.	396.	30.	1265.	914.	137.	91.	0
204	228614.	128552.	-1676.	207.	427.	30.	198.	655.	305.	0	76.	381.	30.	1296.	914.	128.	107.	0
205	232552.	121372.	-1737.	216.	427.	61.	213.	701.	325.	0	71.	396.	61.	1311.	930.	122.	128.	0
206	232552.	112454.	-1829.	219.	335.	46.	351.	732.	380.	0	114.	494.	46.	1305.	930.	122.	122.	0
207	232552.	103537.	-1890.	229.	198.	30.	411.	640.	373.	0	145.	518.	30.	1320.	914.	107.	15.	0
208	232552.	94619.	-1920.	235.	168.	30.	442.	640.	330.	0	249.	579.	30.	1274.	890.	91.	0	0
209	232552.	85702.	-1981.	244.	122.	30.	503.	655.	335.	0	335.	671.	30.	1198.	899.	76.	0	0
210	232552.	76784.	-2134.	244.	152.	30.	457.	640.	366.	0	366.	732.	30.	1241.	914.	61.	0	0
211	232552.	67866.	-2134.	229.	122.	21.	421.	564.	366.	0	366.	732.	21.	1280.	914.	0	0	0
212	232552.	58949.	-1615.	201.	91.	9.	265.	366.	366.	0	366.	732.	9.	1280.	884.	0	0	0
213	232552.	50031.	-1524.	30.	91.	0	91.	183.	402.	0	268.	671.	0	1271.	866.	61.	15.	0
214	249750.	202556.	0	0	15.	15.	0	30.	134.	168.	34.	335.	183.	915.	914.	0	0	2
215	244263.	189788.	-305.	0	49.	30.	43.	122.	183.	152.	0	335.	183.	951.	893.	0	0	1
216	238777.	176556.	-610.	15.	85.	15.	143.	244.	244.	46.	15.	305.	61.	991.	884.	61.	0	0
217	233290.	162861.	-1097.	61.	213.	30.	122.	366.	258.	0	65.	323.	30.	1128.	914.	76.	0	0
218	227803.	148703.	-1433.	146.	366.	30.	122.	518.	293.	0	73.	366.	30.	1189.	732.	122.	0	0
219	234926.	134690.	-1585.	201.	366.	46.	198.	610.	322.	0	44.	366.	46.	1189.	732.	122.	15.	0
220	242049.	120677.	-1737.	216.	381.	61.	229.	671.	311.	0	55.	366.	61.	1220.	823.	131.	91.	0
221	242049.	103045.	-1890.	232.	244.	61.	366.	671.	363.	0	155.	518.	61.	1250.	792.	122.	107.	0
222	242049.	85412.	-2073.	244.	122.	61.	503.	686.	320.	0	320.	640.	61.	1271.	872.	76.	0	0
223	242049.	67780.	-2286.	244.	91.	30.	488.	610.	366.	0	366.	732.	30.	1265.	863.	30.	0	0
224	242049.	50147.	-1981.	152.	91.	6.	299.	396.	351.	0	351.	701.	6.	1265.	838.	30.	0	0
225	257799.	199661.	0	0	15.	15.	30.	61.	96.	168.	56.	320.	183.	884.	890.	0	0	2
226	255396.	193523.	-305.	0	30.	15.	61.	107.	128.	168.	24.	320.	183.	909.	884.	0	0	2
227	252993.	187269.	-457.	0	46.	30.	168.	244.	160.	152.	8.	320.	183.	930.	878.	0	0	2
228	250590.	180899.	-914.	61.	61.	64.	241.	366.	198.	113.	0	311.	177.	930.	853.	0	0	1
229	248186.	174414.	-1097.	91.	82.	91.	268.	442.	213.	61.	0	274.	152.	915.	853.	0	0	0
230	245783.	167812.	-1219.	122.	152.	113.	223.	488.	195.	15.	34.	244.	128.	1037.	792.	30.	0	0
231	243380.	161095.	-1372.	174.	171.	98.	235.	503.	244.	0	61.	305.	98.	1113.	792.	61.	0	0
232	240977.	154262.	-1433.	183.	213.	67.	238.	518.	268.	0	67.	335.	67.	1104.	792.	91.	0	0
233	238574.	147314.	-1463.	186.	274.	46.	229.	549.	293.	0	73.	366.	46.	1152.	732.	101.	0	0
234	241817.	140481.	-1494.	198.	274.	61.	244.	579.	329.	0	37.	366.	61.	1113.	695.	91.	0	0
235	245060.	133648.	-1524.	210.	335.	61.	213.	610.	329.	0	37.	366.	61.	1082.	671.	91.	0	0
236	248302.	126815.	-1615.	244.	335.	46.	244.	625.	311.	0	55.	366.	46.	1131.	680.	122.	0	0
237	251545.	119982.	-1737.	244.	335.	61.	244.	640.	305.	0	76.	381.	61.	1149.	732.	122.	61.	0
238	251545.	111296.	-1829.	213.	396.	76.	198.	671.	338.	0	119.	457.	76.	1174.	732.	116.	152.	0
239	251545.	102610.	-1890.	213.	305.	76.	320.	701.	342.	0	176.	518.	76.	1189.	747.	107.	131.	0
240	251545.	93924.	-1951.	219.	183.	67.	482.	732.	290.	0	290.	579.	67.	1220.	762.	91.	15.	0

Table A-2 (cont.)

Node No.	Coordinates, m		Elev. of cryst. basement, m	Thickness, m											Head in upper aquifer, m	Thickness, m		NCODE
	X	Y		Pre-Penn	Penn. carbonate	Penn. granite wash	Penn. shale	Penn., Total	Wolf. carbonate	Wolf. granite wash	Wolf. shale	Wolf., Total	Granite wash, total	Rock salt		Wolf. porous carbonate	Penn. porous carbonate	
241	251545.	65238.	-2073.	232.	152.	49.	530.	732.	328.	0	328.	655.	49.	1241.	792.	76.	0	0
242	251545.	76552.	-2225.	244.	122.	61.	549.	732.	366.	0	366.	732.	61.	1229.	823.	61.	0	0
243	251545.	67866.	-2377.	244.	91.	30.	488.	610.	366.	0	366.	732.	30.	1226.	823.	30.	0	0
244	251545.	59180.	-2286.	244.	91.	21.	436.	549.	366.	0	366.	732.	21.	1256.	853.	0	0	0
245	251545.	50494.	-1920.	183.	137.	15.	335.	488.	335.	0	335.	671.	15.	1250.	823.	0	0	0
246	265964.	196997.	-61.	0	15.	15.	61.	91.	91.	168.	46.	305.	183.	854.	878.	0	0	2
247	261751.	184924.	-488.	30.	46.	0	198.	244.	122.	152.	30.	305.	152.	899.	853.	0	0	2
248	257538.	172387.	-975.	152.	82.	76.	207.	366.	171.	46.	27.	244.	122.	915.	847.	0	0	1
249	253325.	159387.	-1067.	152.	152.	91.	244.	488.	195.	0	49.	244.	91.	1055.	762.	0	0	0
250	249113.	145924.	-1280.	213.	198.	61.	290.	549.	260.	0	39.	299.	61.	1058.	701.	61.	0	0
251	255077.	132605.	-1524.	213.	244.	61.	305.	610.	299.	0	61.	360.	61.	1043.	640.	107.	0	0
252	261042.	119287.	-1737.	213.	293.	73.	274.	640.	317.	0	79.	396.	73.	1037.	640.	107.	30.	0
253	261042.	102234.	-1890.	213.	366.	88.	247.	701.	363.	0	155.	518.	88.	1098.	701.	91.	137.	0
254	261042.	85180.	-2073.	229.	152.	64.	515.	732.	384.	0	256.	640.	64.	1189.	716.	67.	0	0
255	261042.	68127.	-2347.	244.	183.	27.	521.	732.	439.	0	293.	732.	27.	1198.	732.	30.	0	0
256	261042.	51073.	-1585.	152.	122.	9.	357.	488.	384.	0	256.	640.	9.	1189.	732.	0	0	0
257	274244.	194565.	-183.	0	6.	15.	85.	107.	49.	168.	27.	244.	183.	838.	853.	0	0	2
258	272391.	188716.	-610.	61.	24.	30.	98.	152.	82.	152.	40.	274.	183.	854.	829.	0	0	2
259	270538.	182752.	-671.	91.	43.	76.	125.	244.	116.	107.	67.	290.	183.	869.	792.	0	0	2
260	268685.	176672.	-579.	91.	61.	0	183.	244.	130.	61.	69.	259.	61.	875.	792.	0	0	2
261	266832.	170476.	-610.	122.	79.	46.	149.	274.	146.	15.	82.	244.	61.	902.	808.	0	0	2
262	264979.	164164.	-914.	244.	113.	46.	177.	335.	192.	0	82.	274.	46.	924.	823.	0	0	1
263	263126.	157737.	-792.	107.	146.	30.	189.	366.	247.	0	27.	274.	30.	976.	762.	0	0	0
264	261273.	151193.	-914.	122.	165.	30.	293.	488.	232.	0	58.	290.	30.	1006.	716.	30.	0	0
265	259420.	144534.	-1128.	137.	183.	37.	299.	518.	251.	0	63.	314.	37.	1021.	671.	61.	0	0
266	262200.	138049.	-1280.	152.	198.	43.	308.	549.	268.	0	67.	335.	43.	1018.	649.	98.	0	0
267	264979.	131563.	-1341.	168.	244.	61.	274.	579.	293.	0	73.	366.	61.	1043.	628.	122.	0	0
268	267759.	125078.	-1463.	183.	274.	76.	259.	610.	305.	0	76.	381.	76.	1064.	610.	122.	0	0
269	270538.	118592.	-1646.	198.	335.	91.	198.	625.	293.	0	73.	366.	91.	1073.	610.	61.	15.	0
270	270538.	110254.	-1768.	213.	366.	91.	198.	655.	329.	0	37.	366.	91.	1098.	640.	61.	98.	0
271	270538.	101915.	-1890.	213.	396.	91.	198.	686.	390.	0	98.	488.	91.	1131.	652.	76.	122.	0
272	270538.	93577.	-1920.	213.	335.	76.	305.	716.	347.	0	232.	579.	76.	1146.	646.	76.	15.	0
273	270538.	85238.	-2042.	235.	183.	61.	488.	732.	402.	0	268.	671.	61.	1171.	671.	61.	0	0
274	270538.	76900.	-2195.	241.	168.	30.	533.	732.	439.	0	293.	732.	30.	1195.	692.	30.	0	0
275	270538.	68561.	-2134.	244.	158.	24.	549.	732.	439.	0	293.	732.	24.	1204.	701.	0	0	0
276	270538.	60223.	-1676.	244.	158.	18.	311.	488.	402.	0	268.	671.	18.	1183.	735.	0	15.	0
277	270538.	51884.	-1219.	91.	183.	12.	171.	366.	305.	0	305.	610.	12.	1159.	732.	0	37.	0
278	283046.	194044.	-305.	0	0	15.	107.	122.	37.	168.	40.	244.	183.	802.	844.	0	0	2
279	279803.	182217.	-701.	91.	43.	91.	79.	213.	61.	91.	91.	244.	183.	848.	792.	0	0	2
280	276560.	169984.	-1036.	122.	79.	152.	12.	244.	98.	30.	116.	244.	183.	973.	762.	0	0	2
281	273318.	157346.	-945.	30.	116.	46.	143.	305.	152.	15.	137.	305.	61.	954.	792.	0	15.	1
282	270075.	143897.	-1128.	152.	152.	30.	183.	366.	268.	0	67.	335.	30.	976.	671.	67.	0	0
283	274939.	131129.	-1341.	183.	244.	30.	244.	518.	229.	0	76.	305.	30.	991.	610.	122.	0	0
284	279803.	118592.	-1676.	213.	351.	61.	259.	671.	146.	0	37.	183.	61.	1006.	591.	61.	0	0
285	279803.	102031.	-1890.	244.	384.	91.	256.	732.	299.	0	128.	427.	91.	1055.	610.	64.	137.	0
286	279803.	85470.	-2012.	244.	238.	61.	433.	732.	393.	0	262.	655.	61.	1088.	610.	55.	12.	0
287	279803.	68908.	-1890.	232.	171.	15.	546.	732.	375.	0	250.	625.	15.	1082.	649.	55.	12.	0
288	279803.	52347.	-1067.	30.	122.	0	0	122.	267.	0	267.	533.	0	1037.	671.	30.	91.	0

Table A-2 (cont.)

Node No.	Coordinates, m		Elev. of cryst. basement, m	Thickness, m											Head in upper aquifer, m	Thickness, m		NCODE
	X	Y		Pre-Penn	Penn. carbonate	Penn. granite wash	Penn. shale	Penn., Total	Wolf. carbonate	Wolf. granite wash	Wolf. shale	Wolf., Total	Granite wash, total	Rock salt		Wolf. porous carbonate	Penn. porous carbonate	
289	291848.	193407.	-366.	0	0	15.	107.	122.	24.	168.	52.	244.	183.	759.	808.	0	0	2
290	290458.	187544.	-640.	30.	0	30.	122.	152.	37.	152.	55.	244.	183.	768.	792.	0	0	2
291	289068.	181594.	-671.	91.	15.	67.	101.	183.	44.	116.	84.	244.	183.	784.	747.	0	0	2
292	287678.	175558.	-884.	152.	30.	15.	198.	244.	55.	107.	113.	274.	122.	860.	732.	0	0	2
293	286289.	169434.	-1097.	183.	46.	55.	143.	244.	91.	98.	116.	305.	152.	921.	732.	0	0	2
294	284899.	163224.	-1219.	152.	82.	61.	101.	244.	122.	91.	91.	305.	152.	930.	753.	0	0	2
295	283509.	156926.	-1250.	274.	146.	91.	67.	305.	148.	30.	117.	296.	122.	945.	756.	30.	24.	2
296	282119.	150542.	-1219.	213.	183.	61.	0	244.	198.	0	85.	283.	61.	939.	701.	61.	30.	2
297	280730.	143976.	-1067.	152.	152.	30.	91.	274.	219.	0	55.	274.	30.	951.	671.	76.	24.	1
298	282814.	137006.	-1250.	168.	207.	30.	98.	335.	202.	0	57.	259.	30.	930.	610.	91.	21.	0
299	284899.	130752.	-1402.	183.	244.	30.	213.	488.	185.	0	59.	244.	30.	915.	594.	91.	15.	0
300	286983.	124614.	-1554.	198.	290.	30.	290.	610.	180.	0	63.	244.	30.	921.	579.	91.	0	0
301	289068.	118592.	-1615.	244.	335.	61.	335.	732.	263.	0	102.	366.	61.	933.	579.	67.	0	0
302	289068.	110369.	-1829.	335.	396.	91.	259.	747.	277.	0	119.	396.	91.	970.	579.	15.	30.	0
303	289068.	102147.	-1890.	335.	427.	91.	259.	777.	299.	0	128.	427.	91.	991.	579.	30.	122.	0
304	289068.	93924.	-1920.	244.	396.	79.	317.	792.	329.	0	219.	549.	79.	1006.	579.	15.	152.	0
305	289068.	85701.	-1981.	244.	366.	70.	387.	823.	366.	0	244.	610.	70.	1027.	588.	15.	61.	0
306	289068.	77479.	-1981.	244.	183.	61.	610.	853.	366.	0	244.	610.	61.	1043.	610.	61.	9.	0
307	289068.	69256.	-1829.	152.	207.	24.	622.	853.	293.	0	195.	488.	24.	991.	610.	122.	15.	0
308	289068.	61033.	-975.	61.	213.	0	91.	305.	274.	0	183.	457.	0	915.	634.	122.	61.	0
309	289068.	52811.	-914.	0	244.	0	0	244.	320.	0	137.	457.	0	930.	664.	122.	91.	0
310	300649.	192655.	-610.	0	0	15.	107.	122.	24.	168.	52.	244.	183.	732.	774.	0	0	2
311	298333.	180885.	-945.	152.	24.	46.	174.	244.	52.	137.	70.	259.	183.	732.	732.	0	0	2
312	296017.	168826.	-1128.	305.	49.	76.	119.	244.	82.	107.	85.	274.	183.	823.	707.	0	0	2
313	293701.	156478.	-1280.	213.	146.	122.	37.	305.	174.	61.	55.	290.	183.	875.	671.	0	0	2
314	291384.	142971.	-1311.	274.	152.	46.	229.	427.	235.	15.	85.	335.	61.	854.	640.	30.	15.	2
315	294859.	130434.	-1402.	183.	213.	91.	183.	488.	267.	0	114.	381.	91.	869.	564.	61.	21.	1
316	298333.	118592.	-1737.	213.	305.	122.	305.	732.	341.	0	85.	427.	122.	915.	561.	46.	0	0
317	298333.	102262.	-1890.	366.	427.	91.	274.	792.	288.	0	123.	411.	91.	945.	549.	0	122.	0
318	298333.	85933.	-1920.	244.	488.	61.	290.	838.	329.	0	219.	549.	61.	945.	549.	46.	107.	0
319	298333.	69603.	-1829.	0	305.	61.	488.	853.	320.	0	137.	457.	61.	960.	573.	46.	15.	0
320	298333.	53274.	-914.	0	335.	0	-30.	305.	213.	0	91.	305.	0	829.	610.	122.	61.	0
321	309451.	191786.	-335.	0	0	76.	229.	305.	27.	168.	74.	268.	244.	707.	732.	0	0	2
322	308525.	185966.	-518.	0	0	15.	351.	366.	41.	168.	66.	274.	183.	695.	701.	0	0	2
323	307598.	180089.	-975.	152.	0	30.	351.	381.	56.	152.	72.	280.	183.	716.	668.	0	0	2
324	306672.	174154.	-1067.	168.	24.	61.	341.	427.	72.	122.	93.	287.	183.	726.	671.	0	0	2
325	305745.	168160.	-1128.	183.	43.	76.	338.	457.	88.	107.	98.	293.	183.	777.	680.	0	0	2
326	304819.	162109.	-1219.	183.	61.	91.	305.	457.	136.	91.	75.	302.	183.	793.	671.	0	0	2
327	303892.	156000.	-1280.	183.	79.	122.	226.	427.	170.	61.	89.	320.	183.	793.	640.	0	0	2
328	302966.	149833.	-1311.	213.	143.	152.	70.	366.	205.	30.	106.	341.	183.	823.	613.	0	0	2
329	302039.	142681.	-1433.	213.	146.	168.	235.	549.	252.	15.	120.	387.	183.	854.	588.	0	0	2
330	303429.	136311.	-1676.	244.	149.	183.	399.	732.	284.	0	122.	405.	183.	854.	567.	0	0	2
331	304819.	130173.	-1737.	244.	168.	152.	411.	732.	299.	0	128.	427.	152.	860.	549.	0	0	1
332	306208.	124267.	-1798.	274.	235.	113.	384.	732.	324.	0	139.	463.	113.	866.	546.	0	0	2
333	307598.	118592.	-1829.	305.	290.	91.	351.	732.	317.	0	171.	488.	91.	869.	546.	15.	0	0
334	307598.	110485.	-1829.	305.	427.	122.	305.	853.	299.	0	128.	427.	122.	884.	549.	61.	37.	0
335	307598.	102378.	-1829.	305.	427.	76.	351.	853.	288.	0	123.	411.	76.	884.	549.	30.	101.	0
336	307598.	94271.	-1829.	305.	244.	61.	549.	853.	311.	0	207.	518.	61.	884.	530.	61.	15.	0

Table A-2 (cont.)

Node No.	Coordinates, m		Elev. of cryst. basement, m	Thickness, m											Head in upper aquifer, m	Thickness, m		NCODE
	X	Y		Pre-Penn	Penn. carbonate	Penn. granite wash	Penn. shale	Penn., Total	Wolf. carbonate	Wolf. granite wash	Wolf. shale	Wolf., Total	Granite wash, total	Rock salt		Wolf. porous carbonate	Penn. porous carbonate	
337	307598.	86165.	-1829.	305.	457.	61.	335.	853.	329.	0	219.	549.	61.	890.	530.	61.	37.	0
338	307598.	78058.	-1829.	305.	396.	61.	427.	884.	373.	0	124.	497.	61.	909.	543.	61.	15.	0
339	307598.	69951.	-1829.	305.	259.	61.	533.	853.	333.	0	94.	427.	61.	915.	546.	122.	0	0
340	307598.	61844.	-1341.	152.	198.	0	229.	427.	305.	0	91.	396.	0	823.	564.	137.	9.	0
341	307598.	53737.	-1219.	0	290.	0	76.	366.	389.	0	130.	518.	0	793.	579.	183.	61.	0
342	318253.	190802.	-457.	0	0	91.	366.	457.	55.	152.	67.	274.	244.	701.	671.	0	0	2
343	316863.	179206.	-701.	152.	0	122.	427.	549.	87.	122.	81.	290.	244.	701.	640.	0	0	2
344	315473.	167436.	-1128.	244.	30.	91.	488.	610.	122.	91.	91.	305.	183.	738.	640.	0	0	2
345	314084.	155493.	-1280.	213.	61.	152.	396.	610.	186.	30.	155.	372.	183.	747.	597.	61.	0	2
346	312694.	142507.	-1341.	213.	85.	91.	189.	366.	283.	0	153.	436.	91.	799.	579.	61.	0	2
347	314778.	129971.	-1615.	244.	158.	91.	238.	488.	324.	0	139.	463.	91.	817.	533.	0	0	1
348	316863.	118592.	-1829.	223.	290.	107.	335.	732.	293.	0	195.	488.	107.	829.	530.	61.	24.	0
349	316863.	102494.	-1829.	213.	290.	64.	500.	853.	299.	0	128.	427.	64.	823.	518.	61.	30.	0
350	316863.	86396.	-1829.	213.	335.	61.	457.	853.	415.	0	104.	518.	61.	823.	512.	46.	0	0
351	316863.	70298.	-1829.	152.	122.	61.	671.	853.	390.	0	98.	488.	61.	823.	527.	30.	0	0
352	316863.	54200.	-1585.	183.	213.	3.	424.	640.	428.	0	121.	549.	3.	756.	536.	61.	0	0
353	327055.	189701.	-549.	0	0	122.	488.	610.	58.	122.	110.	290.	244.	671.	610.	0	0	2
354	326591.	183983.	-671.	0	0	131.	479.	610.	74.	113.	109.	296.	244.	655.	610.	0	0	2
355	326128.	178236.	-792.	0	0	143.	466.	610.	91.	101.	111.	302.	244.	671.	610.	0	0	2
356	325665.	172460.	-884.	0	0	152.	457.	610.	110.	91.	113.	314.	244.	701.	600.	0	0	2
357	325202.	166655.	-1219.	259.	0	299.	311.	610.	138.	67.	140.	344.	366.	738.	610.	30.	0	2
358	324738.	160821.	-1402.	268.	0	256.	354.	610.	160.	49.	163.	372.	305.	729.	619.	61.	0	2
359	324275.	154958.	-1433.	274.	30.	213.	366.	610.	186.	30.	180.	396.	244.	732.	604.	61.	0	2
360	323812.	149066.	-1372.	293.	52.	244.	314.	610.	207.	0	207.	415.	244.	732.	549.	61.	0	2
361	323349.	142449.	-1341.	335.	76.	244.	290.	610.	299.	0	128.	427.	244.	735.	536.	61.	0	2
362	324043.	135964.	-1341.	213.	91.	91.	61.	244.	309.	0	133.	442.	91.	777.	524.	46.	0	2
363	324738.	129826.	-1433.	244.	153.	91.	0	244.	341.	0	146.	488.	91.	802.	512.	30.	0	1
364	325433.	124035.	-1676.	244.	232.	110.	268.	610.	293.	0	195.	488.	110.	802.	506.	61.	21.	2
365	326128.	118592.	-1829.	232.	305.	122.	427.	853.	297.	0	160.	457.	122.	796.	512.	61.	55.	0
366	326128.	110601.	-1829.	213.	335.	143.	375.	853.	277.	0	149.	427.	143.	793.	512.	61.	91.	0
367	326128.	102610.	-1829.	207.	290.	91.	472.	853.	305.	0	131.	436.	91.	793.	512.	61.	18.	0
368	326128.	94619.	-1829.	207.	244.	91.	579.	914.	316.	0	135.	451.	91.	793.	488.	30.	0	0
369	326128.	86628.	-1829.	201.	244.	85.	616.	945.	320.	0	137.	457.	85.	799.	488.	61.	0	0
370	326128.	78637.	-1829.	189.	122.	76.	777.	975.	337.	0	144.	482.	76.	799.	503.	61.	0	0
371	326128.	70646.	-1829.	183.	122.	64.	789.	975.	366.	0	122.	488.	64.	774.	503.	61.	0	0
372	326128.	62655.	-1829.	183.	122.	27.	704.	853.	390.	0	98.	488.	27.	738.	503.	61.	0	0
373	326128.	54664.	-1615.	183.	122.	18.	591.	732.	341.	0	146.	488.	18.	716.	488.	61.	0	0
374	335856.	188485.	-640.	0	0	122.	488.	610.	59.	122.	112.	293.	244.	649.	594.	0	0	2
375	335393.	177179.	-884.	0	0	137.	472.	610.	94.	107.	113.	314.	244.	665.	594.	61.	0	2
376	334930.	165815.	-1036.	0	0	152.	457.	610.	139.	91.	135.	366.	244.	732.	564.	61.	0	2
377	334467.	154393.	-1615.	335.	46.	244.	320.	610.	174.	61.	161.	396.	305.	747.	573.	61.	0	2
378	334003.	142507.	-1585.	305.	91.	198.	320.	610.	212.	15.	197.	424.	213.	793.	524.	55.	0	2
379	334698.	129739.	-1676.	213.	152.	116.	98.	366.	295.	0	223.	518.	116.	793.	488.	61.	15.	1
380	335393.	118592.	-1829.	244.	296.	183.	405.	884.	293.	0	195.	488.	183.	777.	527.	61.	76.	0
381	335393.	102726.	-1829.	244.	290.	122.	564.	975.	293.	0	195.	488.	122.	777.	494.	55.	18.	0
382	335393.	86859.	-1829.	198.	183.	82.	771.	1036.	293.	0	195.	488.	82.	777.	488.	61.	0	0
383	335393.	70993.	-1798.	186.	122.	61.	853.	1036.	293.	0	195.	488.	61.	698.	494.	61.	0	0
384	335393.	55127.	-1676.	183.	168.	15.	671.	853.	293.	0	195.	488.	15.	634.	472.	61.	0	0

Table A-2 (cont.)

Node No.	Coordinates, m		Elev. of cryst. basement, m	Thickness, m											Head in upper aquifer, m	Thickness, m		NCODE
	X	Y		Pre-Penn	Penn. carbonate	Penn. granite wash	Penn. shale	Penn., Total	Wolf. carbonate	Wolf. granite wash	Wolf. shale	Wolf., Total	Granite wash, total	Rock salt		Wolf. porous carbonate	Penn. porous carbonate	
385	344658.	187153.	-762.	0	0	131.	783.	914.	60.	113.	126.	299.	244.	631.	579.	0	0	2
386	344658.	181594.	-914.	0	0	134.	780.	914.	76.	110.	119.	305.	244.	640.	579.	46.	0	2
387	344658.	176035.	-975.	0	0	137.	777.	914.	101.	107.	128.	335.	244.	662.	579.	61.	0	2
388	344658.	170476.	-1036.	0	0	140.	774.	914.	113.	104.	149.	366.	244.	726.	564.	61.	0	2
389	344658.	164917.	-1097.	0	0	143.	771.	914.	126.	101.	155.	381.	244.	726.	555.	61.	0	2
390	344658.	159358.	-1128.	0	15.	146.	753.	914.	139.	98.	160.	396.	244.	732.	543.	61.	0	2
391	344658.	153799.	-1707.	0	40.	210.	360.	610.	148.	94.	169.	411.	305.	762.	527.	61.	0	2
392	344658.	148240.	-1737.	335.	91.	152.	366.	610.	162.	91.	173.	427.	244.	848.	509.	30.	0	2
393	344658.	142681.	-1768.	335.	98.	183.	329.	610.	178.	46.	233.	457.	229.	838.	497.	30.	0	2
394	344658.	135964.	-1798.	317.	98.	198.	314.	610.	215.	15.	258.	488.	213.	823.	488.	61.	15.	2
395	344658.	129710.	-1829.	213.	168.	183.	15.	366.	274.	0	274.	549.	183.	756.	488.	61.	30.	1
396	344658.	123919.	-1829.	244.	235.	183.	436.	853.	302.	0	247.	549.	183.	765.	488.	61.	61.	0
397	344658.	118592.	-1829.	244.	299.	183.	418.	899.	295.	0	223.	518.	183.	759.	488.	61.	91.	0
398	344658.	110717.	-1829.	244.	335.	152.	488.	975.	253.	0	253.	506.	152.	753.	488.	61.	98.	0
399	344658.	102842.	-1829.	244.	366.	122.	518.	1006.	244.	0	244.	488.	122.	747.	488.	61.	61.	0
400	344658.	94966.	-1829.	244.	137.	88.	841.	1067.	341.	0	146.	488.	88.	741.	488.	61.	0	0
401	344658.	87091.	-1829.	244.	122.	79.	896.	1097.	268.	0	219.	488.	79.	741.	472.	61.	0	0
402	344658.	79216.	-1829.	204.	122.	73.	902.	1097.	244.	0	244.	488.	73.	726.	488.	61.	0	0
403	344658.	71341.	-1768.	192.	122.	30.	945.	1097.	268.	0	219.	488.	30.	662.	488.	61.	0	0
404	344658.	63465.	-1737.	183.	122.	21.	832.	975.	268.	0	219.	488.	21.	604.	472.	61.	0	0
405	344658.	55590.	-1676.	183.	274.	12.	597.	884.	268.	0	219.	488.	12.	573.	457.	61.	0	0

User's Guide for TRAVEL

by

Prakob Wirojanagud

1983

Bureau of Economic Geology
The University of Texas at Austin
Austin, Texas 78712-7508

Section I: Program Identification

1.1 Program Title: Steady-State Flow Analysis

1.2 Program Code Name: TRAVEL

1.3 Program Writer: The original version of this program is George Pinder's ISOQUAD. Randall J. Charbeneau of the Civil Engineering Department, U.T. at Austin, has modified and incorporated the capabilities of computing streamlines, travel times, and the analytical solution for heads around a pumping well (July 1978). Hunder Yeh and Prakob Wirojanagud modified the program for the University of Texas Cyber 750 computer and incorporated zeta plotting subroutines.

Program Documentation: Prakob Wirojanagud

1.4 Organization: Bureau of Economic Geology
The University of Texas at Austin
Austin, Texas 78712-7508

1.5 Date: April 1983

1.6 Source Language: Cyber 750 Computer Systems-FORTRAN IV Version 538.

1.7 Abstract:

Program TRAVEL is a general purpose program for two dimensional steady-state groundwater flow analysis. It can be used to investigate two dimensional, profile or areal, flow and mass transport problems. Two dimensional-profile problems with free surface can be handled provided that the free surface is specified. Two-dimensional-areal problems with leakage from an aquitard can also be handled knowing heads in the aquitard. The flow region may have any complex shape and it may consist of different materials arranged in arbitrary patterns. External and internal boundary conditions that may be specified are: prescribed head; nodal source/sink discharge; element source/sink discharge; and prescribed head in the

aquitard. Analytical solution for head around a pumping well is obtained if the well is specified as a source/sink element. Typical output consists of nodal point values of head and velocity, plots of head contours, streamlines and travel times.

This program was written based on the Galerkin Finite-Element technique and the use of quadratic-quadrilateral elements in discretizing the flow region. Background material, as well as some examples of application, are available in a report entitled "Finite Element Modeling of Groundwater Injection-Extraction Systems" by R. J. Charbeneau and R. L. Street, Technical Report No. 231, Dept. of Civil Engineering, Stanford University, July 1978.

Section II: Program Usage

2.1 Computer Equipment:

Program TRAVEL was written for a Cyber 750 computer. An input terminal, a line printer, a zeta-plotting library, and a plotter are necessary to run the program.

2.2 Source Program: The source listing of Program TRAVEL and its binary version, BTRAVEL, are stored in permanent file 1057 of The University of Texas computer system. The source listing of the program is also given in Section IV of this manual.

2.3 Control Commands:

As run on the University of Texas Cyber 750 through the interactive job processor (TAURUS), the control commands are as follows:

```
MAXFL= 230000/
LDSET,LIB=ZETLIBF/
BTRAVEL, datafile
```

2.4 Storage Requirements:

The present version of Program TRAVEL requires 230000 (octal) words of central memory to execute. This required memory is adequate for problems of up to 740 nodes or 225 elements. The maximum half bandwidth of the global matrix is 50.

2.5 Construction of Finite Element Mesh:

The following gives the procedure for constructing the finite element mesh and the numbering convention which is part of the procedure for preparing an input data file. One should first construct to scale a map or cross-section of the flow region and divide it into subregions according to the geometry of the flow region and/or the material properties.

Each subregion is subdivided into a finite number of elements and then the node and element numbering conventions are specified. The construction of mesh as well as the numbering of node and element can be performed manually or by using an automatic mesh generation program. A general purpose program named "MESHG" is available for the job. Interested users can find detailed information from the user's guide of the program.

Figure 1 shows a map of finite element mesh of 135 nodes and 36 elements. First, the flow region is divided into 3 subregions as indicated by the thick-solid lines according to, for this example, its geometry. In each subregion, if further discretization into elements is performed manually, the size of each element can vary arbitrarily although it is suggested that the dimensions of neighboring elements within a given isotropic material should not differ from each other by more a factor of 2 or 3. If Program MESHG is used, the size of each element can be varied gradually by a given ratio in each direction.

The node and element numbering in Figure 1 starts in sequential order from left to right and from bottom to top. In this manner, the half bandwidth (NHBW) of the resulting global matrix, which is 20, is the minimum for this particular mesh system. Since the half bandwidth is a function of the maximum difference between nodal number occurring on the same element, one should start numbering along the direction with smaller number of elements and then sequentially proceed along the other direction in order to have the minimum half bandwidth. There are three arrayed parameters characterizing the finite element mesh system that need

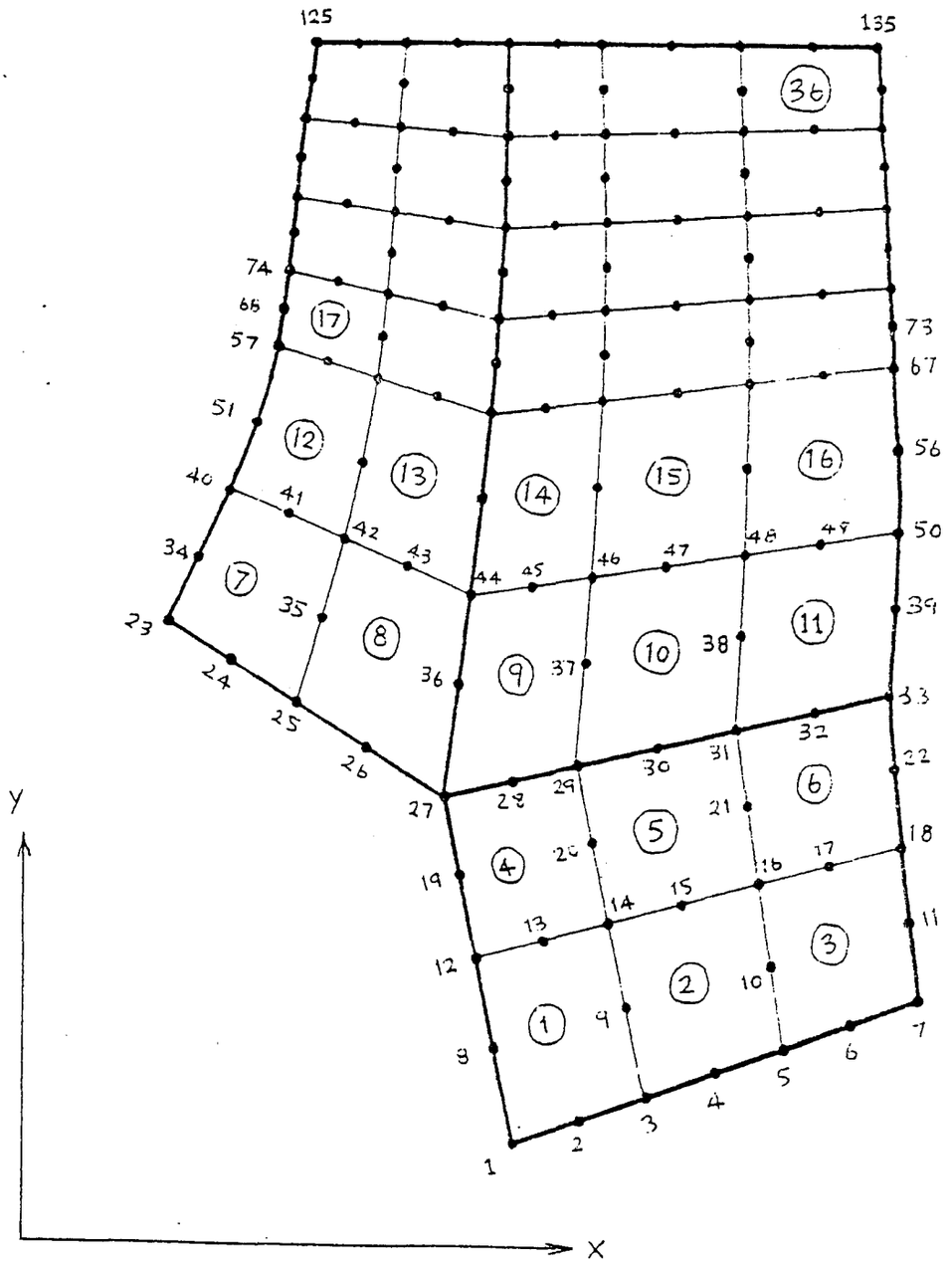
125
135
36
74
66
17
57
73
67
51
12
13
14
15
16
56
40
41
42
43
44
45
46
47
48
49
50
34
7
35
8
9
10
11
39
23
24
25
26
27
36
37
38
33
28
29
30
31
32
22
6
21
5
4
20
18
19
16
17
14
15
13
11
12
3
2
10
1
9
8
7
6
5
4
3
2
1
Y
X

Figure 1

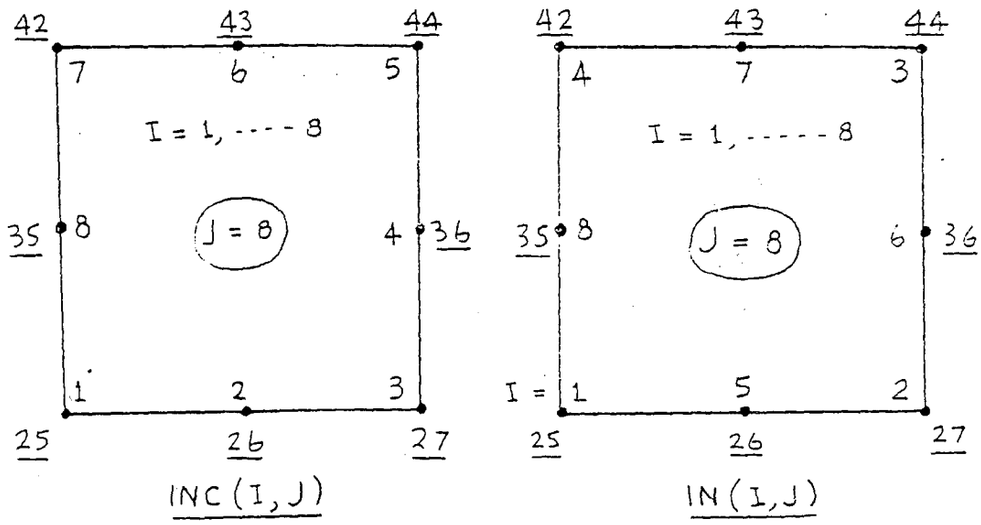

(a) Local-Global Node Numbering Relationship

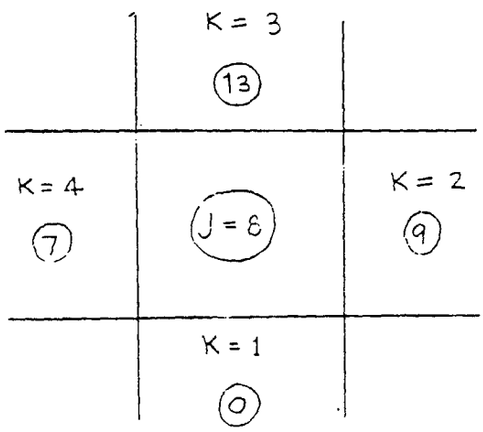

(b) Array of Adjacent Elements, INEL (K, J)

Figure 2

need to be clarified: INC (I,J), IN (I,J), and INEL (K,J).

The integer value of INC (I,J) is the global node number of the local Ith node of the Jth element. As an example, INC (I,J) of the mesh system in Figure 1 has the following integer value for J = 8 (see Figure 2a):

I	=	1	2	3	4	5	6	7	8
INC (I,8)	=	25	26	27	36	44	43	42	35

The counter-clockwise numbering order of INC (I,J) for I = 1 to 8 as shown in Figure 2a is, however, only for convenience in numbering a mesh system manually. The program will convert the array INC (I,J) into array IN (I,J) and use it in the finite element computations. As shown in Figure 2a, the integer value of IN (I,J) for the previous example is:

I	=	1	2	3	4	5	6	7	8
IN (I,8)	=	25	27	44	42	26	36	43	35

Array INEL (K,J) is used to indicate neighboring elements of an element J for use in streamline analysis. Figure 2b shows the counter-clockwise numbering order of INEL (K,J) and its integer value for J = 8.

2.6 Preparation of Data Deck:

The data input has been arranged in groups. Data that do not apply should be left blank, unless otherwise specified.

GROUP	COLUMNS	FORMAT	VARIABLE	DESCRIPTION
A	1-80	20A4	TITLE	Title of problem; information typed on this card is reproduced exactly as a heading on printout.
B	1-5	I5	NN	Number of nodes.
	6-10	I5	NE	Number of elements.
	11-15	I5	NDN	Number of Dirichlet boundary nodes.
	16-20	I5	NHBW	Number in half band width.
	21-25	I5	NLE	Number of leaky elements.
	26-30	I5	NLN	Number of leaky nodes.
	31-35	I5	NQE	Number of source/sink discharge elements.
	36-40	I5	NQN	Number of source/sink discharge nodes.
	41-45	I5	NPLOT	Number of plots of head contours.
	46-50	I5	NTPLOT	Number of plots of transmissivity contours.

GROUP	COLUMNS	FORMAT	VARIABLE	DESCRIPTION
C	1-10	F10.0	ATRANX	Multiplier for x-transmissivity.
	11-20	F10.0	ATRANY	Multiplier for y-transmissivity.
	21-30	F10.0	AFQE	Multiplier for well discharge.
	31-40	F10.0	FACTOR	Multiplier for node coordinates.
	41-50	F10.0	ALEAK	Multiplier for leakage coefficient.

These multipliers are useful when the input values have to be converted due to the inconsistency in units or other needs for transformation. Assign a value of 1.0 if no conversion is needed.

D	1-5	I5	KOD1	Printout of element flow matrices.
	6-10	I5	KOD2	Printout of global flow matrix.
	11-15	I5	KOD3	Printout of element nodal velocities.
	16-20	I5	KOD4	Printout of right hand side vectors.
	21-25	I5	KOD5	Printout of continuous velocity field.
	26-30	I5	KOD6	Plot of hydraulic head contours.
	31-35	I5	KOD7	Plot of transmissivity contours.
	36-40	I5	KOD8	Printout of time of travel along streamlines.
	41-45	I5	KOD9	To flag analytic specification of boundary cond. within the program.
	46-50	I5	KOD10	Plot streamlines.

For these control codes, a value of 1 initiates action, a value of zero suppresses action. For KOD10 to be equal 1, KOD5, KOD8, and either KOD6 or KOD7 must be equal 1.

E	1-5	I5	J	Node number.
	6-15	F10.0	x(J)	x-coordinate of node J.
	16-25	F10.0	y(J)	y-coordinate of node J.
	26-35	F10.0	TRANSX(J)	x-transmissivity at node J.
	36-45	F10.0	TRANSY(J)	y-transmissivity at node J.
	46-55	F10.0	HZERO(J)	Head in the leaking aquitard at node J.

There are NN cards in Group E.

F	1-5	I5	J	Element number.
	6-15	F10.0	PORTH(J)	Product of aquifer porosity and its thickness at element J.
	16-30	F15.0	COEF(J)	Leakage coefficient, which is the aquitard hydraulic conductivity divided by its thickness, at element J.

There are NE cards in Group F.

G	1-5	I5	LL	Element number
	6-10	I5	INC(1)	Integer value of INC(1) is the
	11-15	I5	INC(2)	global node number of node 1 of
	16-20	I5	INC(3)	element LL, and so on . . . .
	21-25	I5	INC(4)	(see details in Section 2.5).
	26-30	I5	INC(5)	
	31-35	I5	INC(6)	
	36-40	I5	INC(7)	
	41-45	I5	INC(8)	

There are NE cards in Group G.

GROUP	COLUMNS	FORMAT	VARIABLE	DESCRIPTION
H	(If NQE > 0)			
	1-5	I5	I	source/sink element number.
	6-15	F10.0	FQE(I)	source/sink discharge at element I.
	16-25	F10.0	RQE(I)	Radius of element I. A source/sink element must have a circular shape.
	26-35	F10.0	BB2(I)	Coefficient used in evaluating Bessel functions for source/sink element (= square root of the characteristic transmissivity divided by the leakage coefficient.
	36-45	F10.0	XQE(I)	x - coordinate of Ith source/sink.
	46-55	F10.0	YQE(I)	y - coordinate of Ith source/sink.
	56-65	F10.0	TRAN(I)	Characteristic transmissivity of source/sink element.

There are NQE cards in Group H.

I	(If NQN > 0)			
	1-5	I5	J	source/sink node number.
	6-15	F10.0	FQ(J)	source/sink discharge at node J.

There are NQN cards in Group I.

J	1-80	20I4	LRT (ITT)	Array used for input of Dirichlet boundary node numbers. ITT is from 1 to NDN. There are 20 values in one card.

Use as many cards as needed.

K	1-80	10F8.0	PH11 (ITT)	Array used for input of Dirichlet boundary head values. There are 10 values in one card.

Use as many cards as needed.

Group LA-LE provides information for plots of transmissivity (If KOD7 = 1).

LA	1-5	I5	NCON	Number of contours for plots.
	6-10	I5	NPTS	Number of search points for contour plots (see example).
	11-15	I5	NFE	First element searched for contour plots.
	16-20	I5	NLT	Last element searched for contour plots.
	21-25	I5	NCIR	0 for rectangular domain, 1 for circular domain.
LB	1-10	F10.0	XMIN	Minimum x-coordinates for plots.
	11-20	F10.0	XMAX	Maximum x-coordinates for plots.
	21-30	F10.0	YMIN	Minimum y-coordinates for plots.
	31-40	F10.0	YMAX	Maximum y-coordinates for plots.

GROUP	COLUMNS	FORMAT	VARIABLE	DESCRIPTION
LC				Information to specify size and position of a rectangular frame of plots.
	1-10	F10.0	XO	Origin of frame in inches from the paper edge in x-direction.
	11-20	F10.0	YO	Origin of frame in inches from the paper edge in y-direction.
	21-30	F10.0	XL	Length of the frame in x-direction, inches.
	31-40	F10.0	YL	Length of the frame in y-direction, inches.
LD	1-80	8F10.0	CON(I)	Contour levels for plots. I = 1 to NCON.

Use as many cards as needed.

LE	1-80	8F10.0	PTS(I)	Contour plotting searched points in local coordinates (see example). I = 1 to NPTS

Use as many cards as needed.

Groups MA-ME provide information for plots of hydraulic heads (If KOD6 = 1). The input variables and formats are exactly the same as those in Group LA to LE.

Groups NA-ND provide information for streamline and travel time analysis (If KOD10 = 1, KOD5 = 1, KOD8 = 1, and either KOD6 = 1 or KOD7 = 1).

NA	1-5	I5	NSL	Number of streamlines.
	6-10	I5	NSTPRT	Number of integration between each printout of streamline travel.
	11-15	I5	NTIME	Number of contours of travel time.
	16-25	F10.0	STEP	Stepping length for integration long streamlines in local coordinates.
	26-35	F10.0	TMAX	Maximum travel time along streamlines.
NB	1-80	8F10.0	TT(I)	Travel-time level to be plotted along streamlines. I = 1 to NTIME.

Use as many cards as needed.

NC	1-5	I5	L	Element number.
	6-10	I5	INEI(1,L)	Array of adjacent elements.
	11-15	I5	INEL(2,L)	(see details in Section 2.5).
	16-20	I5	INEL(3,L)	
	21-25	I5	INEL(4,L)	

There are NE cards in Group NC.

GROUP	COLUMNS	FORMAT	VARIABLE	DESCRIPTION
ND	1-5	I5	NEL	Element number in which starting points of streamlines are specified.
	6-15	F10.0	XI1	ξ-η coordinates of a starting point of streamline in the NELth element.
	16-25	F10.0	ETA1	

Use as many cards as needed.

2.7 OUTPUT:

Printed output are in file OUTPUT.

Plotted output are in file PLOT.

Tape 1 contains, in each line, node number, x and y coordinates of node, nodal values of head and x-y seepage velocities with the format (I5, 3F10.2, 2E15.6).

SECTION III: SAMPLE PROBLEM

Table 1 is a listing of data input of the sample problem shown in Figure 3. Figure 4 shows the node and element numbering convention. Figures 5 and 6 are plotted output in file PLOT. Different examples of the program's application are available in the report by Carbeneau and Street (1978).

Table 1 Data Input of the Sample Problem

```
 TEST PROBLEM FOR PROGRAM TRAVEL
40     9    14    14     0     0     0     0     1     0
    1.00        1.00        1.00        1.00        1.00
 1     1     1     0     1     1     0     1     0     1
 1          .00          .00        50.00        50.00          .00
 2        50.00          .00        50.00        50.00          .00
 3       100.00          .00        50.00        50.00          .00
 4       150.00          .00        50.00        50.00          .00
 5       200.00          .00        50.00        50.00          .00
 6       250.00          .00        50.00        50.00          .00
 7       300.00          .00        50.00        50.00          .00
 8          .00        50.00        50.00        50.00          .00
 9       100.00        50.00        50.00        50.00          .00
10       200.00        50.          50.          50.            .00
11       300.          50.          50.          50.            .00
12         0.         100.          50.          50.            .00
13        50.         100.          50.          50.            .00
14       100.         100.           5.           5.            .00
15       150.         100.           5.           5.            .00
16       200.         100.           5.           5.            .00
17       250.         100.          50.          50.            .00
18       300.         100.          50.          50.            .00
19         0.         150.          50.          50.            .00
20       100.         150.           5.           5.            .00
21       200.         150.           5.           5.            .00
22       300.         150.          50.          50.            .00
23         0.         200.          50.          50.            .00
24        50.         200.          50.          50.            .00
25       100.         200.           5.           5.            .00
26       150.         200.           5.           5.            .00
27       200.         200.           5.           5.            .00
28       250.         200.          50.          50.            .00
29       300.         200.          50.          50.            .00
30         0.         250.          50.          50.            .00
31       100.         250.          50.          50.            .00
32       200.         250.          50.          50.            .00
33       300.         250.          50.          50.            .00
34         0.         300.          50.          50.            .00
35        50.         300.          50.          50.            .00
36       100.         300.          50.          50.            .00
37       150.         300.          50.          50.            .00
38       200.         300.          50.          50.            .00
39       250.         300.          50.          50.            .00
40       300.         300.          50.          50.            .00
 1        2.50          .00
 2        2.50          .00
 3        2.50          .00
 4        2.50          .00
 5        2.50          .00
```

Table 1 (continue)

```
6       2.50         .00
7       2.50         .00
8       2.50         .00
9       2.50         .00
1     1     2     3     9    14    13    12     8
2     3     4     5    10    16    15    14     9
3     5     6     7    11    18    17    16    10
4    12    13    14    20    25    24    23    19
5    14    15    16    21    27    26    25    20
6    16    17    18    22    29    28    27    21
7    23    24    25    31    36    35    34    30
8    25    26    27    32    38    37    36    31
9    27    28    29    33    40    39    38    32
1    2    3    4    5    6    7  34   35   36   37   38   39   40
30.00    30.00    30.00    30.00    30.00    30.00    30.00    20.00    20.00    20.0
20.00    20.00    20.00    20.00
 9     5     1     9     0
    .00     300.00         .00     300.00
   1.50       2.75        6.00       6.00
  29.00      28.00       27.00      26.00      25.00      24.00      23.00      22.0
  21.00
   -.80       -.30         .00        .30        .80
15     5     8          .10  10000.00
 200.00     400.00     600.00     800.00    1000.00    1200.00    1400.00    1600.0
 1     0     2     4     0
 2     0     3     5     1
 3     0     0     6     2
 4     1     5     7     0
 5     2     6     8     4
 6     3     0     9     5
 7     4     8     0     0
 8     5     9     0     7
 9     6     0     0     8
 1       -.70       -.99
 1       -.30       -.99
 1        .10       -.99
 1        .50       -.99
 1        .90       -.99
 2       -.70       -.99
 2       -.30       -.99
 2        .10       -.99
 2        .50       -.99
 2        .90       -.99
 3       -.70       -.99
 3       -.30       -.99
 3        .10       -.99
 3        .50       -.99
 3        .90       -.99
```

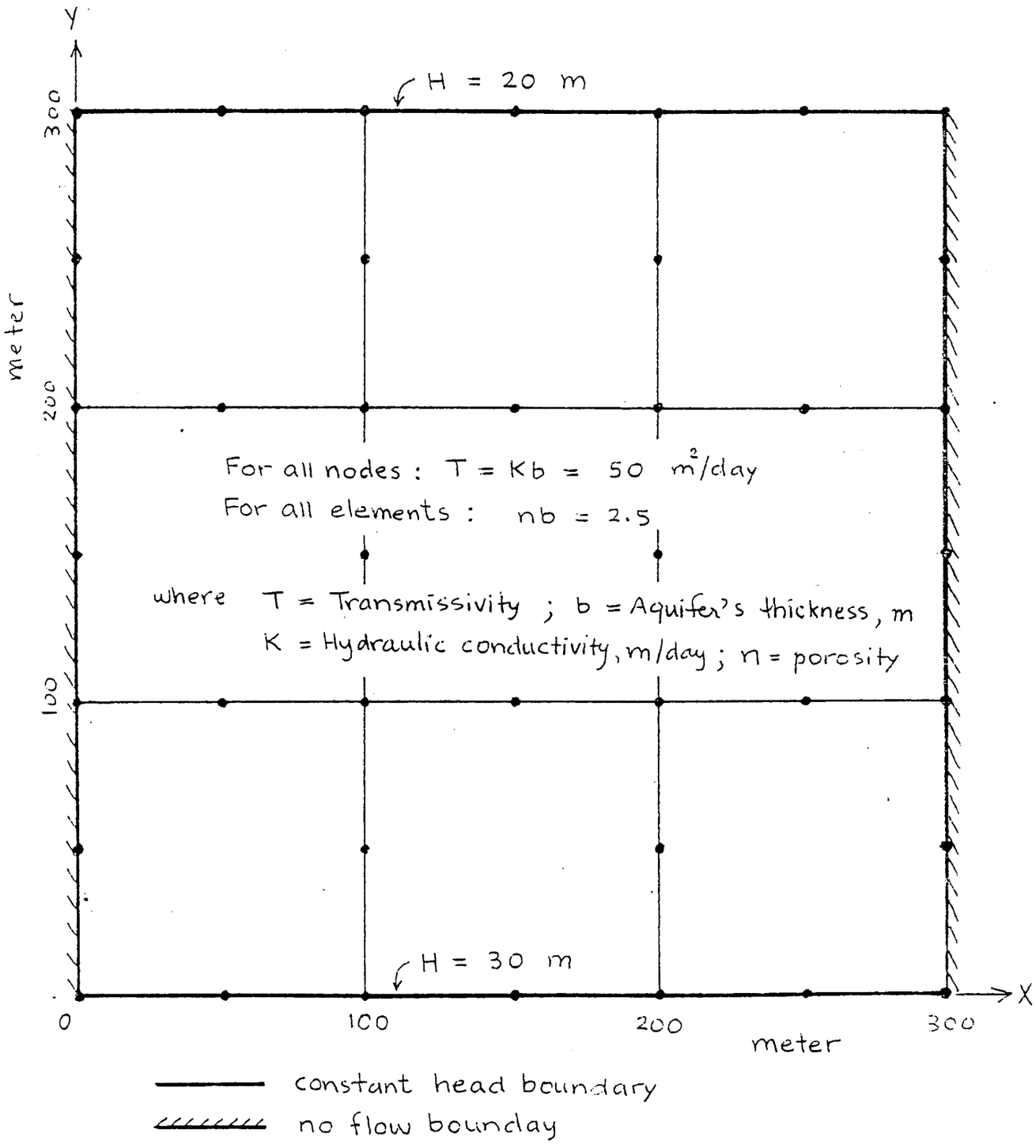

Figure 3 Sample Problem

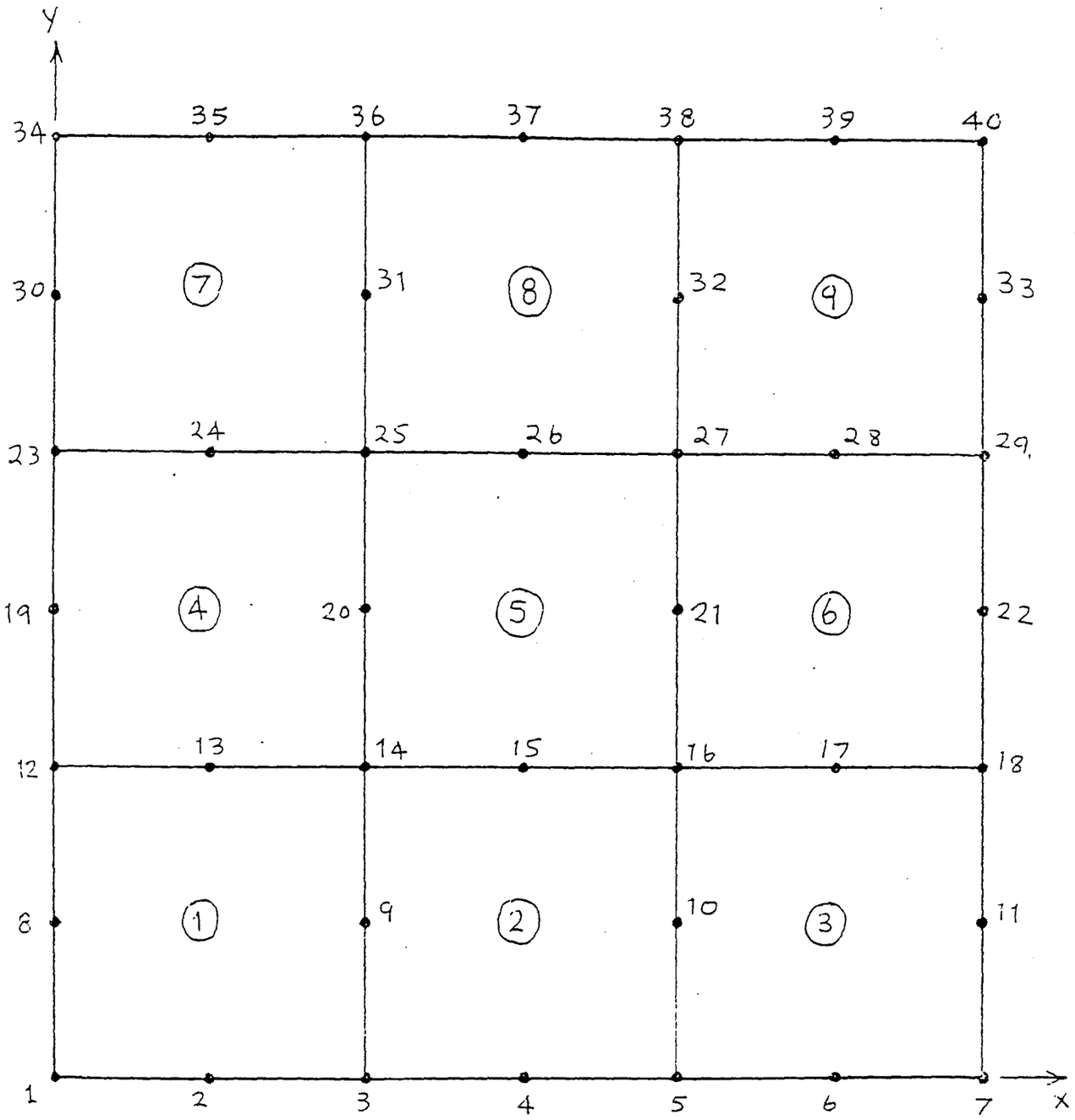

Half Bandwidth = 14

Figure 4 Numbering Convention for the Sample Problem

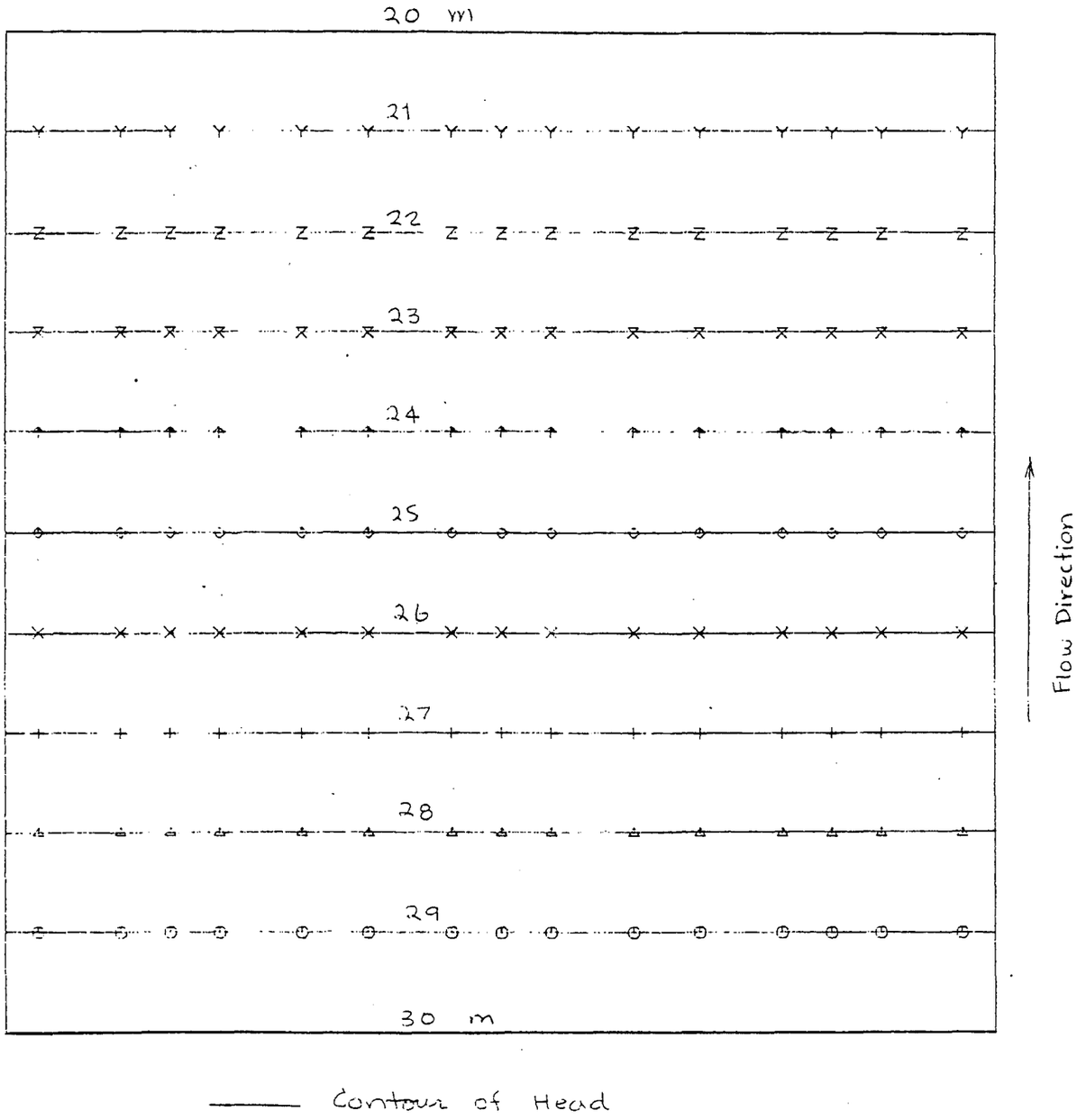

Figure 5 Sample Output - Contours of Head

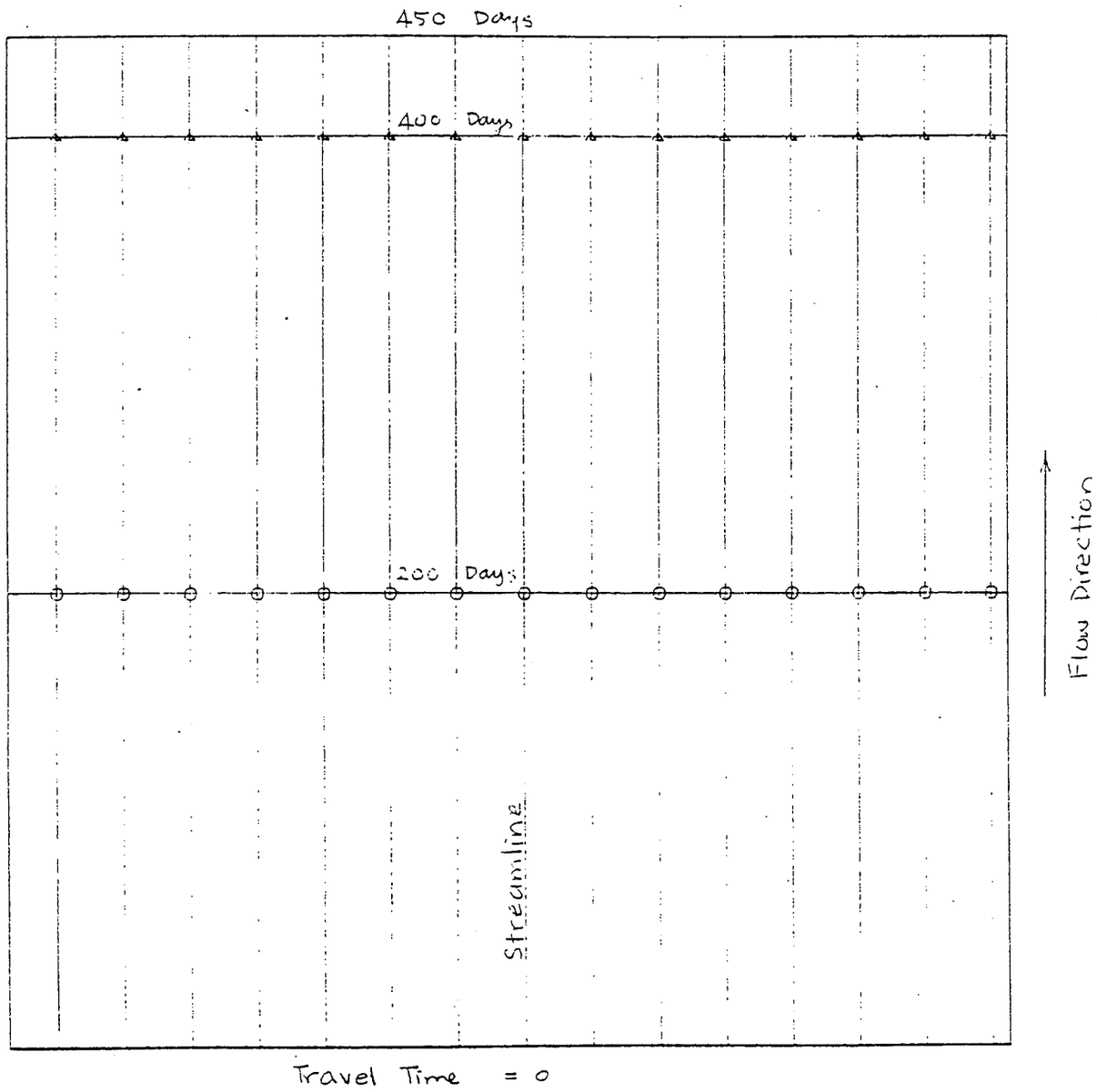

Figure 6 Sample Output - Streamlines and Travel Times

SECTION IV: PROGRAM LISTING

```
      PROGRAM TRAVEL (INPUT,OUTPUT,TAPE5=INPUT,TAPE6=OUTPUT,TAPE1,
     1               TAPE2,PLOT)
C                          T R A V E L
C          S T E A D Y  S T A T E  F L O W  A N A L Y S I S
C
C
C     THE ORIGINAL VERSION OF THIS PROGRAM IS PINDER'S ISOQUAD,
C     RANDALL J. CHARBENEAU OF THE CIVIL ENGINEERING DEPARTMENT,U.T. AT
C     AUSTIN, HAS MODIFIED AND INCORPORATED THE CAPABILITIES OF COMPUTING
C     STREAMLINES, TRAVEL TIMES, AND THE ANALYTICAL SOLUTION FOR HEADS
C     AROUND A PUMPING WELL (1978), MUNDER YEH AND PRAKOB WIROJANAGUD
C     MODIFIED THE PROGRAM FOR U.T. CYBER 750 COMPUTER AND INCOPORATED
C     ZETA PLOTTING SUBROUTINES. THE PROGRAM WAS DOCUMENTED FOR USE IN
C     THE WEST TEXAS WASTE ISOLATION PROJECT BY PRAKOB WIROJANAGUD (1983).
C
C
C     D E F I N I T I O N   O F   V A R I A B L E S
C
C     AFQE--------MULTIPLIER FOR WELL DISCHARGE
C     ALEAK-------MULTIPLIER FOR LEAKAGE COEFFICIENT
C     ATRANX------MULTIPLIER FOR X-TRANSMISSIVITY
C     ATRANY------MULTIPLIER FOR Y-TRANSMISSIVITY
C     BESI0-------MODIFIED BESSEL FUNCTION OF THE FIRST KINK OF ORDER ZERO
C     BESI1-------MODIFIED BESSEL FUNCTION OF THE FIRST KINK OF ORDER ONE
C     BESK0-------MODIFIED BESSEL FUNCTION OF THE SECOND KIND OF ORDER ZERO
C     BESK1-------MODIFIED BESSEL FUNCTION OF THE SECOND KIND OF ORDER ONE
C     BES1(I)-----ARRAY OF MODIFIED BESSEL FUNCTIONS OF ORDER ONE
C                 EVALUATED ON THE SOURCE/SINK ELEMENT BOUNDARY
C     BB2(I)------COEFFICIENT USED IN EVALUATING BESSEL FUNCTIONS FOR
C                 SOURCE/SINK ELEMENTS=  SQUARE ROOT OF THE CHARACTERISTIC
C                 TRANSMISSIVITY DIVIDED BY THE LEAKAGE COEFFICIENT.....L
C     COEF(I)-----LEAKAGE COEFFICIENT (AQUITARD PERMEABILITY DIVIDED
C                 BY ITS THICKNESS).........1/T
C     CON(I)------CONTOUR LEVELS FOR PLOTS
C     DETJ(I)-----VALUE OF THE JACOBIAN DETERMINANT AT EACH INTEGRATION
C                 POINT
C     DX(I,J)-----VALUE OF THE X-DERIVATIVE OF THE ITH BASIS FUNCTION AT
C                 THE JTH INTEGRATION POINT
C     DY(I,J)-----VALUE OF THE Y-DERIVATIVE OF THE ITH BASIS FUNCTION AT
C                 THE JTH INTEGRATION POINT
C     ETA1--------STARTING LOCAL ETA COORDINATE FOR INTEGRATION ALONG
C                 STREAMLINES
C     F(I,J)------VALUE OF THE ITH BASIS FUNCTION AT THE JTH INTEGRATION
C                 POINT
C     FQ(I)-------NODAL SOURCE/SINK DISCHARGE
C     FQE(I)------ELEMENT SOURCE/SINK DISCHARGE.............L**3/T
C     FM(I)-------STORAGE VECTOR
C     FACTOR------MULTIPLIER FOR NODE COORDINATES
C     H(I,J)------GLOBAL FLOW MATRIX
C     HK(I)-------SUM OF THE HEAD IN ADJACENT AQUIFER AT THE ITH
C                 INTEGRATION POINT
C     IN(I,L)-----INCIDENCE RELATIONS=  ITH NODE OF ELEMENT L
C     INC(I)------DUMMY ARRAY FOR INPUT OF INCIDENCE RELATIONS
C     INEL(I,L)---ARRAY OF ADJACENT ELEMENTS FOR STREAMLINE ANALYSIS
C     JACOB(I)----1 FOR PARALLELOGRAM SHAPED ELEMENTS, 2 FOR NON-CONSTANT
C                 JACOBIAN ELEMENTS (NON-PARALLELOGRAM TYPE)
C     KOD1--------1 FOR PRINTOUT OF ELEMENT FLOW MATRICES, 0 OTHERWISE
C     KOD2--------1 FOR PRINTOUT OF GLOBAL FLOW MATRIX, 0 OTHERWISE
C     KOD3--------1 FOR PRINTOUT OF ELEMENT NODAL VELOCITIES, 0 OTHERWISE
C     KOD4--------1 FOR PRINTOUT OF RIGHT HAND SIDE VECTORS, 0 OTHERWISE
C     KOD5--------1 FOR PRINTOUT OF CONTINUOUS VELOCITY FIELD, 0 OTHERWISE
```

```
C      KOD6---------1 FOR PLOT OF HYDRAULIC HEAD CONTOURS, 0 OTHERWISE
C      KOD7---------1 FOR PLOT OF TRANSMISSIVITY CONTOURS, 0 OTHERWISE
C      KOD8---------1 FOR PRINTOUT OF TIME OF TRAVEL ALONG STREAMLINES,
C                     0 OTHERWISE
C      KOD9---------1 TO FLAG ANALYTIC SPECIFICATION OF BOUNDARY CONDITIONS
C                     WITHIN THE PROGRAM
C      KOD10--------PLOT STREAMLINES, (KOD5=1,KOD8=1,FOR KOD10=1)
C      KR(I)--------NODE NUMBER OF THE ITH DIRICHLET BOUNDARY NODE
C      LR(I)--------INDEX WHICH EQUALS 1 FOR DIRICHLET BOUNDARY NODES AND
C                     0 OTHERWISE
C      LRC(I)-------RUNNING SUM OF DIRICHLET BOUNDARY NODES
C      LRT(I)-------DUMMY ARRAY FOR INPUT OF DIRICHLET BOUNDARY NODES
C      N----------NUMBER OF ACTIVE NODES     (NN=NDN)
C      NCIR---------0 FOR RECTANGULAR DOMAIN, 1 FOR CIRCULAR DOMAIN
C      NCON---------NUMBER OF CONTOURS FOR PLOTS
C      NDN----------NUMBER OF DIRICHLET BOUNDARY NODES
C      NE-----------NUMBER OF ELEMENTS
C      NEL----------STARTING ELEMENT FOR INTEGRATION ALONG STREAMLINES
C      NFE----------FIRST ELEMENT SEARCHED FOR CONTOUR PLOTS
C      NHBW---------NUMBER IN HALF BANDWIDTH
C      NLE----------NUMBER OF LEAKY ELEMENTS
C      NLE----------LAST ELEMENT SEARCHED FOR CONTOUR PLOTS
C      NLN----------NUMBER OF LEAKY NODES
C      NN-----------NUMBER OF NODES
C      NPLOT--------NUMBER OF PLOTS OF HYDRAULIC HEAD CONTOURS IN OUTPUT
C      NPTS---------NUMBER OF SEARCH POINTS FOR CONTOUR PLOTS
C      NQE----------NUMBER OF SOURCE/SINK DISCHARGE ELEMENTS
C      NQN----------NUMBER OF SOURCE/SINK DISCHARGE NODES
C      NSL----------NUMBER OF STREAMLINES
C      NSTPRT-------NUMBER OF INTEGRATIONS BETWEEN PRINTOUT OF STREAMLINE
C                     TRAVEL
C      NTIME--------NUMBER OF CONTOURS OF TRAVEL TIME
C      NTPLOT-------NUMBER OF PLOTS OF TRANSMISSIVITY CONTOURS IN OUTPUT
C      PHI(I)-------CALCULATED HYDRAULIC HEADS
C      PHII(I)------DIRICHLET BOUNDARY NODE HEAD
C      PHIIN(I)-----DUMMY ARRAY FOR INPUT OF DIRICHLET BOUNDARY NODE HEADS
C      PORTH(I)-----PRODUCT OF ELEMENT POROSITY AND AQUIFER THICKNESS,...L
C      PTS(I)-------CONTOUR PLOTTING SEARCH POINTS
C      Q(I)---------VECTOR OF  KINETIC ENERGY  TO BE LOADED IN ELEMENT
C                     FLOW MATRIX
C      RQE(I)-------RADIUS OF SOURCE/SINK ELEMENT,.............L
C      RT(I)--------FORCING FUNCTION (RIGHT HAND SIDE)
C      SE(I,J)------ELEMENT FLOW MATRIX
C      SRCL---------UNKNOWN PART OF LEAKAGE FOR ELEMENT (LOADED INTO
C                     ELEMENT FLOW MATRIX)
C      SRCLT(I)-----UNKNOWN PART OF LEAKAGE AT INTEGRATION POINT I
C      SRCR(I)------KNOWN PART OF LEAKAGE FOR NODE I
C      SRCRT(I)-----KNOWN PART OF LEAKAGE FOR INTEGRATION POINT I
C      STEP---------STEPPING LENGTH FOR INTEGRATION ALONG STREAMLINES
C      TMAX---------MAXIMUM TRAVEL TIME ALONG STREAMLINES
C      TRAN(I)------CHARACTERISTIC TRANSMISSIVITY OF SOURCE/SINK ELEMENT,.
C                     ..,L**2/T
C      TRANSX(I)----X-TRANSMISSIVITY OF NODE I.....,.....L**2/T
C      TRANSY(I)----Y-TRANSMISSIVITY OF NODE I.....,.....L**2/T
C      X(I)---------X-COORDINATE OF NODE I.....,.....L
C      XII----------STARTING LOCAL XI COORDINATE FOR INTEGRATION ALONG
C                     STREAMLINES
C      XMAX---------MAXIMUM X-COORDINATE FOR PLOTS
C      XMIN---------MINIMUM X-COORDINATE FOR PLOTS
C      XQE(I)-------X-COORDINATE OF ITH SOURCE/SINK,.....L
C      XV(I)--------MODIFIED FE X-VELOCITY FOR SOURCE/SINK ELEMENTS
C      Y(I)---------Y-COORDINATE OF NODE I.....,.....L
```

```
C      YMAX--------MAXIMUM Y-COORDINATE FOR PLOTS
C      YMIN--------MINIMUM Y-COORDINATE FOR PLOTS
C      YQE(I)------Y-COORDINATE OF ITH SOURCE/SINK.......L
C      YV(I)-------MODIFIED FE Y-VELOCITY FOR SOURCE/SINK ELEMENTS
C
C
C
C     ------------------------------------------------------------------
       REAL AG(4),H1,H2
C
       COMMON /SCALAR/
      1   NN, NE, NHBW, SRCL, KOD8, KOD10, IQE
       COMMON /VECTOR/
      1   X(740), Y(740), FM(740), PHI(740), PHII(740), XV(740),
      2   RT(740), TRANSX(740), TRANSY(740), COEF(225), PORTH(225),
      3   FQE(20), XQE(20), YQE(20), RQE(20), BB2(20), BES1(20),
      4   SRCRT(16), SRCLT(16), Q(16), SRCR(8), DGX(8), DGY(8), YV(740),
      5   FQ(50)
       COMMON /MATRIX/
      1   H(700,50), IN(8,225), SE(8,8)
C
       DIMENSION
      1   HZERO(740), LR(740), LRC(740), KR(740), TRANS(740),
      2   TITLE(20), INC(8), LRT(100), PHIIH(100), HK(16), F(8,16),
      3   DETJ(16), DX(8,16), DY(8,16), TRAN(20), FF(8)
       DATA AG/-.86113631159405З,
      1   -.33998104358485б, .33998104358485б, .86113631159405З/
       DATA KR(1)/0/
C     ------------------------------------------------------------------
C
C      R E A D   A N D   W R I T E   D A T A
       READ (5,840) TITLE
       WRITE (6,850)
       WRITE (6,860) TITLE
C
       READ (5,910) NN,NE,NDN,NHBW,NLE,NLN,NQE,NQN,NPLOT,NTPLOT
       WRITE (6,920)
       WRITE (6,930) NN,NE,NDN,NQE,NHBW,NLE,NLN,NPLOT,NTPLOT
C
C
       READ (5,1040) ATRANX,ATRANY,AFQE,FACTOR,ALEAK
       WRITE (6,1050) ATRANX,ATRANY,AFQE,FACTOR,ALEAK
C
      READ (5,910) KOD1,KOD2,KOD3,KOD4,KOD5,KOD6,KOD7,KOD8,KOD9,
     .             KOD10
C
C      WRITE OUT CODE INTERPRETATION
       WRITE (6,25)
       IF (KOD1.EQ.2) WRITE (6,1)
       IF (KOD1.NE.2) WRITE (6,2)
       IF (KOD2.EQ.3) WRITE (6,3)
       IF (KOD2.NE.3) WRITE (6,4)
       IF (KOD3.EQ.2) WRITE (6,5)
       IF (KOD3.NE.2) WRITE (6,6)
       IF (KOD4.EQ.3) WRITE (6,7)
       IF (KOD4.NE.3) WRITE (6,8)
       IF (KOD5.EQ.2) WRITE (6,11)
       IF (KOD5.NE.2) WRITE (6,12)
       IF (KOD6.EQ.2) WRITE (6,13)
       IF (KOD6.NE.2) WRITE (6,14)
       IF (KOD7.EQ.3) WRITE (6,15)
       IF (KOD7.NE.3) WRITE (6,16)
```

```
      IF (KODB.EQ.0) WRITE (6,17)
      IF (KODB.NE.0) WRITE (6,18)
      IF(KODT.EQ.0) WRITE (6,19)
      IF(KODT.NE.0) WRITE (6,20)
C
C     FILL DUMMY ARRAYS FOR NODE AND ELEMENT NUMBERS
C
C
C     READ GENERAL INPUT DATA FOR CODE
C     --------------------------------
C
C
C     READ NODE COORDINATES AND PARAMETERS=
C     TRANSMISSIVITY AND HEAD IN ADJACENT AQUIFER
      READ (5,980) (J,X(J),Y(J),TRANSX(J),TRANSY(J),HZERO(J),K=1,NN)
      DO 40 J=1,NN
      X(J)=X(J)*FACTOR
      Y(J)=Y(J)*FACTOR
   40 CONTINUE
C
C     READ ELEMENT PARAMETERS=  POROSITY AND LEAKAGE COEFFICIENT
      READ (5,985) (J,PORTH(J),COEF(J),K=1,NE)
C
C     READ ELEMENT INCIDENCES
C
      DO 50 L=1,NE
      READ (5,1110) LL,(INC(K),K=1,8)
      DO 50 I=1,4
      J=I+4
      IN(I,L)=INC(2*I-1)
      IN(J,L)=INC(2*I)
   50 CONTINUE
C
C
C     WRITE GENERAL INPUT DATA FOR CODE
C     ---------------------------------
C
C     WRITE NODE COORDINATES
      WRITE (6,990)
      WRITE (6,1000)
      WRITE (6,1010) (J,X(J),Y(J),J=1,NN)
C
C     WRITE ELEMENT INCIDENCES
      WRITE (6,1140)
      WRITE (6,1150)
      DO 100 L=1,NE
  100 WRITE (6,1160) L,(IN(I,L),I=1,8)
C
C     WRITE NODAL TRANSMISSIVITIES AND HEAD IN ADJACENT AQUIFER
      WRITE (6,1170)
      WRITE (6,1190) (J,TRANSX(J),TRANSY(J),HZERO(J),J=1,NN)
C     WRITE ELEMENT POROSITY TIMES AQUIFER THICKNESS AND LEAKAGE
C     COEFFICIENT
C
      WRITE (6,1180)
      WRITE (6,1200) (J,PORTH(J),COEF(J),J=1,NE)
      DO 120 J=1,NE
  120 COEF(J)=COEF(J)*ALEAK
C
C
C
C     READ AND WRITE DATA FOR SOURCE/SINK ELEMENTS,
```

```
C      SOURCES ARE POSITIVE.  FOR THIS CODE THE SOURCE/SINK
C      IS ALWAYS LOCATED AT THE ELEMENTS ORIGIN
C
       III=NE+1
       DO 150 I=1,III
       RQE(I)=0.
       BB2(I)=0.
       XQE(I)=0.
       YQE(I)=0.
       TRAN(I)=0.
       BES1(I)=0.
  150  FQE(I)=0.
       IF (NQE.EQ.0) GO TO 201
       WRITE (6,1020)
       DO 200 JJ=1,NQE
       READ (5,70) IQE,FQE(IQE),RQE(IQE),BB2(IQE),XQE(IQE),YQE(IQE),
      1            TRAN(IQE)
C
C      EVALUATE MODIFIED BESSEL FUNCTIONS OF THE FIRST AND SECOND KINDS
C      OF ORDERS 0 AND 1=  I0, I1, K0, AND K1
C
       IF (COEF(IQE).EQ.0.) GO TO 170
       XXX=RQE(IQE)/BB2(IQE)
       BES1(IQE)=BESK1(XXX)*BESK0(XXX)*BESI1(XXX)/BESI0(XXX)
  170  CONTINUE
C
       WRITE (6,1040) IQE,FQE(IQE),RQE(IQE),XQE(IQE),YQE(IQE),BB2(IQE),
      .               TRAN(IQE)
       TRAN(IQE)=TRAN(IQE)*ATRANX
  200  FQE(IQE)=FQE(IQE)*AFQE
  201  CONTINUE
C
C      READ NODAL DISCHARGE
C
       DO 210 I=1,NN
       PHII(I)=0.
  210  FQ(I)=0.
       IF(NQN.EQ.0) GO TO 230
       DO 220 I=1,NQN
  220  READ (5,1460) J,FQ(J)
  230  CONTINUE
C
C      IDENTIFY DIRICHLET BOUNDARY NODES FOR FLOW (INDICATED BY LR=1)
C
       WRITE (6,1230)
       DO 270 I=1,NN
  270  LR(I)=0
       IF (NQN.EQ.0) GO TO 310
       NST=0
  280  READ (5,1240) (LRT(ITT),ITT=1,20)
       IA=0
       DO 290 I=1,20
       IF (LRT(I).EQ.0) GO TO 300
       IA=I
       J=LRT(I)
       NST=NST+1
       IF (J.LE.NN) GO TO 290
       WRITE (6,1250) J
       GO TO 1600
  290  LR(J)=1
  300  WRITE (6,1260) (LRT(IIT),IIT=1,IA)
       IF (NST.GE.NQN) GO TO 310
```

```
      IF (IA.EQ.20) GO TO 280
      IF (NST.NE.NON) WRITE (6,1270) NST,NON
  310 CONTINUE
C
C     READ DIRICHLET NODE HEADS
      IF (KOD9.EQ.1) GO TO 325
      IA=0
      IA1=1
      IA2=10
  315 READ (5,500) (PHIIH(ITT),ITT=IA1,IA2)
      IF (IA2.GE.NON) GO TO 318
      IA1=IA2+1
      IA2=IA2+10
      GO TO 315
  318 DO 320 I=1,NN
      IF (LR(I).NE.1) GO TO 320
      IA=IA+1
  320 PHII(I)=PHIIH(IA)
C
      GO TO 340
C
C     ***************************************
C     ANALYTIC SPECIFICATION OF BOUNDARY CONDITIONS.
C     SPECIFY FOR PARTICULAR PROBLEM.
  325 CONTINUE
      DO 330 J=1,NOE
      DO 328 K=1,NE
      IF(FOE(K).LE.0.) GO TO 327
      DO 326 I=1,NN
      IF (LR(I).NE.1) GO TO 324
      XN=X(1)-XOE(K)
      XXN=XN*XN
      YN=Y(1)-YOE(K)
      YYN=YN*YN
      XD=X(I)-XOE(K)
      XXD=XD*XD
      YD=Y(I)-YOE(K)
      YYD=YD*YD
      SUMH=114.6*FOE(K)*ALOG((XXN+YYN)/(XXD+YYD))/TRANSX(I)
      PHII(I)=PHII(I)+SUMH
  324 CONTINUE
  326 CONTINUE
  327 CONTINUE
  328 CONTINUE
  330 CONTINUE
C     ***************************************
  340 CONTINUE
C
C
C
C
C     SUM DIRICHLET BOUNDARY NODES
      LRC(1)=LR(1)
      DO 370 J=2,NN
  370 LRC(J)=LRC(J-1)+LR(J)
      NR=LRC(NN)
      N=NN-NR
      WRITE (6,1310) NN,NR,N
C
C     CONSTANT BOUNDARY MATRIX ROW INDICES
      K=0
      DO 390 J=1,NN
```

```
372         IF (LR(J).LT.1) GO TO 390
373         K=K+1
374         KR(K)=J
375     390 CONTINUE
376   C
377   C
378   C     PLOT CONTOURS OF TRANSMISSIVITY
379         IF (KOD7.NE.1) GO TO 402
380         DO 394 I=1,NN
381     394 FM(I)=TRANSX(I)
382         DO 396 I=1,NTPLOT
383     396 CALL ZPLOT
384     402 CONTINUE
385   C
386         DO 406 J=1,NN
387         TRANSX(J)=TRANSX(J)*ATRANX
388     406 TRANSY(J)=TRANSY(J)*ATRANY
389   C
390   C     CONSTANTS
391   C
392   C     CLEAR GLOBAL FLOW MATRIX
393   C
394         DO 410 I=1,N
395         FM(I)=0.
396         DO 410 J=1,NHBW
397     410 H(I,J)=0.
398   C
399   C     CLEAR GLOBAL FORCING FUNCTION (RIGHT HAND SIDE VECTOR)
400   C
401         II=0
402         DO 415 I=1,NN
403         IF (LR(I).GT.0) GO TO 415
404         II=II+1
405         RT(II)=0.
406     415 CONTINUE
407   C
408   C
409   C     GENERATE COEFFICIENT MATRIX FOR FLOW
410   C     ------------------------------------
411   C
412   C
413   C     CHANGE FORCING FUNCTION FOR NODAL LOCATION OF WELLS
414         IF (NON.EQ.0) GO TO 419
415         DO 417 I=1,NN
416         IF (FQ(I).EQ.0.) GO TO 417
417         JDJ=I-LRC(I)
418         RT(JDJ)=RT(JDJ)-FQ(I)
419     417 CONTINUE
420     419 CONTINUE
421   C
422   C     START ELEMENT LOOP FOR GENERATING FLOW MATRICES AND VECTORS
423   C
424         L=0
425     420 L=L+1
426   C
427   C
428   C     GENERATE AND EVALUATE BASIS FUNCTIONS, THEIR DERIVATIVES AND
429   C     THE JACOBIAN DETERMINANT AT EACH INTEGRATION POINT
430   C     INTEGRATION BY GAUSSIAN QUADRATURE
431   C     4X4 RULE FOR ALL ELEMENTS
432         DO 440 I=1,4
433         DO 440 J=1,4
```

```
434         K=(I-1)*4+J
435     425 XI=AG(J)
436         YI=AG(I)
437     432 CONTINUE
438   C     ******************************
439         CALL SHAPE (L,XI,YI,FF,DET)
440   C     ******************************
441         DO 435 JJ=1,8
442         F(JJ,K)=FF(JJ)
443         DX(JJ,K)=DGX(JJ)
444     435 DY(JJ,K)=DGY(JJ)
445         DETJ(K)=DET
446     440 CONTINUE
447   C
448   C     SUM HEAD IN ADJACENT AQUIFER FOR EACH NODE POINT AT EACH
449   C     INTEGRATION POINT
450   C
451         IF (COEF(L).EQ.0.) GO TO 446
452         DO 445 K=1,16
453         HK(K)=0.
454         DO 444 J=1,8
455         JDJ=IN(J,L)
456     444 HK(K)=HK(K)+F(J,K)*HZERO(JDJ)
457     445 CONTINUE
458     446 CONTINUE
459   C
460   C     CHANGE FORCING FUNCTION FOR MODIFIED SOURCE/SINK ELEMENTS
461   C
462         IF (FQE(L).EQ.0.) GO TO 454
463         FQEE=FQE(L)
464         IF (COEF(L).EQ.0.) GO TO 448
465         FQEE=FQE(L)*RQE(L)*BES1(L)/BB2(L)
466     448 CONTINUE
467         DO 450 I=1,4
468         JDJ=IN(I,L)
469         IR=JDJ-LRC(JDJ)
470     450 RT(IR)=RT(IR)-0.090845*FQEE
471         DO 452 I=5,8
472         JDJ=IN(I,L)
473         IR=JDJ-LRC(JDJ)
474     452 RT(IR)=RT(IR)-0.159155*FQEE
475     454 CONTINUE
476   C
477   C     GENERATE UPPER HALF OF FLOW COEFFICIENT MATRIX
478   C
479         DO 460 I=1,8
480         DO 460 J=I,8
481         DO 459 K=1,16
482         TRANX=0.
483         TRANY=0.
484         DO 458 JJ=1,8
485         JDJ=IN(JJ,L)
486         TRANX=TRANX+TRANSX(JDJ)*F(JJ,K)
487     458 TRANY=TRANY+TRANSY(JDJ)*F(JJ,K)
488         SRCLT(K)=COEF(L)*F(I,K)*F(J,K)*DETJ(K)
489         Q(K)=(TRANX*DX(I,K)*DX(J,K)+TRANY*DY(I,K)*DY(J,K))*DETJ(K)
490     459 CONTINUE
491   C     ********************
492         CALL MATGEN (I,J)
493   C     ********************
494     460 SE(I,J)=SE(I,J)+SRCL
495   C
```

```
C       FILL LOWER HALF OF SE ARRAY
        DO 462 I=2,8
        I1=I-1
        DO 462 J=1,I1
  462 SE(I,J)=SE(J,I)
C
C       EVALUATE CONTRIBUTIONS TO FORCING FUNCTION FROM HEAD IN
C       ADJACENT AQUIFER
C
        IF (COEF(L).EQ.0.) GO TO 467
        DO 466 I=1,8
        DO 464 K=1,16
  464 SRCRT(K)=COEF(L)*HK(K)*F(I,K)*DETJ(K)
C       **************
  466 CALL MATGENA (I,1)
C       **************
        GO TO 469
  467 DO 468 I=1,8
        SRCR(I)=0.
  468 CONTINUE
  469 CONTINUE
C
C       PRINT ELEMENT MATRICES FOR FLOW
        IF (KOD1.NE.1) GO TO 470
        IF (L.GT.1) GO TO 470
        WRITE (6,490)
        WRITE (6,130) L
        DO 80 I=1,8
   80 WRITE (6,140) I,(SE(I,J),J=1,8)
  130 FORMAT (////,10X,7HELEMENT,I4,5X,16HSTIFFNESS MATRIX/)
  140 FORMAT (I5,8E15.6//)
  470 CONTINUE
C
C       LOAD GLOBAL COEFFICIENT MATRIX AND FORCING FUNCTION
C       ---------------------------------------------------
C
C
        DO 478 I=1,8
        JDI=IN(I,L)
        IF (LR(JDI).GT.0) GO TO 474
C       ROW NUMBER IN GLOBAL MATRIX
        IR=JDI-LRC(JDI)
C
C       SUBTRACT INFLUENCE OF HEAD IN ADJACENT AQUIFER FROM FORCING
C       FUNCTION
        RT(IR)=RT(IR)-SRCR(I)
        DO 472 J=1,8
        JDJ=IN(J,L)
        IF (LR(JDJ).GT.0) GO TO 472
C       COLUMN NUMBER IN GLOBAL MATRIX (NUMBER FROM MAIN DIAGONAL)
        JC=JDJ-LRC(JDJ)-IR+1
        IF (JC.LE.NHBW) GO TO 471
        WRITE (6,560) L,JC,NHBW
        GO TO 472
  471 IF (JC.LT.1) GO TO 472
C
C       LOAD ELEMENT FLOW MATRIX INTO GLOBAL FLOW MATRIX
        H(IR,JC)=H(IR,JC)+SE(I,J)
  472 CONTINUE
        GO TO 478
  474 CONTINUE
        DO 476 J=1,8
```

```
      JDJ=IN(J,L)
      IF (LR(JDJ).GT.0) GO TO 476
C     NOW NUMBER OF FORCING FUNCTION
      JC=JDJ-LRC(JDJ)
C
C     MOVE INFLUENCE OF DIRICHLET BOUNDARY NODE HEAD TO FORCING FUNCTION
      RT(JC)=RT(JC)+SE(J,I)*PHII(JDJ)
  476 CONTINUE
  478 CONTINUE
  480 CONTINUE
  485 IF (L.LT.NE) GO TO 420
C
C     END ELEMENT LOOP FOR GENERATING FLOW MATRICES AND VECTORS
C
      IF (KOD2.NE.1) GO TO 489
      WRITE (6,530)
      WRITE (6,540)
      DO 486 I=1,N
  486 WRITE(6,570) I,(H(I,J),J=1,NWBW)
      WRITE (6,590)
      WRITE (6,600) (RT(I),I=1,N)
  489 CONTINUE
C
C
C
C     DECOMPOSE
C     *********
      CALL DBAND (N,IEX)
C     *********
C     IF DBAND FAILS, GO TO THE END
C
      IF (IEX.EQ.1) GO TO 1500
C
C     COMPUTE VECTOR OF KNOWN VALUES
C     ------------------------------
C
C     CHANGE SIGN OF FORCING FUNCTION
      DO 670 I=1,N
  670 FM(I)=-RT(I)
      IF (KOD4.NE.1) GO TO 690
      WRITE (6,1350)
      WRITE (6,1080)
      WRITE (6,1090) (I,FM(I),I=1,N)
C
C     BACK SUBSTITUTE
C     ***************
  690 CALL SBAND (N)
C     ***************
C
C
C     ADJUST FOR CORRECT NODAL SEQUENCE - USE FM FOR TEMPORARY STORAGE
      IP=0
      DO 770 I=1,NN
      IF (LR(I).GT.0) GO TO 760
      IP=IP+1
      FM(I)=PHI(IP)
      GO TO 770
  760 FM(I)=PHII(I)
  770 CONTINUE
C     END CALCULATIONS FOR HEAD
C
C
```

```
C
C       O U T P U T
C       -----------
C
C       WRITE VALUES OF HYDRAULIC HEAD
        WRITE (6,1372)
        WRITE (6,1082)
        WRITE (6,1092) (I,PHI(I),I=1,NN)
C
C       WRITE ELEMENT NODAL VELOCITIES
        IF (KOD3.EQ.1) CALL VCAL
C
C
C       WRITE CONTINUOUS GLOBAL VELOCITY FIELD
        IF (KOD5.EQ.0) GO TO 800
        DO 790 II=1,NN
        PHI(II)=0.
        PHII(II)=0.
  790   RT(II)=0.
        CALL VGLOB2
  800   CONTINUE
C
C       PLOT CONTOURS OF HYDRAULIC HEAD
        IF (KOD6.NE.1) GO TO 820
        DO 812 I=1,NPLOT
  810   CALL ZPLOT
  820   CONTINUE
C
C
C
C       WRITE TIME OF TRAVEL ALONG STREAMLINES
        IF (KOD8.NE.1) GO TO 828
        CALL STRM2
  828   CONTINUE
C
 1580   CONTINUE
 1600   CONTINUE
C
C       END OUTPUT
C
C
C       F O R M A T S
     1  FORMAT (11X,*SUPPRESS PRINTOUT OF ELEMENT FLOW MATRICES*)
     2  FORMAT (11X, *PRINT ELEMENT FLOW MATRICES*)
     3  FORMAT (11X,*SUPPRESS PRINTOUT OF GLOBAL FLOW MATRIX*)
     4  FORMAT (11X,*PRINT GLOBAL FLOW MATRIX*)
     5  FORMAT (11X,*SUPPRESS PRINTOUT OF NODAL VELOCITIES*)
     6  FORMAT(11X,*PRINT NODAL VELOCITIES*)
     7  FORMAT(11X, *SUPPRESS PRINTOUT OF RIGHT HAND SIDE VECTORS*)
     8  FORMAT(11X, *PRINT RIGHT HAND SIDE VECTORS*)
    11  FORMAT (11X,*SUPPRESS PRINTOUT OF CONTINUOUS VELOCITY FIELD*)
    12  FORMAT (11X,*PRINT CONTINUOUS VELOCITY FIELD*)
    13  FORMAT (11X,*SUPPRESS PLOT OF HYDRAULIC HEAD CONTOURS*)
    14  FORMAT (11X,*PLOT HYDRAULIC HEAD CONTOURS*)
    15  FORMAT (11X,*SUPPRESS PLOT OF TRANSMISSIVITY CONTOURS*)
    16  FORMAT (11X,*PLOT TRANSMISSIVITY CONTOURS*)
    17  FORMAT (11X,*SUPPRESS PRINTOUT OF TIME OF TRAVEL ALONG STREAMLINES
     1       *)
    18  FORMAT (11X,*PRINT TIME OF TRAVEL ALONG STREAMLINES*)
    19  FORMAT(11X,*SUPPRESS PLOT OF STREAMLINES*)
    20  FORMAT(11X,*PLOT STREAMLINES*)
    25  FORMAT (////11X,*CODE OPTIONS*/11X,12(1H=)//)
```

```
682      70 FORMAT (I5,6F10.3)
683     500 FORMAT (10F8.0)
684     490 FORMAT (1H1,////11X,25HELEMENT MATRICES FOR FLOW/11X,25(1H=))
685     530 FORMAT (1H1,10X,36HGLOBAL COEFFICIENT MATRICES FOR FLOW/11X,36(1H=
686        1))
687     540 FORMAT (1H0,20X,37HA COEFFICIENT MATRIX - UPPER HALFBAND/11X,37(1H
688        1=)//)
689     560 FORMAT (1H0,10X,7HELEMENT,I4,5X,38HINSUFFICIENT H4LF-BAND WIDTH -
690        1REQUIRE,I5,2X,10HINSTEAD OF,I5)
691     570 FORMAT(I5,10E12.4/(8X,10E12.4))
692     590 FORMAT (/////,11X,20HF COEFFICIENT MATRIX/11X,20(1H=)//)
693     600 FORMAT (11X,10E12.3)
694     840 FORMAT (20A4)
695     850 FORMAT (1H1,36X,12HT R A V E L //36X,35HGROUNDWATER FLOW
696        1             //25X,41HWITH ISOPARAMETRIC QUADRILATERAL ELEMENTS//35
697        2X,20HSTEADY STATE PROGRAM//)
698     860 FORMAT (11X,70(1H*)//11X,20A4//11X,70(1H*)///)
699     910 FORMAT (15I5)
700     920 FORMAT (///11X,19HFINITE ELEMENT DATA/11X,19(1H=)/)
701     930 FORMAT (1H ,10X,11HNUMBER OF =,2X,5HNODES,I24/21X,1H=,2X,8HELEMENT
702        1S,I21/21X,1H=,2X,24HDIRICHLET BOUNDARY NODES,I5/21X,1H=,2X,23HSOUR
703        2CE OR SINK ELEMENTS,I5/21X,1H=,2X,20HELEMENTS IN HALFBAND,I9/
704        321X,1H=,2X,14HLEAKY ELEMENTS,I15/21X,1H=,2X,
705        419HLEAKY ELEMENT NODES,I10/21X,1H=,2X,20HHYDRAULIC HEAD PLOTS,I9/
706        521X,1H=,2X,20HTRANSMISSIVITY PLOTS,I9)
707     980 FORMAT (I5,5F10.0)
708     985 FORMAT (I5,F10.0,F15.0)
709     990 FORMAT (////11X,16HNODE COORDINATES/11X,16(1H=)/)
710    1000 FORMAT (1H ,2(11X,4HNODE,12X,1HX,15X,1HY,2X))
711    1010 FORMAT (1H ,2(10X,I4,2F16.2)/(11X,I4,2F16.2,10X,I4,2F16.2))
712    1020 FORMAT (////11X,43HSOURCE/SINK ELEMENTS=  SOURCES ARE POSITIVE/11
713        1X,43(1H=)//11X,97HELEMENT   DISCHARGE (CU.M/DAY)   ELEMENT RADIUS
714        2  X-COORDINATE   Y-COORDINATE   B-COEFFICIENT (M),16H  TRANSMISSIV
715        3ITY)
716    1040 FORMAT (13X,I3,9X,F7.1,11X,F6.1,9X,F8.2,7X,F8.2,10X,F7.1,F20.1)
717    1080 FORMAT (/11X,6(4HNODE,5X,5HVALUE,5X))
718    1090 FORMAT (/(11X,6(I4,F10.3,5X)))
719    1100 FORMAT (////11X,*ELEMENT POROSITY TIMES THICKNESS (M)  AND LEAKAG
720        1E COEFFICIENT (1/DAY)*/11X,76(1H=)//11X,*ELEMENT     POROSITY TIME
721        2S THICKNESS     LEAKAGE COEFFICIENT*//)
722    1110 FORMAT (9I5)
723    1140 FORMAT (////11X,18HELEMENT INCIDENCES/11X,16(1H=)/)
724    1150 FORMAT (1H ,10X,7HELEMENT,5X,1H/,3(1H-),9H CORNERS ,4(1H-),1H/,7X,
725        11H/,4(1H-),7H SIDES ,5(1H-),1H/)
726    1160 FORMAT (1H ,4X,I10,5X,4I5,5X,4I5)
727    1170 FORMAT (////11X,61HTRANSMISSIVITIES (SQ.M/DAY) AND CONSTANT HEAD
728       1(M) FOR LEAKAGE/11X,61(1H=)//11X,53H  NODE   X-TRANSMISSIVITY  Y-T
729        2RANSMISSIVITY     HEAD  //)
730    1190 FORMAT (13X,I3,7X,F10.2,8X,F10.2,6X,F7.2)
731    1200 FORMAT (13X,I3,17X,0PF5.2,18X,F15.12)
732    1230 FORMAT (////11X,33HDIRICHLET BOUNDARY NODES FOR FLOW/11X,33(1H=))
733    1240 FORMAT (20I4)
734    1250 FORMAT (11X,10(1H*),33H DIRICHLET BOUNDARY NODE FOR FLOW,I4,38HDOE
735        1S NOT EXIST - EXECUTION TERMINATED ,10(1H*))
736    1260 FORMAT (11X,20I5)
737    1270 FORMAT (1H0,10(1H*),49H NUMBER OF DIRICHLET BOUNDARY NODES FOR FLO
738        1W READ,I10,35H DISAGREES WITH NUMBER ANTICIPATED ,I10,10(1H*))
739    1310 FORMAT (///11X,19HFINITE ELEMENT DATA/11X,19(1H=)/11X,21HTOTAL NUM
740        1BER OF NODES,I19/11X,33HDIRICHLET BOUNDARY NODES FOR FLOW,I7/11X,2
741        27HDEGREES OF FREEDOM FOR FLOW,I13///)
742    1350  FORMAT (/////11X,31HVECTOR OF KNOWN VALUES FOR HEAD/11X,31(1H=))
743    1370 FORMAT (//11X,14HHYDRAULIC HEAD/11X,14(1H=))
```

```
 1440 FORMAT (5F10.2)
 1450 FORMAT(1H0,///11X,21HPARAMETER MULTIPLIERS /11X,21(1H=)/11X,
     16HATRANX,F19.9/11X,6HATRANY,F19.9/11X,4HAFQE,F21.9/11X,
     26HFACTOR,F19.9/11X,5HALEAK,F20.9)
 1460 FORMAT (I5,F10.0)
      END
C
      SUBROUTINE YCAL
C
C     PURPOSE - CALCULATE VELOCITIES AT THE NODES OF EACH ELEMENT
C     ------------------------------------------------------------------
      COMMON /SCALAR/
     1   NN, NE, NHBW, SRCL, KOD8, KOD10, IQE
      COMMON /VECTOR/
     1   X(740), Y(740), FM(740), PHI(740), PHII(740), XV(740),
     2   RT(740), TRANSX(740), TRANSY(740), COEF(225), PORTH(225),
     3   FQE(20), XQE(20), YQE(20), RQE(20), BB2(20), BES1(20),
     4   SRCRT(16), SRCLT(16), G(16), SRCR(8), DGX(8), DGY(8), YV(742),
     5   FQ(50)
      COMMON /MATRIX/
     1   H(700,50), IN(8,225), SE(8,8)
      DIMENSION VX(8), VY(8), INDX(8), FF(8)
C     ------------------------------------------------------------------
C
      WRITE(6,210)
      L=0
   20 L=L+1
      WRITE(6,200) L
      DO 10 I=1,8
      VX(I)=0.
   10 VY(I)=0.
      DO 130 I=1,8
      JDJ=IN(I,L)
      XCOND=TRANSX(JDJ)/PORTH(L)
      YCOND=TRANSY(JDJ)/PORTH(L)
      IF (I.GT.4) GO TO 40
      XI=1.
      YI=1.
      IF (I.EQ.1.OR.I.EQ.4) XI=-1.
      IF (I.EQ.1.OR.I.EQ.2) YI=-1.
      GO TO 70
   40 XI=0.
      YI=0.
      IF (I.EQ.6) XI=1.
      IF (I.EQ.8) XI=-1.
      IF (I.EQ.5) YI=-1.
      IF (I.EQ.7) YI=1.
   70 CONTINUE
C     ******************************
      CALL SHAPE (L,XI,YI,FF,DET)
C     ******************************
      EX=0.
      EY=0.
      DO 90 K=1,8
      J1=IN(K,L)
C
C     COMPUTE PRESSURE DERIVATIVES
      EX=EX+DGX(K)*FM(J1)
      EY=EY+DGY(K)*FM(J1)
   90 CONTINUE
      INDX(I)=JDJ
      VY(I)=-YCOND*EY
```

```
806         VX(I)=-XCOND*EX
807     130 CONTINUE
808         WRITE (6,220) (INDX(I),VX(I),VY(I),I=1,8)
809         IF (L.LT.NE) GO TO 20
810         RETURN
811   C
812     210 FORMAT(///11X,16HPOINT VELOCITIES/11X,16(1H=))
813     200 FORMAT( /11X,7HELEMENT,I8/11X,3(4HNODE,2X,11HX-COMPONENT,2X,11HY-C
814        1OMPONENT,6X) )
815     220 FORMAT((11X,3(I4,2E13.3,7X)))
816         END
817   C
818   C
819   C
820         SUBROUTINE VGLOB2
821   C
822   C       PURPOSE - CALCULATE A CONTINUOUS QUADRATIC VELOCITY FIELD
823   C                 (CALCULATED BY AVERAGING ELEMENT NODAL VELOCITIES
824   C                  AND SINGULAR SOLUTION FOR SOURCE/SINK ELEMENTS)
825   C
826   C       ------------------------------------------------------------------
827         COMMON /SCALAR/
828        1    NN, NE, NHBW, SRCL, KOD8, KOD10, IQE
829         COMMON /VECTOR/
830        1    X(740), Y(740), FM(740), PHI(740), PHII(740), XV(740),
831        2    RT(740), TRANSX(740), TRANSY(740), COEF(225), PORTH(225),
832        3    FQE(20), XQE(20), YQE(20), RQE(20), BB2(20), BES1(20),
833        4    SRCRT(16), SRCLT(16), Q(16), SRCR(8), DGX(8), DGY(8), YV(740),
834        5    FQ(50)
835         COMMON /MATRIX/
836        1    H(700,50), IN(8,225), SE(8,8)
837         DIMENSION FF(8)
838   C       ------------------------------------------------------------------
839   C
840         WRITE (6,300)
841         DO 200 L=1,NE
842         DO 150 I=1,8
843         JDJ=IN(I,L)
844         XCOND=TRANSX(JDJ)/PORTH(L)
845         YCOND=TRANSY(JDJ)/PORTH(L)
846         IF (I.GT.4) GO TO 40
847         XI=1.
848         YI=1.
849         IF (I.EQ.1.OR.I.EQ.4) XI=-1.
850         IF (I.EQ.1.OR.I.EQ.2) YI=-1.
851         GO TO 80
852      40 XI=0.
853         YI=0.
854         IF (I.EQ.5) YI=-1.
855         IF (I.EQ.6) XI=1.
856         IF (I.EQ.7) YI=1.
857         IF (I.EQ.8) XI=-1.
858      80 CONTINUE
859   C       ****************************
860         CALL SHAPE (L,XI,YI,FF,DET)
861   C       ****************************
862         EX=0.
863         EY=0.
864         DO 100 K=1,8
865         J1=IN(K,L)
866         EX=EX+DGX(K)*FM(J1)
867     100 EY=EY+DGY(K)*FM(J1)
```

```
      PHI(JDJ)=PHI(JDJ)-XCOND*EX
      PHII(JDJ)=PHII(JDJ)-YCOND*EY
      RT(JDJ)=RT(JDJ)+1.
      IF (FQE(L).EQ.0.) GO TO 125
      IF (CDEF(L).EQ.0.) GO TO 110
      PHI(JDJ)=PHI(JDJ)+FQE(L)*BES1(L)*(X(JDJ)-XQE(L))/(6.2831853*
     1BB2(L)*RQE(L)*PORTH(L))
      PHII(JDJ)=PHII(JDJ)+FQE(L)*BES1(L)*(Y(JDJ)-YQE(L))/(6.2831853
     1*BB2(L)*FQE(L)*PORTH(L))
      GO TO 125
  110 PHI(JDJ)=PHI(JDJ)+FQE(L)*(X(JDJ)-XQE(L))/(6.2831853*RQE(L)**2*
     1PORTH(L))
      PHII(JDJ)=PHII(JDJ)+FQE(L)*(Y(JDJ)-YQE(L))/(6.2831853*RQE(L)
     1**2*PORTH(L))
  125 CONTINUE
  150 CONTINUE
  200 CONTINUE
      DO 250 J=1,NN
      PHI(J)=PHI(J)/RT(J)
      PHII(J)=PHII(J)/RT(J)
  250 CONTINUE
C
C
      IF (KOD8.EQ.0) GO TO 290
      DO 260 I=1,NN
      XV(I)=0.
  260 YV(I)=0.
      DO 280 L=1,NE
      IF (FQE(L).EQ.0.) GO TO 280
      DO 270 I=1,8
      JDJ=IN(I,L)
      XV(JDJ)=PHI(JDJ)-FQE(L)*(X(JDJ)-XQE(L))/(6.2831853*RQE(L)**2*
     1PORTH(L))
      YV(JDJ)=PHII(JDJ)-FQE(L)*(Y(JDJ)-YQE(L))/(6.2831853*RQE(L)**2
     1*PORTH(L))
      IF (CDEF(L).EQ.0.) GO TO 270
      XV(JDJ)=PHI(JDJ)-FQE(L)*BES1(L)*(X(JDJ)-XQE(L))/(6.2831853*
     1BB2(L)*RQE(L)*PORTH(L))
      YV(JDJ)=PHII(JDJ)-FQE(L)*BES1(L)*(Y(JDJ)-YQE(L))/(6.2831853
     1*BB2(L)*RQE(L)*PORTH(L))
  270 CONTINUE
  280 CONTINUE
  290 CONTINUE
      WRITE(1,305)(J,X(J),Y(J),FM(J),PHI(J),PHII(J),J=1,NN)
      WRITE (6,350)  (J,X(J),Y(J),PHI(J),PHII(J),XV(J),YV(J),J=1,NN)
      RETURN
  300 FORMAT (/////11X,41HCONTINUOUS VELOCITY DISTRIBUTION  (M/DAY)/11X,
     141(1H=)//11X,*NODE         X-COOR,         Y-COOR,      X-VELOCITY
     1  Y-VELOCITY*)
  305 FORMAT (I5,3F10.2,2E15.6)
  350 FORMAT (11X,I4,2F15.2,4E15.4)
      END
C
C
      SUBROUTINE MATGEN (I,J)
C
C     PURPOSE - PERFORM GAUSSIAN QUADRATURE OVER EACH ELEMENT
C
C     ------------------------------------------------------------------
      REAL H1, H2
      COMMON /SCALAR/
     1   NN, NE, NH8W, SRCL, KOD8, KOD10, IQE
```

```
      COMMON /VECTOR/
     1   X(740), Y(740), FM(740), PHI(740), PHII(740), XV(740),
     2   RT(740), TRANSX(740), TRANSY(740), COEF(225), PORTH(225),
     3   FGE(20), XGE(20), YGE(20), RGE(20), BB2(20), BES1(20),
     4   SRCRT(16), SRCLT(16), Q(16), SRCR(8), DGX(8), DGY(8), YV(740),
     5   FG(50)
      COMMON /MATRIX/
     1   H(700,50), IN(8,225), SE(8,8)
      DATA H1/.347854845137454/,H2/.652145154862546/
C     ------------------------------------------------------------------
C
      H11=H1*H1
      H12=H1*H2
      H22=H2*H2
   30 SE(I,J)=H11*(Q(1)+Q(4)+Q(13)+Q(16))+H12*(Q(2)+Q(3)+Q(5)+Q(8)+Q(9)+
     1Q(12)+Q(14)+Q(15))+H22*(Q(6)+Q(7)+Q(10)+Q(11))
   40 SRCL=H11*(SRCLT(1)+SRCLT(4)+SRCLT(13)+SRCLT(16))+H12*(SRCLT(2)+SRC
     1LT(3)+SRCLT(5)+SRCLT(8)+SRCLT(9)+SRCLT(12)+SRCLT(15)+SRCLT(14))+H2
     2*(SRCLT(6)+SRCLT(7)+SRCLT(10)+SRCLT(11))
   50 CONTINUE
      RETURN
C
C
      ENTRY MATGEN
      H11=H1*H1
      H12=H1*H2
      H22=H2*H2
   60 SRCR(I)=H11*(SRCRT(1)+SRCRT(4)+SRCRT(13)+SRCRT(16))+H12*(SRCRT(2)+
     1SRCRT(3)+SRCRT(5)+SRCRT(8)+SRCRT(9)+SRCRT(12)+SRCRT(15)+SRCRT(14))
     2+H22*(SRCRT(6)+SRCRT(7)+SRCRT(10)+SRCRT(11))
   70 CONTINUE
      RETURN
      END
      SUBROUTINE DRAND (N,IEX)
C
C     PURPOSE - DECOMPOSE GLOBAL FLOW MATRIX
C
C     ------------------------------------------------------------------
      COMMON /SCALAR/
     1   NN, NE, NHBW, SRCL, KOD8, KOD10, IGE
      COMMON /MATRIX/
     1   H(700,50), IN(8,225), SE(8,8)
C     ------------------------------------------------------------------
      IEX=0
      DO 50 I=1,N
      IP=N-I+1
      IF (NHBW.LT.IP) IP=NHBW
      DO 50 J=1,IP
      IQ=NHBW-J
      IF ((I-1).LT.IQ) IQ=I-1
      SUM=H(I,J)
      IF (IQ.LT.1) GO TO 20
      DO 10 K=1,IQ
      II=I-K
      JZ=J+K
   10 SUM=SUM-H(II,K+1)*H(II,JZ)
   20 IF (J.NE.1) GO TO 40
      IF (SUM.LE.0.) GO TO 30
      TEMP=1./ SQRT(SUM)
      H(I,J)=TEMP
      GO TO 50
   30 WRITE (6,60) I
```

```
      WRITE (6,70) N,NHBW,IP,IQ,I,J,SUM
      IEX=1
      RETURN
   40 H(I,J)=SUM*TEMP
   50 CONTINUE
      RETURN
C
   60 FORMAT (1H1,10X,19HBRAND FAILS AT ROW ,I4)
   70 FORMAT (1H0,6I5,E20.8)
      END
C
C
      SUBROUTINE SBAND (N)
C
C     PURPOSE - BACK SUBSTITUTE FOR GLOBAL SOLUTION
C
C     ------------------------------------------------------------------
      COMMON /SCALAR/
     1   NN, NE, NHBW, SRCL, KOD8, KOD10, IQE
      COMMON /VECTOR/
     1   X(740), Y(740), PM(740), PHI(740), PHII(740), XV(740),
     2   RT(740), TRANSX(740), TRANSY(740), COEF(225), PORTH(225),
     3   FQE(20), XQE(20), YQE(20), RQE(20), B82(20), BES1(20),
     4   SRCRT(16), SRCLT(16), Q(16), SRCR(8), DQX(8), DQY(8), YV(740),
     5   FQ(50)
      COMMON /MATRIX/
     1   H(700,50), IN(8,225), SE(8,8)
C     ------------------------------------------------------------------
      DO 30 I=1,N
      J=I-NHBW+1
      IF ((I+1).LE.NHBW) J=1
      SUM=PM(I)
      K1=I-1
      IF (J.GT.K1) GO TO 20
      DO 10 K=J,K1
      II=I-K+1
   10 SUM=SUM-H(K,II)*PHI(K)
   20 PHI(I)=SUM*H(I,1)
   30 CONTINUE
      DO 60 I1=1,N
      I=N-I1+1
      J=I+NHBW-1
      IF (J.GT.N) J=N
      SUM=PHI(I)
      K2=I+1
      IF (K2.GT.J) GO TO 50
      DO 40 K=K2,J
      KK=K-I+1
   40 SUM=SUM-H(I,KK)*PHI(K)
   50 PHI(I)=SUM*H(I,1)
   60 CONTINUE
      RETURN
      END
C
C
C
      SUBROUTINE SHAPE (L, XI, YI, F, DET)
C
C     PURPOSE - EVALUATION OF BASIS FUNCTIONS, THEIR DERIVATIVES,
C               AND THE JACOBIANS AND INVERSE JACOBIANS
C
C     A NODE QUADRALATER ELEMENT,1,2,3,4,ARE CORNER NODES
C     ------------------------------------------------------------------
```

```
      COMMON /SCALAR/
     1   NN, NE, NMBW, SRCL, KCOS, KOD10, IQE
      COMMON /VECTOR/
     1   X(740), Y(740), FM(740), PHI(740), PHII(740), XV(740),
     2   RT(740), TRANSX(740), TRANSY(740), COEF(225), PORTM(225),
     3   FQE(20), XQE(20), YQE(20), RQE(20), SS2(20), SES1(20),
     4   SRCRT(16), SRCLT(16), Q(16), SRCR(8), DGX(8), DGY(8), YY(740),
     5   FQ(50)
      COMMON /MATRIX/
     1   H(700,50), IN(8,225), SE(8,8)
      DIMENSION F(8),DFX(8),DFY(8)
C     ------------------------------------------------------------------
C
      XI1=1.-XI
      XI2=1.+XI
      XI3=1.-XI*XI
      YI1=1.-YI
      YI2=1.+YI
      YI3=1.-YI*YI
C
C     F(I):SHAPE FUNCTIONS
C
      F(1)=.25*XI1*YI1*(-XI-YI-1.)
      F(2)=.25*XI2*YI1*(XI-YI-1.)
      F(3)=.25*XI2*YI2*(XI+YI-1.)
      F(4)=.25*XI1*YI2*(-XI+YI-1.)
      F(5)=.5*XI3*YI1
      F(6)=.5*XI2*YI3
      F(7)=.5*XI3*YI2
      F(8)=.5*XI1*YI3
C
C     DFX,DFY: DERIVATIVES OF SHAPE FUNCTIONS
C
      XY1=2.*XI+YI
      XY2=2.*XI-YI
      YX1=2.*YI+XI
      YX2=2.*YI-XI
C
      DFX(1)=.25*YI1*XY1
      DFX(2)=.25*YI1*XY2
      DFX(3)=.25*YI2*XY1
      DFX(4)=.25*YI2*XY2
      DFX(5)=-XI*YI1
      DFX(6)=.5*YI3
      DFX(7)=-XI*YI2
      DFX(8)=-DFX(6)
      DFY(1)=.25*XI1*YX1
      DFY(2)=.25*XI2*YX2
      DFY(3)=.25*XI2*YX1
      DFY(4)=.25*XI1*YX2
      DFY(5)=-.5*XI3
      DFY(6)=-YI*XI2
      DFY(7)=-DFY(5)
      DFY(8)=-YI*XI1
C
C     JACOBIAN
      SUM1=0.
      SUM2=0.
      SUM3=0.
      SUM4=0.
      DO 260 I=1,8
      XI=IN(I,L)
```

```
1116          SUM1=SUM1+DFX(I)*X(KI)
1117          SUM2=SUM2+DFX(I)*Y(KI)
1118          SUM3=SUM3+DFY(I)*X(KI)
1119          SUM4=SUM4+DFY(I)*Y(KI)
1120      260 CONTINUE
1121          DET=SUM1*SUM4-SUM2*SUM3
1122          DET1=1./DET
1123          C11=DET1*SUM4
1124          C12=-DET1*SUM2
1125          C21=-DET1*SUM3
1126          C22=DET1*SUM1
1127    C
1128    C     SHAPE FUNCTION DERIVATIVES - GLOBAL
1129          DO 270 J=1,8
1130          DGX(J)=C11*DFX(J)+C12*DFY(J)
1131          DGY(J)=C21*DFX(J)+C22*DFY(J)
1132      270 CONTINUE
1133          RETURN
1134          END
1135          SUBROUTINE STRM2
1136    C
1137    C     PURPOSE - CALCULATE THE TIME OF TRAVEL ALONG STREAMLINES=  QUADRATIC
1138    C
1139    C     TT(J) TRAVEL TIME (DAYS) ALONG STREAMLINES
1140    C
1141    C     ------------------------------------------------------------------
1142          COMMON /SCALAR/
1143         1   NN, NE, NBBW, SRCL, KOD8, KOD10, IDE
1144          COMMON /VECTOR/
1145         1   X(740), Y(740), FH(740), VX(740), VY(740), XV(740),
1146         2   RT(740), TRANSX(740), TRANSY(740), COEF(225), PORTH(225),
1147         3   FQE(20), XQE(20), YQE(20), RQE(20), BB2(20), BES1(20),
1148         4   SRCRT(16), SRCLT(16), Q(16), SRCR(8), DGX(8), DGY(8), YV(740),
1149         5   FQ(52)
1150          COMMON /MATRIX/
1151         1   H(700,50), IN(8,225), SE(8,8)
1152          COMMON/XY/XO,YO,XL,YL,XMAX,YMAX,XMIN,YMIN,SCALE,NCIR
1153          COMMON/TIME/INEL(4,225),TT(16)
1154    C
1155    C     ------------------------------------------------------------------
1156          READ (5,310) NSL, NSTPRT, NTIME,STEP, TMAX
1157          READ (5,320), (TT(I),I=1,NTIME)
1158          DO 10 L=1,NE
1159          READ (5,300) LL, (INEL(K,L),K=1,4)
1160       10 CONTINUE
1161          WRITE (6,339)
1162          A1 = B1 = 0.
1163          IF(KOD10.NE.1) GO TO 15
1164          CALL PLOTS(55,0,4LPLOT)
1165          CALL PLOT(XO,YO,-3)
1166          IF(NCIR.EQ.0) GO TO 12
1167          RL=XL/2.
1168          CALL CIRCLE(RL,0.,-90.,270.,RL,2)
1169          GO TO 15
1170       12 CONTINUE
1171          CALL PLOT (XMIN,YMIN,3)
1172          DO 14 IP=1,2
1173          CALL PLOT(XMAX,YMIN,2)
1174          CALL PLOT(XMAX,YMAX,2)
1175          CALL PLOT(XMIN,YMAX,2)
1176          CALL PLOT(XMIN,YMIN,2)
1177       14 CONTINUE
```

```
   15 CONTINUE
C
      N=0
   20 N=N+1
C
      IF(N.LE.NSL) GO TO 21
C
      XEND=8.5-XO
      IF(KOD10.EQ.1) CALL PLOT(XEND,-YO,999)
C
      GO TO 390
   21 CONTINUE
      READ (5,330) NEL, XI1, ETA1
      JCOS=0
C
      IF (KOD10.NE.1) GO TO 23
      J = 1
   23 CONTINUE
      DT=0.
C
      TIME=0.
      NSTEP=0
   30 K1=IN(1,NEL)
      K2=IN(2,NEL)
      K3=IN(3,NEL)
      K4=IN(4,NEL)
      K5=IN(5,NEL)
      K6=IN(6,NEL)
      K7=IN(7,NEL)
      K8=IN(8,NEL)
      L=NEL
C
C     EVALUATE TERMS IN FUNCTION EXPANSION FOR X, Y, VX AND VY
C
      T1X=(-X(K1)-X(K2)-X(K3)-X(K4)+2.0*(X(K5)+X(K6)+X(K7)+X(K8)))/4.0
      T1Y=(-Y(K1)-Y(K2)-Y(K3)-Y(K4)+2.0*(Y(K5)+Y(K6)+Y(K7)+Y(K8)))/4.0
      T1VX=(-VX(K1)-VX(K2)-VX(K3)-VX(K4)+2.0*(VX(K5)+VX(K6)+VX(K7)+
     1     VX(K8)))/4.0
      T1VY=(-VY(K1)-VY(K2)-VY(K3)-VY(K4)+2.0*(VY(K5)+VY(K6)+VY(K7)+
     1     VY(K8)))/4.0
      T2X=(X(K6)-X(K8))/2.0
      T2Y=(Y(K6)-Y(K8))/2.0
      T2VX=(VX(K6)-VX(K8))/2.0
      T2VY=(VY(K6)-VY(K8))/2.0
      T3X=(-X(K5)+X(K7))/2.0
      T3Y=(-Y(K5)+Y(K7))/2.0
      T3VX=(-VX(K5)+VX(K7))/2.0
      T3VY=(-VY(K5)+VY(K7))/2.0
      T4X=(X(K1)-X(K2)+X(K3)-X(K4))/4.0
      T4Y=(Y(K1)-Y(K2)+Y(K3)-Y(K4))/4.0
      T4VX=(VX(K1)-VX(K2)+VX(K3)-VX(K4))/4.0
      T4VY=(VY(K1)-VY(K2)+VY(K3)-VY(K4))/4.0
      T5X=(X(K1)+X(K2)+X(K3)+X(K4)-2.0*(X(K5)+X(K7)))/4.0
      T5Y=(Y(K1)+Y(K2)+Y(K3)+Y(K4)-2.0*(Y(K5)+Y(K7)))/4.0
      T5VX=(VX(K1)+VX(K2)+VX(K3)+VX(K4)-2.0*(VX(K5)+VX(K7)))/4.0
      T5VY=(VY(K1)+VY(K2)+VY(K3)+VY(K4)-2.0*(VY(K5)+VY(K7)))/4.0
      T6X=(X(K1)+X(K2)+X(K3)+X(K4)-2.0*(X(K6)+X(K8)))/4.0
      T6Y=(Y(K1)+Y(K2)+Y(K3)+Y(K4)-2.0*(Y(K6)+Y(K8)))/4.0
      T6VX=(VX(K1)+VX(K2)+VX(K3)+VX(K4)-2.0*(VX(K6)+VX(K8)))/4.0
      T6VY=(VY(K1)+VY(K2)+VY(K3)+VY(K4)-2.0*(VY(K6)+VY(K8)))/4.0
      T7X=(-X(K1)-X(K2)+X(K3)+X(K4)+2.0*(X(K5)-X(K7)))/4.0
      T7Y=(-Y(K1)-Y(K2)+Y(K3)+Y(K4)+2.0*(Y(K5)-Y(K7)))/4.0
```

```
      T7VX=(-VX(K1)-VX(K2)+VX(K3)+VX(K4)+2.0*(VX(K5)-VX(K7)))/4.0
      T7VY=(-VY(K1)-VY(K2)+VY(K3)+VY(K4)+2.0*(VY(K5)-VY(K7)))/4.0
      T8X=(-X(K1)+X(K2)+X(K3)-X(K4)+2.0*(-X(K6)+X(K8)))/4.0
      T8Y=(-Y(K1)+Y(K2)+Y(K3)-Y(K4)+2.0*(-Y(K6)+Y(K8)))/4.0
      T8VX=(-VX(K1)+VX(K2)+VX(K3)-VX(K4)+2.0*(-VX(K6)+VX(K8)))/4.0
      T8VY=(-VY(K1)+VY(K2)+VY(K3)-VY(K4)+2.0*(-VY(K6)+VY(K8)))/4.0
C
C     USE MODIFIED VELOCITY DISTRIBUTION FOR SOURCE/SINK ELEMENTS
C
      IF (FQE(L).EQ.0.0) GO TO 35
      T1VX=(-XV(K1)-XV(K2)-XV(K3)-XV(K4)+2.0*(XV(K5)+XV(K6)+XV(K7)+
     1     XV(K8)))/4.0
      T1VY=(-YV(K1)-YV(K2)-YV(K3)-YV(K4)+2.0*(YV(K5)+YV(K6)+YV(K7)+
     1     YV(K8)))/4.0
      T2VX=(XV(K6)-XV(K8))/2.0
      T2VY=(YV(K6)-YV(K8))/2.0
      T3VX=(-XV(K5)+XV(K7))/2.0
      T3VY=(-YV(K5)+YV(K7))/2.0
      T4VX=(XV(K1)-XV(K2)+XV(K3)-XV(K4))/4.0
      T4VY=(YV(K1)-YV(K2)+YV(K3)-YV(K4))/4.0
      T5VX=(XV(K1)+XV(K2)+XV(K3)+XV(K4)-2.0*(XV(K5)+XV(K7)))/4.0
      T5VY=(YV(K1)+YV(K2)+YV(K3)+YV(K4)-2.0*(YV(K5)+YV(K7)))/4.0
      T6VX=(XV(K1)+XV(K2)+XV(K3)+XV(K4)-2.0*(XV(K6)+XV(K8)))/4.0
      T6VY=(YV(K1)+YV(K2)+YV(K3)+YV(K4)-2.0*(YV(K6)+YV(K8)))/4.0
      T7VX=(-XV(K1)-XV(K2)+XV(K3)+XV(K4)+2.0*(XV(K5)-XV(K7)))/4.0
      T7VY=(-YV(K1)-YV(K2)+YV(K3)+YV(K4)+2.0*(YV(K5)-YV(K7)))/4.0
      T8VX=(-XV(K1)+XV(K2)+XV(K3)-XV(K4)+2.0*(-XV(K6)+XV(K8)))/4.0
      T8VY=(-YV(K1)+YV(K2)+YV(K3)-YV(K4)+2.0*(-YV(K6)+YV(K8)))/4.0
   35 CONTINUE
C
C     EVALUATE THE EXPANSIONS FOR X, Y, VX AND VY
C
      XX1=T1X+T2X*XI1+T3X*ETA1+T4X*XI1*ETA1+T5X*XI1*XI1+T6X*ETA1*ETA1+
     1    T7X*XI1*XI1*ETA1+T8X*XI1*ETA1*ETA1
      YY1=T1Y+T2Y*XI1+T3Y*ETA1+T4Y*XI1*ETA1+T5Y*XI1*XI1+T6Y*ETA1*ETA1+
     1    T7Y*XI1*XI1*ETA1+T8Y*XI1*ETA1*ETA1
      WRITE (6,340) NEL, XX1, YY1, TIME
C
      IF(KOD10.NE.1) GO TO 37
      XXA=XX1/SCALE
      YYA=YY1/SCALE
      IF (TIME.GT.0.0000001) GO TO 32
      CALL PLOT (XXA,YYA,3)
      GO TO 36
   32 CALL PLOT(XXA,YYA,2)
      IF (J.GT.NTIME) GO TO 36
      IF(TIME.LT.TT(J)) GO TO 36
      CALL SYMBOL(XXA,YYA,0.07,J,0.,-1)
      J=J+1
   36 CONTINUE
   37 CONTINUE
C
      XI=XI1
      ETA=ETA1
      XXX=XX1
      YYY=YY1
C
C     LOOP FOR SECOND ORDER RUNGE-KUTTA INTEGRATION
C
      K=1
   38 CONTINUE
      VVXX=T1VX+T2VX*XI+T3VX*ETA+T4VX*XI*ETA+T5VX*XI*XI+
```

```
     1     T6VX*ETA*ETA+T7VX*XI*XI*ETA+T8VX*XI*ETA*ETA
      VVYY=T1VY+T2VY*XI+T3VY*ETA+T4VY*XI*ETA+T5VY*XI*XI+
     1     T6VY*ETA*ETA+T7VY*XI*XI*ETA+T8VY*XI*ETA*ETA
C
      IF (FQE(L),EQ,0,0) GO TO 45
      RR=SQRT((XXX-XQE(L))**2+(YYY-YQE(L))**2)
      VVX=FQE(L)*(XXX-XQE(L))/(6,2831853*PORTH(L)*RR**2)
      VVY=FQE(L)*(YYY-YQE(L))/(6,2831853*PORTH(L)*RR**2)
      IF (COEF(L),EQ,0,0) GO TO 40
      ARG1=RR/BB2(L)
      ARG2=RQE(L)/BB2(L)
      VVX=FQE(L)*(XXX-XQE(L))*(BESK1(ARG1)+BESK0(ARG2)*BESI1(ARG1)/
     1     BESI0(ARG2))/(6,2831853*PORTH(L)*RR*BB2(L))
      VVY=FQE(L)*(YYY-YQE(L))*(BESK1(ARG1)+BESK0(ARG2)*BESI1(ARG1)/
     1     BESI0(ARG2))/(6,2831853*PORTH(L)*RR*BB2(L))
   40 VVXX=VVXX+VVX
      VVYY=VVYY+VVY
   45 CONTINUE
C
C     CALCULATE X AND Y DERIVATIVES
C
      DXXI=T2X+T4X*ETA+2,0*T5X*XI+2,0*T7X*XI*ETA+T8X*ETA*ETA
      DXETA=T3X+T4X*XI+2,0*T6X*ETA+T7X*ETA*ETA+2,0*T8X*XI*ETA
      DYXI=T2Y+T4Y*ETA+2,0*T5Y*XI+2,0*T7Y*XI*ETA+T8Y*ETA*ETA
      DYETA=T3Y+T4Y*XI+2,0*T6Y*ETA+T7Y*ETA*ETA+2,0*T8Y*XI*ETA
C
C     CALCULATE A AND B
C
      A=VVYY*DXXI-VVXX*DYXI
      B=VVXX*DYETA-VVYY*DXETA
C
      IF (K,EQ,1) GO TO 48
      A=0,5*(A+A1)
      B=0,5*(B+B1)
      DXI=STEP/SQRT(1,0+(A/B)**2)
      IF (B,LT,0,0) DXI=-DXI
      DETA=STEP/SQRT(1,0+(B/A)**2)
      IF (A,LT,0,0) DETA=-DETA
      GO TO 50
C
   48 DXI=STEP/SQRT(1,0+(A/B)**2)
      IF (B,LT,2,0) DXI=-DXI
      DETA=STEP/SQRT(1,0+(B/A)**2)
      IF (A,LT,0,0) DETA=-DETA
      XI=XI1+DXI
      ETA=ETA1+DETA
      IF (ABS(XI),GT,1,0,OR,ABS(ETA),GT,1,0) GO TO 60
   49 CONTINUE
      A1=A
      B1=B
      VX1=VVXX
      VY1=VVYY
      XXX=T1X+T2X*XI+T3X*ETA+T4X*XI*ETA+T5X*XI*XI+T6X*ETA*ETA+
     1     T7X*XI*XI*ETA+T8X*XI*ETA*ETA
      YYY=T1Y+T2Y*XI+T3Y*ETA+T4Y*XI*ETA+T5Y*XI*XI+T6Y*ETA*ETA+
     1     T7Y*XI*XI*ETA+T8Y*XI*ETA*ETA
      K=2
      GO TO 38
C
   50 CONTINUE
C
      XI=XI1+DXI
```

```
1364          ETA=ETA1+DETA
1365    C
1366    C     CHECK TO SEE IF STEP LEAVES THE ELEMENT
1367    C
1368          IF (ABS(XI).GE.1.0.OR.ABS(ETA).GE.1.0) GO TO 60
1369    C
1370    C     FIND X, Y, VX AND VY AT THE END OF THE STEP
1371    C
1372          XX2=T1X+T2X*XI+T3X*ETA+T4X*XI*ETA+T5X*XI*XI+T6X*ETA*ETA+
1373         1    T7X*XI*XI*ETA+T8X*XI*ETA*ETA
1374          YY2=T1Y+T2Y*XI+T3Y*ETA+T4Y*XI*ETA+T5Y*XI*XI+T6Y*ETA*ETA+
1375         1    T7Y*XI*XI*ETA+T8Y*XI*ETA*ETA
1376          JCOS=JCOS+1
1377          VX2=T1VX+T2VX*XI+T3VX*ETA+T4VX*XI*ETA+T5VX*XI*XI+T6VX*ETA*ETA+
1378         1    T7VX*XI*XI*ETA+T8VX*XI*ETA*ETA
1379          VY2=T1VY+T2VY*XI+T3VY*ETA+T4VY*XI*ETA+T5VY*XI*XI+T6VY*ETA*ETA+
1380         1    T7VY*XI*XI*ETA+T8VY*XI*ETA*ETA
1381    C
1382          IF (FQE(L).EQ.0.0) GO TO 53
1383          RR=SQRT((XX2-XQE(L))**2+(YY2-YQE(L))**2)
1384          VVX=FQE(L)*(XX2-XQE(L))/(6.2831853*PORTH(L)*RR**2)
1385          VVY=FQE(L)*(YY2-YQE(L))/(6.2831853*PORTH(L)*RR**2)
1386          IF (CQEF(L).EQ.0.0) GO TO 52
1387          ARG1=RR/BB2(L)
1388          ARG2=RQE(L)/BB2(L)
1389          VVX=FQE(L)*(XX2-XQE(L))*(BESK1(ARG1)+BESK0(ARG2)*BESI1(ARG1)/
1390         1    BESI0(ARG2))/(6.2831853*PORTH(L)*RR*BB2(L))
1391          VVY=FQE(L)*(YY2-YQE(L))*(BESK1(ARG1)+BESK0(ARG2)*BESI1(ARG1)/
1392         1    BESI0(ARG2))/(6.2831853*PORTH(L)*RR*BB2(L))
1393       52 VX2=VX2+VVX
1394          VY2=VY2+VVY
1395       53 CONTINUE
1396    C
1397    C     CALCULATE THE TIME OF TRAVEL
1398    C
1399          DX=XX2-XX1
1400          DY=YY2-YY1
1401          DELTA=SQRT(DX*DX+DY*DY)
1402          COSIN=DX/DELTA
1403          IF (JCOS.EQ.1) FCOSIN=COSIN
1404          VBAR=.5*(SQRT(VX1*VX1+VY1*VY1)+SQRT(VX2*VX2+VY2*VY2))
1405          DT=DELTA/VBAR
1406          TIME=TIME+DT
1407          IF (FQE(L).GE.0.0) GO TO 54
1408          IF (ABS(XI).GE.STEP.OR.ABS(ETA).GE.STEP) GO TO 54
1409          WRITE (6,376) N, L, TIME, XX2, YY2
1410          GO TO 20
1411       54 CONTINUE
1412          IF (TIME.LE.TMAX) GO TO 55
1413          WRITE (6,380) TIME, TMAX, N, XX2, YY2
1414          GO TO 20
1415       55 NSTEP=NSTEP+1
1416    C
1417          IF(KOD10.NE.1) GO TO 156
1418          XXA=XX2/SCALE
1419          YYA=YY2/SCALE
1420          CALL PLOT(XXA,YYA,2)
1421          IF (J.GT.NTIME) GO TO 156
1422          IF(TIME.LT.TT(J)) GO TO 155
1423          CALL SYMBOL(XXA,YYA,0.07,J,0.,-1)
1424          J=J+1
1425      155 CONTINUE
```

```
1426     156 CONTINUE
1427   C
1428         IF (NSTEP.NE.NSTART) GO TO 56
1429         WRITE (6,350) XX2, YY2, TIME
1430         NSTEP=0
1431      56 CONTINUE
1432         XI1=XI
1433         ETA1=ETA
1434         XX1=XX2
1435         YY1=YY2
1436         XXX=XX2
1437         YYY=YY2
1438         K=1
1439         GO TO 38
1440   C
1441   C      ADJUST THE STEP SO THAT IT ONLY GOES TO THE BOUNDARY
1442   C      STEP ONLY CROSSES ONE BOUNDARY
1443   C
1444      60 NSTEP=0
1445         IF (ABS(XI).GE.1.0.AND.ABS(ETA).GE.1.0) GO TO 100
1446         IF (ABS(ETA).GE.1.0) GO TO 80
1447         IF (XI.LE.-1.0) GO TO 70
1448         XI=1.0
1449         ETA=ETA1+(A/B)*(1.0-XI1)
1450         IBL=2
1451         GO TO 170
1452      70 XI=-1.0
1453         ETA=ETA1+(A/B)*(-1.0-XI1)
1454         IBL=4
1455         GO TO 170
1456      80 IF (ETA.LE.-1.0) GO TO 90
1457         ETA=1.0
1458         XI=XI1+(B/A)*(1.0-ETA1)
1459         IBL=3
1460         GO TO 170
1461      90 ETA=-1.0
1462         XI=XI1+(B/A)*(-1.0-ETA1)
1463         IBL=1
1464         GO TO 170
1465   C
1466   C      STEP CROSSES CORNER FOR TWO BOUNDARIES
1467   C
1468     100 IF (XI.LE.-1.0) GO TO 130
1469         ETAT=ETA1+(A/B)*(1.0-XI1)
1470         IF (ABS(ETAT).GT.1.0) GO TO 110
1471         XI=1.0
1472         ETA=ETAT
1473         IBL=2
1474         GO TO 160
1475     110 IF (ETAT.LT.-1.0) GO TO 120
1476         ETA=1.0
1477         XI=XI1+(B/A)*(1.0-ETA1)
1478         IBL=3
1479         GO TO 160
1480     120 ETA=-1.0
1481         XI=XI1+(B/A)*(-1.0-ETA1)
1482         IBL=1
1483         GO TO 160
1484     130 ETAT=ETA1+(A/B)*(-1.0-XI1)
1485         IF (ABS(ETAT).GT.1.0) GO TO 140
1486         XI=-1.0
1487         ETA=ETAT
```

```
      IBL=4
      GO TO 160
  140 IF (ETAT.LT.-1.0) GO TO 150
      ETA=1.0
      XI=XI1+(B/A)*(1.0-ETA1)
      IBL=3
      GO TO 160
  150 ETA=-1.0
      XI=XI1+(B/A)*(-1.0-ETA1)
      IBL=1
  160 IF (ABS(XI).EQ.ABS(ETA)) ETA=ETA-SIGN(0.0001,ETA)
  170 CONTINUE
C
      IF (K.EQ.1) GO TO 49
C
C     DETERMINE TRAVEL TIME
C
      XX2=T1X+T2X*XI+T3X*ETA+T4X*XI*ETA+T5X*XI*XI+T6X*ETA*ETA+
     1    T7X*XI*XI*ETA+T8X*XI*ETA*ETA
      YY2=T1Y+T2Y*XI+T3Y*ETA+T4Y*XI*ETA+T5Y*XI*XI+T6Y*ETA*ETA+
     1    T7Y*XI*XI*ETA+T8Y*XI*ETA*ETA
      VX2=T1VX+T2VX*XI+T3VX*ETA+T4VX*XI*ETA+T5VX*XI*XI+T6VX*ETA*ETA+
     1    T7VX*XI*XI*ETA+T8VX*XI*ETA*ETA
      VY2=T1VY+T2VY*XI+T3VY*ETA+T4VY*XI*ETA+T5VY*XI*XI+T6VY*ETA*ETA+
     1    T7VY*XI*XI*ETA+T8VY*XI*ETA*ETA
C
      IF (FQE(L).EQ.0.0) GO TO 174
      BB=SQRT((XX2-XQE(L))**2+(YY2-YQE(L))**2)
      VVX=FQE(L)*(XX2-XQE(L))/(6.2831853*PORTH(L)*RR**2)
      VVY=FQE(L)*(YY2-YQE(L))/(6.2831853*PORTH(L)*RR**2)
      IF (COEF(L).EQ.0.0) GO TO 172
      ARG1=RR/BB2(L)
      ARG2=BQE(L)/BB2(L)
      VVX=FQE(L)*(XX2-XQE(L))*(BESK1(ARG1)+BESK0(ARG2)*BESI1(ARG1)/
     1    BESI0(ARG2))/(6.2831853*PORTH(L)*RR*BB2(L))
      VVY=FQE(L)*(YY2-YQE(L))*(BESK1(ARG1)+BESK0(ARG2)*BESI1(ARG1)/
     1    BESI0(ARG2))/(6.2831853*PORTH(L)*RR*BB2(L))
  172 VX2=VX2+VVX
      VY2=VY2+VVY
  174 CONTINUE
C
C     CALCULATE THE TIME OF TRAVEL
C
      DX=XX2-XX1
      DY=YY2-YY1
      DELTA=SQRT(DX*DX+DY*DY)
      VBAR=.5*(SQRT(VX1*VX1+VY1*VY1)+SQRT(VX2*VX2+VY2*VY2))
      DT=DELTA/VBAR
      TIME=TIME+DT
C
      IF(KOD10.NE.1) GO TO 165
      XXA=XX2/SCALE
      YYA=YY2/SCALE
      CALL PLOT(XXA,YYA,2)
      IF (J.GT.NTIME) GO TO 165
      IF(TIME.LT.TT(J)) GO TO 165
      CALL SYMBOL(XXA,YYA,0.07,J,0.,-1)
      J=J+1
  165 CONTINUE
C
C     DETERMINE THE ADJACENT ELEMENT AND THE CHANGE IN COORDINATES
C
```

```
      II=NEL
      NEL=INEL(IBL,II)
      IF (NEL.NE.0) GO TO 175
      WRITE (6,300) N, II, TIME, XX2, YY2
      WRITE (2,363) TIME
      WRITE (6,301) FCOSIN
      WRITE(6,362) COSIN
      GO TO 20
  175 CONTINUE
      IF (INEL(1,NEL).EQ.II) IBE=1
      IF (INEL(2,NEL).EQ.II) IBE=2
      IF (INEL(3,NEL).EQ.II) IBE=3
      IF (INEL(4,NEL).EQ.II) IBE=4
      II=IBL-IBE
      IF (II.EQ.-2.OR.II.EQ.0.OR.II.EQ.2) GO TO 190
      II=IBL+IBE
      IF (II.NE.5) GO TO 180
      XI1=ETA
      ETA1=XI
      GO TO 30
  180 XI1=-ETA
      ETA1=-XI
      GO TO 30
  190 II=IBL+IBE
      IF (II.EQ.2.OR.II.EQ.6) GO TO 200
      XI1=XI
      ETA1=-ETA
      GO TO 30
  200 XI1=-XI
      ETA1=ETA
      GO TO 30
C
  300 FORMAT (5I5)
  310 FORMAT (3I5,2F10.0)
  320 FORMAT (8F10.0)
  330 FORMAT (I5,2F10.1)
  339 FORMAT(////)
  340 FORMAT (/11X,*ELEMENT=*,I5,10X,*X-COOR.=*,F11.3,10X,
     1         *Y-COOR.=*,F11.3,10X,*TIME=*,F10.2)
  350 FORMAT (34X,*X-COOR.=*,F11.3,10X,*Y-COOR.=*,F11.3,
     .         10X,*TIME=*,F10.2)
  360 FORMAT(/7X,*STREAMLINE NUMBER...*,I3,6X,*LEAVES THE DOMAIN *,
     .*THROUGH ELEMENT NUMBER*,I5,3X,*AT      TIME=*,F10.2/34X,
     .*X-COOR.=*,F11.3,10X,*Y-COOR.=*,F11.3///)
  361 FORMAT(11X,*COS VALUE AT THE INFLOW BOUNDARY =*,F11.3)
  362 FORMAT(11X,*COS VALUE AT THE OUTFLOW BOUNDARY =*,F11.3///)
  363 FORMAT(F12.3)
  370 FORMAT (///11X,*STREAMLINE NUMBER*,I5,3X,*REACHES THE VICINITY OF
     1THE SINK IN ELEMENT*,I5,3X,*AT TIME=*,F10.2/20X,*X-COOR.=*,F10.2,
     210X,*Y-COOR.=*,F10.2)
  380 FORMAT (//11X,*TIME=*,F10.2,5X,*EXCEEDS TMAX=*,F10.2,5X,*FOR ST
     1REAMLINE NUMBER=*,I5/20X*X-COOR.=*,F10.2,*Y-COOR.=*,F10.2///)
  390 CONTINUE
      RETURN
      END
C
C
C
C
C     FUNCTION SUBROUTINES OF SERIES EXPANSIONS FOR MODIFIED BESSEL
C     FUNCTIONS
```

```
C
      FUNCTION BESI0(X)
      BESI0=1.0+(X**2)/4.+(X**4)/64.+(X**6)/2304.
      RETURN
      END
C
C
      FUNCTION BESI1(X)
      BESI1=X/2.+(X**3)/16.+(X**5)/384.
      RETURN
      END
C
C
      FUNCTION BESK0(X)
      G=0.5772156649
      BESK0=-(ALOG(X/2.)+G)*BESI0(X)+(X**2)/4.+3.*(X**4)/128.+
     1      11.*(X**6)/13824.
      RETURN
      END
C
C
      FUNCTION BESK1(X)
      G=0.5772156649
      BESK1=1./X+ALOG(X/2.)*BESI1(X)-(-G/2.+1./4.)*X-(-G/16.+5./64.)*
     1      (X**3)-(-G/384.+10./2304.)*(X**5)
      RETURN
      END
      SUBROUTINE ZPLOT
C
C     PURPOSE - PLOT CONTOURS OF HYDRAULIC HEAD AND TRANSMISSIVITY
C
C     ISYMBL : FIVE SYMBOLS CHOSEN FOR HYDAULIC CONDUCTIVITIES,
C              SEE ZETA MANNUAL P.A-5
C
      COMMON /SCALAR/
     1   NN, NE, NHBW, SRCL, KOD8, KOD10, IQE
      COMMON /VECTOR/
     1   XN(740), YN(740), FM(740), PHI(740), PHII(740), XV(740),
     2   RT(740), TRANSX(740), TRANSY(742), COEF(225), PORTH(225),
     3   FQE(20), XQE(20), YQE(20), RQE(20), BB2(20), BES1(20),
     4   SRCRT(16), SRCLT(16), Q(16), SRCR(8), DGX(8), DGY(8), YV(740),
     5   FQ(50)
      COMMON /MATRIX/
     1   H(700,50), IN(8,225), SE(8,8)
      COMMON/XY/XO,YO,XL,YL,XMAX,YMAX,XMIN,YMIN,SCALE,NCIR
      DIMENSION CON(20),PTS(20),TITLE(8),ISYMBL(20)
      DIMENSION X(740),Y(740)
      DATA ISYMBL /12,76,143,77,8/
C
C
      WRITE (6,20)
   20 FORMAT(////,11X,*PLOTTING INFORMATION*/11X,20(1H-)//)
      READ(5,1000) NCON, NPTS, NFE, NLE, NCIR
      READ(5,1020) XMIN,XMAX,YMIN,YMAX
      READ(5,1020) XO,YO,XL,YL
      READ(5,1020) (CON(J),J=1,NCON)
      READ(5,1020) (PTS(J),J=1,NPTS)
      WRITE (6,1005) NCON,NPTS,NFE,NLE,NCIR
 1005 FORMAT (11X,22HNCON,NPTS,NFE,NLE,NCIR,10I5)
      WRITE (6,1006) XMIN,XMAX,YMIN,YMAX
 1006 FORMAT (11X,19HXMIN,XMAX,YMIN,YMAX,6F10.1)
      WRITE (6,1007) XO,YO,XL,YL
```

```
1674    1007 FORMAT (11X,11HXO,YO,XL,YL,6F10.1)
1675         WRITE (6,1008) (CON(J),J=1,NCON)
1676    1008 FORMAT (11X,3HCON,8F10.1)
1677         WRITE (6,1009) (PTS(J),J=1,NPTS)
1678    1009 FORMAT (11X,3HPTS,6F10.1//)
1679    C
1680    C       SET UP AND SCALE PLOT
1681    C
1682         XTOT=XMAX-XMIN
1683         YTOT=YMAX-YMIN
1684         SCALE=XTOT/XL
1685         SCALE1=YTOT/YL
1686         IF(SCALE.LT.SCALE1) SCALE = SCALE1
1687         XTOT = XTOT/SCALE
1688         YTOT = YTOT/SCALE
1689         XMAX=XMAX/SCALE
1690         XMIN=XMIN/SCALE
1691         YMAX=YMAX/SCALE
1692         YMIN=YMIN/SCALE
1693         DO 506 I=1,NN
1694         X(I)=XN(I)/SCALE
1695         Y(I)=YN(I)/SCALE
1696     506 CONTINUE
1697         CALL PLOTS(55,0,4LPLOT)
1698         CALL PLOT(XO,YO,-3)
1699         IF(NCIR.EQ.0) GO TO 155
1700         RL=XL/2.
1701         CALL CIRCLE (RL,0.,-90.,270.,RL,2)
1702         GO TO 165
1703     155 CONTINUE
1704         CALL PLOT (XMIN,YMIN,3)
1705         DO 160 IP=1,2
1706         CALL PLOT(XMAX,YMIN,2)
1707         CALL PLOT(XMAX,YMAX,2)
1708         CALL PLOT(XMIN,YMAX,2)
1709         CALL PLOT(XMIN,YMIN,2)
1710     160 CONTINUE
1711     165 CONTINUE
1712    C
1713    C       START ELEMENT LOOP
1714         DO 500 L=NFE,NLE
1715         HMAX=-1.0E+50
1716         HMIN=1.0E+50
1717    C
1718    C       PLOT NODE COORDINATES
1719         DO 200 J=1,8
1720         K=IN(J,L)
1721         IF (FM(K).LT.HMIN) HMIN=FM(K)
1722         IF (FM(K).GT.HMAX) HMAX=FM(K)
1723    C
1724         IF (X(K).GT.XMAX.OR.X(K).LT.XMIN) GO TO 170
1725         IF (Y(K).GT.YMAX.OR.Y(K).LT.YMIN) GO TO 180
1726         GO TO 200
1727     170 CONTINUE
1728         WRITE(6,601) K,X(K)
1729         RETURN
1730     180 CONTINUE
1731         WRITE(6,602) K,Y(K)
1732         RETURN
1733     200 CONTINUE
1734    C
1735    C       SET UP AND SOLVE QUADRATIC EQUATIONS FOR XI AND ETA
```

```
      DO 450 NC=1,NCON
      HCON=CON(NC)
      IF (HCON.GT.HMAX.OR.HCON.LT.HMIN) GO TO 450
      K1=IN(1,L)
      K2=IN(2,L)
      K3=IN(3,L)
      K4=IN(4,L)
      K5=IN(5,L)
      K6=IN(6,L)
      K7=IN(7,L)
      K8=IN(8,L)
C
C     EVALUATE TERMS IN FUNCTION EXPANSION FOR HEAD, X, AND Y
      T1H=(-FM(K1)-FM(K2)-FM(K3)-FM(K4)+2.0*(FM(K5)+FM(K6)+FM(K7)
     1   +FM(K8)))/4.0
      T1X=(-X(K1)-X(K2)-X(K3)-X(K4)+2.0*(X(K5)+X(K6)+X(K7)+X(K8)))/4.0
      T1Y=(-Y(K1)-Y(K2)-Y(K3)-Y(K4)+2.0*(Y(K5)+Y(K6)+Y(K7)+Y(K8)))/4.0
      T2H=(FM(K6)-FM(K8))/2.0
      T2X=(X(K6)-X(K8))/2.0
      T2Y=(Y(K6)-Y(K8))/2.0
      T3H=(-FM(K5)+FM(K7))/2.0
      T3X=(-X(K5)+X(K7))/2.0
      T3Y=(-Y(K5)+Y(K7))/2.0
      T4H=(FM(K1)-FM(K2)+FM(K3)-FM(K4))/4.0
      T4X=(X(K1)-X(K2)+X(K3)-X(K4))/4.0
      T4Y=(Y(K1)-Y(K2)+Y(K3)-Y(K4))/4.0
      T5H=(FM(K1)+FM(K2)+FM(K3)+FM(K4)-2.0*(FM(K5)+FM(K7)))/4.0
      T5X=(X(K1)+X(K2)+X(K3)+X(K4)-2.0*(X(K5)+X(K7)))/4.0
      T5Y=(Y(K1)+Y(K2)+Y(K3)+Y(K4)-2.0*(Y(K5)+Y(K7)))/4.0
      T6H=(FM(K1)+FM(K2)+FM(K3)+FM(K4)-2.0*(FM(K6)+FM(K8)))/4.0
      T6X=(X(K1)+X(K2)+X(K3)+Y(K4)-2.0*(X(K6)+X(K8)))/4.0
      T6Y=(Y(K1)+Y(K2)+Y(K3)+Y(K4)-2.0*(Y(K6)+Y(K8)))/4.0
      T7H=(-FM(K1)-FM(K2)+FM(K3)+FM(K4)+2.0*(FM(K5)-FM(K7)))/4.0
      T7X=(-X(K1)-X(K2)+X(K3)+X(K4)+2.0*(X(K5)-X(K7)))/4.0
      T7Y=(-Y(K1)-Y(K2)+Y(K3)+Y(K4)+2.0*(Y(K5)-Y(K7)))/4.0
      T8H=(-FM(K1)+FM(K2)+FM(K3)-FM(K4)+2.0*(-FM(K6)+FM(K8)))/4.0
      T8X=(-X(K1)+X(K2)+X(K3)-X(K4)+2.0*(-X(K6)+X(K8)))/4.0
      T8Y=(-Y(K1)+Y(K2)+Y(K3)-Y(K4)+2.0*(-Y(K6)+Y(K8)))/4.0
      DO 400 NP=1,NPTS
      XI1=0.0
      XI2=0.0
      ETA1=0.0
      ETA2=0.0
C
C     PICK A VALUE OF ETA AND SOLVE FOR XI
      ETA=PTS(NP)
      A=T5H+T7H*ETA
      B=T2H+T4H*ETA+T8H*ETA*ETA
      C=T1H+T3H*ETA+T6H*ETA*ETA-HCON
      IF (A.EQ.0.0.AND.B.NE.0.0) GO TO 230
      DISCR=B*B-4.0*A*C
      IF (DISCR.GE.0.0) GO TO 210
      GO TO 270
  210 IF (DISCR.NE.0.0) GO TO 220
      IF (B.NE.0.0) GO TO 220
      IF (A.NE.0.0) GO TO 250
      IF (C.NE.0.0) GO TO 270
      WRITE (6,1040) L, HCON, ETA
      GO TO 270
  220 XI1=-((B+SIGN(1.,B)*SQRT(DISCR))/(2.0*A))
      XI2=C/(A*XI1)
      GO TO 240
```

```
      230 XI1=-C/B
          XI2=-100.0
      240 IF (XI1.GE.-1.0.AND.XI1.LE.1.0.OR.XI2.GE.-1.0.AND.
     1   XI2.LE.1.0) GO TO 250
          GO TO 270
C
C     IF THE ROOT LIES WITHIN THE ELEMENT, FIND ITS LOCATION
      250 DO 260 I=1,2
          XI=XI1
          IF (I.EQ.2) XI=XI2
          IF (XI.LT.-1.0.OR.XI.GT.1.0) GO TO 260
          XX=T1X+T2X*XI+T3X*ETA+T4X*XI*ETA+T5X*XI*XI+T6X*ETA*ETA+
     1    T7X*XI*XI*ETA+T8X*XI*ETA*ETA
          YY=T1Y+T2Y*XI+T3Y*ETA+T4Y*XI*ETA+T5X*XI*XI+T6Y*ETA*ETA+
     1    T7Y*XI*XI*ETA+T8X*XI*ETA*ETA
C
C     PLOT THE LOCATION OF THE ROOT
          IF (XX.LT.XMIN.OR.XX.GT.XMAX) GO TO 260
          IF (YY.LT.YMIN.OR.YY.GT.YMAX) GO TO 260
          IF(NCON.EQ.3) GO TO 252
          IF(NCON.EQ.5) GO TO 253
          CALL SYMBOL(XX,YY,0.07,NC,0.,-1)
          GO TO 260
      252 CONTINUE
          JNC=NC*2-1
          CALL SYMBOL(XX,YY,0.07,ISYMBL(JNC),0.,0)
          GO TO 260
      253 CONTINUE
          CALL SYMBOL(XX,YY,0.07,ISYMBL(NC),0.,0)
      260 CONTINUE
C
C     PICK A VALUE OF XI AND SOLVE FOR ETA
      270 XI=PTS(NP)
          A=T6H+T8H*XI
          B=T3H+T4H*XI+T7H*XI*XI
          C=T1H+T2H*XI+T5H*XI*XI-HCON
          IF (A.EQ.0.0.AND.B.NE.0.0) GO TO 330
          DISCR=B*B-4.0*A*C
          IF (DISCR.GE.0.0) GO TO 310
          GO TO 400
      310 IF (DISCR.NE.0.0) GO TO 320
          IF (B.NE.0.0) GO TO 320
          IF (A.NE.0.0) GO TO 350
          IF (C.NE.0.0) GO TO 400
          WRITE (6,1039) L,HCON,XI
          GO TO 400
      320 ETA1=-((B+SIGN(1.,B)*SQRT(DISCR))/(2.0*A))
          ETA2=C/(A*ETA1)
          GO TO 340
      330 ETA1=-C/B
          ETA2=-100.0
      340 IF (ETA1.GE.-1.0.AND.ETA1.LE.1.0.OR.ETA2.GE.-1.0.AND.
     1   ETA2.LE.1.0) GO TO 350
          GO TO 400
C
C     IF THE ROOT LIES WITHIN THE ELEMENT, FIND ITS LOCATION
      350 DO 360 I=1,2
          ETA=ETA1
          IF (I.EQ.2) ETA=ETA2
          IF (ETA.LT.-1.0.OR.ETA.GT.1.0) GO TO 360
          XX=T1X+T2X*XI+T3X*ETA+T4X*XI*ETA+T5X*XI*XI+T6X*ETA*ETA+
     1    T7X*XI*XI*ETA+T8X*XI*ETA*ETA
```

```
      YY=T1Y+T2Y*XI+T3Y*ETA+T4Y*XI*ETA+T5Y*XI*XI+T6Y*ETA*ETA+
     1   T7Y*XI*XI*ETA+T8Y*XI*ETA*ETA
C
C     PLOT THE LOCATION OF THE ROOT
      IF (XX.LT.XMIN.OR.XX.GT.XMAX) GO TO 360
      IF (YY.LT.YMIN.OR.YY.GT.YMAX) GO TO 360
      IF(NCON.EQ.3) GO TO 352
      IF(NCON.EQ.5) GO TO 353
      CALL SYMBOL(XX,YY,0.07,NC,0.,-1)
      GO TO 360
  352 CONTINUE
      JNC=NC*2-1
      CALL SYMBOL(XX,YY,0.07,ISYMBL(JNC),0.,0)
      GO TO 360
  353 CONTINUE
      CALL SYMBOL(XX,YY,0.07,ISYMBL(NC),0.,0)
  360 CONTINUE
  400 CONTINUE
  450 CONTINUE
  500 CONTINUE
      CALL PLOT(0.,0.,3)
      XEND=8.5-X0
      CALL PLOT(XEND,-Y0,999)
C
  601 FORMAT(/5X,10HX-VARIABLE,I3,F10.3,5X,17HEXCEED THE DOMAIN)
  602 FORMAT(/5X,10HY-VARIABLE,I3,F10.3,5X,17HEXCEED THE DOMAIN)
 1000 FORMAT(10I5)
 1020 FORMAT (8F10.1)
 1039 FORMAT(//10X,I5,2X,F6.1,3X,F6.3,5X,*CONTOUR LINE IS XI LINE*)
 1040 FORMAT(//10X,I5,2X,F6.1,3X,F6.3,5X,*CONTOUR LINE IS ETA LINE*)
      RETURN
      END
```

July 1978
Technical Report No. 231

FINITE ELEMENT MODELING OF GROUNDWATER INJECTION-EXTRACTION SYSTEMS

by

Randall J. Charbeneau

Robert L. Street

COPIED FOR QA FILES

Supported by

U.S. Environmental Protection Agency
Research Grant EPA-R-804431

Department of CIVIL ENGINEERING
STANFORD UNIVERSITY

Department of Civil Engineering
Stanford University
Stanford, California 94305

FINITE ELEMENT MODELING OF GROUNDWATER INJECTION-EXTRACTION SYSTEMS

by

Randall J. Charbeneau

Robert L. Street

Technical Report No. 231

July 1978

This research was supported by

Groundwater Research Branch
Robert S. Kerr Environmental Research Laboratory
U.S. Environmental Protection Agency
Ada, Oklahoma 74820
Research Grant EPA-R-804431

Project Officer
Marion R. Scalf

This study was conducted in cooperation with
Water Resources Control Board, Department of Water Resources
and Department of Health, State of California,
Sacramento, California 95814

and

Santa Clara Valley Water District
San Jose, California 95118

ABSTRACT

Artificial recharge of groundwater resources through wells leads to a need for computer simulation of the hydraulics and transport of contaminants in groundwater flowfields. The Palo Alto Baylands injection-extraction project motivated the present work. A numerical model was developed for simulating steady-state groundwater flow in a confined, leaky aquifer system. The basic numerical technique used is the Galerkin-finite-element method. Greatly improved accuracy of the simulation near wells is achieved by removing the singular behavior of the flow with an analytic solution for the near-well zone, solving the remaining non-singular problem, and combining the results. The resulting solutions compare favorably with known analytic solutions for confined leaky aquifers (both isotropic and anisotropic). No additional computation time is required for this method compared to standard FE programs. Velocity fields were derived through differentiation of the head solution; smoothing and averaging are then used for generating systems of streamlines and determining times of travel to points of interest (including breakthrough curves). Specific applications of the model include investigation of the gross hydraulic characteristics of a nonhomogeneous groundwater aquifer containing injection-extraction well combinations, the times of travel and breakthrough curves being appropriate only for "nondispersive" contaminants. In an appendix the recent geologic history, stratigraphy and geomorphology of Wisconsin age alluvial deposits beneath the Palo Alto baylands are reviewed; then a comprehensive picture of the hydrogeologic environment is drawn and its impact on the modeling effort is noted.

ACKNOWLEDGEMENTS

The authors are grateful to the individuals associated with the groundwater recharge project who have contributed to this work in many ways. A special note of thanks is due Dr. Paul V. Roberts, manager of the Stanford University research project, and Dr. Bernard Hallet, whose suggestions pointed the way for the investigations of Appendix I. Dr. George F. Pinder of Princeton University provided the original computer code and Albert Valocchi helped with some of the computer programming. Finally, the authors are grateful for the financial support received under U.S. Environmental Protection Agency Grant EPA-R-804431.

TABLE OF CONTENTS

ABSTRACT		iii
ACKNOWLEDGEMENTS		iv
LIST OF TABLES		vii
LIST OF FIGURES		viii
I.	INTRODUCTION	1
II.	SCOPE OF WORK	4
III.	BAYLANDS PROJECT	5
IV.	FINITE ELEMENT MODELING OF INJECTION-EXTRACTION SYSTEMS	8
	A. Galerkin Finite Element Method	9
	B. Basis Functions, Function Representations and Transformation Between Domains	12
	C. Problems with Wells; Local Solution Improvement Methods	18
	D. A Technique for Singularity Removal	21
	E. Evaluation of the Interelement Boundary Integral	24
	F. Velocity Fields	32
	1. Quadratic Velocity Field	33
	2. Smoothed Linear Velocity Field	36
	G. Streamlines	38
	H. Times of Travel	40
	I. Plotting Contours	41
V.	APPLICATIONS	43
	A. Thiem Problem	44
	B. Source and Sink in Infinite Aquifer: Isotropic Cases	44
	C. Source and Sink in Infinite Aquifer: Anisotropic Cases	46
	D. Velocity Fields, Streamlines and Times of Travel	47

VI. DISCUSSION 51

A. Simulation Model and Results 51

B. Dispersion 55

C. Generalization and Time Dependent Problems 57

VII. CONCLUSIONS AND RECOMMENDATIONS FOR FUTURE WORK 63

REFERENCES 65

APPENDIX I 70

Hydrogeology of the Palo Alto Baylands 70

Recent Geologic History 71

Stratigraphy 71

Geomorphology 73

SCVWD Injection-Extraction Site 74

Injection Well I-2 78

Doublet Pair I-1, E-1 80

APPENDIX II 82

Properties of the Anisotropic Solution 82

Evaluation of Interelement Boundary Integral 84

LIST OF TABLES

1. Correspondence Between Function Representation Coefficients 88
2. Bilinear Basis Functions 88
3. Transmissivity Values for SCVWD Injection-Extraction Wells (Preliminary Data) 89

23. Fence Diagram at I-2 113
24. Simulation of Hydraulic Head Contours Around I-2 114
25. Hydraulic Head Contours for I-1, E-1 Pair 115
26. Contours of Transmissivity Used in Simulation of Figure 25 116
27. Breakthrough Curve (Nondispersive) at E-1 117
28. Ellipse Containing the Well 118
a. Streamlines Crossing Boundary
b. Normal Vector to Boundary
c. Unit Normal and Streamlines at Boundary

I. INTRODUCTION

An increased interest in the use of groundwater resources has been seen in recent years. Ambroggi (1977) discussed regulation of underground reservoirs, including overexploitation and artificial recharge, as a means of long-term control of the water cycle. He noted the various functions of these reservoirs: supply, storage, mixing and conveying water. Except in California and Israel, where the storage function is partially exploited, the primary use of underground reservoirs has been that of supply. In certain coastal areas extensive use of underground reservoirs for supply has led to a reversal in the normal direction of water movement. In some of these areas artificial recharge programs are currently underway with their principal purpose being prevention of saltwater intrusion into potable water supplies. Such programs are found in Orange County (Los Angeles area) and Santa Clara County (San Francisco area), where systems of injection and extraction wells are used to prevent the intrusion of saltwater into near-shore aquifers. In both programs the water being injected is reclaimed wastewater. Injection of this water raises a number of interesting questions concerned with the fate of certain contaminants, the answers to which can only be obtained through use of mathematical models.

Mathematical modeling of contaminants in groundwater systems requires a description of the hydraulics and transport of contaminants as well as a description of chemical reactions within the environment of the porous media. In trying to achieve a realistic model of the fate of injected reacting contaminants one must first adequately account for the hydraulic properties, i.e., the convection and dispersion of the contaminants. Unless the hydraulics are modeled correctly throughout the flowfield, anticipated reactions can only serve to compound the error and make quantitative interpretation of field results impossible. Now, according to the work of de Jong (1958), Bear (1961) and Scheidegger

(1961), as well as many others, the magnitude of the coefficient of dispersion is proportional to the first power of the velocity. Because the velocity is greatest in the immediate vicinity of a well (and in fact becomes singular at the well in a two-dimensional source-sink model of wells), an adequate model of convection and dispersion must be especially accurate near wells. This need for accuracy near wells has been a major problem in the simulation of well fields. Neither the finite difference nor finite element techniques are able to model point singularities or even very rapidly varying quantities. Analytical methods can easily provide accurate solutions near wells but they are generally applicable only to idealized homogeneous groundwater systems, an exceptional case when large-scale field systems are considered.

Complexities inherent within actual field sites may be classified under two general headings: anisotropic fields and nonhomogeneous fields. Anisotropy refers to preferred directional characteristics of a property of the media at a particular point. With hydraulic conductivity being the media property of most interest in groundwater flow, an anisotropic medium is one in which the flow has an easier time going in one direction than in another. A nonhomogeneous field is one in which the property of interest varies from one point to another. In an anisotropic and nonhomogeneous aquifer the magnitude of hydraulic conductivity, as well as the direction of the principal axes of the conductivity tensor, may vary from one point to another.

In the case of a confined groundwater aquifer, where the aquifer is usually characterized as a two-dimensional surface, the ability of the "surface" to transmit flow is measured by the product of the hydraulic conductivity of the media and the thickness of the aquifer. This product is called the coefficient of transmissivity. In a nonhomogeneous field it may vary due to changes in either hydraulic conductivity or thickness of the aquifer.

Because large-scale groundwater systems are characterized by their nonhomogeneous nature, analytical simulation methods have found much less use than numerical methods. Of the many methods of numerical analysis available, the finite element method has been shown to be particularly effective for problems in groundwater flow and contaminant transport (Pinder and Frind, 1972; Pinder, 1973).

II. SCOPE OF WORK

The present work has two relatively distinct foci. We are on one hand interested in the hydrogeology of post-Wisconsin alluvial deposits beneath the Palo Alto baylands and, on the other, concerned with development of a two-dimensional model for groundwater hydraulics around wells located in a confined, leaky, nonhomogeneous aquifer. Both topics stem from a single project concerned with groundwater recharge and extraction. The project is being carried out by the Santa Clara Valley Water District (SCVWD), with the intent of establishing a hydraulic barrier to salt-water intrusion from South San Francisco Bay. As shown below, conclusions drawn from the hydrogeologic investigation (see Appendix I) limit application of the numerical model to only part of the injection-extraction field.

In Section III the SCVWD Project is described and the predesign test status is reviewed. Introduction of this material provides motivation for Section IV in which a steady-state hydraulics model for flow in a confined, leaky aquifer is developed for a nonhomogeneous porous medium containing injection/extraction wells. Section V provides applications of the model presented in Section IV. Sections VI and VII present the discussion and the conclusions and recommendations for future work. In Appendix I the geologic history, stratigraphy and geomorphology of the baylands are discussed and a comprehensive picture of the hydrogeologic environment is drawn. In Appendix II the analysis of Section IV is extended to anisotropic problems.

III. BAYLANDS PROJECT

The Santa Clara Valley Water District (SCVWD) has proposed to carry out advanced waste treatment and injection of municipal wastewater into an aquifer in the Palo Alto Bayfront area to serve as a barrier against seawater intrusion into the groundwater. Figure 1 shows the design for this project. Nine injection wells are located along a 3.2 kilometer line running parallel to the bayfront. Ten extraction wells are located landward of these injection wells. Design of the intrusion barrier is based on the idea that the line of injection wells will form a pressure ridge which will block the landward movement of the denser seawater. Extraction occurs so that there will be no net input of reclaimed water into the aquifer. Ideally, all of the injected water is eventually extracted.

The predesign phase of the project suggested that modeling of groundwater flow within the shallow aquifers of the area would be a straightforward task. Wells were drilled along the northwestern edge of the study area (near I-1). Logs and well tests showed that there were two shallow zone aquifers (at depths of 6 and 14 meters) separated by a leaky aquitard. A third, thicker aquifer was found in the deeper zone (55 meters). The deeper aquifer was hydraulically separate from the shallow zone aquifers. The description of the shallow zone given in the predesign report (Jenks and Adamson, 1974, pg. 4) was that "the alluvium consists of a series of essentially flat lying sand and gravel aquifers separated by extensive clay aquicludes and aquitards." A qualified warning was given, but its implications were not appreciated at the time:

> "Concerning the shallow deposits, there is evidence of variation in thickness of these aquifers throughout the area and evidence that particular thin zones may pinch out and interfinger with other similar zones. However, due to leakage between the various individual zones, the shallow deposits

can be considered a single extensive aquifer throughout the area." (Jenks and Adamson, pg. 4)

Since it was felt that the test site was representative of the entire area the design of the injection-extraction system was carried out on the basis of the predesign tests. These tests suggested a transmissivity of 108 m^2/day (8700 gpd/ft) and a coefficient of storativity of 0.000036 for injection well I-1 in the lower (14 meter) aquifer (Jenks and Adamson). The vertical hydraulic conductivity of the confining aquitard was calculated to be 0.13 cm/day (0.032 gpd/ft^2) with a storativity of 0.001. The maximum injection rate was determined to be 1020 m^3/day (187 gpm).

A 7600 m^3/day (two million gallons per day) advanced waste treatment facility was proposed (and subsequently constructed). Assuming that all of the high quality effluent was injected to establish the hydraulic barrier an average injection rate of 844 m^3/day (154 gpm) would be required for each well in the injection system.

As a long-term goal, the SCVWD facility will be used for research to determine the feasibility of such a system for reclaiming water for potable uses. To answer questions relevant to this long-term goal, Stanford University proposed a three-year program designed to acquire fundamental knowledge concerning the transformations of contaminants and aquifer material resulting from the injection of treated wastewater. This research was funded by the U.S. Environmental Protection Agency under Grant EPA-R-804431, authorized for three years beginning May 1, 1976. The major objectives of the research project are as follows (Roberts, et al., 1978):

1. To determine the effects which the injected wastewater will have on the chemical, physical, and biological quality of the basin and injected waters.

2. To determine the effect which injected wastewater will have on the hydrologic and mineralogic characteristics of the aquifer.
3. To seek the optimum quality for injected water which will result in a high quality groundwater and minimum damage to the hydrologic characteristics of the aquifer.
4. To develop generalized mathematical models for describing the movement of water, the changes in hydrologic characteristics, and resulting changes in water quality from wastewater injection in order to make the results of most value for application in other similar projects.

The objective of primary interest in the present work is the first part of 4, i.e., development of generalized mathematical models for describing the movement of water in the hydrogeologic environment.

IV. FINITE ELEMENT MODELING OF INJECTION-EXTRACTION SYSTEMS

As pointed out in the Introduction, the first task in achieving a realistic model of the fate of injected reacting contaminants is to adequately model the groundwater flow hydraulics. The equation governing the hydraulics of a leaky aquifer system is obtained by combining Darcy's law with the principle of conservation of mass (Bear, 1972). Consider steady flow in an aquifer of areal extent lying on an impermeable bed and confined from above by a slightly permeable aquitard of specified thickness and permeability. Above the aquitard is a second (adjacent) aquifer. Treating the lower aquifer as two-dimensional in the horizontal plane with a transmissivity $T_{\alpha\beta}$ one finds that the governing equation for steady-state flow is

$$\frac{\partial}{\partial x_\alpha}\left(T_{\alpha\beta}\frac{\partial h}{\partial x_\beta}\right) - \frac{K}{b}\left(h - h_a\right) + Q = 0 \qquad (1)$$

where

h	= hydraulic head	(L)
$T_{\alpha\beta}$	= transmissivity tensor	(L^2/T)
x_α	= location vector	(L)
K	= permeability of confining bed (aquitard)	(L/T)
b	= thickness of confining bed	(L)
h_a	= head in adjacent aquifer	(L)
Q	= $\sum_k Q_k \delta(x - x_k,\ y - y_k)$	
Q_k	= source strength per unit area	(L/T)
N_w	= number of source-sink wells	
$\delta(\circ,\circ)$	= Dirac delta function	
(x_k, y_k)	= location of source-sink wells, $k = 1, 2, \ldots, N_w$	
α, β	= indices which run from 1 to 2	

The first term in equation (1) represents the divergence of the velocity field written in terms of Darcy's law, the second term represents leakage to the adjacent aquifer and the third term represents sources and sinks (Q_k being positive or negative, respectively).

To simplify the presentation which follows it is convenient to work with the operator L defined by

$$L(h) = \frac{\partial}{\partial x_\alpha}\left(T_{\alpha\beta}\frac{\partial}{\partial x_\beta}h\right) - \frac{K}{b}h \qquad (2)$$

Then equation (1) may be written

$$L(h) + \frac{K}{b}h_a + Q = 0 \qquad (3)$$

A. Galerkin-Finite-Element Method

Application of the Galerkin-finite element procedure to aquifer analysis has been described by Pinder and Frind (1972)[also see Pinder and Gray (1977)]; only a brief review will be given here. To solve equation (3) we assume a trial solution of the form

$$\hat{h}(x, y) = \sum_{j=1}^{N_n} h_j \varphi_j(x, y) \qquad (4)$$

where the $\varphi_j(x, y)$ are a system of linearly independent functions (basis functions) chosen beforehand, h_j are undetermined coefficients, and N_n is the total number of nodes (basis functions) in the finite element net. The domain Ω having boundary Γ, as shown in Figure 2, is divided into a number N_e of subdomains (elements). Each of these has, for the type of basis functions used here, eight node points on its boundary. The type of basis functions used in this work were introduced by Ergatoudis,

et al. (1968) and are for use with curved isoparametric quadrilateral elements. The term isoparametric means that the functional representation of the curved boundaries and the functional representation of the approximate solution (4) are given by the same system of functions, φ_j (Pinder and Gray, 1977, pg. 122). As shown in Figure 3, the basic shape of one of these elements is a quadrilateral, but the sides are distorted in a way prescribed by the location of the node points. There exist many other types of basis functions used in finite element analysis. [See for instance Pinder and Gray (1977, Chapter 4) for an extensive list.]

The basis function $\varphi_i(x,y)$ has a non-zero value only over those elements which have node i on their boundary; $\varphi_i(x,y)$ has the value unity at node i and zero at all other nodes:

$$\varphi_i(x_j, y_j) = \delta_{ij} = \begin{cases} 1 & i=j \\ 0 & i \neq j \end{cases}$$

One can see that the unknown coefficients h_i in (4) are the values of the approximate solution to (3) at the nodes points (x_i, y_i). Now, if (4) is the true solution to (3), the following identity must hold:

$$L(\hat{h}) + \frac{K}{b} h_a + Q = 0 \tag{5}$$

In general (5) is not satisfied exactly; however, we can try to make it an identity by finding a solution $\hat{h}$ such that (5) is orthogonal to the set of basis functions $\varphi_j (j = 1, 2, \ldots N_n)$ over the domain Ω:

$$\iint_{\Omega} \left\{ L(\hat{h}) + \frac{K}{b} h_a + Q \right\} \varphi_i \, d\Omega = 0 \qquad i = 1, 2, \ldots N_n \tag{6}$$

Equation (6) forms the heart of the Galerkin-finite element method. It can be shown (Oden and Reddy, 1976, pg. 326) that if the coefficients h_j

are determined so that (6) holds, the resulting solution (4) is the "best approximation" to the true solution (3) in terms of the basis functions $\varphi_j (j = 1, 2, \ldots N_n)$. Before applying (6) we may eliminate the second derivatives, which otherwise would impose unnecessary continuity conditions between elements, by application of Green's theorem. First we define the symmetric bilinear operator

$$E(\varphi_i, \hat{h}) \doteq T_{\alpha\beta} \frac{\partial \varphi_i}{\partial x_\alpha} \frac{\partial \hat{h}}{\partial x_\beta} + \frac{K}{b} \varphi_i \hat{h}$$

Then Green's theorem may be written

$$\int_\Omega L(\hat{h}) \varphi_i d\Omega = - \iint_\Omega E(\varphi_i, \hat{h}) d\Omega + \int_\Gamma \varphi_i T_{\alpha\beta} \frac{\partial \hat{h}}{\partial x_\beta} \ell_\alpha d\Gamma$$

$$= - \iint_\Omega E(\varphi_i, \hat{h}) d\Omega - \int_\Gamma \varphi_i q_n d\Gamma \qquad (7)$$

where we have used Darcy's law to write q_n, the outward normal velocity to the boundary, in place of $-T_{\alpha\beta} \frac{\partial \hat{h}}{\partial x_\beta} \ell_\alpha$ (ℓ_α being the direction cosines of the outward unit normal vector to Γ). Applying Green's theorem (7) to equation (6) we obtain

$$\iint_\Omega E(\varphi_i, \hat{h}) d\Omega = \iint_\Omega \left\{ Q + \frac{K}{b} h_a \right\} \varphi_i d\Omega - \int_\Gamma q_n \varphi_i d\Gamma \qquad (8)$$

Substitution of the expression for the approximate solution (4) into equation (8) gives the matrix equation for determination of the unknown coefficients:

$$\sum_{j=1}^{N_n} h_j \iint_{\Omega} E(\varphi_i, \varphi_j)\, d\Omega = \iint_{\Omega} \left\{ Q + \frac{K}{b} h_a \right\} \varphi_i\, d\Omega - \int_{\Gamma} q_n \varphi_i\, d\Gamma \qquad (9)$$

or

$$E_{ij} h_j = f_i \qquad (i = 1, 2, \ldots N_n)$$

The matrix $\iint_{\Omega} E(\varphi_i, \varphi_j)\, d\Omega$ is called the "stiffness" matrix and the right hand side vector of (9) is the generalized forcing function. The stiffness matrix is symmetric. Because the basis functions φ_i are defined to be non-zero only over those elements which have node i on their boundary, we see that, with a proper numbering of nodes, the stiffness matrix is also banded and sparse.

B. Basis Functions, Function Representation and Transformation Between Domains

As evidenced by equation (9), application of the finite element method requires evaluation of areal integrals over the non-simple domains of elements. This is accomplished by carrying out the integration over a simple domain which may be uniquely mapped into the physical domain of the elements. The physical plane is called the global domain while the corresponding simple domain is called the local domain (see for instance Pinder and Gray, 1977, pg. 110). When using quadratic, isoparametric, quadrilateral elements the local domain consists of a two unit by two unit square in ξ - η coordinates. Figure 3 shows an example of the local and global representations of an element. The mapping from the local to the global domain is uniquely determined by

$$x = \sum_{i=1}^{8} x_i \varphi_i(\xi, \eta)$$

$$y = \sum_{i=1}^{8} y_i \varphi_i(\xi, \eta) \tag{10}$$

where x and y are the global domain coordinates of a point of the element, x_i and y_i are the ith node coordinates in the global domain, and φ_i are the basis functions of the element. The basis functions are polynomials in the local domain coordinates (Ergatoudis, et al., 1968):

corner nodes

$$\varphi_i = -\frac{1}{4}(1 + \xi_o)(1 + \eta_o)(1 - \xi_o - \eta_o)$$

where $\xi_o = \xi \xi_i$ and $\eta_o = \eta \eta_i$, ξ_i and η_i are the node coordinates (either ± 1)

side nodes (see Figure 3)

For nodes 5 and 7,

$$\varphi_i = \frac{1}{2}(1 - \xi^2)(1 + \eta_o)$$

and for nodes 6 and 8,

$$\varphi_i = \frac{1}{2}(1 + \xi_o)(1 - \eta^2)$$

Representation of an arbitrary function in local coordinates is given by an expansion similar to (10):

$$A(\xi, \eta) = \sum_{i=1}^{8} a_i \varphi_i(\xi, \eta) \tag{11}$$

where a_i are the nodal values of the function. To specify the function in global coordinates all three expansions in (10) and (11) are required; (11) is used to find the value at a particular point (ξ, η) and (10) is used to find the

corresponding global point (x, y). The problem of going from the global to local representation is not simple since the transformations in (10) and (11) are not easily inverted. Fortunately, it is seldom necessary to go in this direction.

Equation (11) may be cast into a more useful form for analysis within a particular element. Each of the basis functions is a polynomial in ξ and η. If (11) is expanded and equivalent terms are grouped, one obtains the expression

$$A(\xi, \eta) = c_1 + c_2\xi + c_3\eta + c_4\xi\eta + c_5\xi^2 + c_6\eta^2 + c_7\xi^2\eta + c_8\xi\eta^2 \qquad (12)$$

The correspondence between the coefficients in (11) and (12) is shown in Table 1. Equation (12) has advantages over (11). If one were interested in evaluating the function at a number of points one need only use the (ξ, η) points directly in (12). In (11) one would have to regenerate the basis functions for each (ξ, η) point and then carry out the expansion. (In typical FE codes the basis functions are generated in a separate subroutine. One enters with the (ξ, η) point and returns with the values of the functions, their derivatives, etc., at that point.) A second advantage of (12) is that for a particular ξ (or η) the form is an explicit quadratic in η (or ξ). This is the key to generating contour plots, as is shown below.

Now consider the mapping of boundaries or the values of a function along the boundary of an element. Along each side of the element boundary the basis functions for all nodes not situated on the particular side have zero value. Choose the side $\xi = 1$ for example (see Figure 3 for the numbering scheme). Then the expansion in (11) becomes

$$\begin{aligned} A(1, \eta) &= a_2\varphi_2 + a_3\varphi_3 + a_6\varphi_6 \\ &= a_6 + \frac{1}{2}(a_3 - a_2)\eta + \frac{1}{2}(a_3 + a_2 - 2a_6)\eta^2 \end{aligned} \qquad (13)$$

and the tangential derivative along the boundary is

$$\frac{d\,A(1,\eta)}{d\eta} = \frac{1}{2}(a_3 - a_2) + (a_3 + a_2 - 2a_6)\eta \tag{14}$$

In particular the mapping of the boundary is specified by

$$x = x_6 + \frac{1}{2}(x_3 - x_2)\eta + \frac{1}{2}(x_3 + x_2 - 2x_6)\eta^2$$

$$y = y_6 + \frac{1}{2}(y_3 - y_2)\eta + \frac{1}{2}(y_3 + y_2 - 2y_6)\eta^2 \tag{15}$$

In evaluating the integrals of equation (9), or similar integrals which follow, the mapping or transformation between local and global domains is of little value unless it is unique and can be inverted (at least numerically). Courant and John (1974), p. 261) show that a transformation is unique and invertable if the determinant of the Jacobian of the transformation is not zero. In the transformation between local and global coordinates the regions most sensitive to violation of the condition on the Jacobian are the corner nodes of an element. It is well known that to keep the element from folding over on itself, thus destroying the uniqueness and invertability of the transformation, the angle at the corner node must be greater than zero and less than 180 degrees. Using the results from the last few paragraphs on mapping of boundaries one can constrain the location of nodes of the element so that uniqueness and invertability are preserved.

As an example consider corner node number 3 of Figure 3. The slope of the side 2-6-3 at node 3 is, according to (15),

$$\frac{dy}{dx} = \frac{dy}{d\eta}\frac{d\eta}{dx}\bigg|_{\eta=1} = \frac{\frac{3}{2}y_3 + \frac{1}{2}y_2 - 2y_6}{\frac{3}{2}x_3 + \frac{1}{2}x_2 - 2x_6} \tag{16}$$

Similarly, for the 4-7-3 the slope at node 3 is

$$\frac{dy}{dx} = \frac{dy}{d\xi}\frac{d\xi}{dx}\bigg|_{\xi=1} = \frac{\frac{3}{2}y_3 + \frac{1}{2}y_4 - 2y_7}{\frac{3}{2}x_3 + \frac{1}{2}x_4 - 2x_7} \tag{17}$$

The conditions on the node points for the two sides may then be written

$$\theta_2 + 180 > \theta_1 > \theta_2 \tag{18}$$

where

$$\theta_1 = \tan^{-1}\left(\frac{\frac{3}{2}y_3 + \frac{1}{2}y_2 - 2y_6}{\frac{3}{2}x_3 + \frac{1}{2}x_2 - 2x_6}\right)$$

$$\theta_2 = \tan^{-1}\left(\frac{\frac{3}{2}y_3 + \frac{1}{2}y_4 - 2y_7}{\frac{3}{2}x_3 + \frac{1}{2}x_4 - 2x_7}\right)$$

If these conditions are not fulfilled then the mapping is degenerate and cannot be used. The constraints for other corners of the element are formulated in a similar fashion. These constraints carry over to complete Lagrangian isoparametric quadratic elements (but then the Jacobian is also sensitive to the location of the center node). Use is made of these constraints when checking the conditions on isoparametric "circles" and "ellipses" (see section IV. E and Appendix II).

Before leaving this discussion of basis functions and function expansions it is of interest to mention a particular problem which arises with specification of nonhomogeneous parameter fields (such as the transmissivity). When functional coefficients are used (see Pinder, Frind and Papadopulos, 1973) the nodal values are assigned and the field is interpolated using the basis function expansion. Most parameter fields are inherently positive valued (transmissivity, porosity, leakage

coefficient, aquifer thickness, dispersivity, etc.). When the variance of the assigned values is small and the magnitudes are fairly large there is little difficulty. But, when there is a large range in assigned values a problem of negative values may arise, even if all of the assigned values are positive. For instance, assume that the value of 3 is assigned to all of the corner nodes and the value of 1 is assigned to the side nodes. Then the interpolated value at the center of the element is -1 (see (12) and Table 1). It is difficult to develop useful general conditions to guarantee positive definiteness of the entire parameter field but it is easy to develop such conditions for values on the element boundaries. Indeed, from (14) the extremum is at $\eta = -\frac{a_3 - a_2}{2(a_3 + a_2 - 2a_6)}$; if this lies between -1 and 1, then it is within the element. Substituting this value of η into (13) one finds

$$A_{\text{extremum}} = a_6 - \frac{(a_3 - a_2)^2}{8(a_3 + a_2 - 2a_6)}$$

If $A_{\text{extremum}} < 0$ and $|\eta| \leq 1$ then there is trouble. A more useful condition follows if it is recognized that in practice one is usually interested in specifying a uniform (not necessarily constant) gradient across an element. This is accomplished by keeping the extremum points outside of the range $-1 < \eta < 1$ (or ξ instead of η). This leads to the following condition along the side 2-6-3:

$$\frac{a_2 + 3a_3}{4} \leq a_6 \leq \frac{3a_2 + a_3}{4}$$

when $a_2 > a_3$ and

$$\frac{3a_2 + a_3}{4} \leq a_6 \leq \frac{a_2 + 3a_3}{4}$$

when $a_3 > a_2$. Similar conditions are found for the other sides. If these conditions are met for all sides then there will be no problem with violating the positive definite condition within the element. As a second example consider specifying $a_3 = 4000$ and $a_2 = 400$. Then to guarantee a uniform gradient one must have $1300 \leq a_6 \leq 3100$.

Finally an interesting theorem concerning the specification of a parameter along a boundary, or even specification of the boundary itself, is mentioned.

Theorem: The slope of an interpolated parameter representation at the side node is equal to the slope of the line drawn through the two corner node values.

This theorem follows directly from (14) with $\eta = 0$ and is of great value when visualizing the shape of a function or the shape of the boundary through specified points. The validity of this theorem does not depend upon the location of the mid-node and, thus, is of great value when visualizing the effect on the interpolated shape of the boundary (and thus on the Jacobian of the transformation) of moving the mid-side node.

C. Problems with Wells; Local Solution Improvement Methods

An actual well has a finite radius and the magnitude of the velocity at the well wall is very large but still finite. In the chosen model the flowfield is envisioned as being two dimensional and injection and extraction wells are assumed to exist at specific points. To get a finite discharge into or out of a point the velocity must be infinite, and this is the main difficulty presented by wells. Neither the finite difference nor finite element methods are able to accurately simulate rapidly varying fields, let alone those which become singular.

General problems presented by the presence of singular functions in the true solution are well recognized in the finite element literature. Each of the following produces a particular type of singularity: the

point-load or point-source, the presence of a corner in a structure, the presence of a fracture or crack tip, and specification of discontinuous data. There are three general approaches to improving the solution in the local region around a singularity. First, the finite element mesh may be refined. Second, a singularity may be introduced through use of a singular transformation between the local and global domains. The third approach is to augment the solution space [the function space spanned by the set of basis functions $\varphi_j(x, v)(j = 1, 2, \ldots N_n)$] by adding higher order functions or functions of a particular nature specific to the problem at hand. Carey (1976) and Gartling and Becker (1976) present two examples of the first approach (mesh refinement), the work of Carey being more readily applicable to problems containing singular regions. For a discussion of the second approach, that of introducing a singularity through the local-global transformation, see Henshell and Shaw (1975) and the references therein. The third approach, solution space augmentation, has found greater application and is of primary interest here.

For a general discussion of the third approach see Strang and Fix (1973, Chapter 8). Pian (1964 A & B) added higher powers to the polynomial basis functions of particular rectangular elements. Krahula and Polhemus (1968) used the same technique, but with trigonometric functions as well as higher powers added to the set of polynomial basis functions. The work of Cavendish, Price and Varga (1969, presented at the Symposium on Numerical Simulation of Reservoir Performance of the Society of Petroleum Engineers of AIME, April 22-23, 1968) is very interesting in that they dealt with the same problem considered here. They presented a general discussion of the Galerkin method and included the problem of calculating accurate pressure distributions and pressure gradients around wells. The technique is essentially the same as that of Krahula and Polhemus: trigonometric functions are added to the

existing set of basis functions of a rectangular element containing a well. These trigonometric functions are then treated like ordinary basis functions with their coefficients determined by the regular finite element method.

An extension of the third approach to non-rectangular elements, as applied in the structural engineering field, has been given by Morley (1970) and Rao, Raju and Murty (1971). Morley dealt with methods for incorporating special solutions into the finite element analysis of the problem of the bending of a square plate with a square hole in its middle. These special solutions are the biharmonic eigenfunctions of the problem; the solutions describe the exact analytical structure in the vicinity of discontinuities, and in particular the eigenfunctions describe the singularities in the moments at the corners of the hole. In one respect Morely's method differs from the others mentioned: the eigenfunctions are those of the entire domain rather than those of a particular sub-region. Rao, et al., divide the domain into large primary elements containing "stress concentrations" and secondary elements which are regular finite elements. The solution within a primary element is composed of functions, not necessarily eigenfunctions, satisfying the differential equation and certain boundary conditions on the sub-region. Again, the coefficients of these functions are determined from the regular finite element method.

For all of the examples of increased local solution accuracy mentioned thus far each region of desired solution improvement requires an addition of unknown coefficients to the vector $\{h_j\}$ [see eq. (4)]. A problem arises when there are a large number of such regions or a large number of added functions. The size of the "stiffness" matrix, as well as its bandwidth, is greatly increased.

In a quite recent paper Hayes, Kendall and Wheeler (1977) treat the problem of steady-state simulation of well fields and use a technique

which is similar to that presented herein. Rather than increasing the dimension of the FE solution space they changed the form of the approximation to

$$p(x, y) = \sum_j p_j \varphi_j(x, y) + w(x, y)$$

where $p(x, y)$ is the unknown function being approximated, the sum is the usual FE basis function expansion and $w(x, y)$ is a special function of the form

$$w(x, y) = w(r) = \frac{Q}{2\pi T} \ln\left(\frac{r}{R}\right)\left(1 - \frac{r}{R}\right)^2, \quad r \leq R$$

$$= 0, \quad r > R$$

At the well ($r=0$) this function exactly reproduces the source/sink singularity for a non-leaky aquifer. Also, $w(r)$ and its gradient vanish at $r = R$. R is chosen so that the support of w (the region over which w has a nonzero value) is confined to a small number of elements, usually one. In their formulation w becomes part of the forcing function and is integrated over the domain. In this fashion the singularity is locally removed from the problem (although the delta function is still present in the forcing function). The stiffness matrix remains unchanged but the right hand side vector has areal integrals involving products of the gradients of w and the basis functions φ_i.

Next a new technique is presented which is conceptually simpler and computationally more efficient than the methods just discussed.

D. A Technique for Singularity Removal

One approach (not used here) to simulation of a well field problem is to straightforwardly solve the matrix equation (9) for the coefficients h_j. The well discharge $Q_k \delta(x_k, y_k)$ is assigned by having the point

(x_k, y_k) coincide with a node point (corner). The solution obtained in this fashion is perfectly adequate in the far-field region away from the well but the accuracy decreases as the immediate vicinity of the well is approached.

The method presented below is an extension of the following very simple technique. Instead of assigning the well discharge to a particular node we place the well within an element and distribute the discharge among the nodes of that element. If one determines the distribution of discharge by integrating $Q\varphi_i$ over the element one finds that the allocation to the ith node is $Q_k \varphi_i(x_k, y_k)$ where (x_k, y_k) is the location of the well within the element [remember that $Q = Q_k \delta(x-x_k, y-y_k)$].

The technique suggested herein is to approximate the true solution $h(x, y)$ by the combination of what amounts to a Green's function G for a well of strength Q_k within an element plus a finite element solution $\hat{H}$, viz.

$$h \simeq \tilde{h} = G + \sum_{j=1}^{N_n} h_j \varphi_j = G + \hat{H} \tag{19}$$

This concept is shown schematically in Figure 4. We find that the singular part of h is rperesented exactly by G and $\hat{H}$ becomes regular, and hence determinable by the finite-element method, within elements containing wells. The distribution of discharge to nodes of the element is determined by evaluating a boundary integral obtained by applying Green's theorem to the function G.

The boundary value problem describing the Green's function corresponding to a point source of strength Q_k within an element Ω^e with boundary Γ^e is

$$\begin{aligned} L(G) &= -Q_k \delta(x-x_k, y-y_k) \quad \text{in } \Omega^e \\ G &= 0 \quad \text{on } \Gamma^e \end{aligned} \tag{20}$$

where L is defined by equation (2). The finite element solution $\hat{H}$ is continuous over the domain Ω, and addition of G does not destroy this continuity since G = 0 on the boundary of the elements for which it is defined.

Incorporation of the Green's function into the finite element statement of the problem given by equation (9) is easily accomplished. First the domain of integration, Ω, is divided into a number of subdomains (finite elements) Ω^e, e = 1, ... N_e. We want to embed G in a particular subdomain ('singular' element). Substitute equation (19) into (8) [equation (8) is written for an arbitrary element Ω^e; the interelement boundary integrals derived through application of Green's theorem cancel due to interelement continuity] and expand using the linearity of $E(\varphi_i, h)$ to obtain

$$\iint_{\Omega^e} E(\varphi_i, \hat{H}) + E(\varphi_i, G)d\Omega^e = \iint_{\Omega^e} \left\{ Q + \frac{K}{b} h_a \right\} \varphi_i d\Omega^e - \int_{\Gamma} q_n \varphi_i d\Gamma \qquad (21)$$

Next for elements containing wells, multiply (20) by φ_i, integrate over the element Ω^e, and apply Green's theorem to the second-order terms to obtain the identity

$$\iint_{\Omega^e} E(\varphi_i, G)d\Omega^e = \iint_{\Omega^e} \varphi_i Q_k \delta(x-x_k, y-y_k)d\Omega^e + \int_{\Gamma^e} \varphi_i T_{\alpha\beta} \frac{\partial G}{\partial x_\beta} \ell_\alpha d\Gamma^e \qquad (22)$$

In this last equation it is important to note the distinction between the element domain Ω^e and boundary Γ^e, and the entire domain and boundary Ω and Γ. The final result is obtained by subtracting equation (22) from equation (21):

$$\sum_e \iint_{\Omega^e} E(\varphi_i, \hat{H})d\Omega = \sum_e \iint_{\Omega^e} \frac{K}{b} h_a \varphi_i d\Omega - \sum_k \int_{\Gamma_k} \varphi_i T_{\alpha\beta} \frac{\partial G_k}{\partial x_\beta} \ell_\alpha d\Gamma \qquad (23)$$

where $\sum_e$ is over all elements and $\sum_k$ is only over the boundaries of those elements containing wells. In equation (23) the entire domain boundary integral, resulting from specifying flux (Neumann) boundary conditions, has been left out; in problems of aquifer analysis one usually works with either specified head (Dirichlet) boundary conditions or no flow boundaries, in which case $q_n = 0$ and the boundary integral vanishes anyway.

E. Evaluation of the Interelement Boundary Integral

Comparison of equations (23) and (9) shows that the only remaining trace of the well within the finite element statement of the problem is the boundary integral

$$-\int_{\Gamma^e} \varphi_i T_{\alpha\beta} \frac{\partial G}{\partial x_\beta} \ell_\alpha \, d\Gamma^e = \int_{\Gamma^e} q_n \varphi_i \, d\Gamma^e \tag{24}$$

The proper technique for evaluating this integral is the main focus of this subsection. While evaluation of this integral appears straightforward, a review of the literature shows that there are certain subtleties to be overcome. For instance, we shall find that the result presented by Pinder and Gray (1977, pg. 124) is only true for elements with straight sides. The fundamental point to keep in mind when addressing such integrals is that the boundary Γ^e and its behavior within the integral are completely specified once the location of the node points are chosen.

Before the procedure for evaluating the integral in equation (24) is discussed we mention a technique, due to Bear, for investigating homogeneous anisotropic problems in terms of their equivalent isotropic counterparts (the field within the singular element must be homogeneous if we are to find the analytic function G). Using Bear's "modified inspectional analysis" (Bear, 1972, pg. 676) one finds the transformation of

coordinates and parameters which carries an anisotropic problem into an isotropic problem. This transformation is (for the x and y principal axes) (Bear, 1972, pg. 297)

$$X_i = X_a\left(\frac{T_{xa}}{T_{ya}}\right)^{1/4}$$

$$Y_i = Y_a\left(\frac{T_{ya}}{T_{xa}}\right)^{1/4} \qquad (25)$$

$$T_i = \left(T_{xa} T_{ya}\right)^{1/2}$$

$$Q_i = Q_a, \quad h_i = h_a, \quad \left(\frac{K}{b}\right)_i = \left(\frac{K}{b}\right)_a$$

where the subscript a refers to the anisotropic statement of the problem and the subscript i refers to the equivalent isotropic statement of the problem. In equation (25) Q is the total flow crossing any line within the two-dimensional surface of the aquifer. The transformation in (25) carries the equation

$$T_{xa}\frac{\partial^2 h_a}{\partial x_a^2} + T_{ya}\frac{\partial^2 h_a}{\partial y_a^2} - \left(\frac{K}{b}\right)_a h_a = 0$$

into

$$T_i\left(\frac{\partial^2 h_i}{\partial x_i^2} + \frac{\partial^2 h_i}{\partial y_i^2}\right) - \left(\frac{K}{b}\right)_i h_i = 0$$

Thus if we can find a solution for the equivalent isotropic problem we can use the inverse transformation to find the solution for the anisotropic problem (see Appendix II). The function G found by solving

$$T\left(\frac{\partial^2 G}{\partial x^2} + \frac{\partial^2 G}{\partial y^2}\right) - \frac{K}{b} G = -Q_k \delta(x-x_k, y-y_k) \text{ in } \Omega^e$$

$$G = 0 \text{ on } \Gamma^e \tag{26}$$

will suffice for both the isotropic and anisotropic problems, where the principal axes of the latter are coincident with the x and y axes.

Now, the value of the integral in equation (24) depends upon the type of basis functions used, the shape of the singular elements containing wells, and the form of the function G. Since the distribution of head around a well in a two-dimensional model of an isotropic aquifer is a radial function of the distance from the well, a natural shape for singular elements is a circle (i.e., the finite element approximation of a circle) with a well located at the center. For a circular element with a well at its center the differential equation defining the Green's function, equation (26), becomes

$$T\left(\frac{\partial^2 G}{\partial r^2} + \frac{1}{r}\frac{\partial G}{\partial r}\right) - \frac{K}{b} G = -Q_k \delta(x, y) \text{ in } \Omega^e$$

$$G = 0 \text{ on } \Gamma^e$$

Because both representations serve to introduce a discharge Q_k into the flow domain, the delta function description of the well may be replaced by the following condition at the well:

$$\lim_{r \to 0} \left(-T \frac{\partial G}{\partial r}\right) = \frac{Q_k}{2\pi r}$$

Thus the boundary value problem defining G becomes

$$\frac{\partial^2 G}{\partial r^2} + \frac{1}{r}\frac{\partial G}{\partial r} - \frac{K}{Tb} G = 0 \quad \text{in} \quad \Omega^e$$

$$\lim_{r \to 0} r \frac{\partial G}{\partial r} = -\frac{Q_k}{2\pi T} \tag{27}$$

$$G = 0 \quad \text{on} \quad \Gamma^e$$

The solution to equation (27) is

$$G = \frac{Q_k}{2\pi T}\left\{ K_o\left(\frac{r}{B}\right) - \frac{K_o\left(\frac{R}{B}\right)}{I_o\left(\frac{R}{B}\right)} I_o\left(\frac{r}{B}\right)\right\} \tag{28}$$

where I_o and K_o are the modified Bessel functions of the first and second kind of order zero, R is the radius of the singular element, and B is the leakage factor defined by $B = \sqrt{\frac{Tb}{K}}$. In the case of a non-leaky aquifer $B \to \infty$ and (28) becomes

$$G = \frac{Q_k}{2\pi T} \ell n\left(\frac{R}{r}\right) \tag{29}$$

The specific discharge, q_n, across the singular element boundary Γ^e is given by

$$q_n = -T \left.\frac{\partial G}{\partial r}\right|_{r=R} = \frac{Q_k}{2\pi B}\left\{ K_1\left(\frac{R}{B}\right) + \frac{K_o\left(\frac{R}{B}\right)}{I_o\left(\frac{R}{B}\right)} I_1\left(\frac{R}{B}\right)\right\} \underline{\text{leaky}}$$

$$q_n = \frac{Q_k}{2\pi R} \quad \underline{\text{nonleaky}} \tag{30}$$

where I_1 and K_1 are the modified Bessel functions of the first and second kind of order one. Since for a singular element R is a constant,

q_m is equal to a constant and can be taken outside of the integrand of equation (24). Thus we now want to evaluate

$$q_m \int_{\Gamma^e} \varphi_i \, d\Gamma^e \tag{31}$$

In integrating (31) special attention must be paid to the boundary specification. In light of the constraints against degenerate elements a possible problem arises: the interior corner angle between two sides of the isoparametric element might violate the condition that the angle be less than 180 degrees. The discussion which follows presents the case of a circular element (isotropic problem); the case of the elliptic element (anisotropic problem) is presented in Appendix II.

The isoparametric circle has its node points on the true circle and its boundaries are located in accordance with equation (15). Consider an isoparametric circle with the global coordinate system origin located at the circle's center and the x-axis going through node 6 of Figure 3. Nodes 2 and 3 lie along the plus and minus 45 degree rays. Nodal coordinates are as follows:

$$(x_2, y_2) \rightarrow \left(\frac{R}{\sqrt{2}}, -\frac{R}{\sqrt{2}} \right)$$

$$(x_3, y_3) \rightarrow \left(\frac{R}{\sqrt{2}}, \frac{R}{\sqrt{2}} \right)$$

$$(x_4, y_4) \rightarrow \left(-\frac{R}{\sqrt{2}}, \frac{R}{\sqrt{2}} \right)$$

$$(x_6, y_6) \rightarrow (R, 0)$$

$$(x_7, y_7) \rightarrow (0, R)$$

Then according to (18), $\theta_1 = 129.6$ degrees while $\theta_2 = 39.6$ degrees. Thus $\theta_2 + 180 = 140.4$ which is greater than θ_1 and the constraints are satisfied. Figure 5 shows the true circle and its FE approximation.

Actually, because of the symmetrical shape of the isoparametric circle we can go further in discussing its properties. Consider the same orientation of axes mentioned above. If we use equation (11) for the global coordinates, substitute the node points, and use the basis functions, we find after grouping equal powers

$$x = R\xi\left[1 - \left(1 - \frac{1}{2}\right)\eta^2\right]$$

$$y = R\eta\left[1 - \left(1 - \frac{1}{2}\right)\xi^2\right]$$

and

$$|J| = R^2\left\{1 - \left(1 - \frac{1}{\sqrt{2}}\right)\xi^2 - \left(1 - \frac{1}{\sqrt{2}}\right)\eta^2 - 3\left(1 - \frac{1}{\sqrt{2}}\right)^2\xi^2\eta^2\right\}$$

where $|J|$ is the Jacobian determinant of the coordinate transformation. (Note that $R^2 \geq |J| \geq \frac{8\sqrt{2} - 11}{2} R^2 > 0.$) Finally, we mention that Henshell (1976) has discussed the magnitude of the distance between corresponding boundaries of a true circle and its isoparametric model.

We have now reached the point where we can directly evaluate the integral of equation (31), i.e.,

$$I_i = q_n \int_{\Gamma^e} \varphi_i d\Gamma^e$$

We carry out the development for a true circle with the finite element approximation being applied only at the final stage. To start, the following identity for general curves is used, viz.,

$$d\Gamma = \sqrt{1 + \left(\frac{dx}{dy}\right)^2}\, dy$$

A true circle of radius R is specified by $x^2 + y^2 = R^2$ so

$$\left(\frac{dx}{dy}\right)^2 = \frac{y^2}{R^2 - y^2}$$

and

$$\sqrt{1 + \left(\frac{dx}{dy}\right)^2} = \frac{R}{\sqrt{R^2 - y^2}}$$

Along $x^2 + y^2 = R^2$, q_n is indeed constant which justifies our having taken it outside of the integrand. The integral becomes

$$I_i = q_n R \int_{\Gamma^e} \frac{\varphi_i}{\sqrt{R^2 - y^2}}\, dy$$

Now, since q_n is constant along Γ^e, each side node of the boundary will receive the same contribution of the discharge, the same being true for each corner node, and the total discharge to all nodes is $2\pi R q_n$. To simplify matters we need only evaluate the integral for a particular side node (the basis function of a side node has non-zero value only along the side on which the node lies). Also, since the value of the integral must be invariant to changes in orientation, we may translate and rotate the element so that the side node lies along the positive x-axis of a coordinate system whose origin is at the element's center (the well). Finally, along the side for which the basis function has non-zero value one of the local variables, say ξ, is constant, so along that boundary

$$dy = \frac{\partial y}{\partial \xi} d\xi + \frac{\partial y}{\partial \eta} d\eta = \frac{dy}{d\eta} d\eta$$

From Figure 3 we are interested in node 6, whose basis function along the $\xi = 1$ face is $\varphi_6 = 1 - \eta^2$. Using the boundary representation of (15) the final form of the integral to be evaluated is

$$I_6 = q_n R \int_{-1}^{1} \frac{(1 - \eta^2)}{\sqrt{R^2 - y^2}} \frac{dy}{d\eta} d\eta$$

where

$$\frac{dy}{d\eta} = \frac{1}{2}(y_3 - y_2) + (y_3 + y_2 - 2y_6)\eta$$

$$y^2 = \left[y_6 + \frac{1}{2}(y_3 - y_2)\eta + \frac{1}{2}(y_3 + y_2 - 2y_6)\eta^2 \right]^2$$

But with the chosen orientation we know that

$$y_3 = \frac{R}{\sqrt{2}}, \quad y_2 = -\frac{R}{\sqrt{2}} \quad \text{and} \quad y_6 = 0, \text{ so}$$

$$\frac{dy}{d\eta} = \frac{R}{\sqrt{2}}$$

$$y^2 = \frac{1}{2} R^2 \eta^2$$

and

$$I_6 = q_n R \int_{-1}^{1} \frac{1 - \eta^2}{\sqrt{2 - \eta^2}} d\eta = q_n R$$

The corresponding result for a corner node is

$$\frac{2\pi q_n R - 4 \cdot q_n R}{4} = q_n R \left(\frac{\pi}{2} - 1 \right)$$

Thus,

$$\left.\begin{aligned} \Gamma_i \text{ (side node)} &= q_n R \\ \Gamma_i \text{ (corner node)} &= q_n R\left(\frac{\pi}{2}-1\right) \end{aligned}\right\} \qquad (32)$$

Equation (32) gives the primary results of interest. Also, since one part of the transformation between an anisotropic and equivalent isotropic problem stated that the total discharge crossing respective segments of the aquifer is the same, the results of (32) hold for the anisotropic "singular ellipse" as well as the isotropic "singular circle". This is shown in a longer, though more instructive fashion in Appendix II.

Application of the technique is straightforward and only the method for generating the forcing function must be modified in a standard FE computer code. If the element contains a well then the well discharge is allocated according to equation (32). Corner and side nodes have these values from the singular solution added to the forcing function vector [with q_n given by equation (30)].

F. Velocity Fields

Before turning to application of the method presented herein it is worthwhile to mention how the FE solution may be exploited. Direct utilization of the hydraulic head solution is possible because the solution is a continuous function throughout the domain. That the FE solution is in a form which is readily exploitable is one major advantage not shared by finite difference methods. This subsection is concerned with methods for obtaining velocity fields from the hydraulic head solution. Then we examine a method for generating families of streamlines and, finally, an integration scheme for determining time of travel along the streamlines.

1. Quadratic Velocity Field

The simplest means of obtaining a velocity field is to directly use Darcy's law:

$$q_\alpha = - T_{\alpha\beta} \frac{\partial \hat{h}}{\partial x_\beta} \quad ; \quad \alpha, \beta = x, y \tag{33}$$

Since $\hat{h}$ is a polynomial in the local (ξ, η)-coordinate system q_α is finite everywhere (assuming that the Jacobian of the local-global transformation does not vanish). In particular (see Courant and John, 1974, pg. 261),

$$\begin{aligned} q_x &= - T_{xx} \frac{\partial \hat{h}}{\partial x} - T_{xy} \frac{\partial \hat{h}}{\partial y} \\ &= - T_{xx} \left(\frac{\partial \hat{h}}{\partial \xi} \frac{\partial \xi}{\partial x} + \frac{\partial \hat{h}}{\partial \eta} \frac{\partial \eta}{\partial x} \right) - T_{xy} \left(\frac{\partial \hat{h}}{\partial \xi} \frac{\partial \xi}{\partial y} + \frac{\partial \hat{h}}{\partial \eta} \frac{\partial \eta}{\partial y} \right) \\ &= - \frac{T_{xx}}{|J|} \left(\frac{\partial \hat{h}}{\partial \xi} \frac{\partial y}{\partial \eta} - \frac{\partial \hat{h}}{\partial \eta} \frac{\partial y}{\partial \xi} \right) - \frac{T_{xy}}{|J|} \left(- \frac{\partial \hat{h}}{\partial \xi} \frac{\partial x}{\partial \eta} + \frac{\partial \hat{h}}{\partial \eta} \frac{\partial x}{\partial \xi} \right) \\ q_y &= - \frac{T_{yx}}{|J|} \left[\frac{\partial \hat{h}}{\partial \xi} \frac{\partial y}{\partial \eta} - \frac{\partial \hat{h}}{\partial \eta} \frac{\partial y}{\partial \xi} \right] - \frac{T_{yy}}{|J|} \left[- \frac{\partial \hat{h}}{\partial \xi} \frac{\partial x}{\partial \eta} + \frac{\partial \hat{h}}{\partial \eta} \frac{\partial x}{\partial \xi} \right] \end{aligned} \tag{34}$$

For the final forms in (34) we have explicit representations for x, y, $\hat{h}$, T_{xx}, $T_{xy} = T_{yx}$, T_{yy} and $|J|$ in (ξ, η) basis function expansions over each element and thus the representation may be used directly to calculate $q_{x\hat{}}$ and q_y at a specific (ξ, η) point. A convenient representation of the velocity over an element may be found by expanding the nodal velocities from (34) in a basis-function expansion. Thus, if (ξ_j, η_j) is the jth node point, the simplest representation is

$$q_\alpha(\xi, \eta) = \sum_{j=1}^{8} q_\alpha(\xi_j, \eta_j) \varphi_j(\xi, \eta) \quad ; \quad \alpha = x, y \tag{35}$$

Now, while q_α exists [either from (34) or (35)] and is finite throughout the domain it is discontinuous along inter-element boundaries. Indeed, our experience shows that in cases with a strong hydraulic head gradient the jump in q_α may be large compared with its magnitude. Two methods for improving on this straight-forward representation are discussed below.

One method for obtaining an improved velocity field representation is to average the nodal velocities for all elements contiguous with a given node. Then with $\bar{q}_{xj}$ and $\bar{q}_{yj}$ representing the averaged components of q_α at the jth node, the continuous velocity components are given by

$$\bar{q}_x = \sum_{j=1}^{N_m} \bar{q}_{xj}\varphi_j$$
$$\bar{q}_y = \sum_{j=1}^{N_m} \bar{q}_{yj}\varphi_j \qquad (36)$$

where φ_j are the usual basis functions. A problem arises with applying (36) when the Green's function has been embedded in the solution. We do not want the finite element velocity to be continuous across boundaries of elements containing wells because the velocity derived from the Green's function does not vanish on the element boundary. Wishing to take full advantage of the embedded solution, we found a method for alleviating this problem as follows: when determining the average nodal components for elements containing the wells we include the analytic (Green's function) velocity contribution. Thus if q_{Gxj} and q_{Gyj} are the analytic components at node j and if the number of elements contiguous with node j is s, the averages are given by

$$\bar{q}_{xj} = \frac{1}{s}\left[\left(\sum_{e=1}^{s} q_{xj}^{(e)}\right) + q_{Gxj}\right]$$

$$\bar{q}_{yj} = \frac{1}{s}\left[\left(\sum_{e=1}^{s} q_{yj}^{(e)}\right) + q_{Gyj}\right] \tag{37}$$

Using these components in (36) one obtains the desired velocity distribution everywhere except within elements containing wells. To find these components use

$$q_{wxj} = \bar{q}_{xj} - q_{Gxj}$$

$$(j = 1, 2, \ldots 8) \tag{38}$$

$$q_{wyj} = \bar{q}_{yj} - q_{Gyj}$$

Then within the source/sink elements the velocity is given by

$$q_x = \sum_{j=1}^{8} q_{wxj}\varphi_j + q_{Gx}$$

$$q_y = \sum_{j=1}^{8} q_{wyj}\varphi_j + q_{Gy} \tag{39}$$

The velocity field derived from the above equations is continuous everywhere except across element boundaries containing wells. Across these singular element boundaries the velocity is continuous at the node points but there is a jump elsewhere because the basis functions cannot exactly interpolate the x and y components of the Green's function velocity. The discontinuity in velocity is acceptably small.

2. Smoothed Linear Velocity Field

A second approach for obtaining an improved velocity distribution is to smooth the element velocity representation obtained from Darcy's law before averaging the contributions at a node to find the continuous velocity field. This second approach is known as stress averaging in the F. E. structures literature. See Hinton and Campbell (1974) for a discussion of its attributes. To develop the method consider the x-component of the velocity given in equation (34). To smooth this representation we find the least squares fit to (34) in terms of the linear basis function expansion

$$\tilde{q}_x = \sum_{j=1}^{4} \tilde{q}_{xj} \psi_j (\xi, \eta) \tag{40}$$

where ψ_j are the bilinear basis functions (see Table 2). The approximation error is given by $e(\xi, \eta) = q_x(\xi, \eta) - \tilde{q}_x(\xi, \eta)$ and the least squares fit is found by choosing the coefficients in (40) so that the square of the error takes on its least possible value, i.e., find the minimum of $E = \iint_{\Omega^e} e^2 d\Omega$. Accordingly one has the system of equations

$$\frac{\partial E}{\partial \tilde{q}_{xi}} = \frac{\partial}{\partial \tilde{q}_{xi}} \iint_{\Omega^e} e^2(\xi, \eta) d\Omega^e = 0 \quad ; \quad i = 1, 2, 3, 4$$

from which one obtains

$$\left[\iint_{\Omega^e} \psi_i \psi_j dxdy \right]_{4x4} \left\{ \tilde{q}_{xj} \right\}_{4x1} = \left\{ \iint_{\Omega^e} q_x \psi_i dxdy \right\}_{4x1}$$

or, upon transforming to (ξ, η)-coordinates

$$\left[\int_{-1}^{1}\int_{-1}^{1}\psi_i\psi_j|J|\,d\xi\,d\eta\right]\left\{\tilde{q}_{xj}\right\} = \left\{\int_{-1}^{1}\int_{-1}^{1}q_x\psi_i|J|\,d\xi\,d\eta\right\} \qquad (41)$$

For parallelogram shaped elements (including squares and rectangles) Hinton and Campbell (1974) mention that when 2×2 Gaussian quadrature is used to evaluate the integrals in (41) the resulting least squares fit is an interpolate through the four Gauss points. Indeed, for parallelogram shaped elements the Jacobian determinant is a constant and may be cancelled from the system (41). Then each of the coefficients in the matrix and forcing vector is at most a third order polynomial in ξ or η and is integrated exactly by the quadrature scheme. The problem of minimizing the error becomes one of minimizing

$$E = \sum_{k=1}^{4}\left[q_x(\xi_k,\eta_k) - \tilde{q}_x(\xi_k,\eta_k)\right]^2$$

where (ξ_k,η_k) are the Gauss points. The minimum value equals zero when the basis function expansion is an interpolate through the values of (34) at the Gauss points. For parallelogram elements Hinton and Campbell give the following solution to (41)

$$\begin{Bmatrix}\tilde{q}_{x1}\\ \tilde{q}_{x2}\\ \tilde{q}_{x3}\\ \tilde{q}_{x4}\end{Bmatrix} = \begin{bmatrix} 1+\frac{3}{2} & -\frac{1}{2} & 1-\frac{3}{2} & -\frac{1}{2}\\ -\frac{1}{2} & 1+\frac{3}{2} & -\frac{1}{2} & 1-\frac{3}{2}\\ 1-\frac{3}{2} & -\frac{1}{2} & 1+\frac{3}{2} & -\frac{1}{2}\\ -\frac{1}{2} & 1-\frac{3}{2} & -\frac{1}{2} & 1+\frac{3}{2}\end{bmatrix}\begin{Bmatrix}q_x^{I}\\ q_x^{II}\\ q_x^{III}\\ q_x^{IV}\end{Bmatrix} \qquad (42)$$

where q_x^i, $i = I, \ldots, IV$, are the ith Gauss point values of q_x obtained from (34). For the general case of isoparametric elements the matrix system (41) must be inverted (by some type of Gaussian elimination) to find the smoothed corner node values of $\tilde{q}_x$. Again, using 2x2 Gaussian quadrature to evaluate the integrals the interpolate of the Gauss point values is achieved. These smoothed nodal values are then averaged according to the scheme of the first method described above to find the continuous velocity field (which now has only corner nodes in its expansion).

G. Streamlines

From the derived velocity field it is an easy task to generate streamlines. The equation of a streamline is

$$\frac{dy}{dx} = \frac{v}{u} \tag{43}$$

where u and v are the x and y components of the velocity vectors, respectively. Using the transformations $x = \sum_j x_j \varphi_j$, etc. [see equation (10)], for x, y, u and v as well as

$$dy = \sum_j y_i \left(\frac{\partial \varphi_j}{\partial \xi} d\xi + \frac{\partial \varphi_j}{\partial \eta} d\eta \right)$$

$$dx = \sum_j x_j \left(\frac{\partial \varphi_j}{\partial \xi} d\xi + \frac{\partial \varphi_j}{\partial \eta} d\eta \right)$$

one finds that the equation for the streamlines may be transformed to local coordinates as

$$\frac{d\eta}{d\xi} = \frac{A}{B} \tag{44}$$

where

$$A = \left(\sum_j v_j \varphi_j\right)\left(\sum_j x_j \frac{\partial \varphi_j}{\partial \xi}\right) - \left(\sum_j u_j \varphi_j\right)\left(\sum_j y_j \frac{\partial \varphi_j}{\partial \xi}\right)$$

$$B = \left(\sum_j u_j \varphi_j\right)\left(\sum_j y_j \frac{\partial \varphi_j}{\partial \eta}\right) - \left(\sum_j v_j \varphi_j\right)\left(\sum_j x_j \frac{\partial \varphi_j}{\partial \eta}\right)$$

To find the streamlines all one need do is integrate equation (44) in the local coordinate system and transform to global coordinates. The improved Euler's method (which is a second order Runge-Kutta scheme) was chosen for carrying out the integration.

Consider taking a step of length D in local coordinates. Then approximately

$$D^2 \cong \Delta\xi^2 + \Delta\eta^2$$

With $\Delta\eta \cong \frac{A}{B}\Delta\xi$ [from (44)] this becomes

$$D^2 \cong \Delta\xi^2 \left(1 + \left(\frac{A}{B}\right)^2\right)$$

so

$$\Delta\xi = \frac{D}{\left(1 + \left(\frac{A}{B}\right)^2\right)^{1/2}} \tag{45}$$

and similarly

$$\Delta\eta = \frac{D}{\left(1 + \left(\frac{B}{A}\right)^2\right)^{1/2}} \tag{46}$$

Equations (45) and (46) give the step along the streamline in local coordinates. The directions of the step are given by

$$A > 0 \rightarrow \Delta\eta > 0$$

$$B > 0 \rightarrow \Delta\xi > 0 \qquad (47)$$

The algorithm for the second order Runge-Kutta scheme is as follows (see Carnahan, Luther and Wilkes, 1969, pg. 362).

1. start at point $(\xi, \eta)_0$, evaluate A_0 and B_0, and take the step according to (45), (46) and (47) to reach $(\xi, \eta)_1$.
2. if $(\xi, \eta)_1$ does not lie within the element move back along the step to the element boundary.
3. evaluate A_1 and B_1 and average as $A = \frac{1}{2}(A_0 + A_1)$, $B = \frac{1}{2}(B_0 + B_1)$.
4. take the step again from $(\xi, \eta)_0$ using A and B and being sure to remain within or on the element boundary.
5. repeat the step, etc., move on to the next element, and repeat again.

This scheme was used to generate the streamlines shown in the subsection on applications.

H. Times of Travel

The scheme used for generating the times of travel along streamlines is very simple also. Each time the final step is taken in constructing a streamline between two points we evaluate the magnitude of the velocity at both ends. Then, we use

$$t_1 = t_0 + \frac{D_{global}}{\frac{1}{2}(V_0 + V_1)} \qquad (48)$$

which approximates

$$t_1 = t_0 + \int_{t_0}^{t_1} \frac{ds_\alpha}{v_\alpha}$$

where ds_α is the increment in vector length along the streamline and D_{global} is the step used in the Runge-Kutta scheme transformed to global coordinates. To generate breakthrough curves one need note that the closer one gets to a well the more pronounced the effect of the singularity. At the well the flow is essentially radial. If streamlines are set off at equal intervals around the radius of the well, each interval carries the same discharge. Accordingly from the breakthrough times for each streamline at the extraction well, a linear extrapolation may be used to find the breakthrough concentrations.

I. Plotting Contours

A final topic before applications are mentioned is the method for generating contours. The method follows from equation (12). Assume the expansion

$$A(\xi,\eta) = \sum_j a_j \varphi_j(\xi,\eta)$$

is available (that is, the components a_j are known). Then to plot the contour $A = \Phi$ one needs to solve

$$\Phi - (c_1 + c_2\xi + \ldots + c_8\xi\eta^2) = 0$$

where the c_i are given in Table 1. Picking a value of ξ ($\xi = \overset{*}{\xi}$) one may solve the resulting quadratic equation for the roots, $\overset{*}{\eta}$. One has

$$\Phi - \{(c_1 + c_2\overset{*}{\xi} + c_5\overset{*2}{\xi}) + (c_3 + c_4\overset{*}{\xi} + c_7\overset{*2}{\xi})\eta$$

$$+ (c_6 + c_8\overset{*}{\xi})\eta^2 = 0$$

or

$$A(\overset{*}{\xi})\overset{*}{\eta}^2 + B(\overset{*}{\xi})\overset{*}{\eta} + [C(\overset{*}{\xi}) - \Phi] = 0$$

The roots are given by

$$\overset{*}{\eta} = \frac{-B \pm \sqrt{B^2 - 4A[C - \Phi]}}{2A}$$

If $\overset{*}{\eta}$ lies within the range $-1 \leq \overset{*}{\eta} \leq 1$ ($\overset{*}{\xi}$ is chosen to be within this range) then the point $(\overset{*}{\xi}, \overset{*}{\eta})$ is a point on the contour. This may be transformed by equation (10) to find the corresponding global point. One needs to search through a series of ξ points and then through a series of η points to specify the contours within an element [redacted] because the contour may run roughly parallel to one of the local coordinates.

V. APPLICATIONS

As mentioned previously, application of the technique presented herein is straightforward and only the method for generating the forcing function in a standard FE computer code must be modified. If the element contains a well then the well discharge is allocated according to equation (32). Corner and side nodes have these values from the singular solution added to the forcing function vector (with q_n given by equation (30)).

Also mentioned previously are a number of techniques for exploiting the hydraulic head solution to obtain further results. Since the hydraulic head is specified in a basis function expansion its derivatives exist everywhere and may be profitably used in further analysis. These results generated from the basis function expansion of the solution (contours and streamlines) are of great value when visualizing the finite element solution. They represent a particular advantage which the finite difference method does not possess: rather than having to interpolate between node points to find contours one may use the continuous FE solution. But, as is the case with any of the numerical methods which reduce a partial differential equation to an algebraic system, the solution generated will not possess all of the properties of the "true" solution. In the case of the generated contours of hydraulic head this shows up when one follows a contour between elements. While the contour is continuous, its tangent is not. If one required a solution with continuous tangents (which amounts to having continuous first derivatives of the solution), a system of basis functions possessing a higher order of continuity should be used (e.g., Hermitian elements, see Pinder and Gray, 1977). One can always improve on the solution obtained through application of numerical methods, but this will require increased computational expense.

A. The Thiem Problem

As a first example consider the simple Thiem problem of a well located in the middle of a circular island and pumping from a confined non-leaky aquifer under steady state conditions. This purely radial problem was used to determine whether or not the distribution of flow from the singular element containing the well is correct. If the distribution is correct then the head at all nodes on the singular element boundary would be the same. If the distribution is not correct then the heads for the corner and side nodes will differ. The solution (not included here) showed that the heads are the same.

B. Source and Sink in Infinite Aquifer: Isotropic Cases

A more interesting example concerns the combination of source and sink wells pumping an infinite aquifer. The analytic head solutions for both the leaky and non-leaky cases are known; viz.,

$$\left.\begin{aligned} h &= \frac{Q}{2\pi T}\left\{K_o\left(\frac{r_1}{B}\right) - K_o\left(\frac{r_2}{B}\right)\right\} \quad \text{leaky} \\ h &= \frac{Q}{2\pi T}\left\{\ln\left(\frac{r_2}{r_1}\right)\right\} \quad \text{non-leaky} \end{aligned}\right\} \tag{44}$$

As shown in Figure 6, r_1 is the distance from the injection well and r_2 is the distance from the extraction well. For the non-leaky case the contours of constant head form a family of circles (Apolonios circles; Bear, 1972). With $c \equiv \exp\left[\frac{4\pi Th}{Q}\right]$, the equation for this family is

$$x^2 + \left[y - \left(\frac{c+1}{c-1}\right)d\right]^2 = \left[\frac{2d\sqrt{c}}{c-1}\right]^2$$

where 2d is the distance separating the wells (Figure 6).

To obtain the finite element solutions over a finite domain the analytic heads from (49) were used as boundary conditions on the domain. Also, by symmetry, the perpendicular bisector of the line connecting the wells is a line with zero head (zero head at infinity is taken as the datum). Figure 7 shows the element mesh used and a comparison of contours of the finite element head solution with the analytic solution for the non-leaky problem. The distance between wells is 305 meters (1000 ft), the radius of the singular element containing the well is 30.5 meters (100 ft), and the rectangular domain shown is 1830 x 1070 meters (6000 x 3500 ft). In this domain (half the source-sink combination) 23 elements and 86 nodes were used. The transmissivity of the aquifer is 112 meters^2/day (9000 gpd/ft) and the pumping rate is 680 meters^3/day (125 gpm).

With these parameters the analytic solution for the head (in feet) is

$$h = \frac{10}{\pi} \ln\left(\frac{r_2}{r_1}\right)$$

As a measure of the error we have used

$$\text{error} = \frac{\hat{h} - h}{Q/2\pi T} = \frac{\pi}{10}\hat{h} - \ln\left(\frac{r_2}{r_1}\right)$$

The maximum node point error occurs at the two upper corner nodes of the singular element containing the well (in the Figure). The magnitude of the error is -0.063 which corresponds to a negative error in head of 0.1 centimeters. Within the singular element

$$\text{Error} = \frac{\hat{h} - h}{Q/2\pi T} = \frac{2\pi T}{Q}(\hat{H} + G - h)$$

$$= \frac{2\pi T}{Q}\hat{H} + \ln\frac{R}{r_2}$$

where we have used equations (19), (29) and (49). We note again that at the well the Green's function G and actual (analytic) solution h are equal. In our result R = 30.5 (radius of the circular element containing the well), r_2 = 305 and $\tilde{H}$ at the well is equal to half the sum of the side node heads of the element minus one-quarter the sum of the corner node heads ($\tilde{H}_{well}$ = 2.22 m). Thus, at the singular point the error is -0.011 which corresponds to minus 1.1 centimeters.

Figure 8 shows the profile of the analytic head solution along the centerline through the wells for the leaky aquifer counterpart of the previous example. Also included are the finite element node solutions and the solution at the element's center as determined from the basis function expansion. The hydraulic resistance, $\frac{b}{K}$, is 2500 days and the head in the adjacent aquifer is taken as zero. Again, comparison with the analytic solution is seem to be very good. The error within the singular element is given by

$$\text{Error} = \frac{2\pi T}{Q}\hat{H} + K_o\left(\frac{r_2}{B}\right) - K_o\left(\frac{R}{B}\right)$$

At the well we have an error of -0.076 which corresponds to -7.4 centimeters.

C. Source and Sink in Infinite Aquifer: Anisotropic Cases

Figure 9 shows contours for the leaky, anisotropic counterpart of the previous examples. In Figure 9-a the major principal axis of transmissivity coincides with the centerline through the injection-extraction well system. The x and y transmissivities are 55.9 and 223.6 meters^2 per day (in accordance with equation (25), $T_I = (55.9 \times 223.6)^{1/2} = 112$ m^2/day so comparison can be made with the previous examples. The leakage coefficient and discharge are the same as in the other source-sink cases. In Figure 9-b the axes are reversed with T_x = 223.6 and

T_y = 55.9 meters^2/day. A comparison of the two plots shows that the situation depicted in Figure 9-b would be preferable if one were interested in establishing a barrier (e.g., the salt-water barrier mentioned in the Introduction) to flow in the direction of the centerline through the wells. The mound of pressure covers a greater width perpendicular to the direction of flow so an increased spacing between wells could be used.

D. Velocity Fields, Streamlines and Times of Travel

If one's only interest was in determining the hydraulic head throughout the field the analysis could cease at this point. The technique used yields an excellent approximation to the analytic hydraulic head, particularly considering the coarseness of the FE mesh. But, obtaining an improved distribution of head around a well is not an end in itself. The primary goal is to apply the method to problems of contaminant transport where the distribution of velocity around a well is extremely important.

The velocity field is obtained by differentiating the head field. That the head solution is to be differentiated provides one reason for choosing quadratic, isoparametric quadrilateral elements. Linear elements yield a constant velocity over each element while our experience shows that mixed order elements lead to poor results when the solution is differentiated. The type of elements used in this work and the singular solution for elements containing wells combine to provide enough freedom to obtain an accurate solution near wells yet they do not have an excessive number of nodes in the far field region where the solution does not change rapidly.

The discussion now turns to the two methods for obtaining improved velocity distributions with corresponding streamlines and to generation of breakthrough curves. The case of an injection and extraction well in an infinite non-leaky aquifer is again considered. The analytic solution for the streamlines is (Bear, 1972, pg 321)

$$\frac{\psi}{m} = \tan^{-1}\left\{\frac{2xd}{x^2+y^2-d^2}\right\} \qquad (50)$$

where $m = \frac{Q}{2\pi\theta b}$ and 2d is the distance between wells (see Figure 6). Equation (50) may be change into the form

$$(x - d\cot\frac{\psi}{m})^2 + y^2 = d^2(1+\cot^2\frac{\psi}{m})$$

which shows that the streamlines form a family of circles with centers at $(d\cot\frac{\psi}{m}, 0)$ and radii $d(1+\cot^2\frac{\psi}{m})^{1/2} = d|\csc\frac{\psi}{m}|$. Analytic times of travel between points may be calculated either from the original work of Muskat (1934) or from a simpler formula developed by Zaghi (1977). For breakthrough times in an injection-extraction system this latter formula takes the particularly simple form

$$t^* = \frac{4\pi\theta b d^2}{Q}\left\{\frac{1-\frac{\psi}{m}\cot\frac{\psi}{m}}{\sin^2\frac{\psi}{m}}\right\} \qquad (51)$$

Direct integration along the centerline between wells gives the following for the time to initial breakthrough

$$t^*_{min} = \frac{4\pi\theta b d^2}{3Q}$$

Using equations (50) and (51) one can compare the FE solutions with their analytic counterparts.

The same parameters were used in the velocity sample problem as in the hydraulic head problem: $Q = 680\ m^3/day$ (125 gpm), $\theta b = 0.91$ m (3 feet), $d = 152.4$ m (500 feet) and $T = 112\ m^2/day$ (9000 gpd/ft). The chosen mesh consists of 13 x 9 33.9 meter square elements covering

an area 440 x 305 m^2 (396 nodes and 117 elements). The side nodes of the middle element were shifted so as to form the circular element containing the well (radius = 24 m). Again, the mesh covers half the injection-extraction well combination, the other half being identical by symmetry.

Figures 10 and 11 compare the numerically generated streamlines (dashed line) from the smoothed linear and quadratic velocity fields with the analytic streamlines (solid line) for the first quadrant of Figure 6. Note that the agreement is excellent. The FE streamlines were found by starting at a point on the analytic streamline near the well and integrating the equation of the streamline using the second-order Runge-Kutta method described earlier. The local error is defined by $E(x, y) = \frac{1}{m}\{\psi(x, y) - \psi(x_o, y_o)\}$ and thus is equal to zero at the injection well [actually at the initial point for the streamline near the well, (x_o, y_o)] . $\psi(x, y)/m$ is given by . equation (50). Examination of computed values of E, or more simply examination of Figure 11, shows that the error for the quadratic field streamlines alternates in sign for the various streamlines. This type of behavior is well known in the structural FE literature where the FE stresses are known to oscillate about their analytic values (see Hinton and Campbell, 1974). Figure 10 shows that this oscillatory behavior of E is not as apparent for the stress averaged linear field streamlines. From these two figures it appears that the solution derived from the smoothed linear velocity field is preferable as far as the computed streamlines are concerned. But the values of $E(x, y)$ also show that the smoothed linear and quadratic velocity field methods give equivalent results within the circular element containing the well (which is to be expected since the velocity within the circular element is primarily determined by the analytic Green's function). Thus the improvement in the smoothed linear method is achieved outside of the circular element.

Figures 12 and 13 compare the corresponding analytic and FE breakthrough curves for the smoothed linear and quadratic velocity field

methods. Again, the agreement is excellent. The quadratic method predicts a more accurate time to initial breakthrough but the overall fit is better for the smoothed linear method.

VI. DISCUSSION

In this section a number of points related to the present work are discussed. The first topic for consideration is the chosen simulation model and the results generated therefrom. The second topic is dispersion phenomena. Generalization of the method and time dependent problems comprise the third topic.

A. Simulation Model and Results

The finite element model presented in Section IV is a very general model for steady-state analysis. But, consideration of practical problems suggests that the restriction to steady-state problems might seriously limit application of the model. For instance, there is an unsteady start-up period when pumping is initiated as well as variation in the injection and extraction rates over time. Also, it is anticipated that after the initial start-up there will be periods when the pumps will be shut off. These considerations suggest that the steady-state assumption is impractical. The basis for the steady-state assumption is the long time frame to be considered in the movement of contaminants. Transport between wells in the present case will take from months to years. Considered over these time frames the variations in well discharge will act as a small perturbation on the overall transport process. During periods of well shut-down the flow within the aquifer will, for practical purposes, stop. The hydraulic head distribution will rapidly return to its "natural" state and leakage between adjacent aquifers will be important only over very long time frames (the difference in hydraulic head between adjacent aquifers is usually much less under "natural" conditions than when water is being injected into or extracted from one of the aquifers). In simulation of short to moderate length no-flow periods only the kinetic components of chemical reaction models need be run. If chemical equilibrium models are used then these no-flow periods may be completely removed

from the input record for both the hydraulic and contaminant transport models. In sum, since the central focus of the present investigation is convection-dispersion-reaction of contaminants, the steady-state flow assumption seems adequate.

There are a number of severe restrictions implied by the use of a steady-state flow model. For the present work the most severe of these is that the density field must be uniform throughout the region of flow. If the density field is not uniform the dynamics will change as the field moves about (it takes more force to change the momentum of a heavier liquid so the velocity field must change). A second restriction is that one cannot consider the interaction between chemical and biological species and the porous media, e.g., clogging due to precipitation, ion exchange, or bacterial growth.

In the computer code used in the FE simulation of hydraulics the aquifer transmissivity is specified as a continuous parameter field over the domain. Our experience in simulation of nonhomogeneous fields suggests that this restriction to continuous parameter fields is more a requirement of conceptual aesthetics than a requirement for reasonable simulation results. For a field consisting of sand and gravel lenses embedded in a silt and clay matrix it is conceptually preferable to specify the transmissivity as a discontinuous field. This is because the transition between the sand and silt is abrupt. A simulation attempt of such a problem using a continuous field runs into severe problems with keeping the transmissivity non-negative (see Section IV.B). The other parameters (porosity and leakage coefficient) were specified as constants over each individual element. These parameters could also be specified as a continuous field, but then the order of the Gaussian quadrature scheme used to evaluate the integrals within the stiffness matrix would have to be increased. It was felt that the added expense was not justified.

When evaluating the usefulness of the numerical model presented herein one must compare it not only with analytic solutions but also with FE solutions obtained from placing wells at node points. For the far field (away from the well) the two FE methods produce equivalent results. This is because of the local character of the finite element solution (emphasized by Oden (1972); the type of solution, or constraints on the solution, in a particular area are not felt in regions far removed from that area). It is only as the well is approached that the distinctive features of the type of approximation used for the well show up. To compare the two FE techniques the problem used in Section V. D for examining the generated streamlines was simulated with the well placed at a corner node. The region 427 by 305 meters (1400 by 1000 feet) was modeled using 560 15.2 meter (50 feet) square elements and 1777 nodes. The hydraulic head at the well was found to be 5.63 meters (18.5 feet) rather than the analytic infinite head. At the adjacent side nodes 7.6 meters from the well the simulated head was 17 cm greater than the analytic head and the error slowly decreased with increasing distance from the well. Except very near the well the simulated results were acceptable but the solution obtained through use of the model of Section IV was superior throughout the domain.

A moments consideration makes it apparent that the velocity obtained by differentiating the head solution near the node-placed well (equation 34) will not be very good but it is not clear how one should go about assigning a velocity at the well itself. (A velocity component at the well is required if we wish to simulate the transport of an injected contaminant). If the field is not averaged in some way then it is impossible to send off streamlines in the direction of the element boundaries; since the magnitude of the x and y velocity components are approximately equal the only direction a streamline can take at the well is along the bisector of the element. Also, the jumps in velocity magnitude and

direction are very large when crossing element boundaries. If the velocity field is averaged using either of the methods suggested in Section IV. F then the velocity field becomes continuous but there is still considerable error in magnitude near the well. At the well itself the averaged velocity is nearly zero! Thus, one can see that there are some very real problems with placing the well at a node point. For contaminant transport modeling these problems dictate that some type of improved approximation technique be used.

Concerning the hydraulic head solution generated from the technique of Section IV. D, there is very little to be added to that mentioned in Section V. The generated head is very close to its analytic value throughout the domain. Completely satisfactory results can be obtained using a very coarse mesh (see Figure 7).

The object of most interest is the velocity field obtained from the hydraulic head solution. This velocity field is used directly in the contaminant transport model. Based on the results presented herein it is not possible to conclude which of the two improved velocity field methods presented in Section IV. F is preferable. Conceptually the smoothed linear field is preferable. There are three reasons for this. First, while the node points are the best sampling points for the primary variable (hydraulic head), they are the worst sampling points for the derivatives of the primary variable (velocity). Hinton and Campbell (1974) suggest that this might be related to the fact that interpolation functions tend to behave badly near the extremities of the interpolation region. Sampling at internal points should therefore give better results. (See Strang and Fix, 1973, pg. 168, for a note on why the node points are the best points for sampling the primary variables.) The second reason for preferring the smoothed linear velocity method is that the process of smoothing serves to filter out unwanted modes of deformation or flow due to the incomplete higher degree terms of the quadratic polynomial

velocity field. Third, it is contrary to one's "analytic" expectations to represent the hydraulic head and velocity field by the same series of functions when the latter is derived from the former through differentiation. If we did not have to consider the transformation between local and global representations of a function, it follows that differentiation of a quadratic representation would yield a linear representation. But, as the examples of Section V. D show, none of the above reasons can be compelling. Apparently, averaging the contributions to the velocity at a node from surrounding elements serves to do the same type of smoothing as the least squares fit of the linear velocity field to the quadratic one. It is left to future work to determine which of the velocity field generation schemes is the best.

B. Dispersion

In modeling the transport of contaminants in a porous media the velocity field is used in two distinguishable ways: convection of contaminants and mechanical dispersion. Since mechanical dispersion of contaminants is so intimately connected with the velocity field a few qualitative comments on the role of the velocity field are called for. Mechanical dispersion is the name given to the mixing and spreading of a contaminant or tracer as it is convected through the porous media. The two basic elements which contribute to this type of mixing are the flow and the presence of the pore system through which the flow takes place (Bear, 1972). The basic equation which describes the transport of an ideal tracer (i.e., one of uniform density which will not enter into chemical reactions) is

$$\frac{\partial c}{\partial t} = \frac{\partial}{\partial x_\alpha}\left(D'_{\alpha\beta} \frac{\partial c}{\partial x_\beta}\right) - \frac{\partial}{\partial x_\alpha}(v_\alpha c)$$

where $D'_{\alpha\beta}$ is the coefficient of hydrodynamic dispersion, a second

order symmetric tensor. $D'_{\alpha\beta}$ is the sum of the coefficient of mechanical dispersion ($D_{\alpha\beta}$) and the coefficient of molecular diffusion in the porous media. Unless the field velocity is very small, mixing due to molecular diffusion may usually be ignored and $D'_{\alpha\beta} \cong D_{\alpha\beta}$.

There have been many theoretical derivations expressing the coefficient of mechanical dispersion in terms of fundamental properties of the porous media and characteristics of the flow. A number of these models are reviewed by Bear (1972). The major point of interest here is that all expressions for $D_{\alpha\beta}$ require the velocity vector $v_\alpha = \frac{q_\alpha}{\theta}$, where q_α is the Darcy velocity and θ is the porosity (v_α is the actual velocity at which a parcel of water moves through the porous media). The most widely used representation is that of Scheidegger (1961):

$$D_{\alpha\beta} = a_{II} V \delta_{\alpha\beta} + (a_I - a_{II}) \frac{v_\alpha - v_\beta}{V}$$

This expression is valid for isotropic dispersion where a_I and a_{II} are the media's longitudinal and transverse dispersivities and V is the magnitude of the velocity vector. The longitudinal and transverse dispersivities are properties of the media only, being independent of the flow. Scheidegger's model suggests that the coefficient of dispersion is proportional to the first power of the velocity.

As discussed by Cherry, et al. (1975), determination of the magnitude of the longitudinal and transverse coefficients of dispersion (dispersivity) is very difficult and requires a knowledge of the velocity field. They group the methods for determining the velocity into three classes: 1) artificial tracers, 2) environmental isotopes and 3) application of Darcy's law. They consider the first method to be most accurate.

Problems associated with determination of coefficients of dispersivity are most readily apparent when one compares the magnitudes of coefficients determined in the laboratory and the field. Cherry, et al., quote laboratory values (for uniform materials) on the order of 10^{-2} to 1 centimeter for the longitudinal coefficient a_I in the model

$$D_L = a_I V$$

where D_L is the longitudinal coefficient of mechanical dispersion. Field coefficients are determined by first simulating the hydraulic head distribution and adjusting the coefficient of transmissivity until the simulated field matches the observed head distribution. Then contaminant concentrations are simulated with the dispersion coefficients being adjusted until a match is obtained with observed contaminant values. Coefficients obtained in this fashion are on the order of 10^3 to 10^4 centimeters. Thus we find a difference between laboratory and field values of about a factor of 10^5.

An obvious reason for the large discrepancy between laboratory and field dispersivities is the scale on which flow is occurring. In numerical modeling there are additional problems associated with the scale of resolution of the numerical technique. These problems of scale should be examined in some detail in future work.

C. Generalization and Time Dependent Problems

The technique of embedding an analytic singular solution into the finite element method presented herein is an example of a general rigorous approach to combining analytic and numerical methods. The analytic function is superposed on the approximating solution and does not enter the problem with an unknown multiplying coefficient (i.e., in augmentation of the solution space with extra functions; see Section IV. C).

One can easily envision the use of other analytic solutions, e.g., flows around bodies, certain types of boundary conditions, other types of singularities. The method could be used in other fields, e.g., structural mechanics, heat transfer or electrostatics. The key lies with the problem which remains to be solved after embedding the analytic solution. The situation given in Section IV. D is probably the best conceivable. If, for the leaky aquifer case, we had restricted ourselves to embedding only the Thiem equation (G*), then the forcing function of the resulting system of equations would also contain the term $-\iint_{\Omega} \frac{K}{b} G^* \varphi_i \, d\Omega$ (i.e., the leakage induced by the Thiem equation). Use of the appropriate Green's function of the operator has even removed this term.

From the present point of view the most interesting generalization is that to the leaky-aquifer, time-dependent problem. In analogy with equation (27), the boundary value problem defining the Green's function is

$$\frac{S}{T}\frac{\partial G}{\partial t} = \frac{\partial^2 G}{\partial r^2} + \frac{1}{r}\frac{\partial G}{\partial r} - \frac{K}{Tb} G \quad \text{in } \Omega$$

$$\lim_{r \to 0} r \frac{\partial G}{\partial r} = -\frac{Q}{2\pi T}$$

$$G = 0 \quad \text{on } \Gamma^e$$

$$G = 0 \quad \text{at } t = 0 \quad \text{for all } \Omega$$

where S is the aquifer storage coefficient. Applying the Laplace transformation to this partial differential equation (see Street, 1973) and solving the resulting ordinary differential equation we find

$$\bar{G} = \frac{Q}{2\pi T p} \left\{ K_o(Nr) - \frac{K_o(NR)}{I_o(NR)} I_o(Nr) \right\}$$

where $N^2 = p\frac{S}{T} - \frac{K}{Tb}$ and $\bar{G}$ is the Laplace transformation of the Green's function G, i.e.,

$$\bar{G}(r,p) = \int_0^\infty G(r,t)e^{-tp}dt$$

The convolution of the inverse Laplace transformation of each of the terms of $\bar{G}$, which is the desired solution G, is a far too complicated function to use profitably as the embedded solution. As such we look for a second function $\Lambda(r,t)$ which will cancel the singularity at the well but not necessarily satisfy the other constraints on the problem (in particular the element boundary conditions). Such a function could be that of Hayes, Kendall and Wheeler (1977) but here we look for a function which may be embedded within the FE method in a more systematic fashion.

We consider two problems simultaneously. The first is that of a well (point source) in a nonleaky aquifer and the second is that of a well in a leaky aquifer. For the former the approximate solution is

$$\hat{h} = \hat{H} + \Lambda_1(r,t) - \Lambda_1^*(R,t)$$

where Λ_1 satisfies

$$\frac{S}{T}\frac{\partial \Lambda_1}{\partial t} = \frac{\partial^2 \Lambda_1}{\partial r^2} + \frac{1}{r}\frac{\partial \Lambda_1}{\partial r}$$

$$\lim_{r\to 0} r\frac{\partial \Lambda_1}{\partial r} = -\frac{Q}{2\pi T}$$

$$\Lambda_1 \to 0 \quad \text{as} \quad r \to \infty$$

$$\Lambda_1 = 0 \quad \text{at} \quad t = 0$$

and for the latter the approximate solution is

$$\hat{h} = \hat{H} + \Lambda_2(r,t) - \Lambda_2^*(R,t)$$

where Λ_2 satisfies

$$\frac{S}{T}\frac{\partial \Lambda_2}{\partial t} = \frac{\partial^2 \Lambda_2}{\partial r^2} + \frac{1}{r}\frac{\partial \Lambda_2}{\partial r} - \frac{K}{Tb}\Lambda_2$$

$$\lim_{r\to 0} r\frac{\partial \Lambda_2}{\partial r} = -\frac{Q}{2\pi T}$$

$$\Lambda_2 \to 0 \quad \text{as} \quad r \to \infty$$

$$\Lambda_2 = 0 \quad \text{at} \quad t = 0$$

The solution for the first equation has been given by Theis (1935) while that for the second is given by Hantush and Jacob (1955). These solutions are

$$\Lambda_1(r,t) = \frac{Q}{4\pi T}\int_{\frac{r^2 S}{4Tt}}^{\infty} \frac{1}{u} e^{-u} du$$

and

$$\Lambda_2(r,t) = \frac{Q}{4\pi T}\int_{\frac{r^2 S}{4Tt}}^{\infty} \frac{1}{u} \exp\left(-u - \frac{r^2 K}{4Tbu}\right) du$$

Now, using the same procedure as in Section IV. D the final FE problems to be solved are

$$\iint_{\Omega} S\varphi_i \frac{\partial \hat{H}}{\partial t} + E(\varphi_i, \hat{H})d\Omega = \iint_{\Omega} \left\{ S \frac{\partial \Lambda_1^*}{\partial t} + \frac{K}{b}(h_a - \Lambda_1 + \Lambda_1^*) \right\} \varphi_i d\Omega$$

$$- T \frac{\partial \Lambda_1}{\partial r} \int_{\Gamma^e} - \varphi_i d\Gamma^e - \int_{\Gamma} q_n \varphi_i d\Gamma$$

for the first case and for the second

$$\iint_{\Omega} S\varphi_i \frac{\partial \hat{H}}{\partial t} + E(\varphi_i, \hat{H})d\Omega = \iint_{\Omega} \left\{ S \frac{\partial \Lambda_2^*}{\partial t} + \frac{K}{b}(h_a + \Lambda_2^*) \right\} \varphi_i d\Omega$$

$$- T \frac{\partial \Lambda_2}{\partial r} \int_{\Gamma^e} \varphi_i d\Gamma^e - \int_{\Gamma} q_n \varphi_i d\Gamma$$

In the above note that Λ_1^* is the same function as Λ_1 except that it is evaluated at $r = R$, the radius of the circular element containing the well. At any particular time Λ_1^* is a constant over the singular element and thus $E(\varphi_i, \Lambda_1^*) \equiv \frac{K}{b} \varphi_i \Lambda_1^*$. Similar statements hold for Λ_2^*. Note also that the allocation of the well discharge to the nodes of the singular element is the same as for the problem presented in Section IV. E. Only the magnitude of the normal velocity changes (it is now a function of time). The only obvious distinction between these two results is the presence of the term $-\iint_{\Omega} \frac{K}{b} \Lambda_1 \varphi_i d\Omega$ in the forcing function of the former. The reason for its presence is that the boundary value problem defining the function $\Lambda_1(r, t)$ did not take into account leakage from the adjacent aquifer. Thus, while the representation of $\Lambda_1(r, t)$ is simpler than that of $\Lambda_2(r, t)$, the price is paid for the former by its presence in the forcing function. In each case the starred function serves to cancel the value of the singular solution on the boundary of the circular element so that the approximation $\hat{h}$ is continuous throughout the domain. A second distinction between the two FE problems is in the element boundary integrals

of the normal velocity. The third and last distinction is in the function used in the time correction for the unsteady boundary conditions on Γ^e, $\iint_\Omega S \frac{\Lambda_k^*}{\partial t} \omega_i d\Omega$, $k = 1, 2$. The FE problems can be solved using the usual methods for time dependent problems (i.e., finite difference the time step).

Generalizations to similar problems are easily carried out using the same procedure. A slightly different type of generalization is to change the geometric shape of the singular element containing the well. If a square is used for the nonleaky aquifer (the case where a circle gives the Thiem equation) the Green's function becomes a Fourier series expansion. Our experience shows that evaluation of the boundary integrals of the normal velocity for the first six or seven terms of the Fourier expansion is sufficient as far as the far field FE solution is concerned.

VII. CONCLUSIONS AND RECOMMENDATIONS FOR FUTURE WORK

Conclusions concerning the approximation technique presented herein and the finite element numerical model are given below. Recommendations for further modeling work are also given. Conclusions concerning the Santa Clara Valley Water District Project are given in Appendix I.

The conclusions drawn from the present work are as follows.

1. The approximation technique presented in Section IV.D is an example of a simple but rigorous systematic method for combining analytic and numerical methods. The method as described will handle the analysis of steady-state hydraulics in a confined, leaky aquifer for a nonhomogeneous porous media containing injection-extraction wells. The method is superior to others found in the literature.
2. The technique yields excellent results for both the primary variable (hydraulic head) and for the derivative of the primary variable (velocity). Here "excellent" is judged according to the error in the model simulation result when compared with a known analytic solution. Concerning the fourth of the stated objectives of the Stanford University research project (see Section III), the model presented is certainly more accurate than our knowledge of the required field parameters.
3. Useful constraints were formulated which guarantee uniqueness and invertibility of the transformation between the global and local representations of a function. Also, constraints were formulated which guarantee positive definiteness of appropriate model parameters. These latter constraints are particularly important when considering strongly nonhomogeneous fields.
4. The method presented for generating a family of streamlines and determining the time of travel along respective streamlines is very helpful when visualizing the finite element solution. The

accuracy of the streamline solution (measured by E in Section V.D) is very good, and as the breakthrough curve shows, the time of travel along a streamline is also very accurate.

5. The method presented for plotting contours is of great value when visualizing the hydraulic head solution or nonhomogeneous parameter fields.

The following topics are recommended for future research.

1. Further experiments to determine which of the velocity generation schemes is the best (quadratic velocity field or smoothed linear velocity field). Experimentation with other schemes would be worthwhile.
2. Investigation of methods for incorporating analytic solutions within the Hermitian family of finite elements. The Hermitian family is of special interest because it yields a continuous representation when differentiated; thus, the velocity field could be determined directly from the head solution without averaging. In order to apply the method a way must be found for relaxing the continuity constraints on derivatives across the boundary of the element containing the well.
3. Investigation of time dependent problems using the schemes presented in Section VI.C.
4. Use the model presented in Section IV to investigate the role of unknown coefficients in nonhomogeneous field simulations. A stochastic Monte Carlo scheme could be used to investigate the range and uncertainty in generated results. This would be of particular interest when compared with well test data.

REFERENCES

Ambroggi, P., Underground Reservoirs to Control the Water Cycle, Scientific American, 236(5), 21-27, 1977.

Atwater, B. F., Hedel, C. W. and E. J. Helley, Late Quaternary Depositional History, Holocene Sea-Level Changes, and Vertical Crustal Movement, Southern San Francisco Bay, California, Geological Survey Professional Paper 1014, 15 p., 1977.

Bear, J., On the Tensor Form of Dispersion in Porous Media, J. Geophys. Research, 66(4), 1185-1197, 1961.

Bear, J., Dynamics of Fluids in Porous Media, American Elsevier, New York, 1972.

Blissenbach, E., Geology of Alluvial Fans in Semiarid Regions, Geol. Soc. America Bull, 65, 175-190, 1954.

Bouwer, H., Groundwater Hydrology, McGraw-Hill, New York, 1978.

Carey, E. F., A Mesh-Refinement Scheme for Finite Element Computations, Computer Meth. Appl. Mech. and Engrg., 7, 93-105, 1976.

Carnahan, B., Luther, H. A. and J. O. Wilkes, Applied Numerical Methods, John Wiley and Sons, New York, 1969.

Cavendish, J. C., Price, H. S. and R. S. Varga, Galerkin Methods for the Numerical Solution of Boundary Value Problems, Soc. Petrol. Engrg. J., 246, 204-220, 1969.

Cherry, J. A., Gillham, R. W. and J. F. Pickens, Contaminant Hydrogeology, Part 1, Physical Processes, Geoscience Canada, 2(2), 76-84, 1975.

Courant, R. and F. John, Introduction to Calculus and Analysis, Vol. II, John Wiley-Interscience, New York, 1974.

de Jong, J., Longitudinal and Transverse Diffusion in Granular Deposits, Trans. Amer. Geophys. Union, 39(1), 67-74, 1958.

Dagan, G., Comment on 'A Stochastic-Conceptual Analysis of One-Dimensional Groundwater Flow in Nonuniform Homogeneous Media' by R. A. Freeze, Water Resour. Res., 12(3), 567, 1976.

Ergatoudis, B. M., Irons, B. M. and C. O. Zienkiewicz, Curved Isoparametric, "Quadralateral" Elements for Finite Element Analysis, Int. J. Solids Structures, 4, 31-42, 1968.

Freeze, R. A., A Stochastic-Conceptual Analysis of One-Dimensional Groundwater Flow in Nonuniform Homogeneous Media, Water Resour. Res., 11(5), 725-741, 1975.

Gartling, D. K. and E. B. Becker, Finite Element Analysis of Viscous Incompressible Fluid Flow, Pt. 1, Computer Meth. Appl. Mech. and Engrg., 8, 51-60, 1976.

Gelhar, L. W., Bakr, A. A., Gutjahr, A. L. and J. R. MacMillan, Comments on 'A Stochastic-Conceptual Analysis of One-Dimensional Groundwater Flow in Nonuniform Homogeneous Media' by R. Allan Freeze, Water Resour. Res., 13(2), 477-479, 1977.

Hantush, M. S. and C. E. Jacob, Non-Steady Radial Flow in an Infinite Leaky Aquifer, Trans. Amer. Geophys. Union, 36, 95-100, 1955.

Hayes, L. J., Kendall, R. P. and M. F. Wheeler, The Treatment of Sources and Sinks in Steady-State Reservoir Engineering Simulations, Advances in Computer Methods for Partial Differential Equations II, R. Vichnevetsky (Editor), I.M.A.C.S. (AICA), 1977.

Henshell, R. D., Differences Between Isoparametric Assumptions and True Circles, Int. J. Num. Meth. Engrg., 10(5), 1193-1196, 1976.

Henshell, R. D. and K. G. Shaw, Crack Tip Finite Elements are Unnecessary, Int. J. Num. Meth. Engrg., 9, 495-507, 1975.

Hinton, E. and J. S. Campbell, Local and Global Smoothing of Discontinuous Finite Element Functions Using a Least Squares Method, Int. J. Num. Meth. Engrg., 8, 461-480, 1974.

Holmes, A., Principles of Physical Geology, Ronald Press Co., New York, 1965.

Hooke, R. L., Processes on Arid-Region Alluvial Fans, J. Geol., 75, 438-460, 1967.

Howland, M. D., Hydrogeology of the Palo Alto Baylands, Palo Alto, California, with Emphasis on the Tidal Marches, Thesis for M.S. Degree, Department of Geology, Stanford University, August 1976.

Jenks, J. H. and P. L. Adamson, A Program for Water Reclamation and Groundwater Recharge, Predesign Report, Santa Clara Valley Water District, October 1974.

Krahula, J. L. and J. F. Polhemus, Use of Fourier Series in the Finite Element Method, A.I.A.A. Journal, 6(4), 726-728, 1968.

Morley, L.S.D., A Finite Element Application of the Modified Rayleigh-Ritz Method, Int. J. Num. Meth. Engrg., 2, 85-98, 1970.

Muskat, M., The Flow of Homogeneous Fluids Through Porous Media, McGraw-Hill, New York, 1937.

Oden, J. T., Finite Elements of Nonlinear Continua, McGraw-Hill, New York, 1972.

Oden, J. T. and J. N. Reddy, An Introduction to the Mathematical Theory of Finite Elements, Wiley-Interscience, New York, 1976.

Pian, T.H.H., Derivation of Element Stiffness Matrices, A.I.A.A. Journal, 2(3), 576-577, 1964(A).

Pian, T.H.H., Derivation of Element Stiffness Matrices by Assumed Stress Distributions, A.I.A.A. Journal, 2(7), 1333-1336, 1964(B).

Pinder, G. F., A Galerkin-Finite Element Simulation of Groundwater Contamination on Long Island, New York, Water Resour. Res., 9(6), 1657-1669, 1973.

Pinder, G. F. and E. O. Frind, Application of Galerkin's Procedure to Aquifer Analysis, Water Resour. Res., 8(1), 108-120, 1972.

Pinder, G. F., Frind, E. O. and S. S. Papadopulos, Functional Coefficients in the Analysis of Groundwater Flow, Water Resour. Res., 9(1), 222-226, 1973.

Pinder, G. F. and W. G. Gray, Finite Element Simulation in Surface and Subsurface Hydrology, Academic Press, New York, 1977.

Rao, A. K., Raju, I. S. and A. V. Krishna Murty, A Powerful Hybrid Method in Finite Element Analysis, Int. J. Num. Meth. Engrg., 3, 389-403, 1971.

Reineck, H. E. and I. B. Singh, Depositional Sedimentary Environments, Springer-Verlag, New York, 1975.

Roberts, P. V., et al., Groundwater Recharge by Injection of Reclaimed Water in Palo Alto, Technical Report No. 225, Department of Civil Engineering, Stanford University, February, 1978.

Scheidegger, A. E., General Theory of Dispersion in Porous Media, J. Geophys. Research, 64(10), 3273-3278, 1961.

Sokol, D., The Hydrogeology of the San Francisquito Creek Basin, San Mateo and Santa Clara Counties, California, Ph. D. Dissertation, Department of Geology, Stanford University, December, 1963.

State of California, Department of Water Resources, Evaluation of Groundwater Resources, South Bay, Appendix A: Geology, August 1967.

Strang, G. and G. F. Fix, An Analysis of the Finite Element Method, Prentice-Hall, Englewood Cliffs, N. J., 1973.

Street, R. L., Analysis and Solution of Partial Differential Equations, Brooks/Cole, Monterey, CA, 1973.

Theis, C. V., The Relation Between the Lowering of the Piezometric Surface and the Rate and Duration of Discharge of a Well Using Groundwater Storage, Trans. Amer. Geophys. Union, 16, 519-524, 1935.

Warren, J. E. and H. S. Price, Flow in Heterogeneous Porous Media, Soc. Petrol. Eng. J., 1, 153-169, 1961.

Zaghi, N., Effect of Injection-Production Doublets in Shielding Coastal Aquifers from Brine Intrusion, Ph. D. Dissertation, Department of Petroleum Engineering, Stanford University, May 1977.

APPENDIX I

Hydrogeology of the Palo Alto Baylands Area

In this appendix the relevant geologic history, stratigraphy and geomorphology of the near-surface (60 meters) deposits of the South Bay area are reviewed, the purpose being to provide an understanding of the complex environment chosen for the injection-extraction system. Both local and field groundwater modeling are discussed. The appendix serves to highlight the problems one runs into when investigating actual field sites. There is always a need for more field data and the type of numerical model used must remain open to change.

Four physiographic units are recognized within the basin containing the Palo Alto baylands (Sokol, 1963). These are the northeastern slope of the Santa Cruz mountains, the valley of the San Andreas Fault Zone, the foothill belt and the Santa Clara Valley. For a discussion of the hydrogeology of these units see Sokol (1963). The Santa Clara Valley is a result of a combination of downwarping and faulting. During the Quaternary[1] the valley has accumulated an aggregate thickness of 300 to 450 meters of continental sands, silts and clays interrupted by fairly thick sequences of marine clays (State of California, 1967). In the injection-extraction project we are interested in only the upper 60 meters of deposits. The recent geologic history of this section follows.

---

[1] According to Holmes (1965), the last two or three million years have been geologically classified as the Quaternary period. The Quaternary is further divided into the Pleistocene (Glacial) and Holocene (Recent) periods. The Pleistocene is marked by periods of rising and falling sea level, corresponding to the retreat and advance of the glaciers. Here we are interested in the Sangamon interglacial age (high stand of the seas), the Wisconsin glacial age and the post-Wisconsin or Recent age.

Recent Geologic History

Two principal features stand out in the history of Southern San Francisco Bay deposits: tectonic subsidence and the rise and fall of sea level during the Pleistocene (Glacial age). Atwater, Hedel and Helley (1977) have interpreted the recent geologic history through investigation of sediments and fossils collected for bridge foundation studies. Early estuarine deposits were from the Sangamon interglacial high stand of the sea (70,000 - 130,000 years ago). During the subsequent Wisconsin glacial age the sea level fell and part of the Sangamon estuarine deposits were eroded and covered by alluvial sands, silts and clays. The post-Wisconsin sea level rise has once again introduced estuarine deposits into the Bay area. During the recent rise, the sea level reached the Golden Gate approximately 10,000 to 11,000 years ago. The rising sea spread across the land area as rapidly as 30 meters per year. From 8000 to 6000 years ago the rate of sea level rise decreased and from 6000 years ago to the present has averaged 0.1 to 0.2 centimeters per year. The Bay reached the vicinity of the thalweg (the line marking the deepest points of a stream channel) of the stream draining the "Bay valley" across from Menlo Park 8000 years ago and the Palo Alto baylands 2000 to 3000 years ago. During this period tectonic subsidence was occurring, though at a much smaller rate. Figure 14 (after Atwater, et al.) shows a section of the Bay at Dumbarton bridge (3.2 kilometers northwest of the Palo Alto Baylands).

Stratigraphy

Howland (1976) has investigated the hydrogeology of the Palo Alto baylands. Fortunately, part of his area of study coincides with the site of the injection-extration project. Figure 15 shows his inferred correlations between sediments in the Dumbarton Strait and Palo Alto baylands.

The following sediment descriptions are taken from Howland (1976).

SEDIMENTS FROM 20 TO 60 METERS BELOW THE SURFACE

The sequence is dominated by firm gray silty clay which contains a few minor lenses of sand and gravel. At depths of about 45 to 60 meters the sediments are predominantly mixtures of sand and gravel. The latter deposits are highly variable in thickness. The deposits from 20 to 45 meters are interpreted to be of estuarine origin while those from 45 to 60 meters are alluvium.

SEDIMENTS FROM 20 METERS BELOW THE SURFACE TO THE BAY MUD

Howland described these sediments after investigating approximately 70 engineering borings and 30 well logs. The locations are shown in Figure 16 along with the location of the injection-extraction system. Figure 17 shows a fence diagram constructed by Howland. Two members are delineated on the fence diagram below the artificial fill and Bay mud. The first is a silty and sandy clay group. Minor lenses of gravel and sand of about 30 cm thickness occur throughout this member. The second member consists of loose to dense coarse-grained deposits consisting mainly of sand and gravel with some silt. Sorting is moderate to poor.

The two members are complexly interfingered and variable in areal extent and thickness. Two beds of the sand and gravel deposits can be traced for some distance in the central part of the area (along section G-C). The bed at 14 meters continues in section G-A, whereas the bed at 7.6 meters seems to lense out and become a sandy clay. Toward the southwest the beds seem to coarsen. If they are continuous in this direction they probably thicken and effectly merge. Toward the Bay the section becomes predominantly more fine grained (clayey) with considerable thinning of the coarser deposits.

NEAR-SURFACE DEPOSITS

Toward the Bay the surface is covered by artificial fill and Bay mud. The Bay mud was deposited by the post-Wisconsin rising sea (now).

Geomorphology

The deposits of immediate interest in the SCVWD project are of alluvial origin. To gain further insight to their nature it is necessary to discuss the geomorphology of alluvial fans and alluvial piedmont slopes.

An alluvial fan is a body of rather coarse-grained sediments built up by a mountain stream at the base of a mountain front where a steeper slope passes abruptly into a more gentle slope (Reineck and Singh, 1975). When several alluvial fans occur adjacent to each other they may grow and coalesceto form an alluvial piedmont slope (compound alluvial fan). Fans may be divided into three zones (Blissenbach, 1954): the fanhead (upper fan segment), the midfan and the base. It is the last zone which usually grades into the zone of coalescence with other fans. The characteristics of single alluvial fans are discussed by Blissenbach (1954) and Hooke (1967). Hooke noted that while deposition is localized, shifting of the locus of deposition results in relatively uniform deposits. Blissenbach mentioned the main conditions for formation of alluvial fans: areas of bold relief and arid to semiarid conditions. There must be profound erosion and transportation together with a strong tendency for deposition as the mountain streams reach areas of low gradient. Fans formed in humid environments are usually flatter than those of arid environments. Blissenbach (1954) gives a discussion of depositing agents on alluvial fans.

Streams which carry the sediment load change their course by lateral migration and by overflowing their banks, carving new channels

and abandoning the old ones (downstream). Consequently relatively uniform deposition is found throughout the fan or piedmont slope. The coarser channel deposits downstream on an abandoned channel are left to be covered by finer overbank deposits from flooding of neighboring channels. Thus, discontinuous sand and gravel lenses may be formed.

The material deposited far down the base and within the zone of coalescence is more like floodplain sediments than like sediments from the upper zones of the fan. These deposits are usefully placed with the classification of Reineck and Singh (1975) who mention three major groups: channel deposits, bank deposits and flood basin deposits. (In the case of rivers which migrate actively laterally, recognizable bank deposits may not be found.) Reineck and Singh (1975) present a detailed discussion of the three major groups (and their eight subgroups). The major point here is that the primary type of channel deposit is a point bar. Point bars are deposited along the inside bank of a curve in a stream. The flow traversing the inside bend loses its ability to carry the coarse bedload (the suspended load is not affected). As the stream migrates the coarse point bar deposits are covered first by finer sands and finally by the fine silts and clays of flood plain deposits. Thus, a noticeable characteristic of point bar deposits is a grading from coarse sand and gravel on the bottom to fine silt and clay on the top. Other channel deposits show poorer grading. Flood plain deposits are from the suspended load of a stream when it floods and overtops its banks.

SCVWD Injection-Extraction Site

With the preceding background we turn to description of the site chosen for the injection-extraction project. From the work of Atwater, Hedel and Helley (1977) and the inferred correlations of Howland (1976) we see that the hydraulic barrier separating the deeper zone (55 meter aquifer) from the shallow zone aquifers is composed of Sangamon

estuarine deposits. The 55 meter aquifer is composed of alluvial material from a pre-Sangamon glacial age. The shallow aquifers lie in alluvium deposited during the Wisconsin glacial age. During the period of deposition the ocean shoreline was located out beyond the Golden Gate on the continental shelf. The South Bay and Santa Clara Valley were a river valley with tributaries entering from the adjacent mountains. These tributaries formed alluvial fans along the border of Santa Clara Valley. A particular example is the alluvial fan formed by San Francisquito Creek (see Figure 16).

Palo Alto baylands are located along the southeastern margin of the San Francisquito Creek Basin and the deposits beneath the baylands appear to have been built up mostly from this source. Sokol (1963) has extensively studied the hydrogeology of this basin. From investigation of specific yield[1] maps he determined that the upper reach of San Francisquito Creek (out on the alluvial fan) maintained approximately the same course throughout the Late Pleistocene and Recent time. The same maps suggest that the lower reach has migrated during formation of the fan. On Figures 16 and 17 one can find the present location of San Francisquito Creek. The underlying sand and gravel deposits were probably laid down by the creek as it migrated back and forth across the face of the fan. The center of the arc of migration is toward the northeast (as suggested by the thickness of the unit along section E-D). The deposits which comprise the injection-extraction region of the SCVWD project are in the far southern end of the arc.

---

[1] The specific yield is the volume of water yielded per unit horizontal area per unit drop of water table (Bouwer, 1978). Sands and gravels have greater specific yields than do silts and clays. Greater values of specific yield correspond to coarser deposits which lie closer to the channel than the finer floodplain deposits.

Returning to Figures 16 and 17 (after Howland, 1976) note that the two sand and gravel units shown along the center section G-C correspond to the 7.6 and 14 meter aquifers found in the predesign tests. Figure 17 and the high values of transmissivity (108 and 43 m^2/day for the lower and upper, respectively) suggest that, at least locally, these units are continuous over some distance. But the conclusion of Howland that the 14 meter aquifer continues in section G-A may be inappropriate.

Table 3 gives the transmissivity values for the upper and lower aquifer injection and extraction wells of Figure 1, as determined by step-drawdown pumping tests (preliminary data, Brown and Caldwell). Note the variability in transmissivity values between adjacent wells throughout the field. Also, the well-logs show that it is very difficult to correlate adjacent sand and gravel units.

Figure 18 shows the profile of relative sand and gravel unit concentration for 31 well-logs of the injection-extraction system. Rather than viewing the profile as two distinct aquifers it is easier to view it as a probability distribution function for coarse lenses (versus depth). The expectation of finding a lense is greater than one half only within the ranges 4.9-6.2 and 12.8-13.7 meters. From the well-logs it appears that samples from adjacent wells (except near the I-1, E-1 pair) are statistically independent. While one would certainly expect positive correlation for wells drilled close enough together, adjacent units become uncorrelated within the range of distances between wells found in the injection-extraction field. (Indeed, the example of I-2, to be discussed below, shows that even locally the chances of finding corresponding lenses at depths for adjacent wells may be deemed independent). Figure 19 shows a plot of percent of aquifers thicker than a specified thickness. This plot was generated from the logs of the injection-extraction-observation system and may be viewed as a cumulative distribution function.

The statistical picture drawn in the previous paragraph is further clarified through description of depositional processes at the base of an alluvial fan. Coarse-grained units are mainly channel deposits (particularly point bars). Thin sand lenses may be attributed to the near channel overbank flows of natural levee and crevasse splay deposits (Reineck and Singh, 1975). The streams change their course through a combination of continuous migration (which extends point bars in the lateral direction of migration) and random jumps. When the stream returns it may erode part or all of the previous coarse deposits. Thus, the entire picture may be viewed as a random process.

Accordingly, the best description of the field, apart from the first doublet pair (I-1, E-1), is probably that of a collection of individual sand and gravel lenses (from channel deposits) embedded in an extensive silt and clay matrix (from overbank flows). Figure 18 suggests stronger correlation between deposits at about 5.5 meters and 13.2 meters, but these should not be construed as continuous aquifers. Locally groundwater flow may be simulated using a leaky aquifer model. But field modeling should probably consider the entire thickness of Wisconsin deposits as a single aquifer whose hydraulic conductivity is substantially less than that suggested by the individual coarse-grained lenses.[1]

The discussion in this appendix has implications for the success or failure of the SCVWD injection-extraction project. The principal goal of this project is the establishment of an effective hydraulic barrier against sea-water intrusion into the groundwater aquifers. Design of the

---

[1] Warren and Price (1961) were the first to use stochastic models for investigating flow in nonhomogeneous fields. More recently Freeze (1975) (also see Dagan, 1976 and Gelhar, et al., 1977) has used a stochastic Monte Carlo method for studying one-dimensional flow in a nonuniform media. An extension of this approach is probably the best way to surmount the limitations of a deterministic model for the present field investigation. Applications of such techniques are still in their infancy.

injection-extraction system was based on the conception of two distinguishable, though separate aquifers in the shallow zone (above 20 meters). An important question raised by the present discussion is whether such a barrier is required in this immediate area. The results presented herein show that the conceived aquifers are actually a system of discontinuous lenses which will not readily serve as an avenue to sea-water intrusion. A second question is whether it will prove feasible to establish an effective, continuous pressure ridge along the entire axis of the field. In view of the poor hydraulic conductivity of the upper zone and the discontinuities in the aquifers of interest, injection at a pressure sufficient to establish the barrier would have the undesired effect of causing surface flooding near the well.

Injection Well I-2

To gain experience with direct injection on a field scale the I-2 injection well was investigated in a pilot study (see Figure 1 for location). There are four observation wells surrounding the injection well at a distance of approximately 7.6 meters and one additional well at 16.8 meters. The logs for these wells are shown in Figures 20 and 21. Note the extreme variability, even over such a small area.

With an injection pressure of 103 k Pa (15 psi) a steady-state discharge (into the lower aquifer) of about 82 m^3/day (15 gpm) was originally attained. The steady-state hydraulic head distribution is shown in Figure 22. Immediately one notes the very small drop in head between I-2 and P-4. While this is an extreme departure from a radial distribution of pressure, it may have been anticipated from the logs (note the lense in I-2, P-4 and S-3 of Figure 20). What could not have been anticipated is the drop in head between P-4 and S-3. The magnitude of this drop is nearly the same as that found between I-2 and the other observation wells (where in P-1 for instance, the lense does not even appear). Thus the lense which runs from I-2 to P-4 is hydraulically discontinuous from that found in S-3. The inferred configuration is shown in Figure 23.

An attempt was made to simulate the flowfield using the confined aquifer model developed in Section IV. The inverse problem to be solved was to vary the coefficient of transmissivity until the observed head distribution was reproduced. (The actual discharge and a reasonable leakage coefficient were used.) After some work it became apparent that with this model, solution of the inverse problem required an unreasonable distribution of transmissivity. A high value was used for elements containing the lenses (in an attempt to reproduce the small drop between I-2 and P-4). To reproduce the drop in head between I-2 and observation wells P-1, P-2 and P-3 the transmissivity had to decrease to very low values. But then, to allow all of the flow to leave the region the transmissivity values out beyond the observation wells had to be increased. If this latter increase was not allowed the magnitude of the drop in head was reproduced but the value of the hydraulic head (or pressure) at the injection well was too large.

An alternative to the results of the preceding paragraph was found if the value of the hydraulic resistance of the confining layer was decreased significantly.[1] Using a higher transmissivity for elements representing the lenses and a transmissivity of 1.12 m^2/day for the rest of the field, with a hydraulic resistance of 25 days and a discharge of 82 m^3/day, the hydraulic head contours shown in Figure 24 were derived. The result seems adequate for all the observation wells except P-4. The hydraulic head drop between I-2 and P-4 is still much too large. But a change to the spatial resolustion level necessary to reproduce such a small pressure drop was deemed unjustified since the point of interest is already made if one examines the magnitudes of hydraulic conductivities for the "aquifer" and "aquitard". For the aquifer (K = T/aquifer thickness) the hydraulic conductivity is 0.92 m/day while that

[1] The hydraulic resistance (a scalar quantity) is the ratio of the thickness of the aquitard b and its hydraulic conductivity k. The aquitard hydraulic conductivity was determined to be 0.13 cm/day for I-1 and 0.06 cm/day for I-6. An average of these was used for I-2: k = 0.094 cm/day. From the well logs an aquitard thickness of 5.8 meters was chosen. Thus, the hydraulic resistance is b/k = 6200 days.

for the aquitard (K = b/resistance) is 0.23 m/day. These values are of the same order of magnitude which means that flow through the aquitard should not be strictly in the vertical direction (see the "law of refraction of the gradient", Bear, 1972, pg. 266). Thus the flow is three dimensional (and nearly 3-D radial near the lenses) and confined aquifer models should not be applied.

While one could use this quasi three dimensional model with high vertical leakage there are still a number of obstacles in the way of velocity prediction. One problem is: how should the aquifer thickness values be specified in places where lenses are not found? A second problem stems from the combination of high transmissivity values for the lense connecting I-2 and P-4 and the overly large hydraulic head drop; the resulting velocity is excessively large. It appears that one must leave the two dimensional model for one which is three dimensional, but here the problem of specifying the porous media geometry is even more overwhelming. One alternative, if the possibility of no model is excluded, is to use the stochastic Monte Carlo method of Freeze (1975) extended to three dimensions. The cost is significantly greater but the model is conceptually much superior to a deterministic model of the field.

Doublet Pair, I-1, E-1

A second example for application of the confined leaky aquifer model developed in Section IV is furnished by the doublet pair I-1, E-1. As noted earlier, there is reason to believe that the aquifers found in the predesign tests of I-1 may be continuous over a larger area than is typical of the rest of the field. Reasons for this belief are furnished by the high transmissivity values at the injection and extraction wells, logs of other near-by wells (Jenks and Adams, 1974), and in particular by the fence diagram of Howland (Figure 17).

In setting up the simulation, reliance was placed on Howland's observation that there is a general thinning of the deposits toward the bay. Also, from the logs of I-2 and E-2 we know that the aquifers pinch out in that direction. Toward the foothills we can expect some thickening of the deposits. Finally, as noted by Howland (and shown in the fence diagram, Figure 17), the aquifers thicken and effectively merge to the northwest. With these trends and the transmissivity values for I-1 and E-1 the input data was estimated and the simulation carried out.

With an injection and extraction rate of 680 m^3/day the hydraulic head contours shown in Figure 25 were generated. Transmissivity contours are shown in Figure 26. The breakthrough curve at E-1 (ratio of injected fluid in the withdrawn fluid) is shown in Figure 27. Also shown in this figure is the breakthrough curve for the same conditions except that the field has a uniform transmissivity of 112 m^2/day. Note that the effect of having the aquifer thin out toward the bay is to increase the rate of breakthrough, as would intuitively be expected.

The breakthrough curves were generated directly from the velocity field and as such, do not include the effects of dispersion. It is expected that dispersion would considerably reduce the time to initial breakthrough and the front of the curve would not be as steep.

APPENDIX II

In this appendix we evaluate the interelement boundary integral for the elliptic element of the anisotropic problem. The procedure is more complicated than for the circular isotropic element but the result is the same.

Properties of the Anisotropic Solution

Equation (28) gives the hydraulic head solution for the isotropic problem. Using the transformations of (25) we find that the solution for an anisotropic problem with principal transmissivities T_x and T_y is

$$G = \frac{Q}{2\pi(T_x T_y)^{1/2}} \left\{ K_o\left(\frac{r'}{B'}\right) - \frac{K_o\left(\frac{R'}{B'}\right)}{I_o\left(\frac{R'}{B'}\right)} I_o\left(\frac{r'}{B'}\right) \right\} \qquad \text{(II. 1)}$$

where

$$r' = \left[\frac{x^2}{(T_x/T_y)^{1/2}} + \frac{y^2}{(T_y/T_x)^{1/2}} \right]^{1/2}$$

$$B' = \left[\frac{(T_x T_y)^{1/2}}{(K/b)} \right]^{1/2}$$

and x and y are the global coordinates of the anisotropic problem. From the form of the function G of (II. 1) it is apparent that the head is constant on the ellipse specified by

$$\frac{x^2}{a^2} + \frac{y^2}{b^2} = \text{constant}$$

where $a^2 = 1/b^2 = (T_x/T_y)^{1/2}$. Consider the ellipse corresponding to

the boundary of the singular element, $r' = R'$. The direction of streamlines crossing the ellipse (see Figure 28a) is given by

$$\tan\theta_1 = \frac{q_y}{q_x} = \frac{Y}{x} \qquad \text{(II. 2)}$$

Here,

$$q_y = -T_y \frac{\partial G}{\partial y} = \frac{Q \cdot y}{2\pi B'R'} \left\{ K_1\left(\frac{r'}{B'}\right) + \frac{K_o\left(\frac{R'}{B'}\right)}{I_o\left(\frac{R'}{B'}\right)} I_1\left(\frac{R'}{B'}\right) \right\}$$

and a similar expression is found for q_x. ($K_1(\cdot)$ and $I_1(\cdot)$ are the modified Bessel functions of the second and first kind of order one). The magnitude of q_α is

$$|q_\alpha| = \sqrt{q_x^2 + q_y^2} = \frac{Q}{2\pi B'R'} \left\{ K_1\left(\frac{R'}{B'}\right) + \frac{K_o\left(\frac{R'}{B'}\right)}{I_o\left(\frac{R'}{B'}\right)} I_1\left(\frac{R'}{B'}\right) \right\} \sqrt{x^2 + y^2} \qquad \text{(II. 3)}$$

Next we want to find the direction of the outward unit normal vector to the ellipse. According to Courant and John (1974, pg. 231), the normal to a curve at the point (x, y) is

$$(\xi - x)F_y - (\eta - y)F_x = 0$$

where (ξ, η) is a point on the normal and $F(x, y) = 0$ is the equation of the curve. For the ellipse, $F = \frac{x^2}{a^2} + \frac{y^2}{b^2} - R'^2 = 0$ and the equation of the normal may be written in the form of a straight line:

$$\eta = \frac{ya^2}{xb^2}\xi + \left(y - x\frac{ya^2}{xb^2}\right)$$

This last equation gives the tangent of the normal to the ellipse (see Figure 28b)

$$\tan\theta_2 = \frac{ya^2}{xb^2} = \frac{y}{x}a^4 = \frac{yT_x}{xT_y} \qquad \text{(II. 4)}$$

Evaluation of Interelement Boundary Integral

With equations (II. 2) through (II. 4) we can evaluate the boundary integral given by equation (24)

$$-\int_{\Gamma^e} \varphi_i T_{\alpha\beta} \frac{\partial G}{\partial x_\beta} \ell_\alpha \, d\Gamma^e = \int_{\Gamma^e} \varphi_i q_\alpha \ell_\alpha d\Gamma^e = \int_{\Gamma^e} \varphi_i q_n d\Gamma^e \qquad (15)$$

In Section III Γ^e was a "finite element" circle with q_n constant on the circle, and thus q_n could be moved outside of the integrand. But for the ellipse q_n is a function of the position on the ellipse and must remain within the integrand. Because ℓ_α is a unit vector we can write

$$q_n = q_\alpha \ell_\alpha = |q_\alpha| \cos\theta_3 \qquad \text{(II. 5)}$$

where θ_3 is the angle between the streamline and the unit normal to the surface (see Figure 28c). To find $\cos\theta_3$ we use Equations (II. 2) and (II. 4) in the form

$$F(\xi, \eta) = \eta - \frac{y}{x}\xi - b_1 = 0$$

$$G(\xi, \eta) = \eta - \frac{ya^2}{xb^2}\xi - b_2 = 0$$

Now, according to Courant and John (1974, pg. 234), the cosine of the angle between the curves $F = 0$ and $G = 0$ is

$$\cos\theta = \frac{F_\xi G_\xi + F_\eta G_\eta}{(F_\xi^2 + F_\eta^2)^{1/2}(G_\xi^2 + G_\eta^2)^{1/2}}$$

so

$$\cos\theta_3 = \frac{R'^2}{(y^2a^4 + x^2b^4)^{1/2}(x^2 + y^2)^{1/2}}$$

Then from (II. 3) and (II. 5),

$$q_n = \frac{QR'}{2\pi B'}\left\{K_1\left(\frac{R'}{B'}\right) + \frac{K_o\left(\frac{R'}{B'}\right)}{I_o\left(\frac{R'}{B'}\right)} I_1\left(\frac{R'}{B'}\right)\right\} \cdot (y^2a^4 + x^2b^4)^{-1/2} \qquad \text{(II. 6)}$$

Next we look at the differential along the curve:

$$d\Gamma \equiv \sqrt{1 + \left(\frac{dx}{dy}\right)^2}\, dy$$

Using the equation of the ellipse we find

$$d\Gamma = \sqrt{\frac{R'^2 + a^2y^2(a^4 - 1)}{R'^2 - a^2y^2}}\, dy$$

Finally, we examine the basis function expansion for the boundary (see Section IV. B). Along the boundary (see Figure 3 for numbering scheme)

$$y = y_6 + \frac{1}{2}(y_3 - y_2)\eta + \frac{1}{2}(y_3 + y_2 - 2y_6)\eta^2$$

For the isotropic circle we know that

$$y_2 = -\frac{R}{\sqrt{2}}, \quad y_6 = 0, \quad y_3 = \frac{R}{\sqrt{2}}$$

The corresponding points on the ellipse (with major axis coinciding with the x-axis) are found from equation (25): $y_A = \frac{1}{a} y_I = b y_I$. So for the anisotropic case (with R = R')

$$y_2 = -\frac{R'}{a\sqrt{2}}, \quad y_6 = 0, \quad y_3 = \frac{R'}{a\sqrt{2}}$$

and

$$\frac{dy}{d\eta} = -\frac{R'}{a\sqrt{2}}; \quad y^2 = \frac{R'^2}{2a^2}\eta^2$$

A check for element degeneracy using Section IV. B shows that the element mapping for the ellipse satisfies the conditions for uniqueness and invertability of the transformation between global and local domains. Before assembling the integral we note that

$$(y^2a^4 + x^2b^4)^{-1/2} = \frac{a}{(R'^2 + y^2a^2(a^4 - 1))^{1/2}} \quad . \qquad \text{(II. 8)}$$

Using the same procedure as Section IV. E we evaluate the integral for node 6, whose basis function is $\omega_6 = 1 - \eta^2$. The integral is

$$I_6 = \int_{-1}^{1} (1 - \eta^2) q_n \sqrt{1 + \frac{dx}{dy}^2} \frac{dy}{d\eta} d\eta$$

or, with (2.6), (2.7) and (2.8),

$$I_6 = \frac{QR'}{\pi B'}\left\{K_1\left(\frac{R'}{B'}\right) + \frac{K_o\left(\frac{R'}{B'}\right)}{I_o\left(\frac{R'}{B'}\right)} I_1\left(\frac{R'}{B'}\right)\right\}\int_o^1 \frac{(1-\eta^2)}{\sqrt{2-\eta^2}}\, d\eta$$

$$= \frac{QR'}{2\pi B'}\left\{K_1\left(\frac{R'}{B'}\right) + \frac{K_o\left(\frac{R'}{B'}\right)}{I_o\left(\frac{R'}{B'}\right)} I_1\left(\frac{R'}{B'}\right)\right\} \qquad \text{(II. 9)}$$

Equation (II. 9) is the same result as found for the isotropic case in Section IV. E. Thus the procedure for implementing this approach may be directly extended for an anisotropic problem with the shape of the singular element given by the ellipse

$$\frac{x^2}{(T_x/T_y)^{1/2}} + \frac{y^2}{(T_y/T_x)^{1/2}} = R'^2$$

The side node and corner node flow allocations remain the same.

TABLE 1. Correspondence Between Functional Coefficients in equations (11) and (12)

$$c_1 = -\frac{1}{4}(a_1 + a_2 + a_3 + a_4) + \frac{1}{2}(a_5 + a_6 + a_7 + a_8)$$

$$c_2 = \frac{1}{2}(a_6 - a_8)$$

$$c_3 = \frac{1}{2}(-a_5 + a_7)$$

$$c_4 = \frac{1}{4}(a_1 - a_2 + a_3 - a_4)$$

$$c_5 = \frac{1}{4}(a_1 + a_2 + a_3 + a_4) - \frac{1}{2}(a_5 + a_7)$$

$$c_6 = \frac{1}{4}(a_1 + a_2 + a_3 + a_4) - \frac{1}{2}(a_6 + a_8)$$

$$c_7 = \frac{1}{4}(-a_1 - a_2 + a_3 + a_4) + \frac{1}{2}(a_5 - a_7)$$

$$c_8 = \frac{1}{4}(-a_1 + a_2 + a_3 - a_4) + \frac{1}{2}(-a_6 + a_8)$$

TABLE 2. Bilinear Basis Functions (see Figure 3 for notation)

$$\psi_1 = \frac{1}{4}(1 - \xi)(1 - \eta)$$

$$\psi_2 = \frac{1}{4}(1 + \xi)(1 - \eta)$$

$$\psi_3 = \frac{1}{4}(1 + \xi)(1 + \eta)$$

$$\psi_4 = \frac{1}{4}(1 - \xi)(1 + \eta)$$

TABLE 3. Transmissivity (m^2/day) for SCVWD Wells (See Figure 1) (Preliminary Data)

Wells	Aquifer	
	Shallow	Deep
I-1	43.5	108.0
E-1	134.6	116.7
I-2	33.6	6.4
E-2	7.0	1.0
I-3	29.2	4.8
E-3	12.6	5.0
I-4	-	-
E-4	61.5	22.3
I-5	131.1	1.9
E-5	48.2	-
I-6	6.2	130.8
E-6	15.0	2.6
I-7	6.5	6.8
E-7	32.4	4.7
I-8	62.7	44.5
E-8	11.5	4.7
I-9	51.0	7.9
E-9	33.4	8.7
Mean	40.0	26.5
Std. Dev.	39.0	43.8

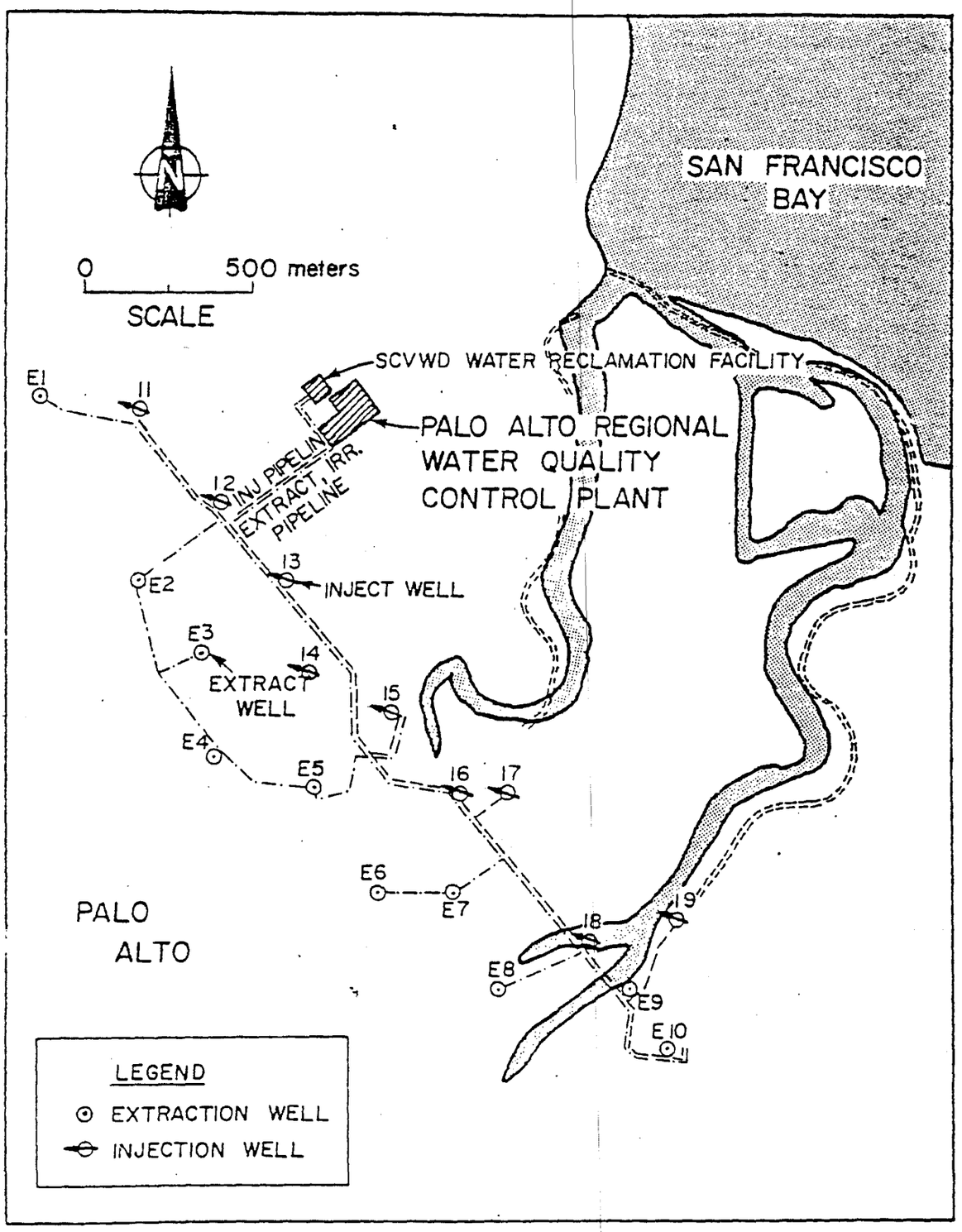

FIGURE 1. Design of SCVWD Project

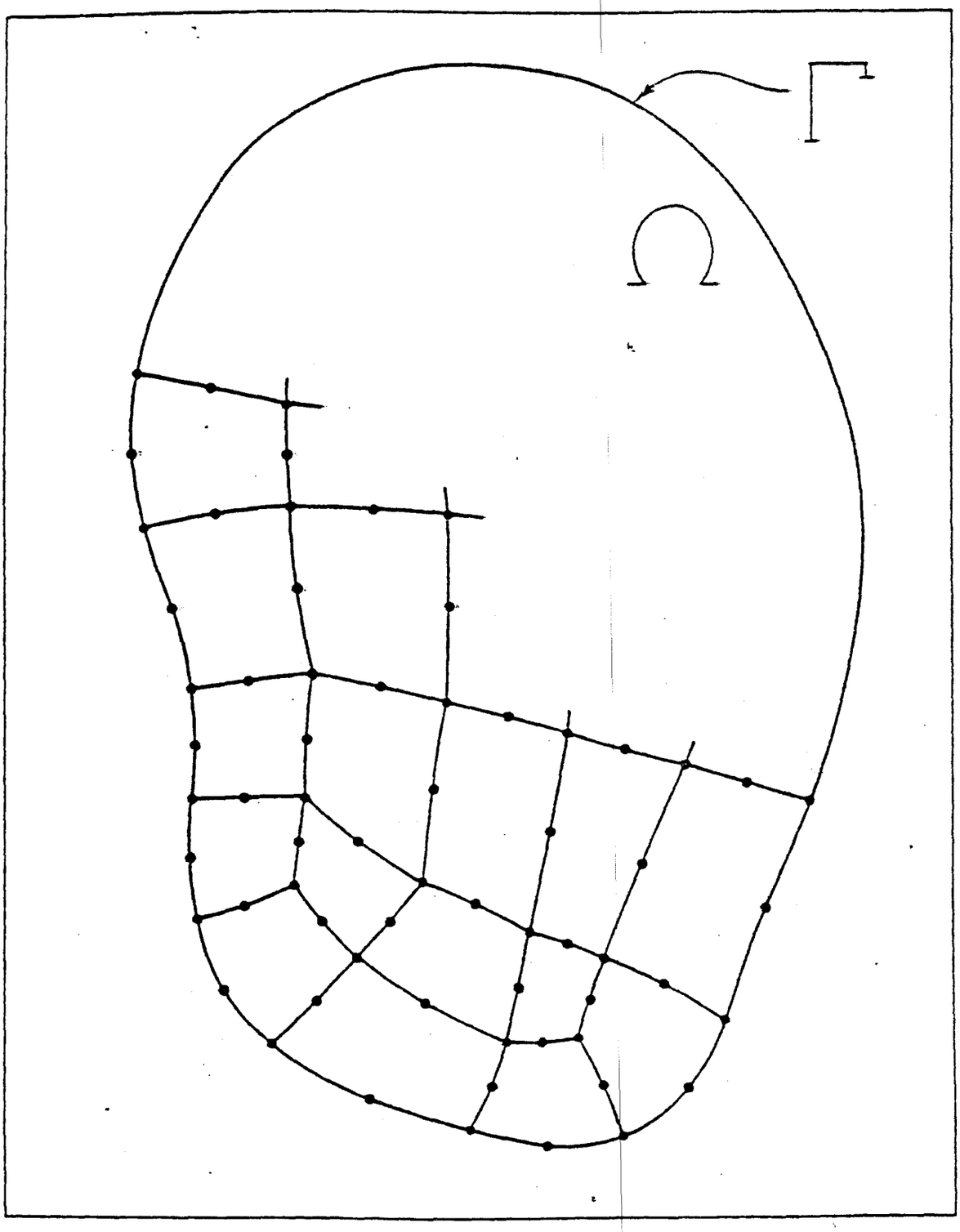

FIGURE 2. Domain Ω with Boundary Γ

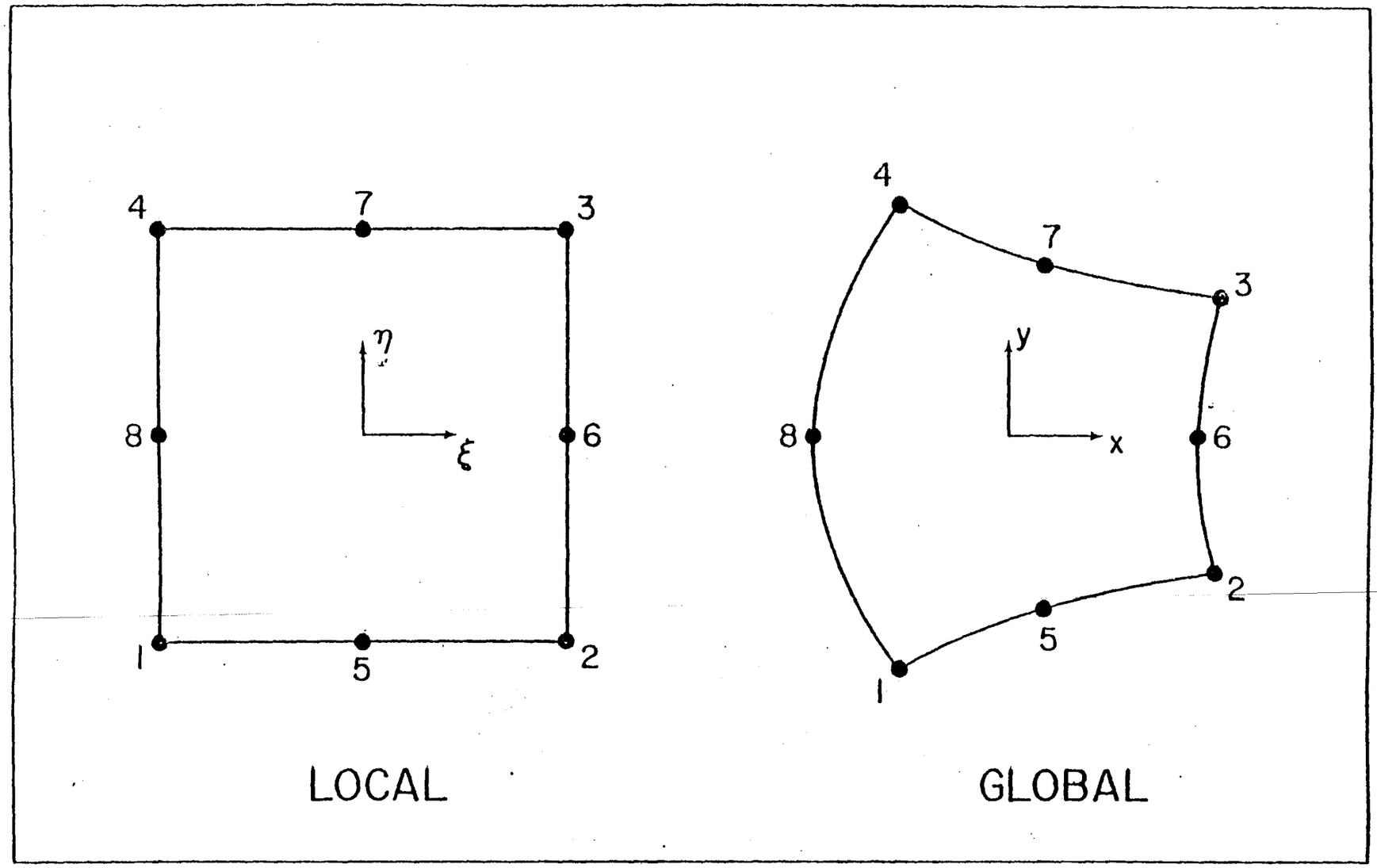

FIGURE 3. Typical Element in Global and Local Coordinates

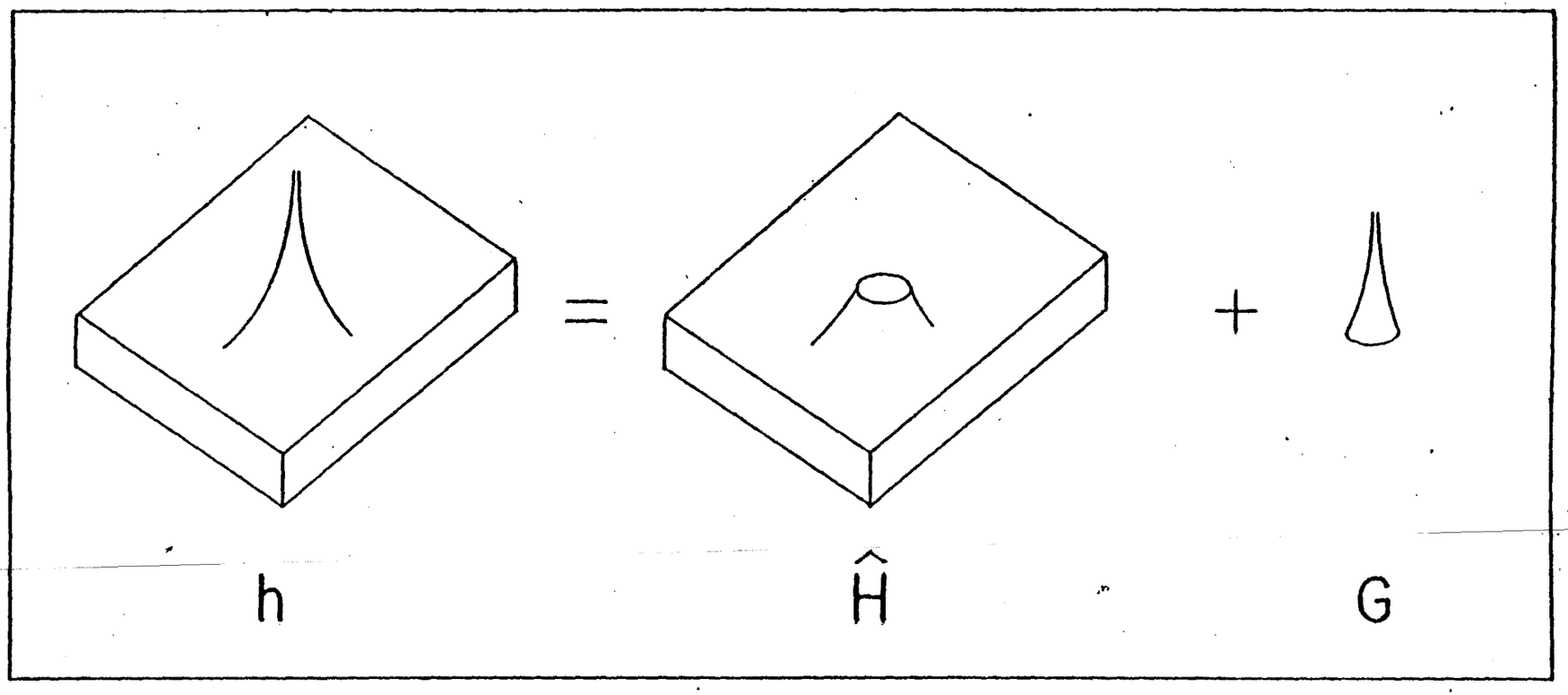

FIGURE 4. Schematic Representation of Approximation Technique

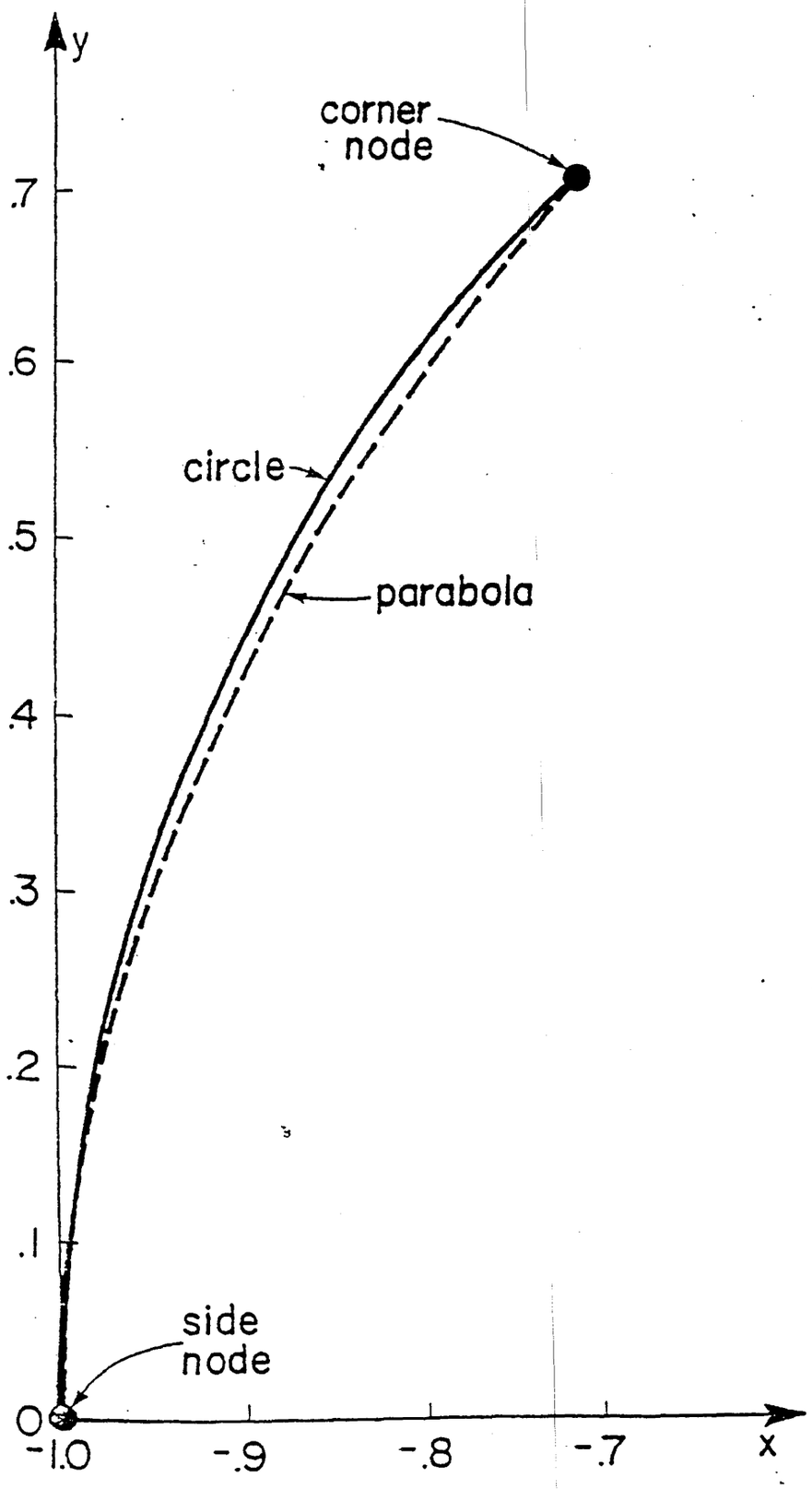

FIGURE 5. True Circle and its FE Approximation

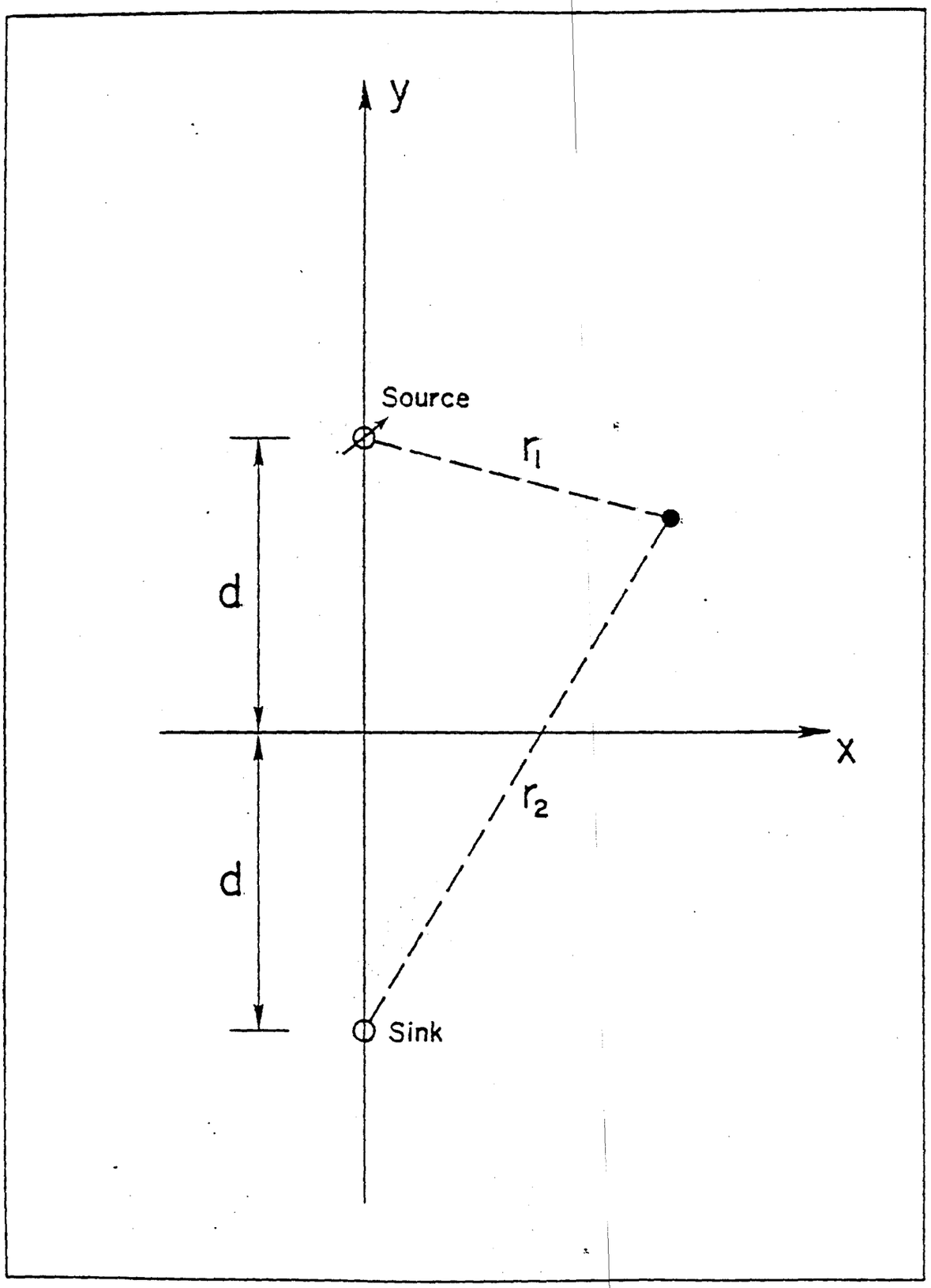

FIGURE 6. Notation for Source and Sink in Infinite Aquifer

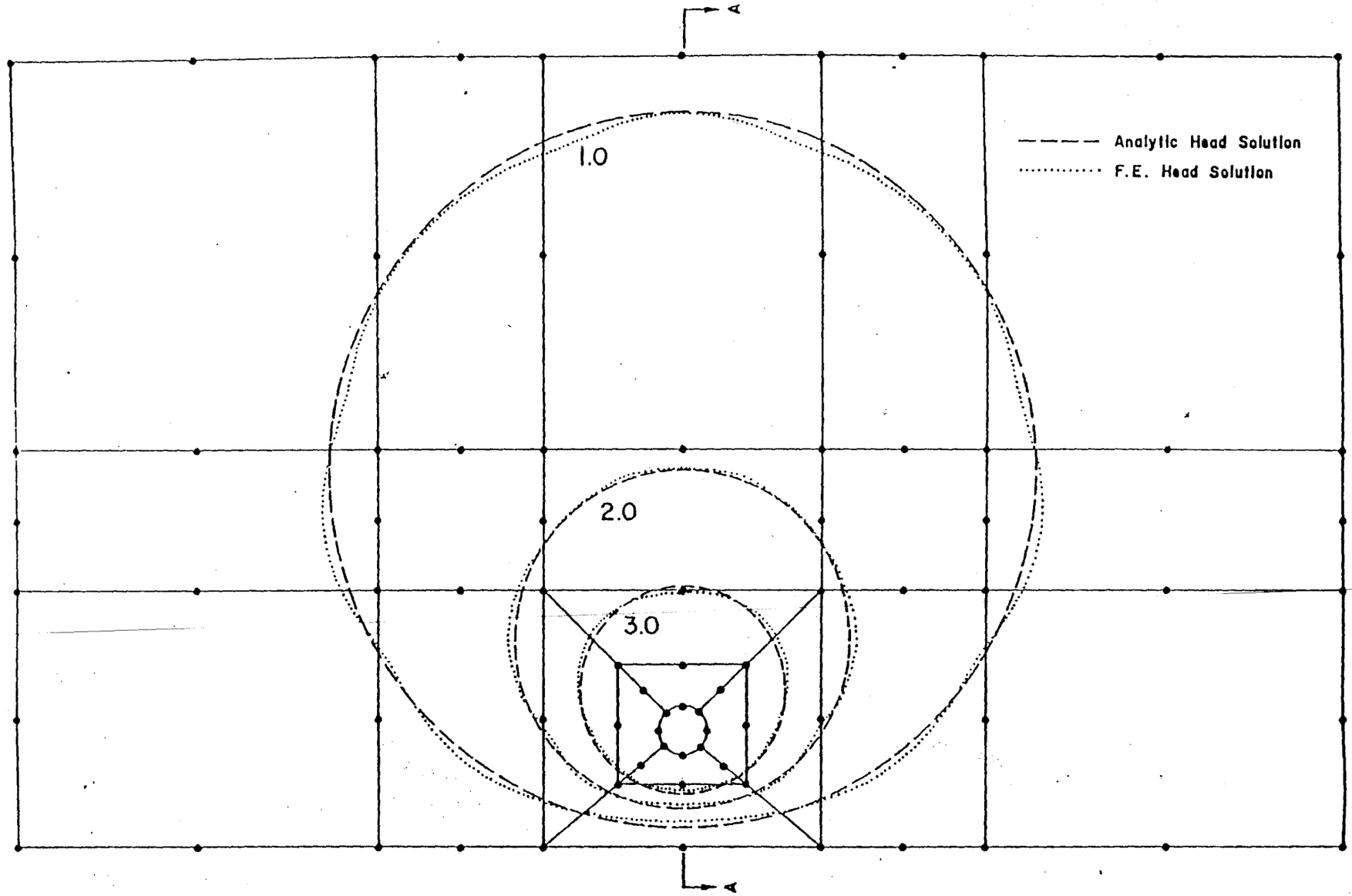

FIGURE 7. FE Mesh and Hydraulic Head Solution (Feet)

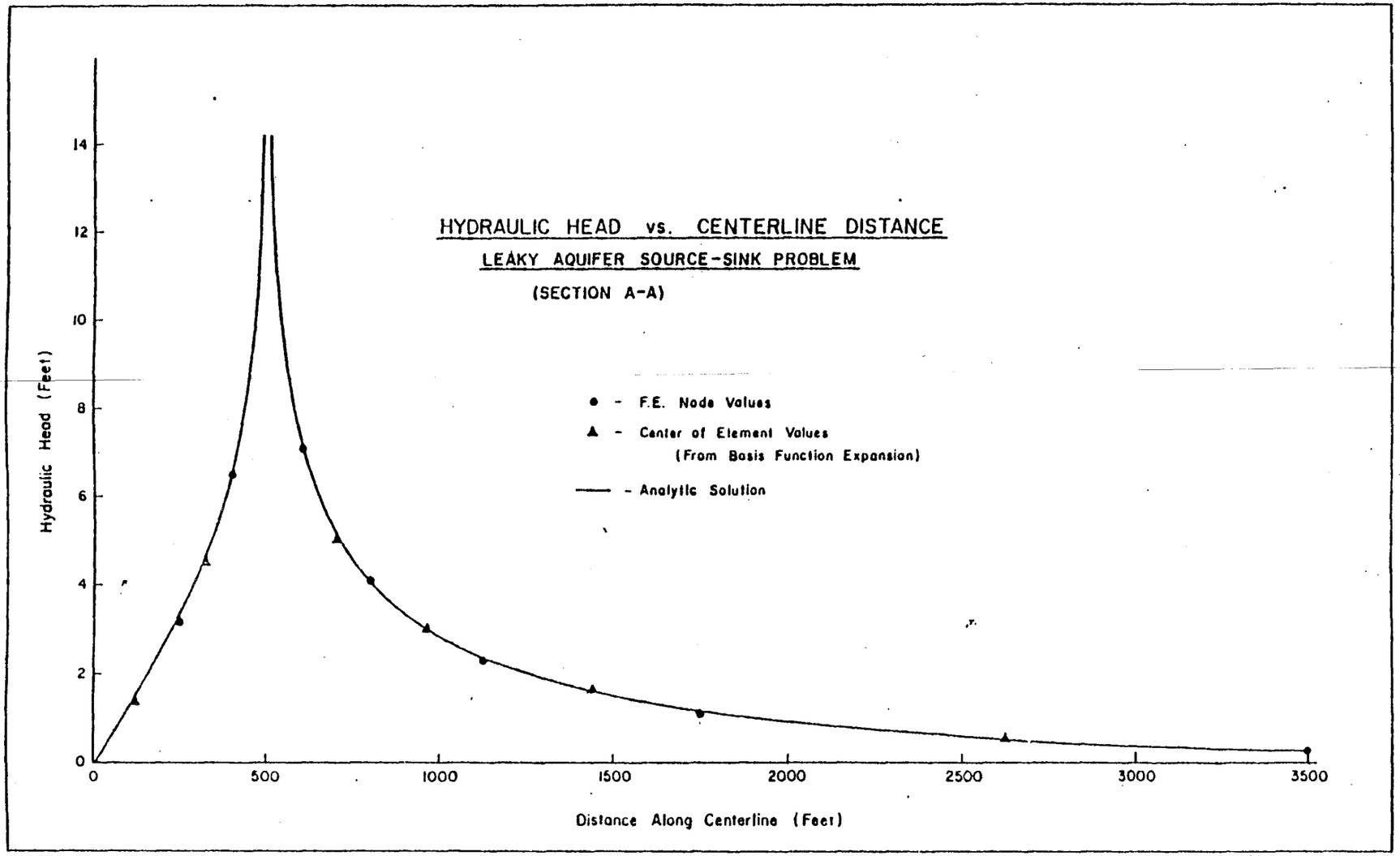

FIGURE 8. Profile of Leaky Aquifer Solution

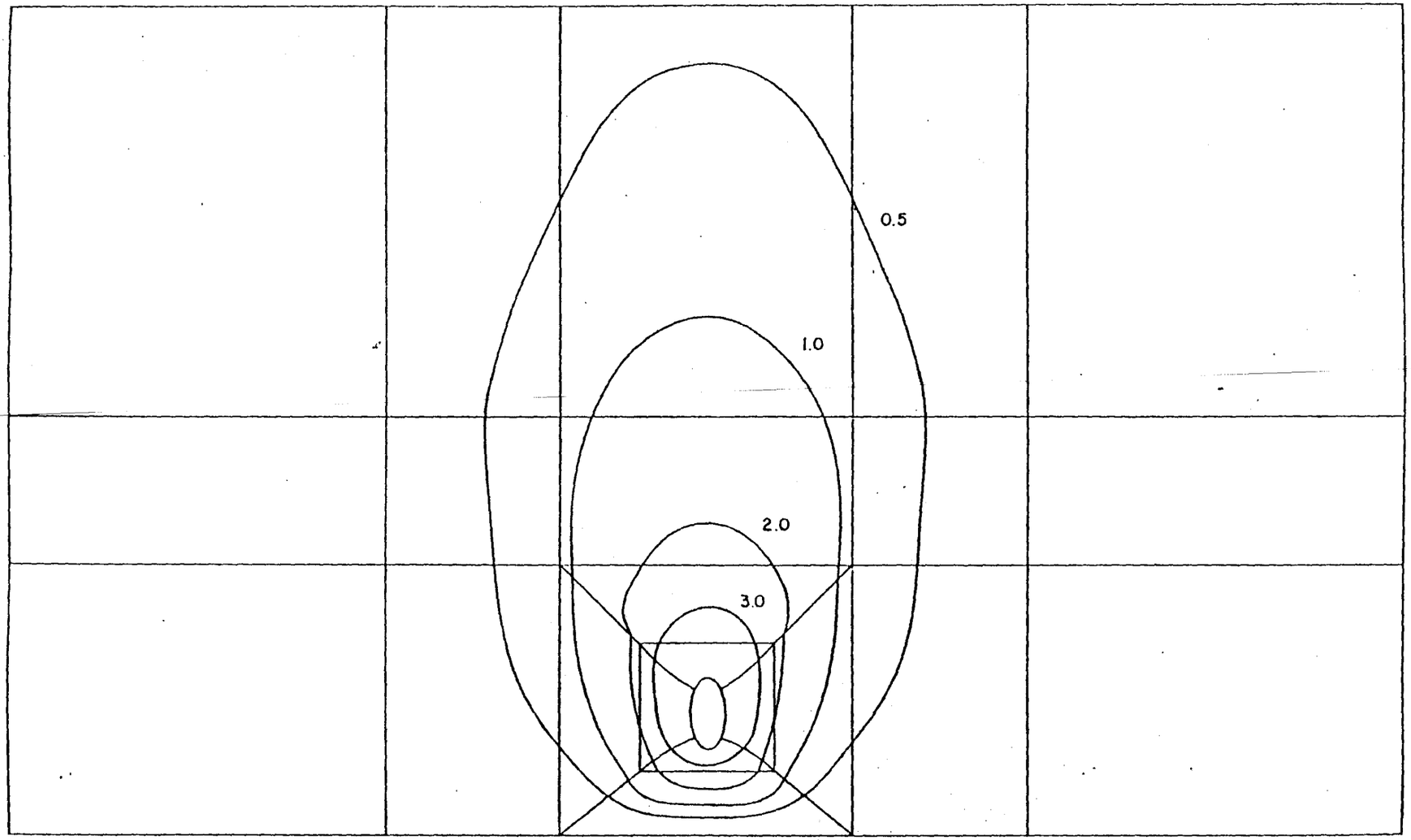

FIGURE 9. Contours from Anisotropic Leaky Aquifer Solution (Feet)
a. Major Principle Axis along Y-Axis

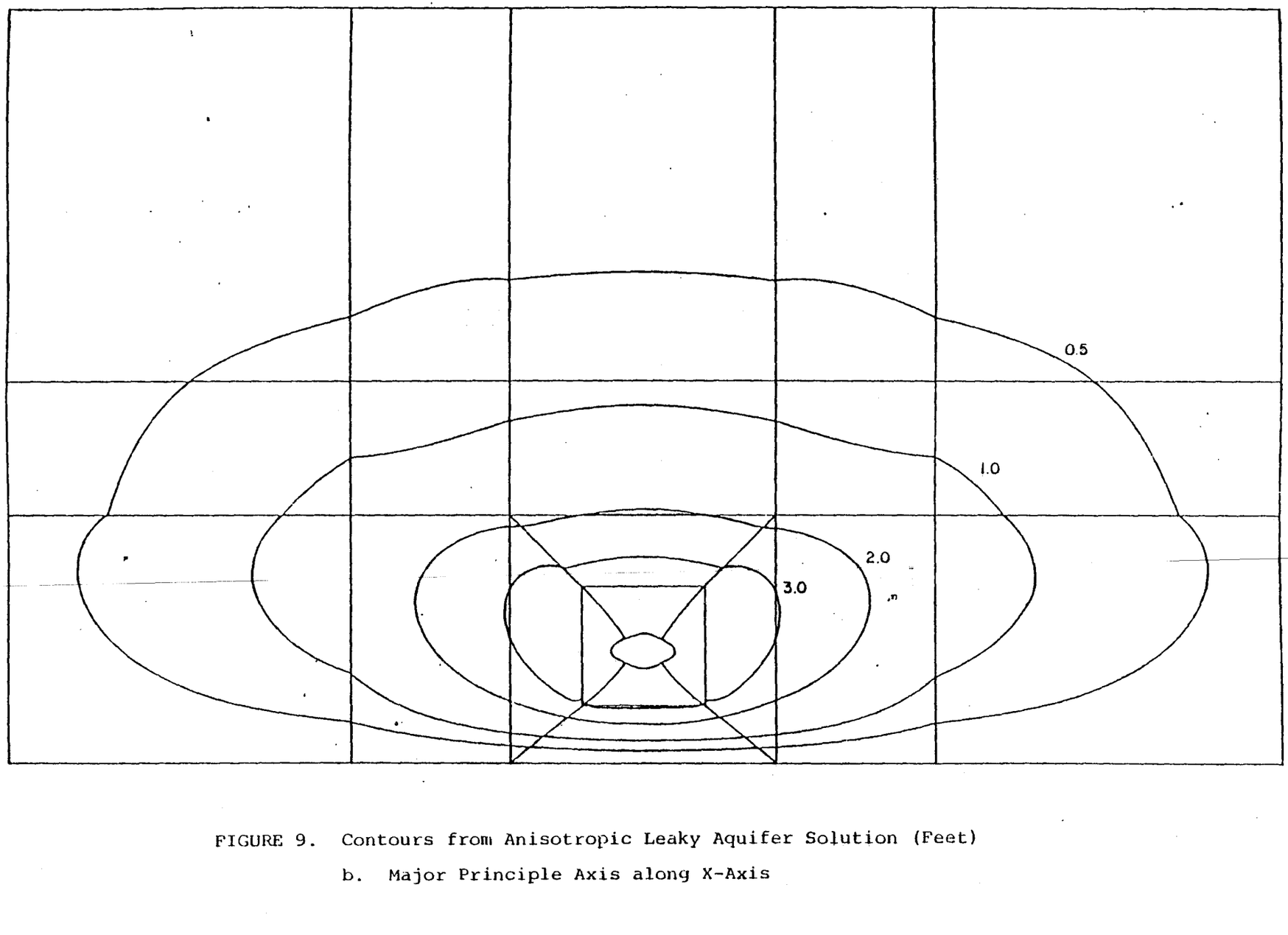

FIGURE 9. Contours from Anisotropic Leaky Aquifer Solution (Feet)

b. Major Principle Axis along X-Axis

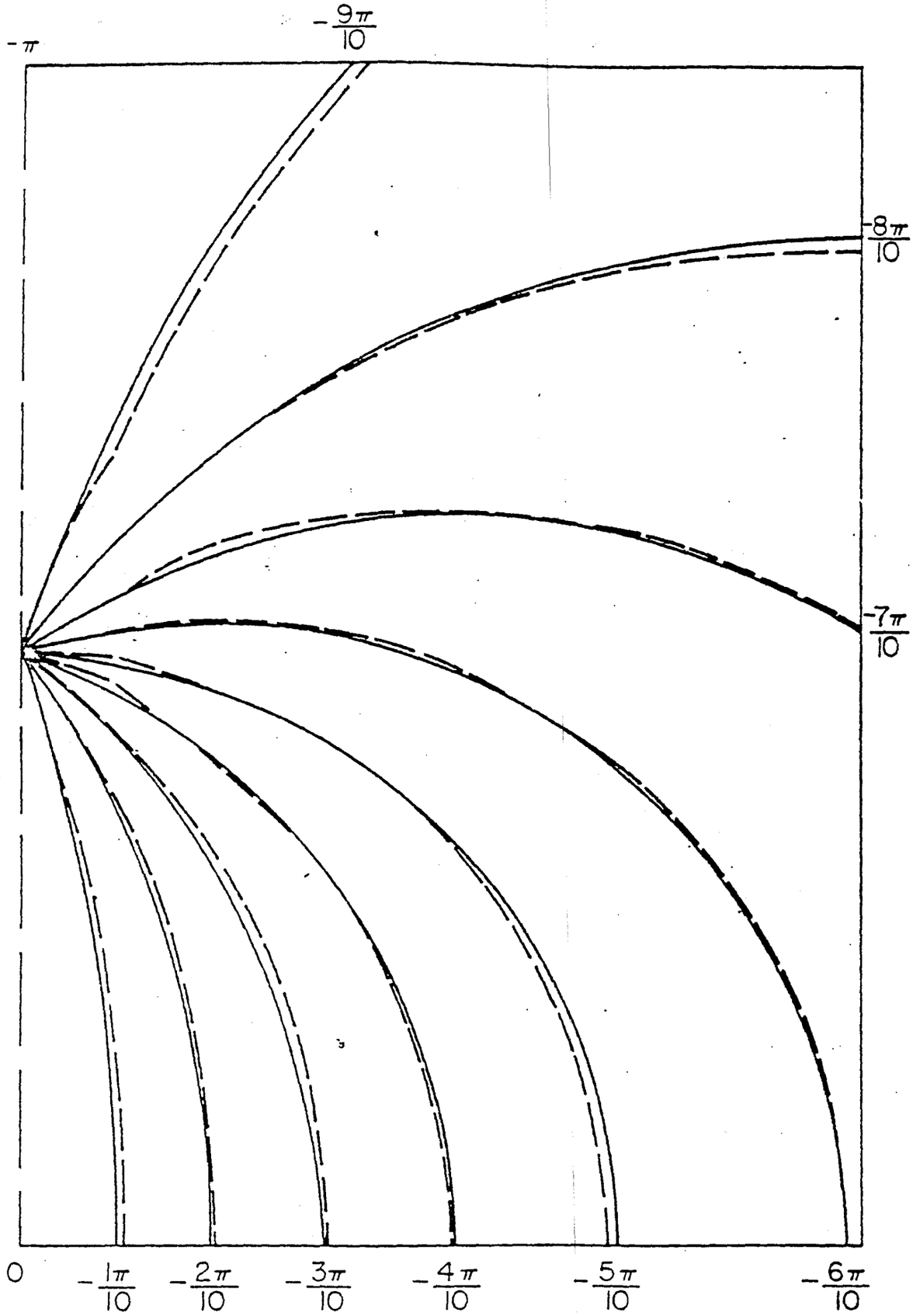

FIGURE 10. Streamlines: Smoothed Linear Velocity Field

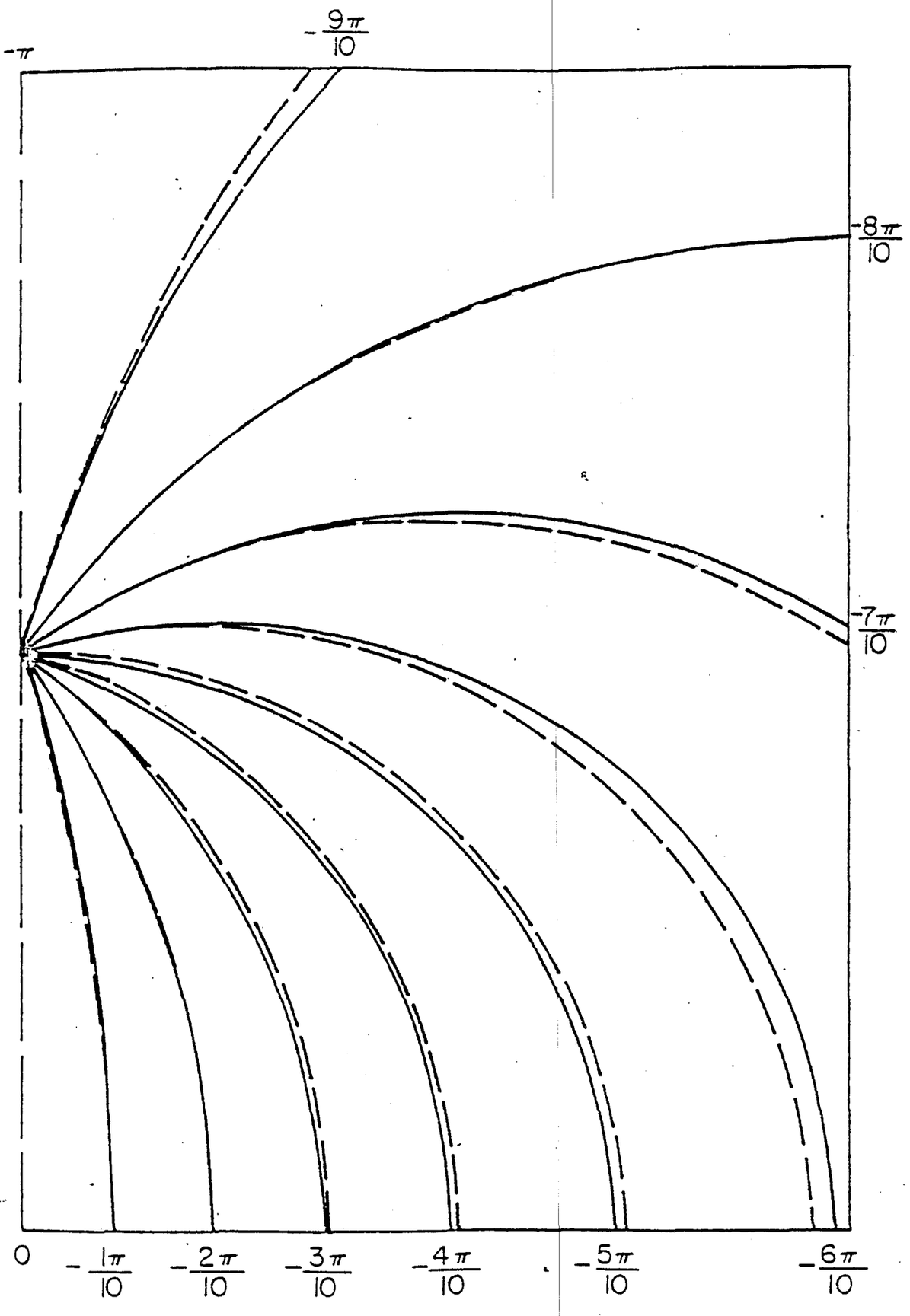

FIGURE 11. Streamlines: Quadratic Velocity Field

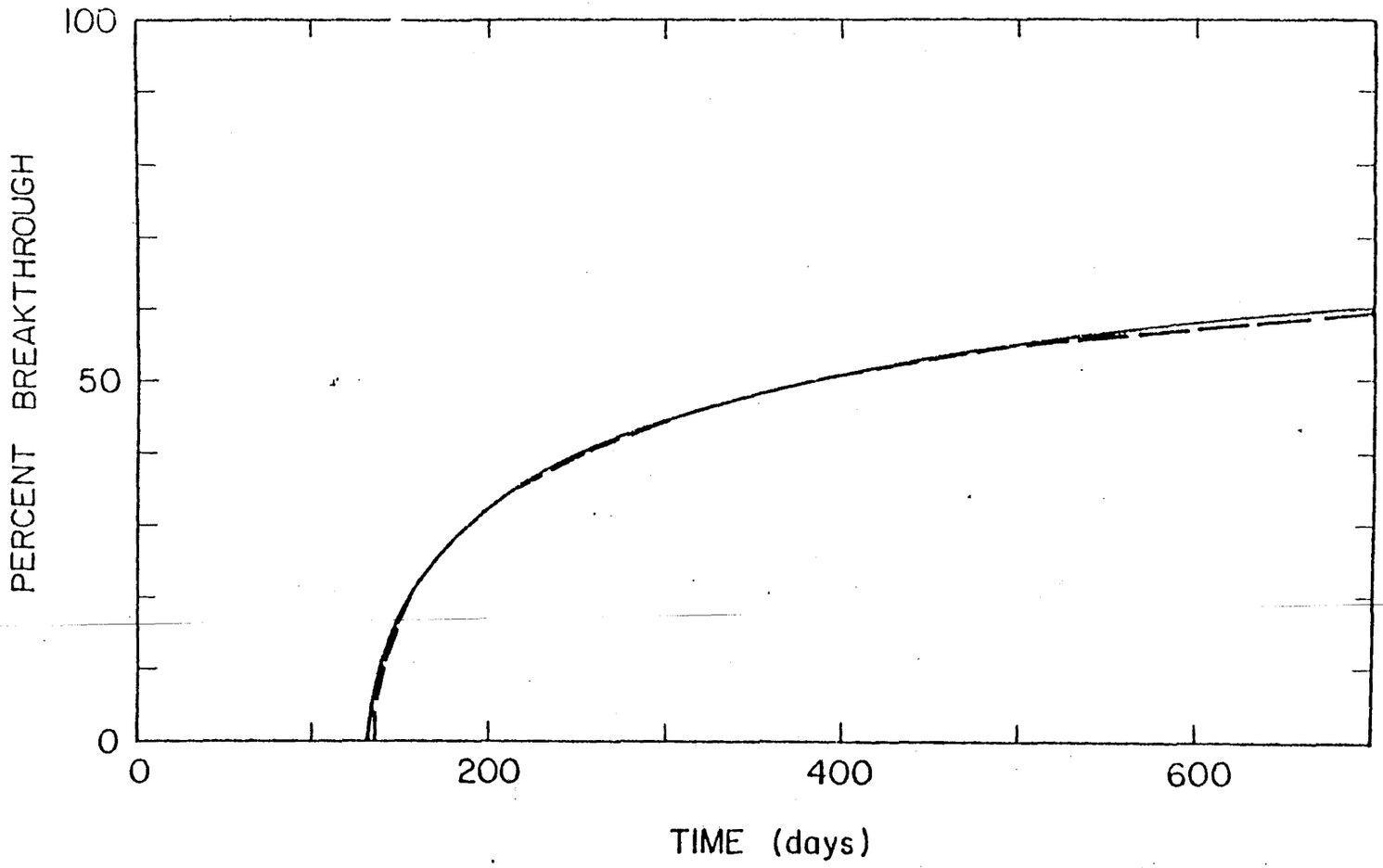

FIGURE 12. Breakthrough Curve from Figure 1?

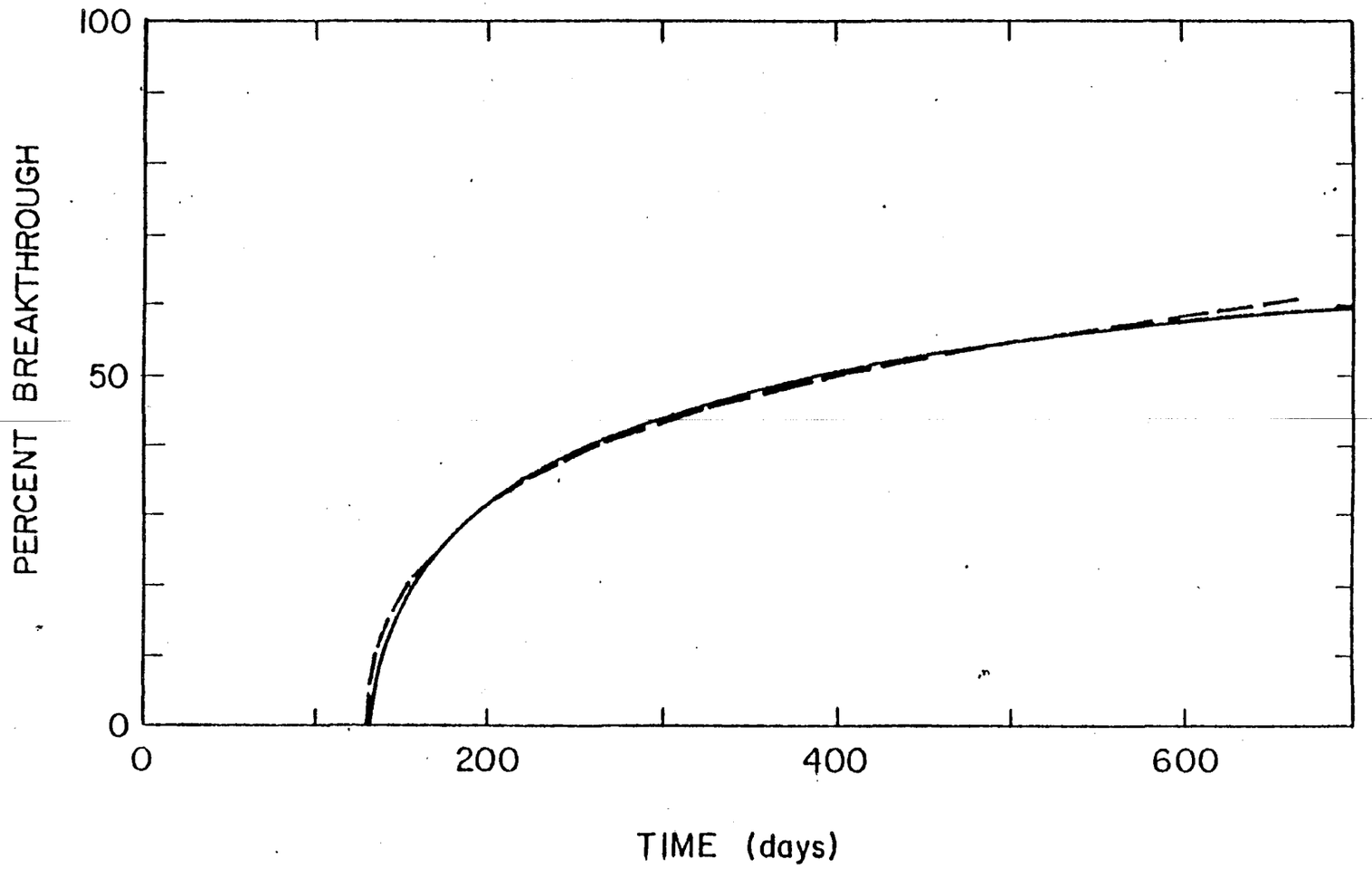

FIGURE 13. Breakthrough Curve from Figure 11

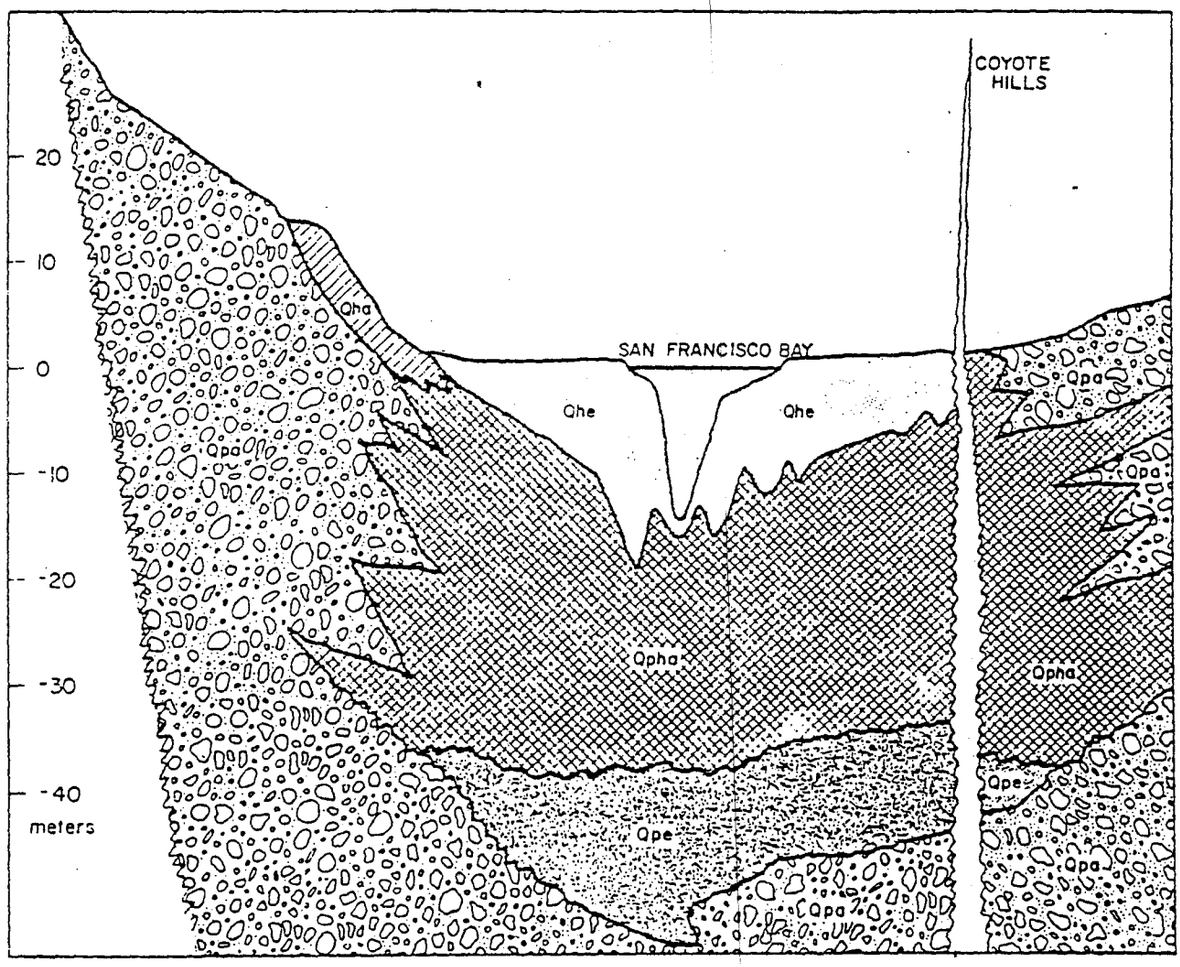

Qhe: Holocene estuarine deposits
Qpha: Late Pleistocene to Holocene alluvial deposits
Qpe: Late Pleistocene estuarine deposits
Qpa: Late Pleistocene alluvial deposits
Qha: Holocene alluvial deposits

FIGURE 14. Geologic Cross-Section of Bay at Dumbarton Bridge (after Atwater, et al., 1977)

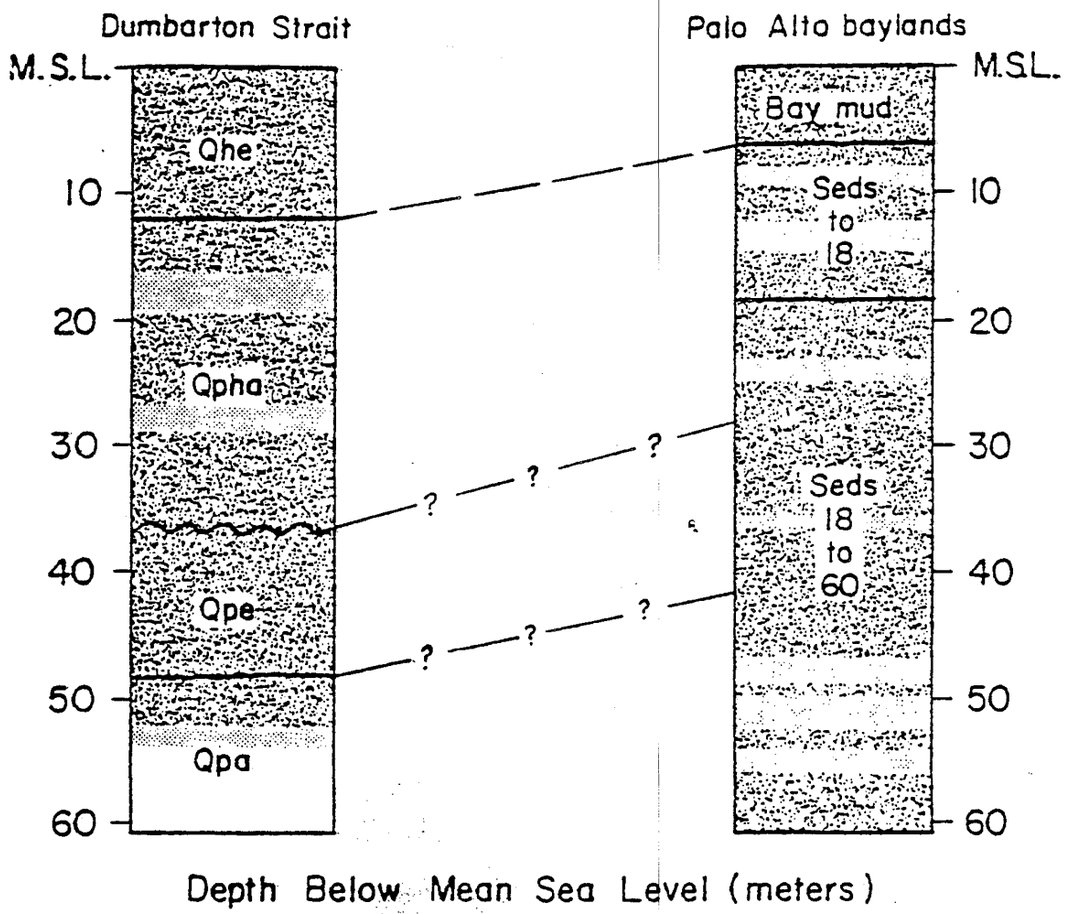

FIGURE 15. Inferred Correlations Between Dumbarton Strait and Palo Alto Baylands (after Howland, 1976)

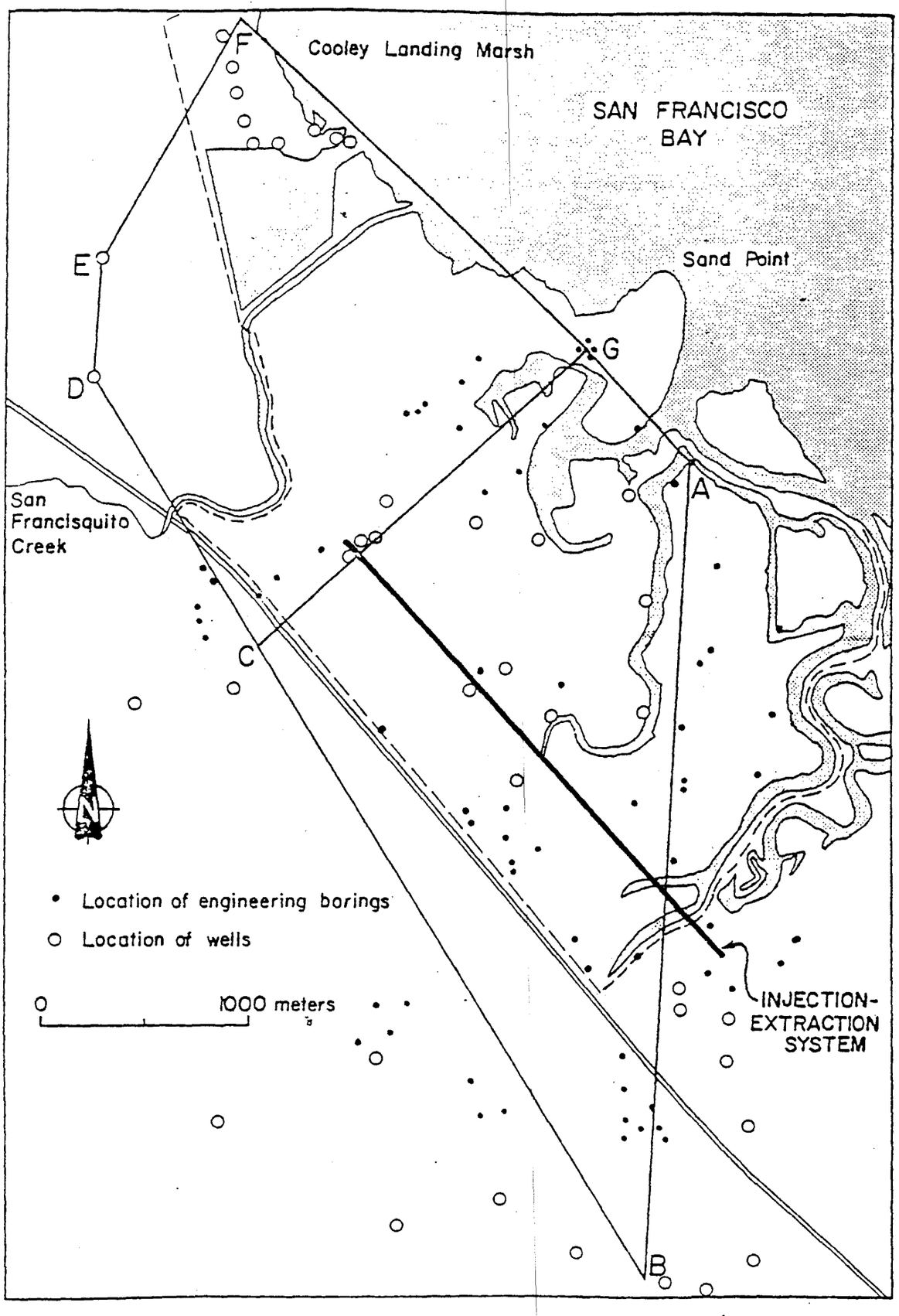

FIGURE 16. Location of Well Logs and Fence Diagram (after Howland, 1976)

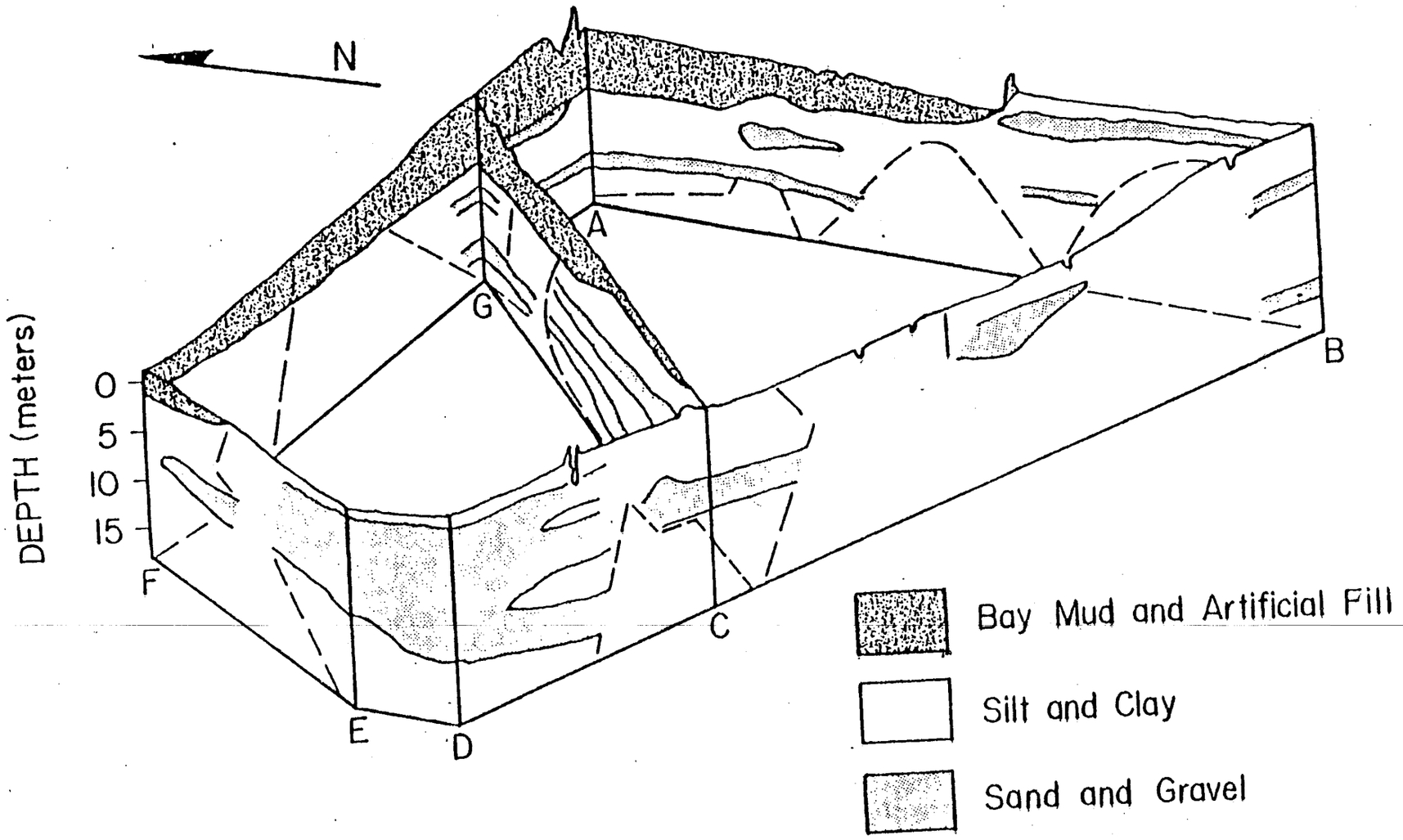

FIGURE 17. Fence Diagram of Baylands Area (after Howland, 1976)

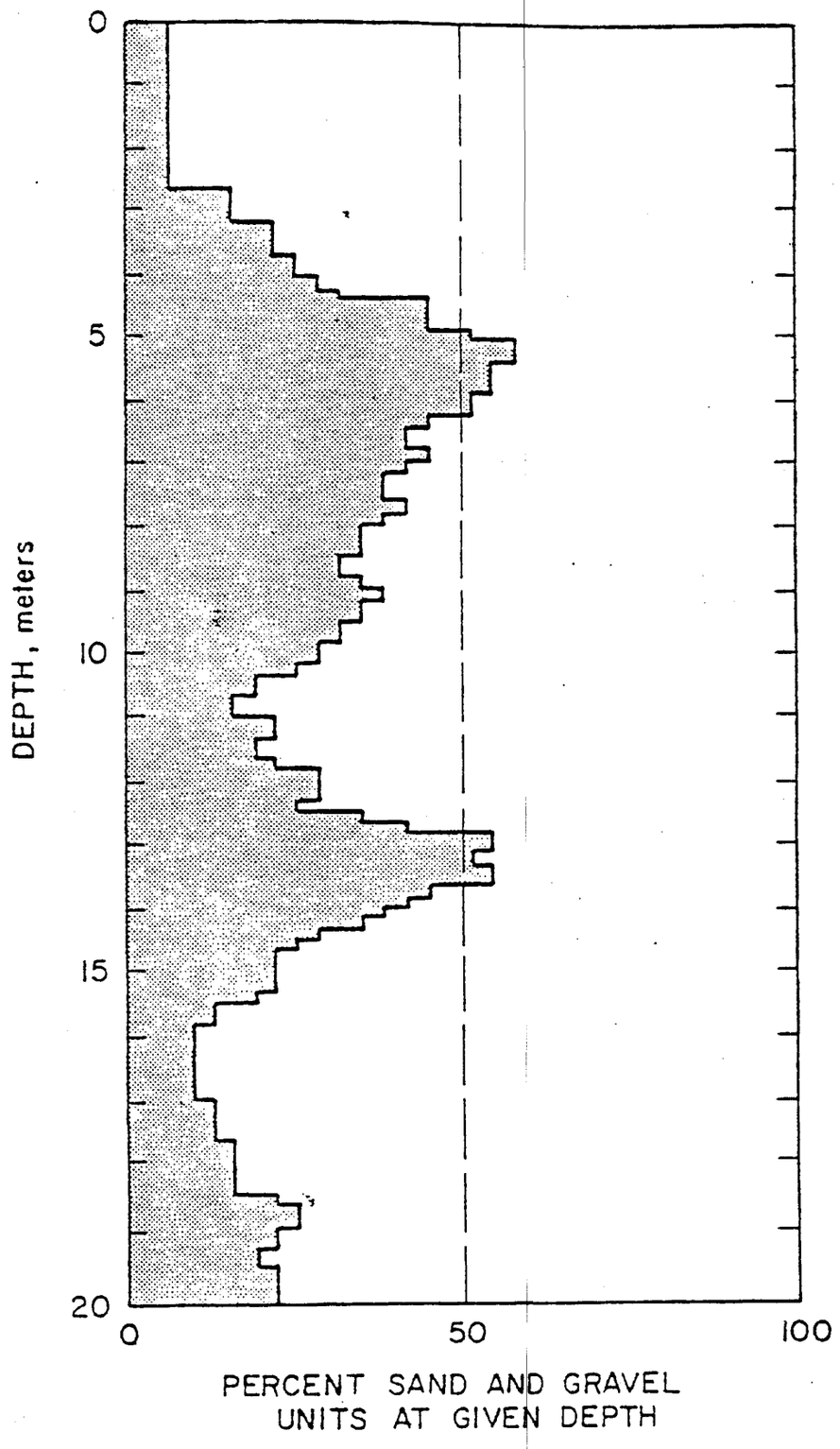

FIGURE 18. Profile of Relative Sand/Gravel Unit Density from SCVWD Well Logs

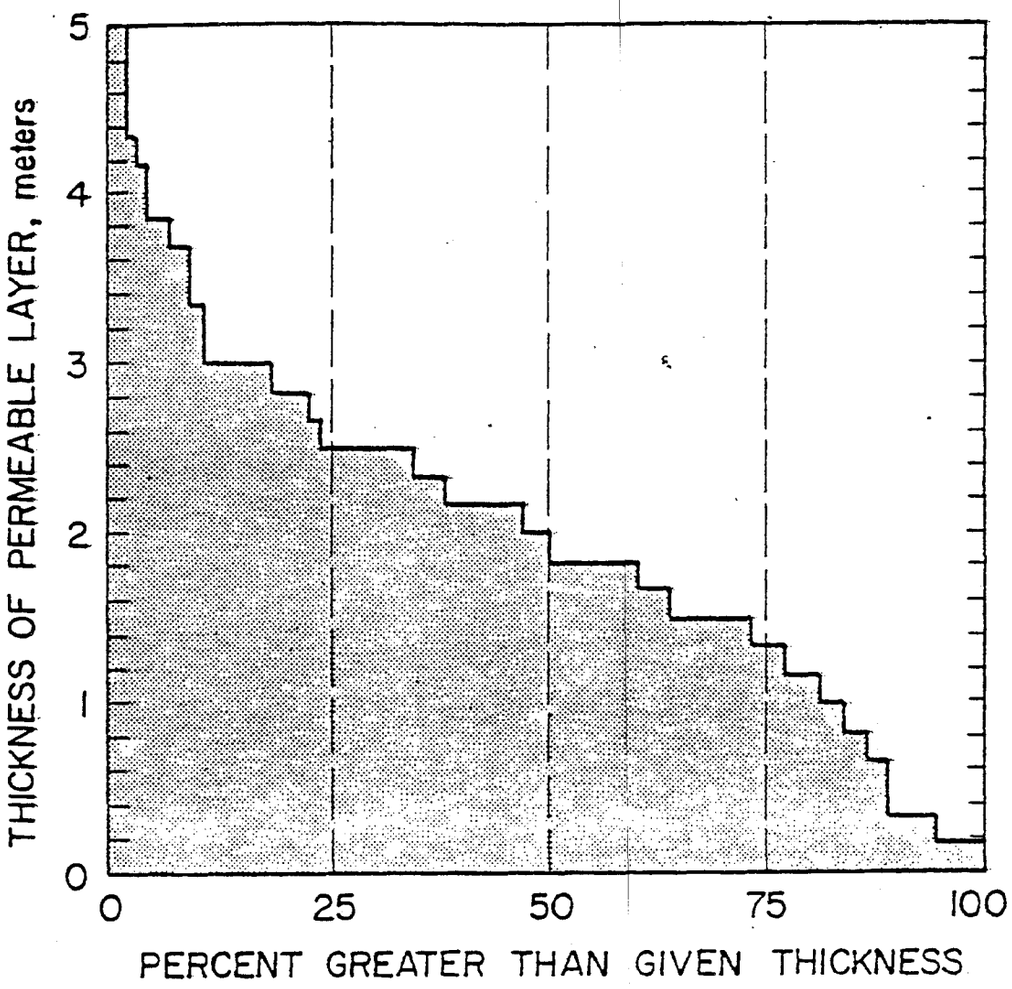

FIGURE 19. Distribution Function for Sand/Gravel Unit Thickness from SCVWD Well Logs

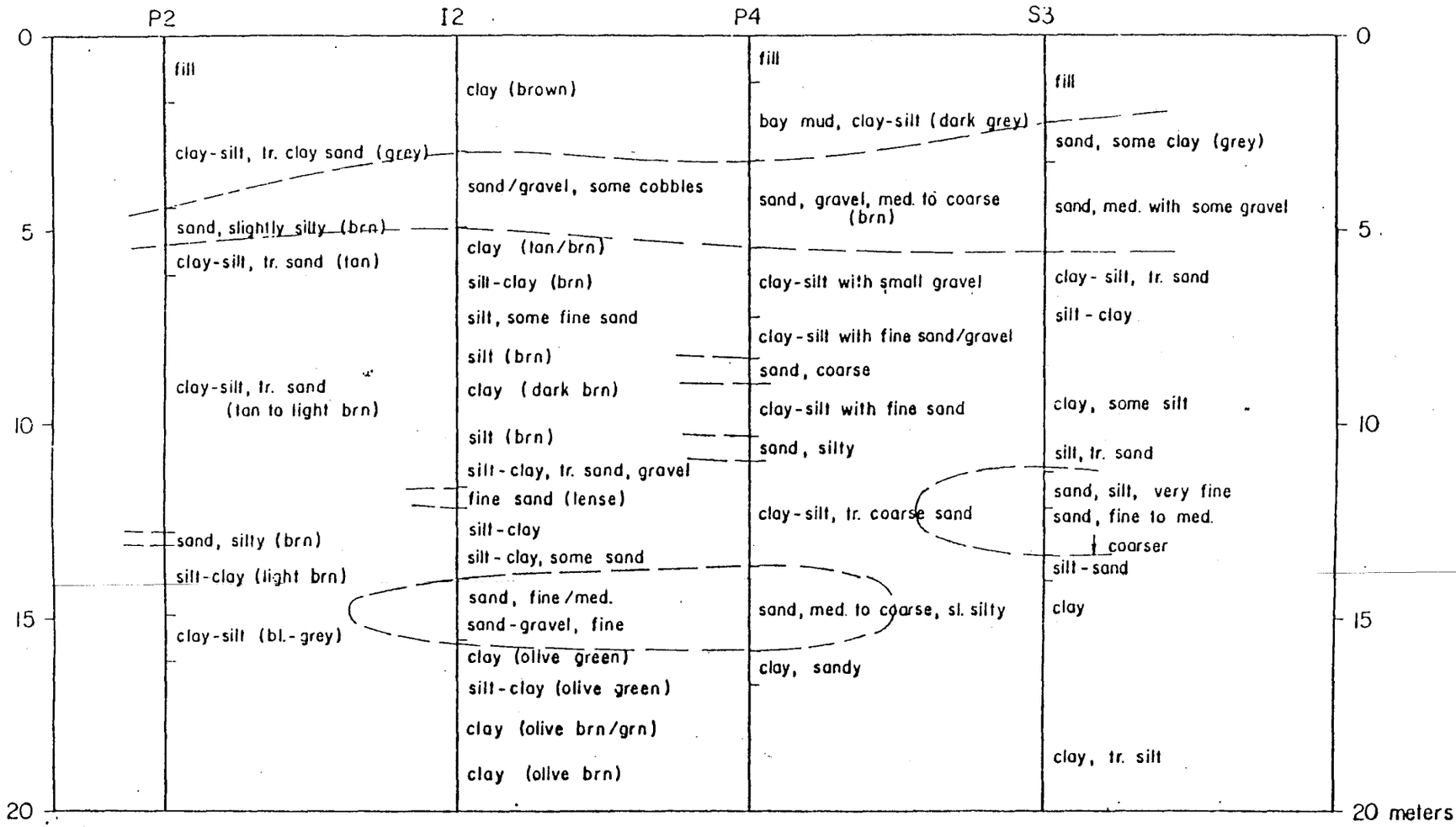

FIGURE 20. Profiles at I-2

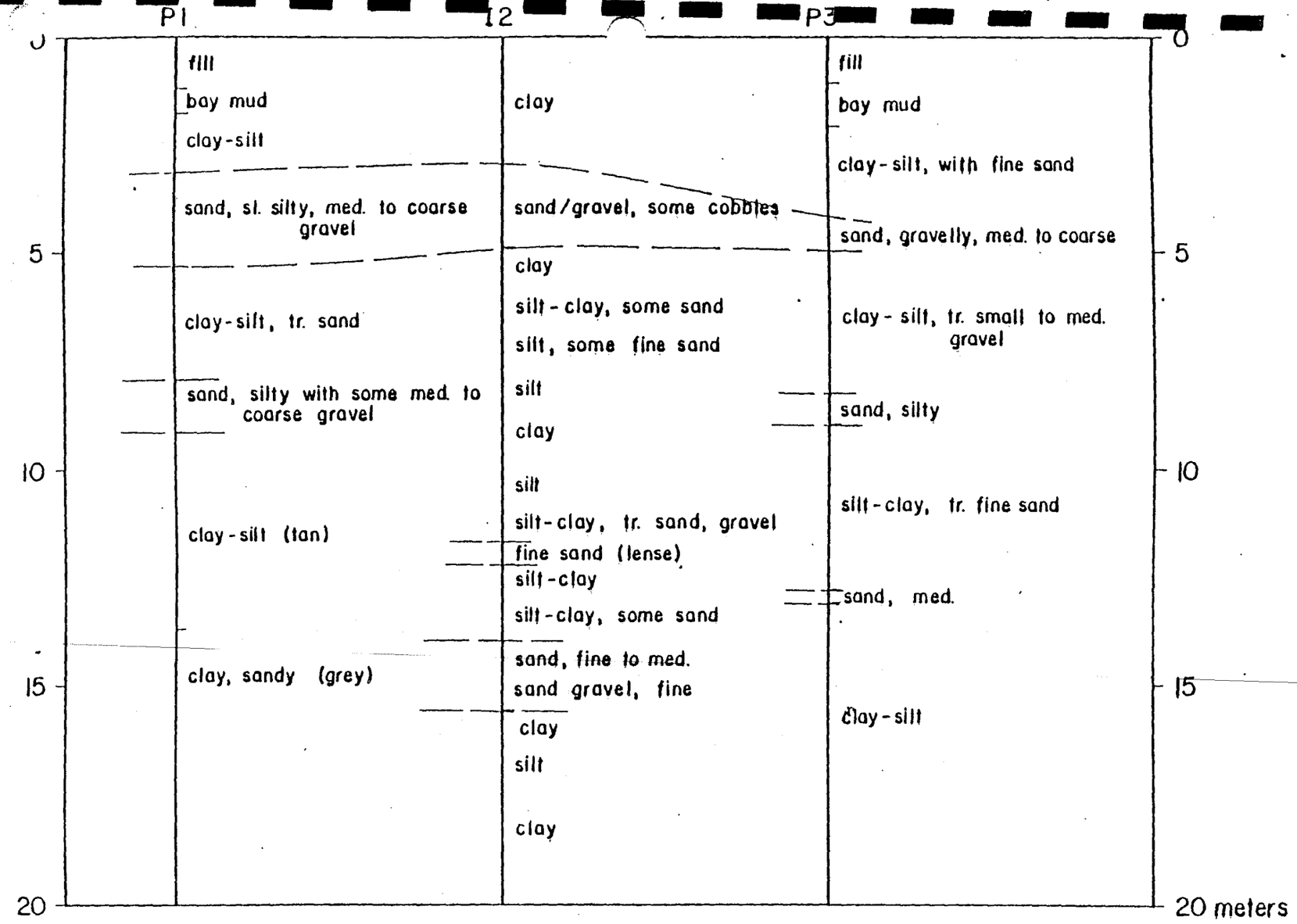

FIGURE 21. Profiles at I-2

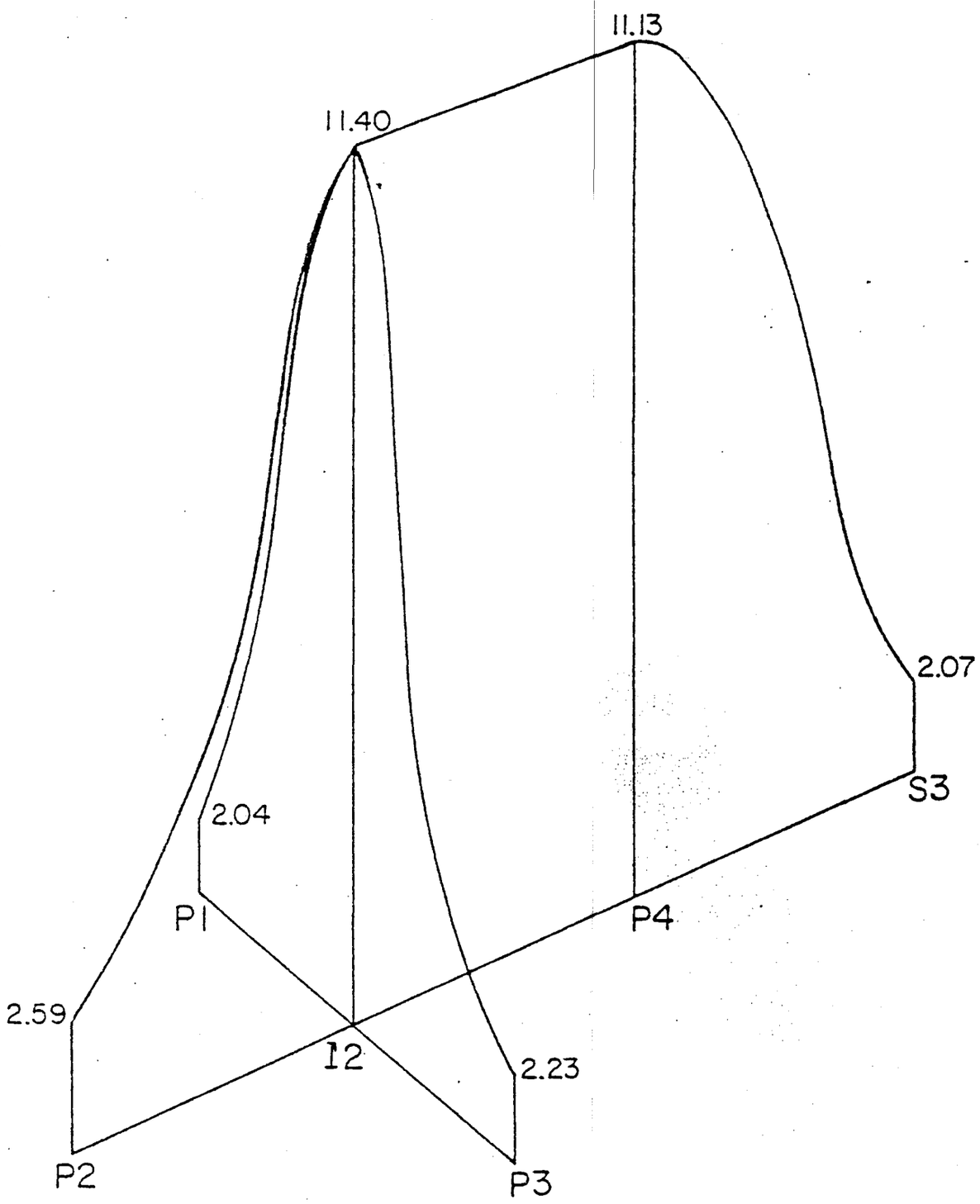

FIGURE 22. Steady State Hydraulic Heat Distribution Around I-2
(Meters)

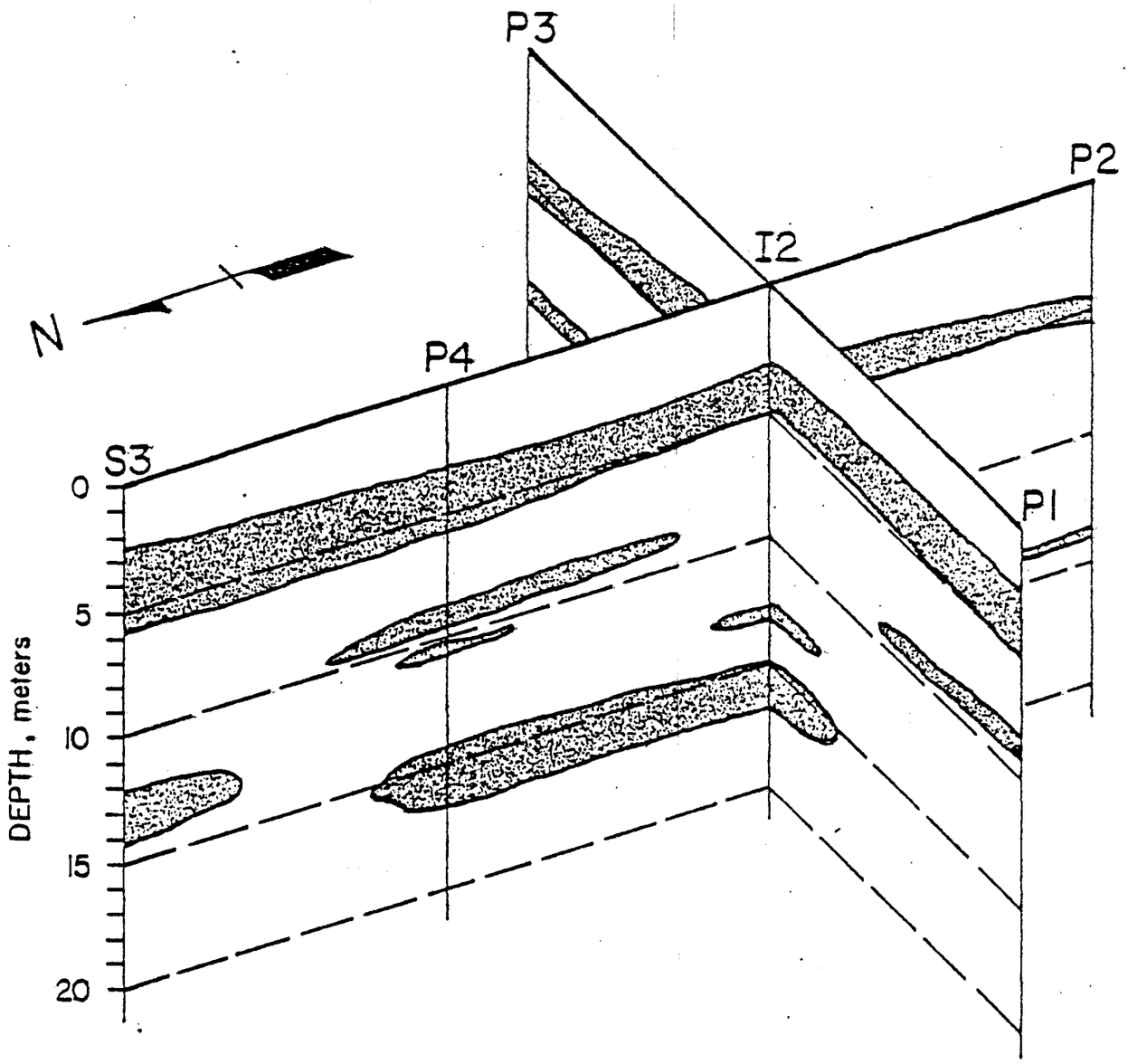

FIGURE 23. Fence Diagram at I-2

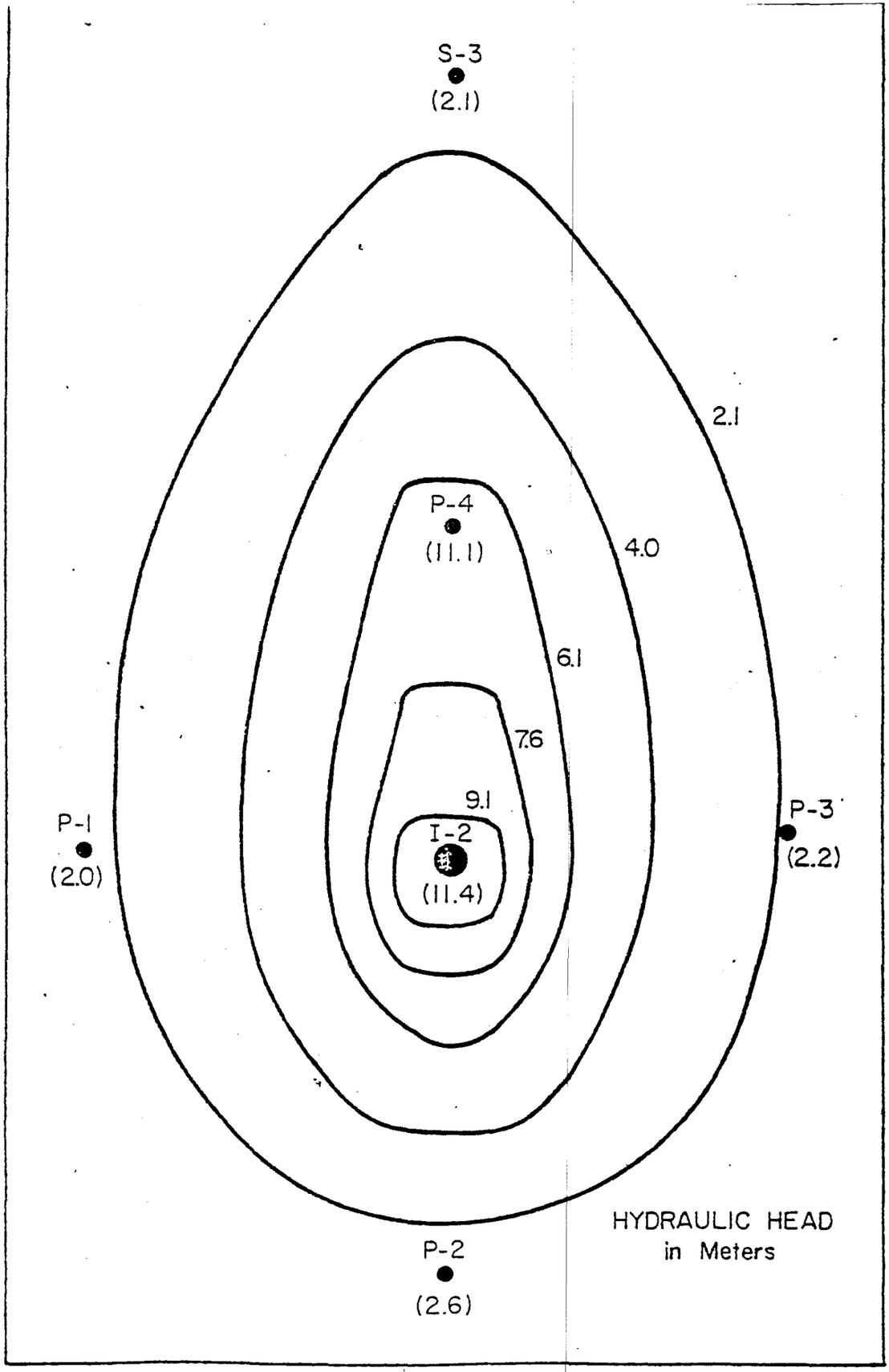

FIGURE 24. Simulation of Hydraulic Head Contours Around I-2

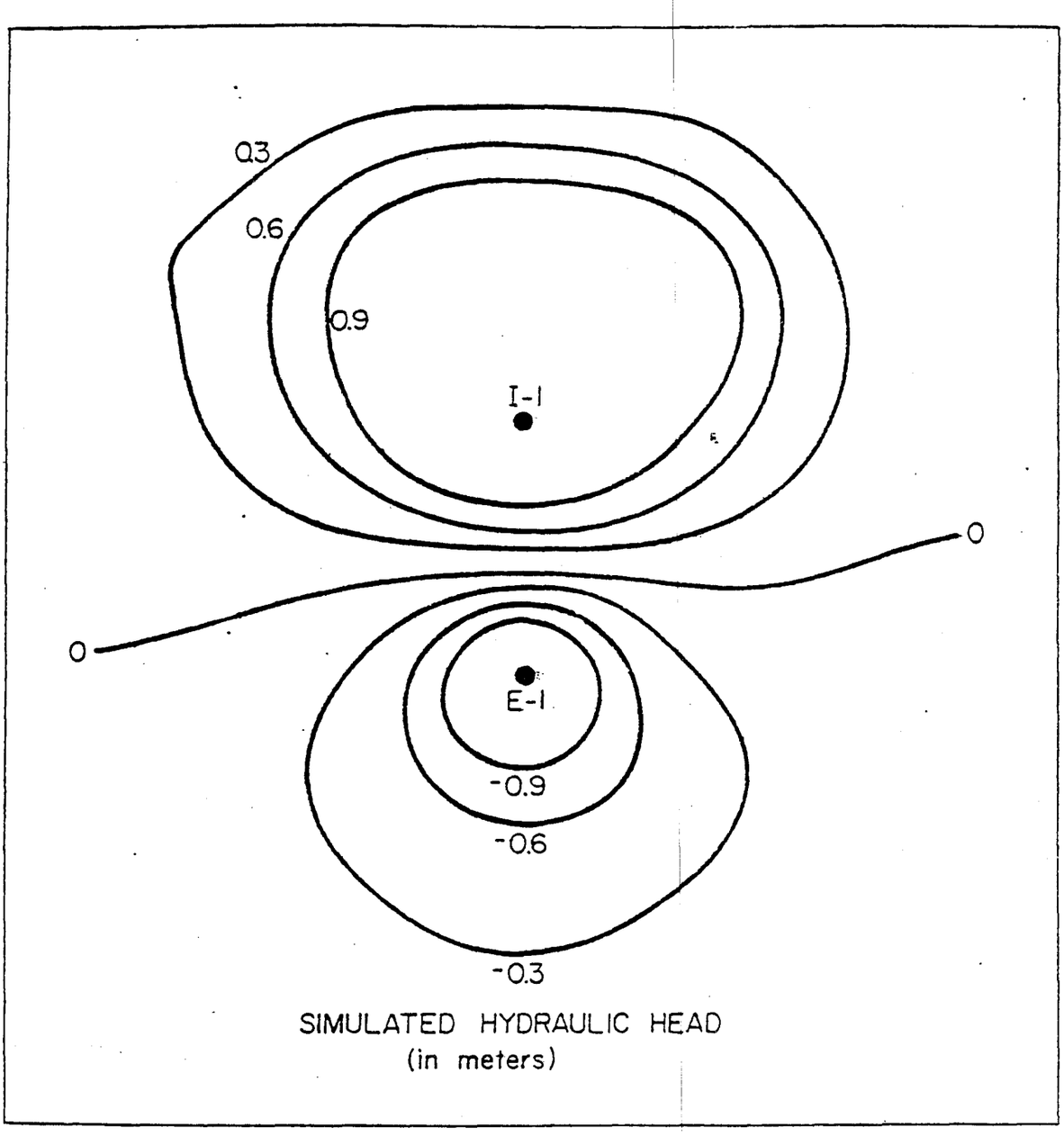

FIGURE 25. Hydraulic Head Contours for I-1, E-1 Pair

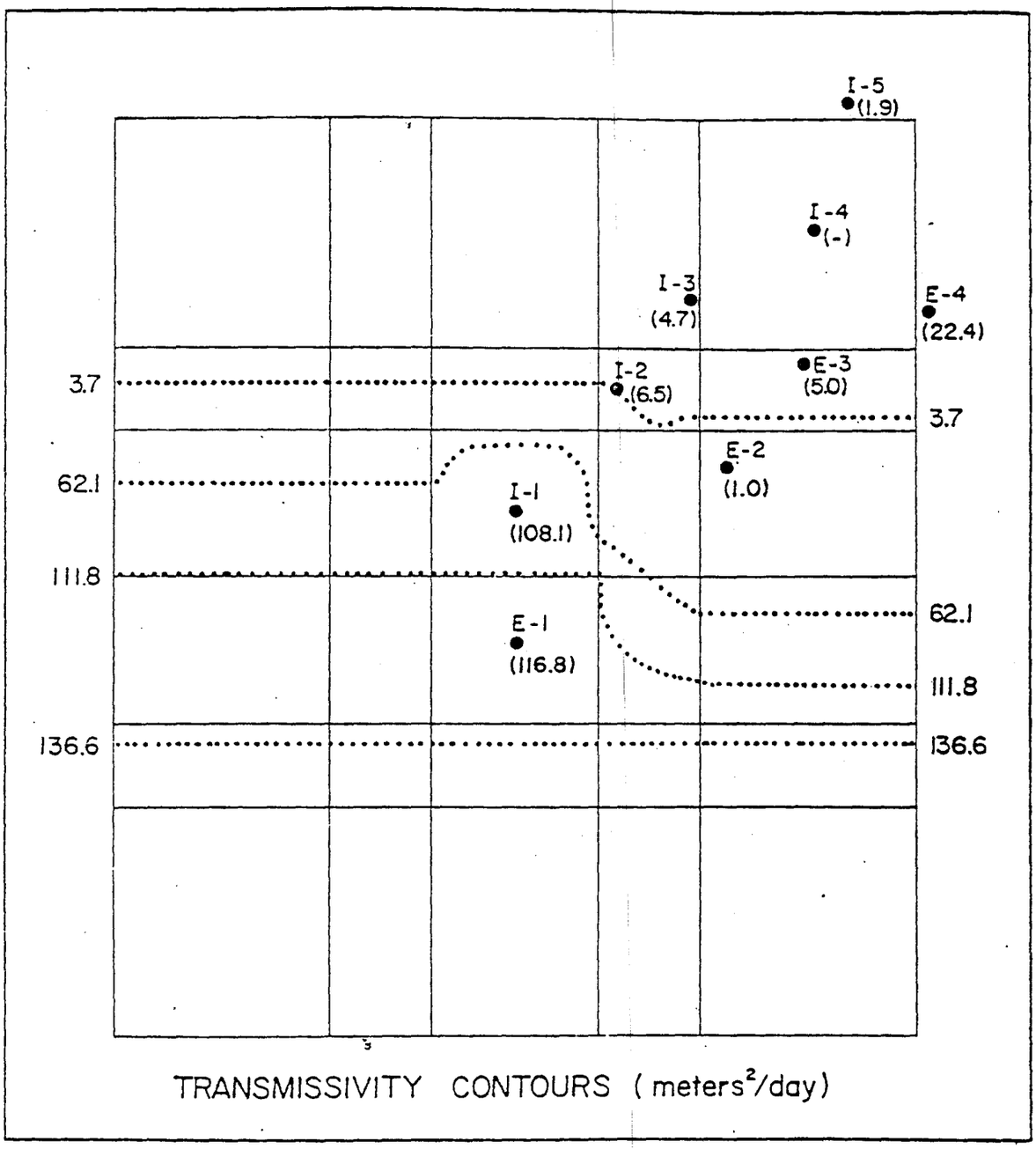

FIGURE 26. Contours of Transmissivity Used in Simulation of Figure 25

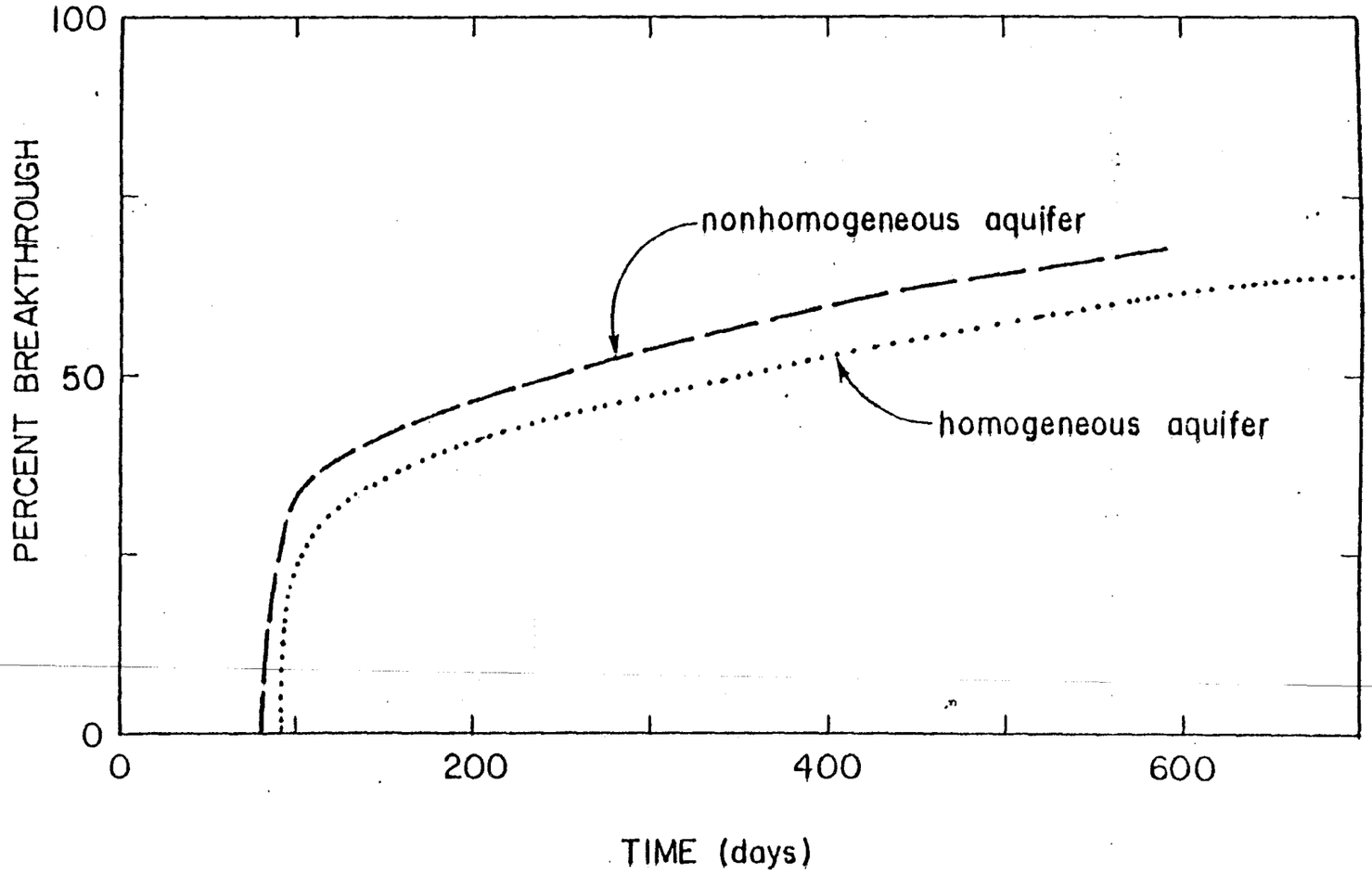

FIGURE 27. Breakthrough Curve (Nondispersive) at E-1

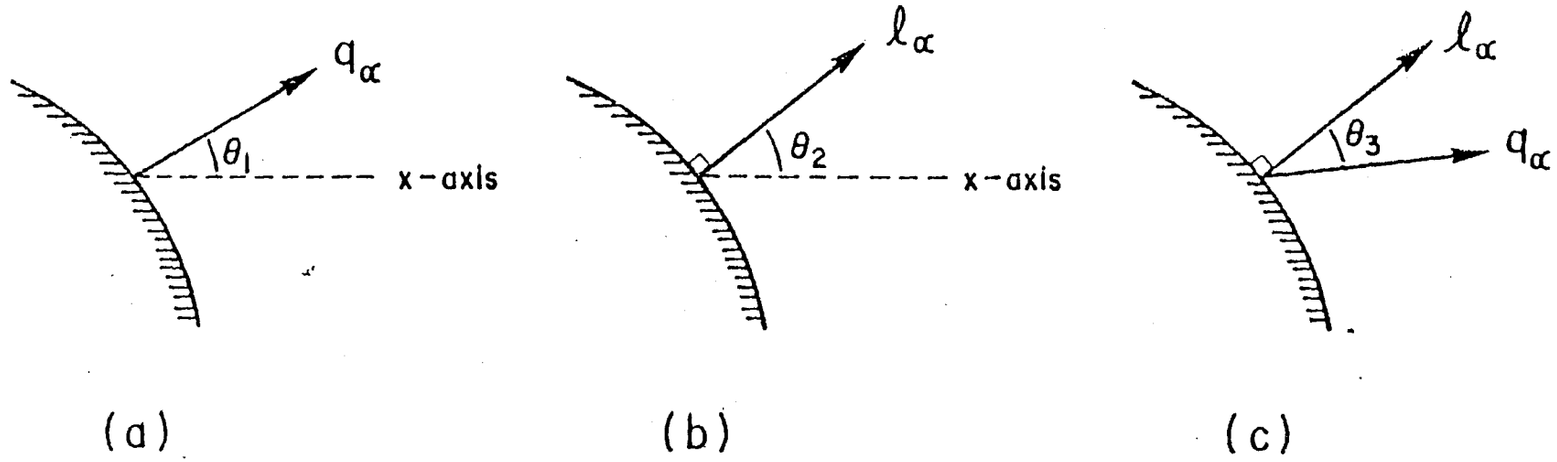

FIGURE 28. Ellipse Containing the Well

a. Streamlines Crossing Boundary

b. Normal Vector to Boundary

c. Unit Normal and Streamlines at Boundary